

University of Nevada, Reno

**Performance Analysis of Multiple Input Multiple Output Free  
Space Optical Communication Systems**

A Dissertation Submitted in Partial Fulfillment of the  
Requirements for the Degree of Doctor of Philosophy in  
Electrical Engineering

by

Xiaoyan Wang

Dr. Banmali Rawat/Dissertation Advisor

August , 2011



University of Nevada, Reno  
Statewide • Worldwide

THE GRADUATE SCHOOL

We recommend that the dissertation  
prepared under our supervision by

**XIAOYAN WANG**

entitled

**Performance Analysis of Multiple Input Multiple Output Free Space Optical  
Systems**

be accepted in partial fulfillment of the  
requirements for the degree of

**DOCTOR OF PHILOSOPHY**

Banmali Rawat, Advisor

M. Sami Fadali, Committee Member

Bruce Johnson, Committee Member

Aaron Covington, Committee Member

Michael Webster, Graduate School Representative

Marsha H. Read, Ph. D., Dean, Graduate School

August, 2011

## ABSTRACT

The Free Space Optical (FSO) communication i.e. optical communication without fibers is slowly becoming quite popular as fiber and its installation cost as well as difficulties involved becomes zero. The FSO communication is already making its impact in deep space communication and is expected to replace the existing optical fiber communication systems in the near future. In order to further speed up the optical communication, the Multiple Input/Multiple Output (MIMO) technology from microwave MIMO systems is being investigated. The characteristics of the Multiple Input/Multiple Output Free Space Optical communication systems using APD receivers have been discussed. The APD-based receivers for MIMO FSO systems under normal working conditions are designed and the characteristics of the components, such as InGaAs APDs, GaAs MESFET transimpedance amplifiers, a matched filter and an equalizer, etc., are considered. The probabilistic analysis of a FSO channel, APDs and noise in the FSO systems has been carried out.

The main contributions in this dissertation are: obtaining the detailed closed-form expressions for the upper bounds of the error probabilities, analyzing the impacts of different parameters in MIMO FSO systems, and thorough analysis of a more complex model of the MIMO FSO system involving Webb distribution for APD-based optical receiver, the probabilistic analysis of the detection for pulse position modulation signaling and the transmitted symbol matrix for MIMO FSO equal gain combining systems. Using this detailed analysis the average symbol error probability, average bit error probability and average pairwise probability are also obtained. The equations have been derived by using the Fourier series analysis method. The

modified Gauss-Chebyshev method for error probability calculation is also proposed. Results for average SEP and average BEP under different parameters are obtained and the impact of these parameters on MIMO FSO systems is also discussed.

## ACKNOWLEDGEMENTS

I would like to express my sincere gratitude to my advisor, Dr. Banmali Rawat, for his constant encouragement and help in my research and preparation of this dissertation. His guidance, advice and undaunted support throughout the duration of this task provided me with the necessary motivation to complete this work.

I would also like to thank Dr. M. Sami Fadali, Dr. Bruch Johnson, Dr. Aaron Covington and Dr. Michael Webster, for serving on my committee. I would like to express my appreciation to Dr. Moncef Tayahi, former faculty of Electrical Engineering Department for this help and support in the beginning of my Ph.D research work.

Finally I am especially grateful to my husband, Bin, for his continued encouragement, support and understanding during my dissertation work and to my parents for giving me immense strength not only to set high goals but also to achieve them. This effort would not have been possible without the support I got from these three amazing people.

## TABLE OF CONTENTS

ABSTRACT.....	i
ACKNOWLEDGEMENTS .....	iii
TABLE OF CONTENTS.....	iv
LIST OF FIGURES.....	viii
LIST OF TABLES.....	x
Chapter 1 Introduction.....	1
References.....	8
Chapter 2 Free Space Optical Communication Systems.....	11
2.1 Comparison of FSO, Radio Frequency and Optical Fiber Communication..	11
2.2 Modulation and Detection Scheme for FSO.....	14
2.2.1 Wavelength Choice.....	14
2.2.2 Direct Detection Modulation.....	16
2.2.3 Pulse Position Modulation .....	18
2.3 Characteristics of Free Space Optical Channel.....	20
2.3.1 Gaussian Beam Propagation.....	20
2.3.2 FSO Channel Model and Turbulence.....	21
2.4 Optical Receiver .....	24
2.4.1 Avalanche Photodetector-Based Receiver Structure.....	24
2.4.2 Webb Distribution of Electrons Given Out by APDs.....	25
2.4.3 Noises in the APD-Based Receivers for FSO.....	26
References.....	33

Chapter 3 Overview of MIMO FSO Communication Systems.....	36
3.1 System Model of MIMO Optical Wireless Links.....	36
3.2 Mathematical Model of MIMO FSO Point-to-Point Communication Systems.....	45
3.2.1 Assumptions for MIMO FSO Point-to-Point Communications.....	45
3.2.2 Laser Beam Transmission and Link Budget.....	47
3.2.3 Statistical Characteristics of Signals in APD-based Receivers.....	53
3.2.4 Receiver Noises in MIMO FSO Systems.....	63
3.2.5 Signal to Noise Ratio Calculation.....	65
3.3 Probability Density Function Calculation of Channel Gains.....	66
References .....	69
Chapter 4 Error Probability Calculation of MIMO FSO Systems .....	72
4.1 Symbol Error Probability Calculation of MIMO FSO Systems .....	72
4.1.1 Symbol Detection of One Q-ary PPM Symbol.....	72
4.1.2 Symbol Detection of Transmitted Matrices.....	81
4.1.3 Symbol Error Probability Calculation of Transmitted Matrices.....	87
4.1.4 Fourier Series Method for Calculating the Average SEP.....	100
4.1.5 Modified Gauss-Chebyshev Method for Calculating the Average SEP.....	105
4.2 Symbol Error Probability Calculation of SISO FSO Systems.....	109
4.2.1 SEP Calculation of SISO FSO Systems By Fourier Series Method....	109
4.2.2 SEP Calculation of SISO FSO Systems By Modified Gauss-Chebyshev Method.....	112

4.3 Error Analysis for SEP and BEP Calculations.....	115
4.3.1 Error Analysis for the Average SEP and BEP Calculation.....	115
References .....	125
Chapter 5 System Model and Analysis Results.....	127
5.1 Calculating Results and Analysis for MIMO FSO Systems.....	127
5.1.1 Model Used for Analysis.....	127
5.1.2 Parameters of MIMO FSO Systems.....	128
5.2 Results and Analysis of the Average Error Probability.....	130
5.2.1 SISO and MIMO Comparison.....	131
5.2.2 Optical Device Impact.....	136
(a) Performance Comparison of APDs.....	136
(b) ADP Gain Impact.....	139
5.2.3 Electrical Device Impact.....	143
(a) Amplifier Impact.....	143
(b) Temperature Impact.....	144
(c) Average BER Comparison of Systems with the different $\gamma_s$ , $I_2$ and $I_3$ .....	147
(d) Bias Resistance Impact.....	148
5.2.4 PPM Symbol Length and MIMO Diversity Impact.....	149
5.2.5 Turbulence Impact.....	151
References .....	153
Chapter 6 Conclusion and Future Research Directions.....	154

APPENDIX A.....	157
APPENDIX B.....	157
APPENDIX C.....	160
APPENDIX D.....	159
APPENDIX E.....	162
APPENDIX F.....	163
APPENDIX G.....	164
APPENDIX H.....	167
APPENDIX I.....	170
APPENDIX J.....	171
APPENDIX K.....	172
APPENDIX L.....	175
APPENDIX M.....	179
APPENDIX N.....	180
APPENDIX O.....	181

## LIST OF FIGURES

Figure 2.1 Atmospheric transmittance for different wavelengths Ref [1] .....	15
Figure 2.2 Example of PPM symbol set.....	19
Figure 2.3 Basic architecture of the APD-based optical receiver.....	25
Figure 3.1 $N_t$ laser sources and $N_r$ photodetectors MIMO FSO system.....	36
Figure 3.2 The detailed architecture of MIMO point-to-point system.....	40
Figure 3.3 Receiver structure of MIMO point-to-point systems.....	44
Figure 3.4 Two processes in APDs.....	56
Figure 4.1 Computing result of the series expression in Eq. (4-73) .....	98
Figure 4.2 Computing result of Eq. (4-73) by Dawson's integral.....	100
Figure 4.3 Plot of $f(x)$ in Eq. (4-109) .....	117
Figure 4.4 Plot of $\frac{d[f(x)]}{dx}$ in Eq. (4-110) .....	118
Figure 4.5 Plot of $g_1(h_{il})$ in Eq. (4-112) .....	119
Figure 4.6 Plot of $g_2(h_{il})$ in Eq. (4-112) .....	120
Figure 4.7 Plot of the functions in Eq. (4-117) and Eq. (4-118) with $M\gamma_1 =$ 1.....	123
Figure 4.8 Plot of the functions in Eq. (4-117) and Eq. (4-118) with $M\gamma_1 =$ 6.....	123
Figure 4.9 Plot of $g(x)$ in Eq. (4-120) .....	124
Figure 5.1(a)Average SEP of SISO FSO systems with $L = 2$ PPM symbols .....	132
Figure 5.1(b)Average SEP of MIMO FSO systems with $L = 2$ PPM symbols .....	132
Figure 5.2(a)Average SEP of SISO FSO systems with $L = 2$ PPM symbol .....	134
Figure 5.2(b)Average SEP of MIMO FSO systems with $L = 2$ PPM symbol .....	134

Figure 5.2(c)Average SEP of SISO FSO systems with $L = 2$ PPM symbol.....	135
Figure 5.2(d)Average SEP of MIMO FSO systems with $L = 2$ PPM symbol .....	135
Figure 5.3(a)Average BEP of Ge APDs and the InGaAs APDs.....	138
Figure5.3(b)Average BEP of InGaAs APDs with the different responsivity.....	138
Figure 5.4 Average BEP with different APD gains $M$ .....	141
Figure 5.5(a)Average BEP with the different $M$ corresponding to $P_s T_b$ (dBJ) .....	141
Figure 5.5(b) Average BEP with the different $M$ corresponding to $P_s$ (dBm) .....	142
Figure 5.6 Average BEP with the different APD gains $M$ and different turbulence .....	143
Figure 5.7 Average BEP with the different amplifier gains.....	144
Figure 5.8 Average BEP under the different temperatures at $P_s T_b = -157.74$ dBJ .....	146
Figure 5.9 Average BEP under the different temperatures at $P_s T_b = -157.74$ dBJ .....	146
Figure 5.10 Average BEP of MIMO FSO systems with the different $\gamma_s$ , $I_2$ and $I_3$ .....	148
Figure 5.11 Average BEP with the different bias resistances $R_b$ .....	149
Figure 5.12 (a) Average BEP with the different $L$ and different $N_t$ and $N_r$ for SISO.....	150
Figure 5.12 (b) Average BEP with the different $L$ and different $N_t$ and $N_r$ for MIMO.....	150
Figure 5.13 Average BEP with the different variance of the log intensity.....	152

**LIST OF TABLES**

Table 5-1 Parameters of MIMO FSO systems.....	129
Table 5-2 Generic operating parameters of Ge and InGaAs APDs.....	137
Table 5-3 Values of the parameters $\gamma_s$ , $I_2$ and $I_3$ for MIMO FSO systems.....	147

## **CHAPTER 1**

### **INTRODUCTION**

Free Space Optical communication, also known as optical wireless communication, has emerged as an attractive technology. It has the potential to bridge the 'last mile' gap that separates homes and businesses from high bandwidth access to the larger wired network or for linking intranets with corporate campus. At the same time, FSO has received significant attention as a technology for deep space ground-to-orbit communication and as a supplement to more conventional radio frequency (RF) or microwave links.

FSO is a method with highly efficient energy usage. It is also cost-effective and offers high-speed wireless connectivity. It uses very narrow and directional beams to achieve smaller divergence than a RF signal. The RF spectrum is becoming increasingly crowded and the demand for available bandwidth is growing rapidly. Since conventional wireless is a broadcast technology, all subscribers within a cell must share the available bandwidth and their base station powers must be limited to allow spectrum reuse in adjacent cells. Thus individual subscribers can obtain only modest bandwidths, especially in dense urban areas. Optical wireless provides an attractive way to circumvent such limitations. This line-of-sight communications technology avoids the wasteful use of both the frequency and spatial domains inherent in broadcast technologies. FSO provides benefits including ultra high wireless bandwidth, secure wireless transmission, license free operation and prompt installation, etc.

However, because the optical wave propagates through the air, which is a medium with inhomogeneous refractive index, the beam experiences fluctuation in

amplitude and phase due to the molecular absorption, aerosol scattering and atmospheric turbulence. This intensity fluctuation, also known as scintillation, is one of the most important factors that degrade the performance of an FSO communication link, even under clear sky conditions. This is caused by changes in signal amplitude known as channel fading. Channel fading causes the attenuation of the optical signal when it makes its way through the FSO channel to the receiver.

Currently, the application of FSO for wireless Local Area Network (LAN) usually has the data rates of 1.5Mb/s to 2.5 Gb/s and covers one or two kilometers. For deep space optical communication applications, Q-switched lasers typically are employed. Their peak power can be several giga-watts for overcoming deep space losses, but this leads to much lower pulse repetition rates, for example, several megahertz (MHz). Thus, there is a tradeoff between bandwidth and transmission distance in optical communication.

The FSO communication link model must be analyzed and simulated accurately, since the choice of a suitable architecture, the optimal algorithms and the demodulation performance directly depend on the characteristics of the FSO channel itself and the properties of the optical components to be used. In the receiver, the discrete time demodulation architecture, which combines the post detection filtering and slot synchronization, is one of the crucial parts of such systems [1-3].

For optical wireless communication, direct detection has more advantages than that of coherent detection. There is no need to detect the signal phase, which has a greater degree of susceptibility due to atmospheric turbulence. In order to fit for the infrared communication requirements, one of the direct detection techniques,

known as Pulse Position Modulation (PPM) is an attractive modulation technique in FSO. In recent years, NASA has been considering optical links for Mars Laser Communication Demonstration (MLCD), and has proposed the use of PPM and its different variants as the modulation format for the links along with PPM capacity formulas [1]. With this coding technique,  $M$  bits of information are encoded onto one of  $L = 2^M$  PPM symbols by establishing a one-to-one correspondence between the possible states of  $M$  binary digits and the location of an optical pulse among  $L$  possible slots [1-2]. A key requirement for optical communication, especially deep space optical communication, is a sufficient peak laser power level for the transmitted signal to survive large deep space losses.

In order to enable transmission under the strong atmospheric attenuation and turbulence, the use of multiple-input multiple-output is introduced to optical communication. It is necessary to combat channel fading, improve system performance and overcome distance limitations [3] [4]. By using the space and time diversity of MIMO, multiple replicas are provided by channel coding, such as Space Time Block Code (STBC), Space Time Trellis Code (STTC) and Bell Labs Layered Space-Time Architecture (BLAST), etc. In theory, by using the multi-laser multi-detector array, the channel capacity, the bandwidth and the transmission distance, can all be improved significantly.

In current RF communication, MIMO techniques have already been developed as practical products and implemented in the market. The IEEE802.16 supports MIMO and uses the Alamouti-based Space Time Block Coding. Although the current products utilize simple MIMO schemes due to technique complexity considerations, MIMO is still a promising technique and is considered as a revolution in wireless communication. However, in order to make MIMO a

practical technique in FSO, many aspects need to be investigated. Although the multi-laser multi-detector array concept is analogous to MIMO in wireless RF communication, the underlying physics is different and several aspects of the MIMO approach applied to the optical problems are different than the RF counterpart.

Firstly, for MIMO FSO communication, PPM is employed and the pulses of laser beam are used to transmit the information data. The PPM signal is transmitted through the block fading FSO channels and is detected by direct detection. The intensities of the received PPM signals are used for detection. Thus the signals of MIMO FSO systems are non-negative and real, and are not complex. But the RF communication generally uses QAM, PSK or other modulation techniques, which require amplitude and phase to transmit the information making them quite complex. The negative symbols in the STBC schemes for RF systems cannot be implemented directly in the FSO system and innovative STBCs for FSO MIMO systems are needed.

Secondly, the PPM is the orthogonal and power-limited signaling technique. In this equal-energy orthogonal signaling scheme, each PPM symbol includes several time slots and each time slot is exposed to noise during transmission. Thus each PPM symbol has the noise impact on different time slots. Whereas in RF communication, the QAM symbol or the PSK symbol occupies one time slot using amplitude and phase modulation and is exposed to the noise only in one slot. Thus the demodulation and the error probability calculations are totally different from those of PPM. Furthermore, efficient STBC schemes and performance analysis suitable for MIMO FSO systems are required.

In recent publications, several different multi-laser multi-detector techniques are studied by using the Chernov bound, the block fading channel and the simplified optical receiver model [3] [4] [5]. Among the different methods of MIMO, Space Time Block Coding (STBC) has more advantages because it is much less complex than others for the same configuration, such as space time trellis code and Bell Labs Layered Space-Time Architecture scheme. For a fixed number of transmission antennas, the decoding complexity of a space time trellis code increases exponentially as a function of the spectral efficiency [6]. The repetition coding scheme is also a simple coding scheme but does not fully use the time diversity for MIMO FSO systems [7]. The Alamouti-based Space Time Block coding is the preferred choice, especially due to its remarkable computational simplicity and satisfactory performance capability [6, 8]. But it uses more energy for transmitting the PPM symbols when the negative symbols are needed to transmit, and results in lower energy efficiency on a per bit basis. Enzo Baccarelli proposed a new family of STBC for MIMO Impulse Radio Ultra-Wideband (IR-UWB) systems, using the orthogonality of different waveforms of pulse to identify the different transmission [9, 10]. Chadi Abou-Rjeily and Wissam Fawaz proposed a STBC scheme for MIMO FSO and IR-UWB systems using the cyclic division algebra [11]. More research on the STBC for MIMO FSO systems is still required.

For performance analysis, many publications have modeled the MIMO FSO system and have analyzed the error probability. Neda Cvijetic and Stephen G. Wilson have obtained the performance analysis for MIMO FSO systems with APD receivers in atmospheric turbulence [12]. But they only gave a simplified expression for the equation, and could not obtain a closed-form expression due to the intractable complexity involved. Ehsan Bayaki and Robert Schober analyzed

the performance of MIMO FSO systems in Gamma–Gamma fading [13]. They only calculated the error probability for OOK and binary PPM using exact equations and approximated the equation for the Q-ary PPM scheme [13]. In Appendix A of [13], the slots in the one Q-ary PPM symbol are treated equally during the calculation of the error probability resulting in errors [13]. In addition, they did not consider the impact of the primary photoemission process and the secondary photo-multiplication process in APD.

The design of coded MIMO FSO configurations for efficient transmission of information can be divided into two basic approaches: the algebraic approach, which is primarily concerned with the design of coding and decoding techniques for specific codes for MIMO FSO systems, and the probabilistic approach, which deals with the performance analysis of a general class of coded signals or configurations. The latter approach yields bounds on the error probability that can be attained for communication over a FSO channel having some specified characteristic and is very important in designing STBC for MIMO FSO systems.

In this dissertation, the probabilistic approach is adopted for MIMO FSO systems. The performance of MIMO systems using PPM over different FSO channels with weak turbulence is analyzed in detail. A detailed method is provided for calculating the performance measures in order to obtain more exact closed-form results or a tighter closed-form upper bound. The average bit error probability, the average symbol error probability and other parameters of the system performance are first calculated in detail for MIMO FSO systems over the block fading FSO channel. Then these results are used to obtain the performance analysis of Single Input Single Output (SISO) FSO system. This is very useful for

analyzing the characteristics of MIMO and SISO FSO systems and for designing a suitable STBC scheme or a better MIMO configuration for FSO systems.

If the impact of each parameter is not considered for a simple PPM demodulation scheme and APD receiver, this results in some errors in the performance analysis. In this dissertation, more detailed models of FSO channels, PPM demodulation, APD devices and optical receivers are considered for more accurate results. Closed-form equations of the upper bounds for the average bit error probability, average symbol error probability and other parameters are obtained. As the parameters change, the diagrams of the average bit error probability, the average symbol error probability and other parameters are obtained and analyzed. The calculation error and truncation error are analyzed in detail. Future research directions are also suggested.

This dissertation is organized as follows. Chapter 1 reviews MIMO FSO technology and summarizes the work accomplished in this dissertation. Chapter 2 presents an overview of Free Space Optical communication systems. Chapter 3 discusses multiple-input multiple-output systems with the free space links. Chapter 4 calculates closed-form upper bounds for the average error probabilities for MIMO and SISO FSO systems. The calculation error and truncation error are discussed in detail. Chapter 5 analyzes the calculated results and diagrams of the average error probabilities and other parameters. Chapter 6 concludes the dissertation with a summary of the contribution of the work in the dissertation and discusses directions for future research and applications.

## REFERENCES

- [1]. Andrew A. Gray, Clement Lee “Discrete-Time Demodulator Architecture for Free Space Broadband Optical PPM,” NASA JPL internal, IPN Progress Report 42-158, August 15, 2004.
- [2]. V. Vilnrotter, A. Biswas, W. Farr, D. Fort, and E. Sigman, “Design and Analysis of a First-Generation Optical Pulse-Position Modulation Receiver,” The Interplanetary Network Progress Report 42-148, October–December 2001.
- [3]. M. Simon and V. Vilnrotter, “Alamouti-type space-time coding for free space optical communication with direct detection,” IEEE Trans. On Wireless Communications, vol. 4, no. 1, pp. 35–39, 2005.
- [4]. S. G. Wilson, M. Brandt-Pearce, Q. Cao, and J.J.H. Leveque, III, “Free-space optical MIMO transmission with Q-ary PPM,” IEEE Trans. Communication. 53, 1402-1412, 2005.
- [5]. I. B. Djordjevic, B. Vasic, M. A. Neifeld, “Multilevel coding in free-space optical MIMO transmission with Q-ary PPM over the atmospheric turbulence channel,” IEEE Photon. Tehnol. Lett. 18, 1491-1493, 2006.
- [6]. Simon Haykin and Michael Moher, “Modern Wireless Communication”, Haykin Moher, LSK 2005 HAY.
- [7]. S. G. Wilson, M. Brandt-Pearce, Q. Cao, M. Baedke, “Optical repetition MIMO transmission with multipulse PPM,” IEEE Selected Areas Comm. 23, 1901-1910 , 2005.
- [8]. S. Alamouti, “A simple transmit diversity technique for wireless communications,” IEEE Journal on Selected Areas in Communications, vol. 16, issue 8, pp. 1451-1458, Oct. 1998.

- [9]. Enzo Baccarelli, Mauro Biagi, Cristian Pelizzoni and Nicola Cordeschi, “A new family of optimized orthogonal Space-Time Codes for PPM-based MIMO systems with imperfect channel ”, *wireless Pers Commun*, 2007, 43:1071-1091, DOI 10.1007/s 11277-007-9284-1.
- [10]. Enzo Baccarelli, Mauro Biagi, Cristian Pelizzoni and Nicola Cordeschi, “Space-Time orthogonal M-ary PPM (STOMP) coding for coverage extension of MIMO UWB-IR systems ”, *IEEE*, 2005, 0-7803-9206-X/05.
- [11]. Chadi Abou-Rjeily and Wissam Fawaz, “Space-Time Codes for MIMO Ultra-Wideband Communications and MIMO Free Space Optical Communications with PPM”, 2008, *IEEE Journal and Selected Areas in Communications*, VOL 26, NO.6, August 2008.
- [12]. Neda Cvijetic, Stephen G. Wilson and Maite Brandt-Perce, “Performance bound for Free Space Optical MIMO systems with APD receivers in Atmospheric Turbulence”, *IEEE Journal and Selected Areas in Communications*, VOL 26, NO.3, April 2008.
- [13] Ehsan Bayaki, Robert Schober and Ranjan K. Mallik, “ Performance analysis of MIMO Free Space Optical Systems in Gamma–Gamma Fading”, *IEEE Transactions on communications*, VOL. 57, NO. 11, November 2009.
- [14]. Seyed Mohammad Navidpour, Murat Uysal, Mohsen Kavehrad , “Performance Bounds for Correlated Turbulent Free-Space Optical Channels”.
- [15]. V. Tarokh, H. Jafarkani, and A. R. Calderbank, “Space-time block codes from orthogonal designs,” *IEEE Trans. Inf. Theory*, vol. 45, no. 5, pp. 1456–1467, Jul. 1999.
- [16]. I. B. Djordjevic, B. Vasic, and M. A. Neifeld, “LDPC coded OFDM over the atmospheric turbulence channel,” *Opt. Express*, vol. 15, pp. 6332–6346, 2007.

- [17]. J. G. Proakis, “Digital Communications”, Boston, MA: McGraw-Hill, 2001.
- [18]. Robert Grover Brown and Patrick Y.C. Hwang, “Introduction to Random Signals and Applied Kalman Filtering”, John Wiley and Sons, Inc, 1997.
- [19]. Stephen G. Wilson, Maite Brandt-Pearce, Michael Baedke, and Qianling Cao, “Optical MIMO Transmission with Multi-pulse PPM” , IEEE ISIT 2004, June 27 – July 2, 2004.

## CHAPTER 2

### FREE SPACE OPTICAL COMMUNICATION SYSTEMS

#### 2.1 Comparison of FSO, Radio Frequency and Optical Fiber Communication

Free Space Optical Communication is a license-free and cost-effective access technique, which has attracted significant attention recently due to a variety of applications. By using laser beams passing through the free space, the information, such as voice, data and video, is transmitted between the users and the servers. Due to this reason, the FSO is also called optical wireless communication. FSO has the same enormous available bandwidth as the optical fiber communication. Optical wireless is becoming an attractive option for the multi-gigabit-per-second (multi-Gb/s) short range (up to 2~3 km) links and a complementary or backup plan for the current fiber or radio frequency network [1]. Through relaying technique, outdoor FSO optical transceivers can also cover long distances. With its high-data-rate capacity and wide bandwidth on unregulated spectrum, FSO communication is a promising solution for the “last mile” problem. However its performance is highly vulnerable to adverse atmospheric conditions.

FSO inherits the advantages of wireless communications over wire communication, such as offering the possibility of rapid wireless deployment, flexibility of establishing temporary communication links, and reducing the cost of reconfiguration and wire placement. FSO also has more advantages than RF and has emerged as a commercially preferred choice and a viable alternative to RF and millimeter wireless communication. It has the following main advantages:

(i) Bandwidth: From a spectrum management point of view, license-free FSO offers potentially huge bandwidths that are currently unregulated worldwide and can therefore support more users compared to RF communication.

(ii) Beam-width: FSO uses very narrow and directional beams to achieve smaller divergence than RF signals. The narrow beam-width is on the order of a few milliradians. FSO is a method with highly efficient use of energy and it is more secure than RF communication.

(iii) Immunity to electromagnetic fields: FSO is immune to electromagnetic interference, which is very useful for applications in special environments.

(iv) Infrared (IR) components: Further advantages of FSO over RF include the low cost, the small size, and the limited power consumption of infrared (IR) components. FSO communication systems can make use of the same opto-electronic devices that have been developed and improved over the past decades for optical fiber communications and other applications.

Comparing with optical fiber communication, the FSO link has the advantages of easy deployment, quick installation, lower cost and the reduced possibility of interference or interception, etc. Firstly, optical wireless technologies have the benefits of mobility for user convenience and flexibility in the placement of terminals. Secondly, by using optical wireless solutions with reliable and rapid deployment, significant reductions in cost and time can be achieved in a number of applications. For instance, reconfiguring computer terminals or microcontroller systems in laboratories, conference rooms, offices, hospitals, production floors, or educational institutions, can be done at relatively reduced cost and faster. For short range links with multi-gigabit bandwidth requirements, laying optical fiber is too expensive or impractical. Usually the cost of fiber communications per kilometer in the range of

1.5 km around the switching center is 100,000~200,000 dollars. About 80% of this cost is used for laying the fibers underneath the ground and equipment installation. On the other hand, maintaining and reconfiguring wired networks, is usually more expensive, time-consuming and complicated. Furthermore, cables are susceptible to damage, which can potentially disrupt network operation. Thirdly, FSO is a good practical choice for some special conditions, especially in situations where cables are grounded or installed in inaccessible locations, as in memorial and historical buildings, hazardous manufacturing plants, temporary and mobile emergency stations or field tests [1- 4]. Currently it is widely believed that optical wireless can be used for multi-Gb/s communication [1].

Besides these advantages, FSO also has the following drawbacks [1- 4]:

- (i) FSO requires line of sight since optical wireless links are susceptible to blocking by persons and objects, which can result in the attenuation of the received signal or in the disruption of the link depending on the configuration of the system.
- (ii) In addition, FSO systems generally operate in environments where other sources of illumination are present. This background illumination, such as the radiation from the sun, the moon or other sources, has part of its energy in the spectral region used by FSO transmitters and receivers. This introduces noise in the photo-detector, which limits the range of the system.
- (iii) FSO systems are also affected by high attenuation due to scattering, absorption and scintillation when the IR signals are transmitted through air. Atmospheric phenomena, such as fog, aerosols, snow and rain droplets further reduce the range of the system and deteriorate the quality of the transmission when operating outdoors.

- (iv) FSO narrow beam-width also implies the need for careful directional pointing. Otherwise building vibration or sway can introduce signal strength fading in the link.

Some of the drawbacks presented by FSO, such as attenuation and background illumination noise, can be compensated to some extent by increasing the optical power level at the transmitter. Unfortunately, due to the fact that high emission power from some emitters can be potentially dangerous to the retina and because of power budget considerations, there is a limit to the optical power that can be safely and efficiently emitted by FSO transmitters [1- 4].

An approach using multiple lasers and multiple photo-detectors, also called MIMO, has recently been proposed and investigated. Due to its complexity, currently practical MIMO FSO systems adopt comparatively simple schemes. However MIMO FSO is still a promising technique and is considered as a revolution in wireless communication.

## **2.2 Modulation and Detection Scheme for FSO**

### **2.2.1 Wavelength Choice**

Many FSO vendors have traditionally used the 780 nm to 850 nm near-infrared spectrum for cost reasons. But the 1550 nm band, the choice of the fiber-optic telecommunication industry, is better suited for optical wireless.

The 1550nm band can transmit more power and is safer for human eyes compared to the 780nm band. Because of the properties of the human eye, the safe or allowable power density at 1550 nm is nearly 50 times than that at 780 nm [1]. Consequently, significantly more power can be transmitted in the 1550 nm band to overcome attenuation by fog. The Food and Drug Administration (FDA) considers a

power density of about  $100 \text{ mW/cm}^2$  at  $1550 \text{ nm}$  (or  $1 \text{ mW/cm}^2$  at  $780 \text{ nm}$ ) safe to the unaided eye [1]. Assuming a beam with a Gaussian profile is transmitted with  $25 \text{ mm}$   $1/e^2$  diameter, approximately  $245 \text{ mW}$  at  $1550 \text{ nm}$  can be transmitted and still be eye-safe[1].

The second benefit is the higher transmittance of this band. The atmospheric transmittance for different wavelengths of radiation is shown in the Fig. 2.1. The commonly used wavelengths close to  $850\text{nm}$  or  $1550\text{nm}$  have transmittance in the range of 75% to 80% [5]. The  $1550 \text{ nm}$  band includes reduced solar background and scattering (attenuation) in light haze and fog [1].

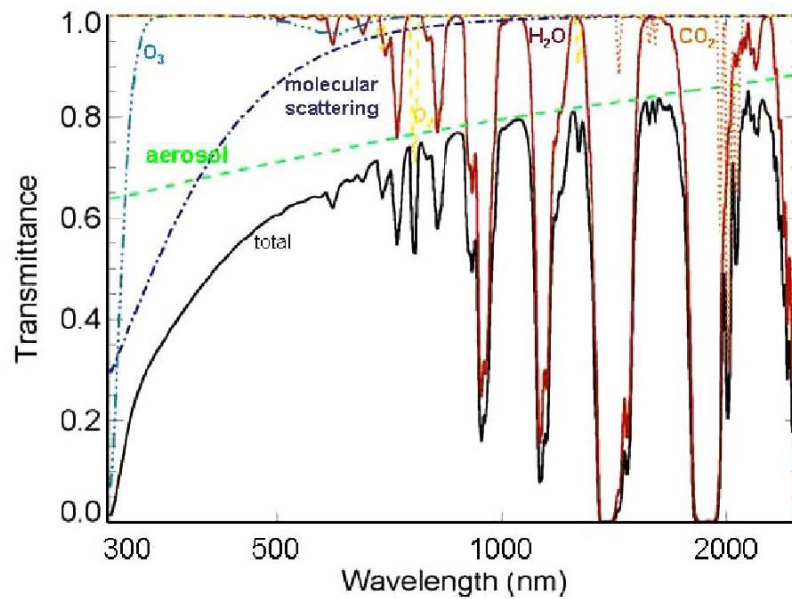


Figure 2.1 Atmospheric transmittance for different wavelengths Ref [1]

The third benefit is a wide range of available components because of the heavy investment in the  $1550 \text{ nm}$  technology for the telecommunication sector.

The disadvantages of this band are: slightly lower detector sensitivity (by a few dB), higher price of components and more difficult alignment [1]. However, all of

these are outweighed by considerably higher available transmitter power. In this dissertation, the 1550 wavelength is employed.

### **2.2.2 Direct Detection Modulation**

There are two kinds of modulation techniques associated with FSO: direct detection modulation and coherent detection modulation. According to the characteristics of FSO communication systems, direct detection modulation has more advantages compared to RF systems [1, 6].

i) Direct detection systems use the intensity of the light pulse to detect the signal.

They can accept a high-order mode beam or even multimode light beam such as LED and multimode laser beams as their light sources. Usually these systems do not require diffraction-limited beams and are easier to sustain compared to coherent detection systems. The multiple mode beams use the lasing volume more efficiently than single mode beams and are easier to generate. Thus they are more electrically efficient and result in better trade-offs between transmitter efficiency and beam quality [6]. According to the characteristics of FSO communication in the range of several kilometers, the main difficulties of FSO transmission are signal attenuation rather than signal dispersion. This is different from the optical fiber communication, where dispersion is considered a more serious problem. The energy efficient multimode beams can provide more energy to combat link fading and signal attenuation.

ii) Direct detection systems have less complex detection circuits than coherent detection systems for the high speed optical communication. Coherent detection systems have phase detection circuits and use a coherent optical

reference, such as a local oscillator, which can add more problems such as time synchronization. Usually coherent detection requires the systems to be diffraction-limited.

- iii) Direct detection systems can use aperture averaging technique to lower the beam perturbations, reduce the fading impact and increase the signal to noise ratio (SNR) of the optical signals. Aperture averaging in coherent detection degrades SNRs.
- iv) Direct detection systems are less complex and are susceptible to phase perturbation due to atmospheric turbulence and surface scatter. Since the coherent detection systems use the amplitude and phase to detect the signals, they are more susceptible to the effects of the atmospheric turbulence due to their sensitivity to phase perturbations across the detector [6]. The impact of atmospheric turbulence on coherent detection systems is quite different from that of direct detection systems. The fact that out-of-phase signal components mixing on a detector surface of heterodyne system can cancel, suggests that the random spatial phase fluctuations of a scintillating beam could also limit the sensitivity [6]. There is an upper limit to the size of the receiver aperture, or equivalently, the range performance of a coherent system operating in a turbulence atmosphere.

The main disadvantage of direct detection is that for small signals or strong noise sources, direct detection receivers may not reach the shot noise limit and consequently may suffer additional performance penalties compared to coherent receivers.

### 2.2.3 Pulse Position Modulation

One suitable direct detection scheme for FSO is Pulse Position Modulation. PPM is considered as an attractive modulation technique for infrared optical wireless communications. The research on optical free-space communication dates back to 1960s. Standard pulse position modulation is an average energy strategy. As the number of slots increases, it also mitigates against the impact of the background radiation. In recent years, NASA has adopted PPM coding for deep space communication systems and has been considering optical links for Mars Laser Communication Demonstration (MLCD). They have proposed the use of PPM and its variants as the modulation format for the links and have provided some PPM capacity formulas [7]. There are many PPM schemes proposed, such as differential PPM and multiple pulses PPM [8, 9]. But these schemes have their drawbacks in some aspects and have difficulties in practical implementation [9]. Standard PPM is still considered as the basis of this technique and is implemented in practical systems.

For the standard Q-ary PPM technique,  $Q$  bits of information are encoded onto one of  $L = 2^Q$  PPM symbols by establishing a one-to-one correspondence between the possible states of  $Q$  binary digits and the location of an optical pulse among  $L$  possible slots [10]. In the demodulation section, each PPM symbol can be decoded into one of  $Q$  bits of information, according to the location of an optical pulse among the  $L$  slots in one PPM symbol duration. The time slot duration is  $T_{slot}$  and one PPM symbol duration is  $T_{symbol} = T_{slot} \times L$ . An example of the PPM symbol set is shown in Figure 2.2.

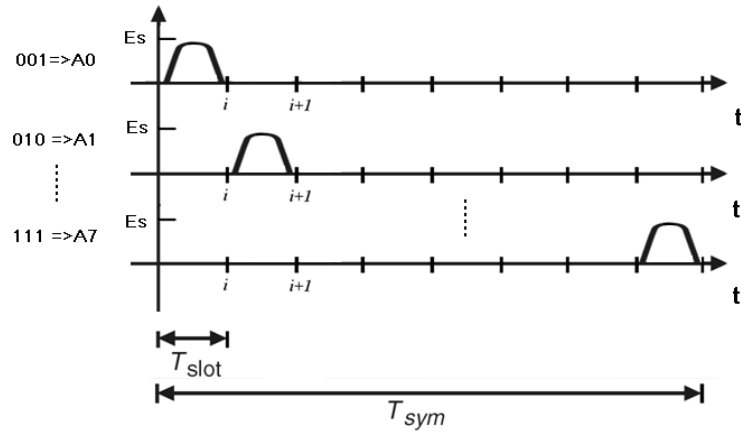


Figure 2.2 Example of PPM symbol set

As a high energy incident laser beam will damage the human retina, there is a limitation of the peak power transmitted by laser pulses in free space applications. This is the main reason for a limited range of FSO in free space applications [11]. As a result, a modified and efficient method of PPM communication without increasing its peak power is of utmost interest.

For deep space applications, the key requirement is a sufficiently large peak power for lasers to survive space losses. Q-switched lasers are typically employed resulting in kilowatt or gigawatt peak power to combat the huge deep space attenuation. A typical Q-switched laser (e.g. a Nd:YAG laser) with a resonator length of 10 cm can produce light pulses of several tens of nanoseconds duration. Even when the average power is well below 1 W, the peak power can be many kilowatts [12].

In this dissertation, the main focus is on free space communication with direct detection, such as standard Q-ary PPM or OOK, which are frequently used in practical systems.

## 2.3 Characteristics of Free Space Optical Channel

### 2.3.1 Gaussian Beam Propagation

In a FSO system, the laser beams are transmitted through free space and are scattered by the air medium. When the laser beams pass through the atmospheric media, there are many aerosol particles in the paths. These particles absorb and scatter the energy of laser beams and cause the attenuation and dispersion of the optical signal. For lower dispersion values, the single mode lasers are selected although multimode lasers can give more power than single mode laser under the same conditions. However, if single mode lasers are used in MIMO systems, the disadvantage of less transmitted power per laser can be overcome by using the multiple lasers to make the total transmitted power sufficiently large. For transmitters with single mode lasers, the propagation of laser beams in free space can be described by Gaussian beam theory. The intensity of a Gaussian beam is given as [6]

$$I = U^*(r, z) \cdot U(r, z) = \frac{a_0^2 \omega_0^2}{\omega^2(z)} e^{\frac{-2r^2}{\omega^2(z)}} = I_0 e^{\frac{-2r^2}{\omega^2(z)}} \quad (2-1)$$

The on-axis intensity at the  $z$  location [6]:

$$I_0 = |U_0(r, z)|^2 = \frac{2P_t}{\pi \omega^2(z)} \quad (2-2)$$

where  $U(r, z)$  is the complex wave amplitude of the Gaussian beam,  $\omega^2(z)$  is the beam radius or spot size of Gaussian beam at the  $z$  location given as [6]

$$\omega^2(z) = \omega_0^2 \left[ 1 + \left( \frac{\lambda z}{\pi \omega_0^2} \right)^2 \right] \quad (2-3)$$

where  $\omega_0^2$  is the beam radius of Gaussian beam at the beam waist  $z = 0$  location.

The total transmitted optical power  $P_t$  of the Gaussian beam is obtained as [6].

$$P_t = \frac{\pi a_0^2 \omega_0^2}{2} \quad (2-4)$$

where  $a_0$  is a constant,  $P_r$  is the received optical power of the Gaussian beam at the  $z$  location of the receiver. In a FSO data link, if only the space loss is considered, the relationship of  $P_t$  and  $P_r$  is the ratio of the received aperture area  $A_r$  to the transmitted beam area  $A_b$  given as [6]

$$P_r = I_0 A_r = \frac{2P_t A_r}{\pi \omega^2(z)} = \frac{2A_r}{A_b} P_t \quad (2-5)$$

where  $A_r$  is the receiving aperture area of the lens at the receiver and  $A_b$  is the half-power spot size's area of the transmitted beam at the receiver  $A_b = \pi \omega^2(z)$ .

### 2.3.2 FSO Channel Model and Turbulence

In FSO communication, when the optical wave propagates through the air, the beam experiences fluctuations in amplitude and phase due to atmospheric turbulence. This is due to the fact that air is a medium with inhomogeneous refractive index due to temperature and pressure variations. This intensity fluctuation, also known as scintillation, is one of the most important factors that degrade the performance of an FSO communication link, even under clear sky conditions. This is also known as channel fading, which changes the signal amplitude and phase for every channel. The dominant atmospheric effect that impacts optical communication is attenuation of the signal by scattering and absorption. Molecular scatter and absorption of major atmospheric constituents is relatively insignificant. Though rain and snow can cause attenuation up to approximately 40 dB/km and 100 dB/km, respectively, fog is by far the most serious problem. In extremely heavy fog, attenuation as high as 300 dB/km has been reported [14].

In the absence of attenuating elements, the atmosphere is best modeled as a random phase medium that changes with time. To a first order approximation, the

atmosphere introduces a random beam deflection. For example, on a sunny day the rising hot air makes the refractive index of air go up with height and in extreme conditions can result in a mirage[1]. Such an index of refraction change near the transmitter tends to deflect the beam causing “beam wander” [1]. The same effect near the receiver, however, causes the beam to appear to have come from a different place known as angle-of-arrival fluctuations [1]. The magnitudes of these effects are largely dependent on the index of refraction fluctuations and propagation distance. In extreme conditions over distances of several kilometers, the atmospheric induced tilt can vary as much as  $100 \mu\text{rad}$  at a rate of tens of Hertz [1].

Second-order effects, i.e. small-scale turbulence, can also play an important role in disrupting optical communication. Small-scale phase fluctuations introduced at the source can result in scintillation (speckle pattern) after several hundred meters of propagation [1]. Depending on the speckle size and receiver aperture, the dynamic atmosphere causes fades in the received signal. Phase perturbations near the receiver make the focused spot size on the detector larger than the diffraction limit [1]. When the detector size is only few tens of microns, this spot size increase reduces minimal allowable transceiver mispointing further [1]. Thus, high bandwidth tracking is made necessary by a turbulent atmosphere for high data rate links.

The FSO channel is a slow fading and frequency-nonselective channel. The characteristics of the channel are treated as flat over the frequency and narrow-band. As the change in the channel gain is slower than the data rate, the channel variation, during which the channel is static, is assumed much smaller than the total duration of the transmission. For example, if the data bandwidth is 1GHz, the slot duration is  $10^{-9}$  second and the symbol duration of Q-ary PPM symbol is  $2^Q \times 10^{-9}$  second. However the temporal correlation time of the optical wireless channel is on the order

of several millisecond [6]. Hence, the channel varies very slow compared to the data speed.

The FSO channel can be modeled as a block fading channel and the channel gain can be modeled as an ergodic random variable. For different degree of turbulence, the intensity attenuation of the laser beams can be described by a lognormal distribution, exponential distribution or gamma-gamma distribution.

Numerous experiments have confirmed that the intensity of laser beams obeys a lognormal distribution under weak turbulence and obeys negative exponential distribution under strong turbulence [6]. For moderate turbulence, the distribution of the intensity fluctuation is not understood and a number of the distributions have been proposed, such as lognormal-Rice distribution, K-distribution and gamma-gamma distribution [6].

For the FSO channel with weak turbulence, the probability density function (PDF) of the laser beam intensity, which is lognormal distribution, is given by

$$p(x) = \frac{1}{x\sigma_l\sqrt{2\pi}} e^{-\frac{(\ln x - m_l)^2}{2\sigma_l^2}} \quad x > 0 \quad (2-6)$$

where  $m_l$  and  $\sigma_l$  are the mean and standard deviation, respectively, of the variable's natural logarithm. By definition, the logarithm of the variable is normally distributed. Since most free space optical communication systems operate under weak turbulence, the error probability analysis in this dissertation focuses on the lognormal distribution.

For a FSO channel with strong turbulence, the PDF of the laser beam intensity, which is a negative exponential distribution, is

$$p(x) = \lambda e^{-\lambda x} \quad x > 0 \quad (2-7)$$

where  $x$  is the rate parameter.

There is a gamma-gamma distribution, which fits the measurement data for a wide range of turbulence conditions (weak to strong) [15]. The PDF of the gamma-gamma distribution is given as

$$p(I_{mn}) = \frac{2(\alpha\beta)^{\frac{(\alpha+\beta)}{2}}}{\Gamma(\alpha)\Gamma(\beta)} I_{mn}^{\frac{(\alpha+\beta)}{2}-1} K_{(\alpha-\beta)}(2\sqrt{\alpha\beta I_{mn}}) \quad I_{mn} > 0 \quad (2-8)$$

where parameters  $\alpha > 0$  and  $\beta > 0$  are linked to the so called scintillation index [15]

$$\text{scintillation index} = \frac{1}{\alpha} + \frac{1}{\beta} + \frac{1}{(\alpha\beta)} \quad (2-9)$$

The parameters  $\alpha$  and  $\beta$  can be adjusted to achieve a good agreement between  $p(I_{mn})$  and measurement data [15]. Alternatively, assuming spherical wave propagation,  $\alpha$  and  $\beta$  can be directly linked to physical parameters [15]

$$\alpha = \left\{ \exp \left[ \frac{0.49\chi^2}{(1 + 0.18d^2 + 0.56\chi^{12/5})^{7/6}} \right] - 1 \right\}^{-1} \quad (2-10)$$

$$\beta = \left\{ \exp \left[ \frac{0.51\chi^2(1 + 0.69\chi^{12/5})^{-5/6}}{(1 + 0.9d^2 + 0.62d^2\chi^{12/5})^{5/6}} \right] - 1 \right\}^{-1} \quad (2-11)$$

where  $\chi^2 = 0.5C_n^2 \kappa^{7/6} L^{11/6}$ ,  $d \triangleq [\kappa D^2 / (4L)]^{1/2}$ ,  $\kappa \triangleq 2\pi / \lambda$ .  $\lambda$ ,  $D$ ,  $C_n^2$  and  $L$  are the wavelength, the diameter of the receiver's aperture, the index of refraction structure parameter and the link distance, respectively [15].

## 2.4 Optical Receiver

### 2.4.1 Avalanche photodetector (APD)-Based Receiver Structure

There are many types of detectors that can be used in optical receivers. The avalanche photodetector is a popular and widely used detector because of its small portable size, low cost, good responsivity and high accuracy, etc.

A typical optical receiver with 1550nm wavelength usually includes a collecting lens, an InGaAs APD, GaAs MESFET transimpedance amplifiers, a matched filter and an equalizer, etc. Some receivers also include optical filters, mirror or other optical components. Occasionally, when the transmission condition is very good and the transimpedance is used, little or no equalization is required [15]. This depends on the receiver design and the transmission environment. In this dissertation, the normal and complicated case including equalizers is considered and analyzed. For simple and special cases, the results can be obtained by changing the parameters. At the end of the equalizer, the processed signal is sent to a decision detector, which implements a Maximum Likelihood (ML) decision to decode or demodulate the data. The basic architecture of the APD-based optical receiver block diagram is shown in Fig. 2.3.

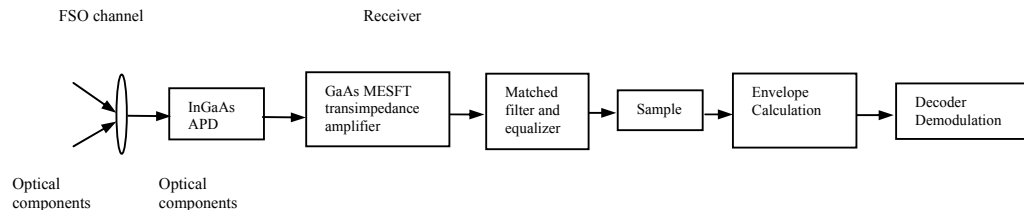


Figure 2.3 Basic architecture of the APD-based optical receiver

#### 2.4.2 Webb Distribution of Electrons Given Out by APDs

In optical receivers, the incident photons are focused and detected by APDs. Inside APDs, there are two processes: the primary photon-injection process and the photon-electron multiplication process. The electron number obtained at the APD obeys the Webb distribution, also called the WMC approximation. It was proposed by Webb, McIntyre and Conradi [6]. The PDF of the electron number  $m_s$  with the mean primary photoelectron number  $\bar{k}$  in the APD is obtained as [6]

$$p_{sw}(m_s) = \frac{\exp \left\{ - \frac{(m_s - \bar{k}M)^2}{2k_s M^2 F \left[ 1 + \frac{(m_s - \bar{k}M)(F-1)}{\bar{k}MF} \right]} \right\}}{\sqrt{2\pi \bar{k}M^2 F} \left[ 1 + \frac{(m_s - \bar{k}M)(F-1)}{\bar{k}MF} \right]^{\frac{3}{2}}} \quad (2-12)$$

This Webb model has the requirement that the emitted electron number is not smaller than the photon-electron number, i.e.  $m_s \geq \bar{k} \geq 0$ , and the photon-electron pairs generated by the first photon-injecting process obey a Poisson distribution [6].

### 2.4.3 Noises in APD-Based Receivers for FSO

When the signal is processed in optical receivers, there are a variety of noise sources that can affect receiver performance. The uncorrelated noise induced in the receivers are shot noise, background noise, backscatter noise, bulk dark current noise, surface dark current noise, thermal noise, amplifier noise and equalizer noise. Any one of these noises induced in receivers can dominate depending on the receiver design and operating environment. In practice, usually these noises induced in receivers are much greater than the path-added additive white Gaussian noise (AWGN) and are considered as dominant factors. Thus the path-added AWGN is negligible for FSO communication systems and therefore is not considered in this dissertation.

Narrow bandpass spectral filters are typically used to reduce the background noise in receivers and can be placed in the “optical components” blocks in Fig 2.3. The filters, as well as lens, mirror, fiber and other optical components in receivers, can cause the loss of optical signals. However, there are other kinds of noises that can mix into the signal bandwidth and cannot be removed by the filtering process. We

must consider their impacts in detail, especially the thermal noise and the shot noise.

The three main types of amplifiers that can be used in the receivers are transimpedance, high-impedance and low-impedance amplifiers [15]. Their noise calculation steps are different. In the multi-Gb/s MIMO systems, the transimpedance amplifier is usually employed because of its lower noise, higher impedance and higher data rate. A number of different field effect transistors (FETs) can be used as the front-end transimpedance amplifier in the receiver design. The typical values of the various parameters for some FETs are given in the reference [15]. As the signal frequency reaches about 25-50 MHz, the gain of the silicon FET approaches unity [15]. Much higher frequencies (4 Gb/s and above) can be achieved with either a GaAs MESFET or a silicon bipolar transistor [15]. For the gigabit-per-second data links, the detailed noise expression for GaAs MESFET transimpedance amplifier is calculated as follows.

The equivalent circuit of a transimpedance receiver design and a simple high-impedance preamplifier design using FET are discussed in reference [15]. The output current of the equalizer is sent to the decision detector to perform Equal Gain Combining (EGC), sampling, maximum likelihood decision, decoding and demodulation. This normally used receiver design has been considered for noise analysis in this dissertation.

If  $i_N(t)$  is the noise current causing the equalizer output current  $i_{out}(t)$  to deviate from the average value  $\langle i_{out}(t) \rangle$ , the actual current  $i_{out}(t)$  is of the form

$$i_{out}(t) = \langle i_{out}(t) \rangle + i_N(t) = \langle i_s(t) \rangle + i_N(t) \quad (2-13)$$

As the total noise  $i_N(t)$  obeys a Gaussian distribution with zero mean and variance  $\sigma^2$ , the average value  $\langle i_{out}(t) \rangle$  equals the signal value  $\langle i_s(t) \rangle$ . The noises in

the APD receiver with InGaAs APD, GaAs MESFET amplifier, matched filter, equalizer, sampling circuit and decision detector can be expressed as

$$\begin{aligned}
\langle i_N^2 \rangle &= \langle i_p^2 \rangle + \langle i_b^2 \rangle + \langle i_c^2 \rangle + \langle i_{db}^2 \rangle + \langle i_{ds}^2 \rangle + \langle i_R^2 \rangle + \langle i_I^2 \rangle + \langle i_E^2 \rangle \\
&= A^2 B_{bae} \left[ 2q\mathcal{R}(P_r + P_b + P_c)M^2F + 2q(I_{db}M^2F + I_{ds}) + \frac{4k_B T}{R_b} \right] + S_I A^2 B_{bae} \\
&\quad + S_E A^2 B_e \\
&= A^2 I_2 B \left[ 2q\langle i_0 \rangle M^2F + 2q\mathcal{R}(P_b + P_c)M^2F + 2q(I_{db}M^2F + I_{ds}) + \frac{4k_B T}{R_b} \right] \\
&\quad + S_I A^2 I_2 B + S_E A^2 \left[ \frac{I_2 B}{R^2} + (2\pi C)^2 I_2 B^3 \right] \\
&= (qAB)^2 \left[ \frac{2\langle i_0 \rangle M^2F + 2\mathcal{R}(P_b + P_c)M^2F + 2(I_{db}M^2F + I_{ds})}{q} T_b I_2 + W_{TZ} \right] \tag{2-14}
\end{aligned}$$

where

$\langle i_N^2 \rangle$  mean-squared total noise current

$\langle i_p^2 \rangle$  mean-squared photon shot noise current

$\langle i_b^2 \rangle$  mean-squared background noise current

$\langle i_c^2 \rangle$  mean-squared backscatter noise current

$\langle i_{db}^2 \rangle$  mean-squared bulk dark current noise

$\langle i_{ds}^2 \rangle$  mean-squared surface dark current noise

$\langle i_R^2 \rangle$  mean-squared thermal noise (or Johnson noise) current

$\langle i_I^2 \rangle$  mean-squared shunt noise current, which results from the amplifier input noise current source  $i_a(t)$

$\langle i_E^2 \rangle$  mean-squared series noise current, which results from the amplifier input voltage noise source  $e_a(t)$

$A$  amplifier gain

$B_{bae}$  noise equivalent bandwidth of the bias circuit, amplifier, equalizer defined for

the positive frequency.  $B_{bae} = I_2 B$

$\mathcal{R}$  responsivity of photodetector

$P_r$  incident photon power in a 1 pulse slot is obtained as

$$P_r = \frac{b_{on}}{T_b} = h\nu\lambda_s B \quad \text{W or J/s} \quad (2-15)$$

$P_b$  background noise power in one slot

$P_c$  backscatter noise power in one slot

$M$  multiplication factor of APD photodetector

$F$  excess noise factor given as

$$F = k_{eff} G + \left(2 - \frac{1}{G}\right) (1 - k_{eff}) \approx M^x \quad (2-16)$$

The parameter  $x$  takes on values of 0.3 for Si, 0.7 for InGaAs and 1.0 for Ge

$k_{eff}$  effective hole/electron ionization rate ratio

$I_{db}$  bulk dark current

$I_{ds}$  surface dark current

$k_B$  Boltzmann's constant  $k_B = 1.38054 \times 10^{-23} \text{ J/K}$

$h$  Planck's constant  $h = 6.6256 \times 10^{-34} \text{ J} \cdot \text{s}$

$T$  temperature (K)

$R_b$  detector bias resistance

$\langle i_0 \rangle$  mean unity gain photocurrent over a bit period  $T_b$

$B$  data bandwidth

$T_b$  time slot or bit period for a 1 pulse or a 0 pulse  $T_b = \frac{1}{B}$

$I_2$  normalized bandwidth integral [11]

$I_3$  normalized bandwidth integral [11]

$B_e$  is noise equivalent bandwidth of the equalizer defined for the positive frequency as

$$B_e = I_2 B + (2\pi RC)^2 I_2 B^3 \quad (2-17)$$

$C$  is the total capacitance of the parallel combination of  $C_d$ ,  $C_a$ ,  $C_{gs}$ ,  $C_{gd}$  for a typical FET amplifier and a good photodiode given as

$$C = C_d + C_a + C_{gs} + C_{gd} = 10pF = 10 \times 10^{-12}F \quad (2-18)$$

$C_d$  detector capacitance

$C_a$  amplifier input capacitance

$C_{gs}$  FET gate-source capacitance

$C_{gd}$  FET gate-drain capacitance

$S_I$  spectral density of the amplifier input noise current source (in  $A^2/Hz$ )

$S_E$  spectral density of the amplifier noise voltage source (in  $V^2/Hz$ )

$R$  is the resistance of the parallel combination of  $R_b$ ,  $R_a$ ,  $R_f$  given as

$$\frac{1}{R} = \frac{1}{R_b} + \frac{1}{R_a} + \frac{1}{R_f} \quad (2-19)$$

$R_b$  detector bias resistor

$R_a$  amplifier input resistance

$R_f$  feedback resistance

$W_{TZ}$  thermal noise characteristic

For GaAs MESFET transimpedance amplifiers, in practice, the feedback resistance  $R_f$  is much greater than the amplifier input resistance  $R_a$  [15]. The thermal noise characteristic for the GaAs MESFET transimpedance amplifier is given as [15]

$$W_{TZ} = \frac{1}{q^2 B} \left( 2qI_{gate} + \frac{4k_B T}{R_b} + \frac{4k_B T \Gamma_e}{g_m \cdot R_b^2} \right) I_2 + \left( \frac{2\pi C}{q} \right)^2 \frac{4k_B T \Gamma_e}{g_m} I_3 B + \frac{T_b}{q^2} \frac{4k_B T}{R_f} I_2 \quad (2-20)$$

where  $\Gamma_e$  is the correlated coefficient of the equalizer.

The detailed noise expression for the GaAs MESFET transimpedance amplifier is obtained as

$$\begin{aligned}
\langle i_N^2 \rangle &= (qAB)^2 \left[ \frac{2\langle i_0 \rangle M^2 F + 2\mathcal{R}(P_b + P_c)M^2 F + 2(I_{db}M^2 F + I_{ds})}{q} T_b I_2 \right. \\
&\quad \left. + \frac{1}{q^2 B} \left( 2qI_{gate} + \frac{4k_B T}{R_b} + \frac{4k_B T \Gamma_e}{g_m \cdot R_b^2} \right) I_2 + \left( \frac{2\pi C}{q} \right)^2 \frac{4k_B T \Gamma_e}{g_m} I_3 B + \frac{T_b 4k_B T}{q^2 R_f} I_2 \right] \\
&= A^2 \left\{ [2\langle i_0 \rangle M^2 F + 2\mathcal{R}(P_b + P_c)M^2 F + 2(I_{db}M^2 F + I_{ds})] q I_2 B + \left( 2qI_{gate} + \frac{4k_B T}{R_b} + \frac{4k_B T \Gamma_e}{g_m \cdot R_b^2} \right) I_2 B \right. \\
&\quad \left. + (2\pi C)^2 \frac{4k_B T \Gamma_e}{g_m} I_3 B^3 + \frac{4k_B T}{R_f} I_2 B \right\}
\end{aligned} \tag{2-21}$$

where  $P_s$  is the signal power for the 1 pulse and  $P_s = P_r$ ,  $b_{on}$  is the energy for a 1 pulse and  $b_{on} = h\nu\lambda_s = h\nu N_t \lambda_{sil} = N_t P_{ril} T_b = P_r T_b$  (J/bit),  $\eta$  is the quantum efficiency,  $\nu$  is the frequency of the optical signal  $\nu = \frac{c}{\lambda}$ ,  $c = 3 \times 10^8$  m/s,  $\lambda$  is the wavelength of the optical signal and  $\gamma_s$  is the fraction of a 1 pulse energy remaining in its time slot.

The variances  $\sigma_{on}^2$  and  $\sigma_{off}^2$  of the equalizer output currents  $i_{out}(t)$  for a 1 pulse slot and a 0 pulse slot, respectively, are the worst-case values of the total noise current  $\langle i_N^2 \rangle$  in Eq. (2-17). The impacts on a 1 pulse slot, due to background noise, backscatter noise, bulk dark current noise, surface dark current noise, thermal noise, amplifier noise and equalizer noise, are similar as those on a 0 pulse slot. But the impact of the shot noise  $\langle i_p^2 \rangle$  on a 1 pulse slot is different than that on a 0 pulse slot. In addition, if the dispersion of the pulses happens in the worst case, there is a part of the pulse energy falling into the adjacent slots and causing the shot noise. As shown in Reference [15, Fig. 7.3], we still use  $\gamma_s$  to represent the fraction of a 1 pulse energy  $P_s$  remaining in its slot.

The worst-case  $\langle i_N^2 \rangle$  in the 1 pulse slot, i.e.  $\sigma_{on}^2$ , happens when the continuous two 1 pulses are transmitted and one pulse is added by the additional energy due to dispersion of the other 1 pulse. For one 1 pulse slot,  $\gamma_s$  fraction of the pulse energy  $P_s$  remains in the slot and  $(1 - \gamma_s)$  fraction of the pulse energy  $P_s$  falls into the adjacent 1 pulse slot. Thus the total photon energy inducing the short noise in the 1 pulse slot is

$$\gamma_s P_s + (1 - \gamma_s) P_s = P_s \quad (2-22)$$

The worst-case of  $\langle i_N^2 \rangle$  in the 0 pulse slot, i.e.  $\sigma_{off}^2$ , happens when the continuous one 1 pulse and one 0 pulse are transmitted and the 0 pulse is added by the additional energy due to dispersion of the adjacent 1 pulse. The worst-case of  $\langle i_N^2 \rangle$  in the 0 pulse slot, i.e.  $\sigma_{off}^2$ , happens when a 1 pulses and a 0 pulse are transmitted continuously. The total energy inducing the short noise in the 0 pulse slot is  $(1 - \gamma_s) P_s$ .

The unity gain mean photocurrents  $\langle i_0 \rangle_{on}$  in a 1 pulse slot and  $\langle i_0 \rangle_{off}$  in a 0 pulse slot, respectively, can be represented as

$$\langle i_0 \rangle_{on} = \frac{\eta q b_{on}}{h\nu T_b} = \mathcal{R} P_s \quad (2-23a)$$

$$\langle i_0 \rangle_{off} = \frac{\eta q b_{on}}{h\nu T_b} (1 - \gamma_s) = \mathcal{R} P_s (1 - \gamma_s) \quad (2-23b)$$

In order to calculate the variance of the noise current in a 1 pulse slot, we assume the worst cases of the  $\langle i_N^2 \rangle$  for continuous 1 pulses happen. So the average power concept can be used. For the receiver architecture shown in Fig. 2.3, the variances of the  $l$  th branch for the 1 pulse slot and the 0 pulse slot are calculated as  $\sigma_{onl}^2$  and  $\sigma_{offl}^2$ , respectively and given as

$$\sigma_{onl}^2 = \langle i_N^2 \rangle_{on}$$

$$\begin{aligned}
&= A^2 \left\{ \left[ 2 \frac{\eta q b_{on}}{h\nu T_b} M^2 F + 2\mathcal{R}(P_b + P_c) M^2 F + 2(I_{db} M^2 F + I_{ds}) \right] q I_2 B \right. \\
&\quad \left. + \left( 2q I_{gate} + \frac{4k_B T}{R_b} + \frac{4k_B T \Gamma_e}{g_m \cdot R_b^2} \right) I_2 B + (2\pi C)^2 \frac{4k_B T \Gamma_e}{g_m} I_3 B^3 + \frac{4k_B T}{R_f} I_2 B \right\} \\
&\hspace{15em} (2-24a)
\end{aligned}$$

$$\begin{aligned}
\sigma_{off l}^2 &= \langle i_N^2 \rangle_{off} \\
&= A^2 \left\{ \left[ 2 \frac{\eta q b_{on}}{h\nu T_b} (1 - \gamma_s) M^2 F + 2\mathcal{R}(P_b + P_c) M^2 F + 2(I_{db} M^2 F + I_{ds}) \right] q I_2 B \right. \\
&\quad \left. + \left( 2q I_{gate} + \frac{4k_B T}{R_b} + \frac{4k_B T \Gamma_e}{g_m \cdot R_b^2} \right) I_2 B + (2\pi C)^2 \frac{4k_B T \Gamma_e}{g_m} I_3 B^3 + \frac{4k_B T}{R_f} I_2 B \right\} \\
&\hspace{15em} (2-24b)
\end{aligned}$$

## REFERENCES

- [1]. Muthu Jeganathan and Pavel Lonov, "Multi-Gigabits-per-second Optical Wireless Communications", Optical Crossing Company, Website: <http://www.citeseerx.ist.psu.edu/viewdoc/download?doi=10.1.1.110>.
- [2]. Neda Cvijetic, Stephen G. Wilson and Maite Brandt-Pearce, "Performance Bounds for Free-Space optical MIMO Systems with APD Receivers in Atmospheric Turbulence," IEEE Journal on Selected Areas in Communications, Vol.26, No.3, April 2008.
- [3]. S. G. Wilson, M. Brandt-Pearce, Q. Cao, and J.J.H. Leveque, III, "Free-space optical MIMO transmission with Q-ary PPM," IEEE Trans. Communication. 53, 1402-1412, 2005.
- [4]. Denis Bushuev and Shlomi Arnon, "Analysis of the performance of a wireless optical multi-input to multi-output communication system," Optical Society of America, J. Opt. Soc. Am. A, vol. 23, No.7, July 2006.

- [5]. J.W. Strohbehn, "Laser Beam Propagation in the Atmosphere," Springer, 1978.
- [6]. Gregory R. Osche, "Optical Detection Theory for laser Applications," 2002, John Wiley & Sons, Inc.
- [7]. S. Dolinar, D. Divsalar, J. Hamkins and F. Pollara "Capacity of Pulse Position Modulation (PPM) on Gaussian and Webb Channels", TMO Progress Report 42-142, August 15, 2000.
- [8]. Hisayoshi Sugiyama and Kiyoshi Nosu, "MPPM: a method for improving the band utilization efficiency in optical PPM," Journal of lightwave technology, Vol. 7, No. 3, March 1989.
- [9]. J. Hamkins and B. Moision "Multipulse pulse position modulation on discrete memoryless channels", INP Progress Report 42-161 May 15, 2005.
- [10]. Andrew A. Gray and Clement Lee "Discrete-Time Demodulator Architecture for Free Space Broadband Optical PPM," IPN Progress Report 42-158, August 15, 2004.
- [11]. "What is Free space Optics (FSO)"  
<http://www.freespaceoptics.org/freespaceoptics/default.cfm> .
- [12]. Q-switching laser Introduction <http://en.wikipedia.org/wiki/Q-switching> .
- [13]. Nick Letzepis and Albert Guillen I Fabregas, "Outage Probability of the MIMO Gaussian Free-Space Optical Channel with PPM," ISIT 2008, Toronto Canada, July 6-11, 2008.
- [14]. Petr Tosovsky and Lucie Dordova, "Free Space Optical Channel Parameters Estimation for High Altitude Platform System," 2008, IEEE, 978-1-4244-2137-4 Microwave Techniques, 2008. COMITE 2008. 14th Conferenc
- [15]. Gerd Keiser, "Optical Fiber Communications", McGraw Hill, Inc, third edition, 2000

- [16]. Simon Haykin and Michael Moher, “Modern Wireless Communication,” 2005 , Pearson Education, Inc
- [17]. Marvin K. Simon and Mohamed-Slim Alouini, “Digital Communication over Fading Channels,” 2005, John Wiley & Sons, Inc., second edition,
- [18]. John G. Proakis and Masoud Salehi, “Digital Communicaitons,” Mc Graw Hill , fifth edition, 2008
- [19]. Robert Grover Brown and Patrick Y.C. Hwang, “Introduction to Random Signals and Applied Kalman Filtering”, John Wiley and Sons, Inc, 1997.
- [20]. Stephen G. Wilson, Maite Brandt-Pearce, Michael Baedke, and Qianling Cao, “Optical MIMO Transmission with Multipulse PPM” , IEEE ISIT 2004, June 27 – July 2, 2004.
- [21]. V. Vilnrotter, A. Biswas, W. Farr, D. Fort, and E. Sigman, “Design and Analysis of a First-Generation Optical Pulse-Position Modulation Receiver,” The Interplanetary Network Progress Report 42-148, October–December 2001, Jet Propulsion Laboratory, Pasadena, California, pp.1–20, February 15, 2002.

## CHAPTER 3

### OVERVIEW OF MIMO FSO SYSTEMS

#### 3.1 System Model of MIMO Optical Wireless Links

Based on the analysis of FSO communication systems in Chapter 2, we present a mathematical model for MIMO FSO communication systems. The statistical characteristics of the FSO channel and MIMO PPM systems are analyzed. Parameters, such as the link budget, receiver noises and signal to noise ratio, etc. are discussed in this chapter.

In MIMO FSO transmission,  $N_t$  laser sources and  $N_r$  photodetectors (PD) are employed as an array and a typical MIMO point-to-point system is shown in Fig. 3.1. The lasers of the transmitters and the photodetectors of the receivers are positioned as arrays, respectively [1]. The laser beams modulated by the user data are transmitted through different FSO paths between the transmitters and the receivers. These beams experience different atmospheric turbulence in the paths. The turbulence causes the channel fading and impacts the amplitude and phase of the received optical signals.

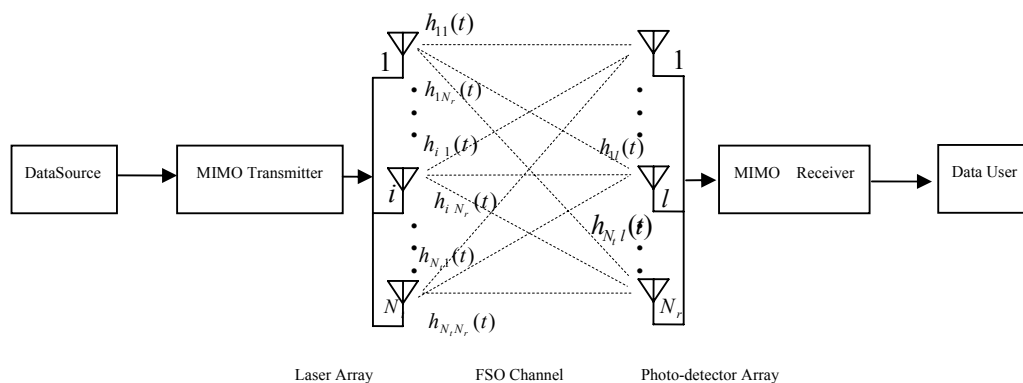


Figure 3.1  $N_t$  laser sources and  $N_r$  photodetectors MIMO FSO system

For MIMO FSO systems, one advantage is that the replicas of the coded data symbols, which are transmitted in the space and time diversity patterns, and combined

and decoded at the receivers, can overcome the channel fading due to atmospheric turbulence. The ability of multiple transmitters and receivers in combating fading is conditioned on reception of uncorrelated copies of signal. The paths in MIMO are usually required to be uncorrelated and independent of each other. As a result, transmit and receive apertures must be placed at least one correlation distance apart [2]. For atmospheric channel this requirement can be easily met since correlation distance (atmospheric coherence length) is about 20cm under good visibility conditions and often drops to 2-4 cm under weak turbulence [2]. The second advantage is that MIMO improves the maximum transmitted power, for the high data rate, e.g. multi-Gb/s, compared with the single laser transmission. Assuming a transmitted beam with a Gaussian profile  $25 \text{ mm } \frac{1}{e^2}$  diameter, approximately 245mW at 1550nm can be transmitted and still be eye-safe [3]. A typical high speed 1550nm laser has a slope efficiency of 0.03~0.2W/A [3]. At present, commercial laser driver chips are capable of only about 100mA modulation current at 2.5 Gb/s [3]. This may result in optical output power about 20mW if the laser efficiency is 0.2W/A. However, there is currently no high speed 1550nm laser with more than 250mW power available in the market [3]. Such a laser would require 1225mA modulation current with an efficiency of 0.2W/A [3]. Thus the MIMO would have to be used in order to achieve the eye-safe maximum power, i.e. 245mW of the 1550 nm wavelength and  $25 \text{ mm } \frac{1}{e^2}$  diameter laser beam for multiple-Gb/s data rate. In order to compare the performance of MIMO, different transmitting schemes from single input single output scheme or other schemes, the total transmitted energy of MIMO for one symbol is fixed as  $E_s$ , the same as that in SISO, during the calculation of this dissertation. The disadvantage of this MIMO approach is that transmitters would have

to be synchronized at the higher data rate, such as multiple-Gb/s, and this is not easy for practical optical and electrical devices.

Optical beams are generally highly directive, and thus isolate themselves spatially from other potential interference. FSO vendors typically use 6-8 milliradian beam divergence for their low data rate products. Higher data rates are usually accomplished by reducing the beam divergence to 2 milliradian [3]. The width of laser beams is quite narrow, but sufficiently wide to illuminate the entire PD array. For example, if the half-power beam width, i.e. divergence, is 1 milliradian, the half-power spot size of the laser beam at a distance of 1 kilometer has 1 meter diameter [1]. Because of the capacitance, the higher bandwidth detectors are inherently smaller in size, typically few tens of micrometers diameter for multi-Gb/s data rate [3]. Commercial photodetectors range in size from 30 $\mu$ m diameter at 10Gb/s to 70 $\mu$ m diameter at 2.5 Gb/s [3]. The diameter of receiver lens apertures is usually a few tens of centimeters, such as 7.5cm or 15cm. In order to keep different FSO paths uncorrelated, the spacing between adjacent receiving antennas of MIMO FSO systems with wavelengths from 780nm to 1550nm, must be 2-4 cm apart under weak turbulence or 20cm under good visibility conditions [2]. This can be satisfied by MIMO FSO systems shown in Fig. 3.1. An optical beam can reach the APD array of receivers at the same time thus making MIMO schemes possible.

For a practical system, we assume that the MIMO FSO system model works under the normal conditions: Accordingly the line-of-sight paths exist between the transmitting laser array and the receiving photo-detector array. The MIMO FSO channel is a frequency non-selective ergodic random channel and can be treated as the block fading channel model. The optical signal is a narrowband signal, i.e. the transmitted signal bandwidth is much smaller than the channel's coherence

bandwidth. The coherence bandwidth measures the frequency range over which the fading process is correlated [4].

To simplify the solution and make it suitable for the normal case, the following assumptions are made. (i) The receivers can get perfect knowledge of the channel information, estimate the signal level of the received symbols and predict the channel condition. (ii) The spatial correlation between the channel paths is negligible, i.e., there are sufficient distances between the individual lasers, APDs and apertures. (iii) There are negligible channel gain estimation errors, negligible synchronization error and acceptable latency in the system. (iv) The active tracking and pointing system is used and makes the mispointing allowance of a FSO data link be about 3dB. This active tracking and pointing scheme ensures that the narrow laser beam is pointed at the receiver aperture, e.g. 150mm diameter, and tightly focused on the relative small detector, typically less than 100 $\mu$ m diameter [3]. (v) The transmitters and receivers are synchronized at the high data rates. (vi) The gain amplitudes of different channel paths can be estimated promptly and correctly for the decoding and demodulation process at the receivers. (vii) The processing delay is acceptable for the network users of voice, data and video. The detailed architecture of the MIMO FSO point-to-point system is shown in Fig 3.2.

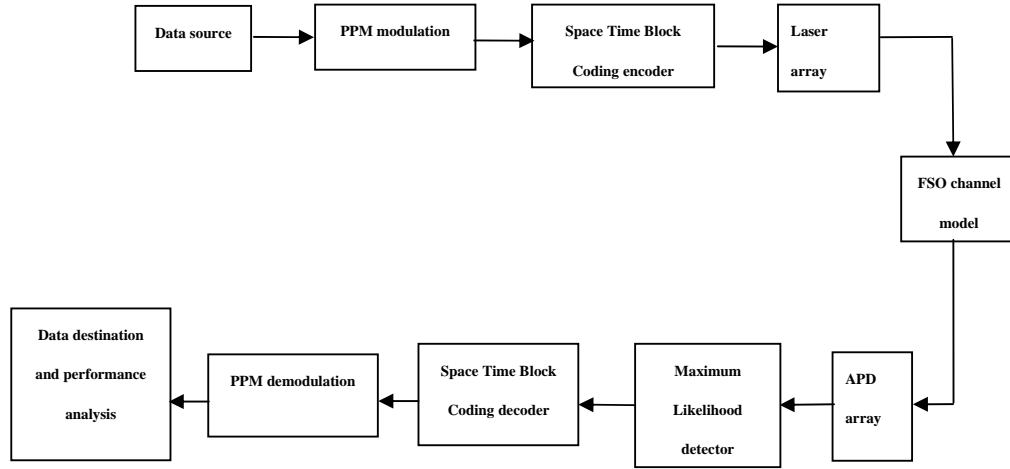


Figure 3.2 The detailed architecture of MIMO point-to-point system

The MIMO system model of Figure 3.2 can be presented by the matrix equation as

$$\mathbf{Y} = \frac{E_s}{N_t} \beta \cdot \mathbf{H} \cdot \mathbf{S} + \mathbf{N} \quad (3-1)$$

where  $\beta$  is the link gain coefficient which makes the mean of the channel gain  $\mathbf{H}$  equal to  $\mathbf{I}$ ,  $E\{\mathbf{H}\} = \mathbf{I}$ ,  $E_s$  is the total energy that transmitted during the 1 pulse slot by the laser array,  $N_t$  is the number of lasers in the transmitting array and  $\mathbf{Y}$  is the received signal ( $N_r \times NL$ ) matrix given as

$$\mathbf{Y} = [\mathbf{y}_1 \quad \mathbf{y}_2 \quad \dots \quad \mathbf{y}_N] = \begin{bmatrix} y_{11} & y_{12} & \dots & y_{1NL} \\ y_{21} & y_{22} & \dots & y_{2NL} \\ \vdots & \vdots & \ddots & \vdots \\ y_{N_r1} & y_{N_r2} & \dots & y_{N_rNL} \end{bmatrix} \quad (3-2)$$

where  $N$  is the number of the PPM symbol in one transmitted matrix,  $L$  is the number of the slots in one Q-ary PPM symbol,  $L = 2^Q$ . There are  $N$  PPM symbols in a transmitted matrix and these  $N$  PPM symbols are independent. The matrix can be coded by the repetition coding scheme or the Space Time Block Coding scheme. In this chapter, we mainly consider the simple repetition coding. In the receiver, these  $N$  symbols in the receiving matrix are decoded together at the same time and then demodulated.  $\mathbf{S}$  is the transmitted symbol ( $N_t \times NL$ ) matrix given as

$$\mathbf{S} = [\mathbf{s}_1 \quad \mathbf{s}_2 \quad \dots \mathbf{s}_N] = \begin{bmatrix} s_{11} & s_{12} & \dots s_{1NL} \\ s_{21} & s_{22} & \dots s_{2NL} \\ \vdots & \vdots & \vdots \\ s_{N_t1} & s_{N_t2} & \dots s_{N_tNL} \end{bmatrix} \quad (3-3)$$

$\mathbf{N}$  is the channel noise matrix represented as

$$\mathbf{N} = [\mathbf{n}_1 \quad \mathbf{n}_2 \quad \dots \mathbf{n}_N] = \begin{bmatrix} n_{11} & n_{12} & \dots n_{1NL} \\ n_{21} & n_{22} & \dots n_{2NL} \\ \vdots & \vdots & \vdots \\ n_{N_r1} & n_{N_r2} & \dots n_{N_rNL} \end{bmatrix} \quad (3-4)$$

The channel gain of each path in the MIMO FSO system is impacted by the fading in this path and the  $(N_r \times N_t)$  channel gain matrix represents the base-band FSO channel impulse response.  $\mathbf{H} = \{h_{il}(t), 0 \leq i \leq N_t, 0 \leq l \leq N_r\}$  is the channel gain matrix given as

$$\mathbf{H} = [\mathbf{h}_1 \quad \mathbf{h}_2 \quad \dots \mathbf{h}_{N_t}] = \begin{bmatrix} h_{11} & h_{12} & \dots h_{1N_t} \\ h_{21} & h_{22} & \dots h_{2N_t} \\ \vdots & \vdots & \vdots \\ h_{N_r1} & h_{N_r2} & \dots h_{N_rN_t} \end{bmatrix} \quad (3-5)$$

We assume that the FSO channel is the frequency non-selective channel and is perfect for the block fading channel model. We also assume that the transmitted optical signal is a narrow bandwidth signal. The basic instantaneous channel equation is the convolution of the input signal and the channel impulse response as

$$y(t) = \frac{E_s}{N_t} \beta \cdot h(t) * s(t) + n(t) \quad (3-6)$$

With the above assumptions about MIMO FSO channels, such as the narrowband signal assumption, we can replace the convolution in Eq. (3-6) by a simple product and rewrite as [5]

$$y(t) = \frac{E_s}{N_t} \beta \cdot h(t) \cdot s(t) + n(t) \quad (3-7)$$

The matrix expressions of MIMO point-to-point communication can be represented as

$$\begin{bmatrix} y_{11} & y_{12} & \dots & y_{1NL} \\ y_{21} & y_{22} & \dots & y_{2NL} \\ \vdots & \vdots & \vdots & \vdots \\ y_{N_r1} & y_{N_r2} & \dots & y_{N_rNL} \end{bmatrix} = \frac{E_s}{N_t} \beta \begin{bmatrix} h_{11} & h_{12} & \dots & h_{1N_t} \\ h_{21} & h_{22} & \dots & h_{2N_t} \\ \vdots & \vdots & \vdots & \vdots \\ h_{N_r1} & h_{N_r2} & \dots & h_{N_rN_t} \end{bmatrix} \begin{bmatrix} s_{11} & s_{12} & \dots & s_{1NL} \\ s_{21} & s_{22} & \dots & s_{2NL} \\ \vdots & \vdots & \vdots & \vdots \\ s_{N_t1} & s_{N_t2} & \dots & s_{N_tNL} \end{bmatrix} + \begin{bmatrix} n_{11} & n_{12} & \dots & n_{1NL} \\ n_{21} & n_{22} & \dots & n_{2NL} \\ \vdots & \vdots & \vdots & \vdots \\ n_{N_r1} & n_{N_r2} & \dots & n_{N_rNL} \end{bmatrix} \quad (3-8)$$

In the received signal matrix  $\mathbf{Y}$ , the element  $y_l(t)$  is the received signal of the  $l$ th branch and can be represented as

$$y_l(t) = \sum_{i=1}^{N_t} \frac{E_s}{N_t} \beta \cdot h_{il}(t) \cdot s_i(t) + n_l(t) \quad (3-9)$$

At the transmitter, the data from the information sources is intensity-modulated by Q-ary PPM or OOK modulation and is sent to encode the Space Time Block Coding. The signal data given out by the STBC component is split into  $N_t$  sub-streams and is added to the  $N_t$  lasers array. The data is modulated on the optical beams and is transmitted to different free space paths experiencing different atmospheric turbulence.

In order to analyze the performance of MIMO FSO systems, we first focus on the standard Q-ary PPM, which is the most frequently used modulation scheme, and the repetition coding scheme, which is one of the simplest MIMO coding schemes.

The other modulation schemes including on-off keying (OOK), multiple pulse position modulation (Multiple PPM) and differential PPM, have their own characteristics and advantages but also have their performance or implementation limitations [6,7]. There are other STBC schemes, such as the modified Alamouti-based STBC, BLAST-based coding and STBC provided by algebraic method [4, 7-

10]. The different STBC schemes can have different coding gains or different diversity gains.

Since PPM is an equal-energy orthogonal technique which requires the non-coherent detection, it is difficult to track the phase of the received signal. In this case, it is practical to use the envelope or square-law detection of PPM in conjunction with post-detection Equal Gain Combining. The EGC receiver processes the  $N_r$  received replicas from the branches, equally weights them, and then sums them to produce the decision statistic. EGC is suboptimum and has acceptable performance and reduced complexity [2, 4]. Although maximum ratio combining (MRC) is optimum and has a better performance but it is more complex and requires the estimation of phase of the received signals [2, 4]. In case of PPM non-coherent modulation, the signal phase is not generally detected. Therefore MRC is not suitable for PPM scheme. There are some other combining methods for the receivers, such as selection combining (SC) and switched combining, but they do not result into optimum implementations and have worse performance than EGC and MRC even though they are less complex than EGC and MRC [2, 4]. In this chapter, the post-detection EGC with the envelope detection is used and its demodulator decision is based on the sum of the envelopes of the PPM symbols.

In the receiver, there are  $N_r$  receiving branches and each branch includes a collecting lens, an InGaAs APD, GaAs MESFET transimpedance amplifiers, a matched filter and an equalizer, etc. Some receivers also include optical filters, mirrors or other optical components. If the transmission condition is very good and the transimpedance is used, little or no equalization is required [11]. In this dissertation, normal cases including equalizers are considered and calculated. For simple and special cases, the results can be obtained by changing the parameters

setting. At the end of these branches, the processed signals are sent to a decision detector, which implements the post-detection EGC with the envelope or square-law detection, maximum likelihood decision, STBC decoding and pulse position demodulation. Then the recovered data is sent to the data destination and the performance analysis is processed. A simple MIMO point-to-point receiver system is shown in Fig. 3.2 and Fig. 3.3.

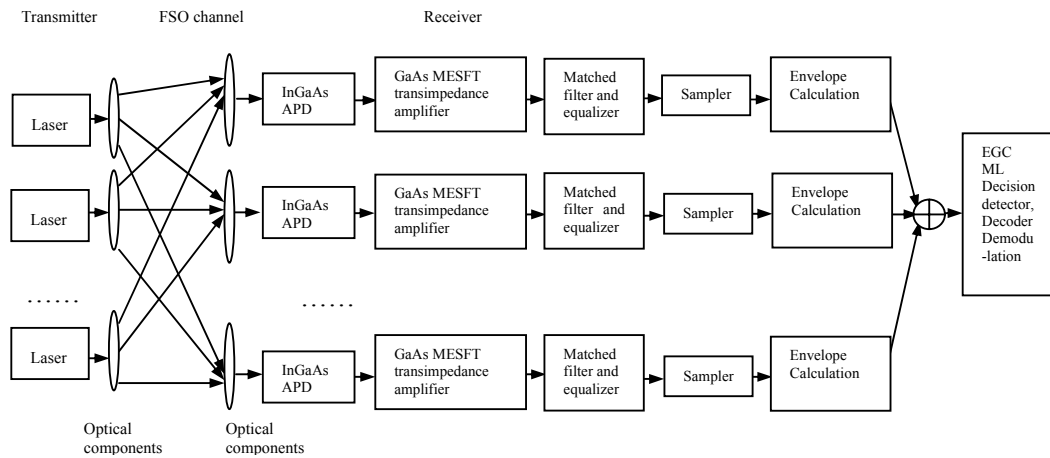


Figure 3.3 Receiver structure of MIMO point-to-point systems

The detection of the transmitted data symbols is implemented by the maximum likelihood algorithm. For different types of detection algorithms for MIMO systems, the maximum likelihood detector is optimum detector and has a better performance than the other detectors, such as Minimum Mean Square Error detector (MMSE), Inverse channel detector (ICD), successive cancellation, sphere detection and lattice reduction [12]. However, the computational complexity of the ML detector grows exponentially as  $L^{N_t}$ , where  $L$  is the number of points in the signal constellation and  $N_t$  is the number of the transmitting lasers. For a small number of transmitting antennas and signal points, the computational complexity of the ML detector is not too high [12].

### 3.2 Mathematical Model of MIMO FSO Point-to-Point Communication Systems

The inhomogeneity of the atmosphere due to temperature and pressure changes, like rising hot air and the moving aerosol particles, the refractive index of the atmospheric media also changes. This causes the amplitude and phase changes of transmitted optical signals.

According to the system model given in Section 3.1, the corresponding mathematical model for MIMO FSO systems is discussed in this section in detail.

#### 3.2.1 Assumptions for MIMO FSO Point-to-Point Communications

In order to make the research model as close to the practical one as possible and simple for analysis, the following basic assumptions and notations are made.

- (i) At the transmitter, the transmitted signal is a  $(N_t \times NL)$  matrix. If the total transmitted power for a 1 pulse in one slot is  $E_s$  and the  $N_t$  lasers in the transmitter array distribute the power equally, the power transmitted by each laser at the transmitter is  $\frac{E_s}{N_t}$ . The laser beams from the transmitter array can be described as Gaussian beams and the transmitted signals have narrow bandwidth. The single mode lasers with the 1550nm wavelength are used in the transmitter.
- (ii) The FSO channel is the slow fading and frequency-nonselective MIMO channel. FSO channels can be modeled as block fading channels and are independently, identically distributed (i.i.d) ergodic channels. In this case, the channel is assumed to be constant during one block or several blocks, each of which has a fixed number of PPM symbols. The channel is assumed to change very little between a number of consecutive blocks compared to the symbol rate, which is assumed to change at a fast space. The channel variation is assumed much

smaller than the total duration of the transmission. For different degrees of turbulence, the intensity of the laser beams can be modeled as lognormal distribution.

- (iii) At the receiver, the received signal is a  $(N_r \times NL)$  matrix. There are  $N_r$  receiving branches and each branch includes a collecting lens, an InGaAs APD, GaAs metal semiconductor field-effect transistor (MESFET) transimpedance amplifiers, a matched filter and an equalizer, etc. The InGaAs APD is selected due to higher responsivity ( $\mathcal{R} = 0.95 \sim 0.98$  at 1550nm) [11], its best performance at 1550nm wavelength [11], and the improved sensitivity [3]. For a 1 pulse slot in the APD, the number of the photon-electron pairs emitted by the first photon-injecting process of APDs obeys the Poisson distribution. For the 1 pulse slot, the number of the electrons emitted by the second photon-electron multiplication process of APDs obeys the Webb distribution and is not smaller than the photon-electron number. The GaAs transimpedance amplifier works in the linear amplifying region and the mean signal current is amplified by the amplifier gain  $A$  in a linear fashion. EGC is implemented in the receiver for improving SNR.
- (iv) At each branch of the receiver, the total noise current transmitted to the decision detector is the i.i.d additive white Gaussian noise. This includes the FSO path AWGN noise, shot noise, background noise, backscatter noise, bulk dark current noise, surface dark current noise, thermal noise and amplifier noise, etc. Since there are many independent noise sources in the FSO paths and receivers, according to the Central Limit Theorem, the total noise of each branch at the decision detector obeys the Gaussian distribution.

Usually the transimpedance amplifier is employed because of its low noise, high impedance and high data rate although the transimpedance amplifier is less

sensitive than the highimpedance amplifier. This difference is usually only about 2-3 dB lower sensitivity for most practical wideband designs [11]. In this dissertation, GaAs MESFET transimpedance amplifiers are employed and the equivalent circuits of a transimpedance receiver are selected according to Ref. [11].

The average symbol error probability, average bit error probability and average pairwise error probability are the performance criterions that exhibit the nature of the system behavior and most often are illustrated in the documents containing system performance evaluations. These are more difficult to compute compared to the signal to noise ratio and the outage probability. For the MIMO FSO system, the PPM symbols are transmitted as a coded matrix by the laser array. In the analysis, we obtain the equations of the average symbol error probability  $P_s(E)$  for one transmitted PPM symbol. Next, we calculate the average symbol error probability  $P_{e\_matrix}(E)$  for one transmitted PPM matrix. Finally the average bit error probability  $P_b(E)$  and the average pairwise error probability  $P_{s \rightarrow s'}(E)$  can be calculated by using  $P_{e\_matrix}(E)$ . Numerical analysis is used in order to obtain the detailed closed-form upper bound expressions of the above error probabilities. The impacts of each parameter of MIMO systems on the error probabilities can be obtained in detail and can be represented by figures. The analysis process results in the system performance, system design, coding and modulation design, etc., for MIMO FSO systems.

### 3.2.2 Laser Beam Transmission and Link Budget

An optical wireless link of MIMO FSO system typically consists of transceivers separated by the distance  $z$ . Each transceiver is made up of a laser array (transmitter) and a photodetector array (receiver). The optical components, such as

telescope, lenses and mirror, shape the transmitted laser beam and focus the received signal on the photodetector. The transmitter transmits enough power  $P_t$  to overcome loss in the path, space, optical components and mispointing resulting in the sufficient received power in the receiver so that the ones and zeros can be distinguished with negligible error. The received power  $P_r$  is given by

$$P_r = \eta_t \cdot \eta_{pt} \cdot \eta_a \cdot \eta_s \cdot \eta_r \cdot \eta_{pr} \cdot P_t \quad (3-10)$$

where  $\eta_t$  and  $\eta_r$  are the optics loss of the transmitter and receiver, respectively,  $\eta_{pt}$  and  $\eta_{pr}$  are the mispointing allowances of the transmitter and receiver, respectively,  $\eta_a$  is the path loss impacted by the weather and  $\eta_s$  is the space loss, which is the fraction of the transmitted power collected by the receiver. The  $\eta_a$  can be calculated by “Beer’s law” and  $\eta_s$  is calculated by using Gaussian beam theory. Depending on the complexity of the optical train in the transmitter and the receiver, the optics loss can vary between 2~5dB [3]. With the active tracking system,  $\eta_{pt}$  and  $\eta_{pr}$  can be about 3dB [3]. The link budget can be calculated as

$$\text{Link margin} = P_{t\_dB} - \eta_{t\_dB} - \eta_{pt\_dB} - \eta_{a\_dB} - \eta_{s\_dB} - \eta_{r\_dB} - \eta_{pr\_dB} - S_{r\_dB} \quad (3-11)$$

where  $P_{t\_dB}$ ,  $\eta_{t\_dB}$ ,  $\eta_{pt\_dB}$ ,  $\eta_{a\_dB}$ ,  $\eta_{s\_dB}$ ,  $\eta_{r\_dB}$ ,  $\eta_{pr\_dB}$  are the variable expressions in dB of  $P_t$ ,  $\eta_t$ ,  $\eta_{pt}$ ,  $\eta_a$ ,  $\eta_s$ ,  $\eta_r$ ,  $\eta_{pr}$ , respectively,  $S_{r\_dB}$  is the sensitivity of the receiver in dB. It is desirable to have as much excess link margin as possible to mitigate atmospheric effects, such as fog, etc. On a sunny day, the atmosphere is clear and the link margin is useful to overcome fades caused by turbulence. On a foggy day, the link margin is used to overcome signal attenuation. Thus the link distance or link availability has to be compromised according to weather conditions. It is obvious that

more link margin can be allotted to the atmospheric attenuation, for better compromise. In the presence of severe atmospheric attenuation, an optical link with narrow beam and tracking has an advantage over a link without tracking.

In a FSO data link, when only the space loss  $\eta_s$  is considered, the relationship of  $P_t$  and  $P_r$  are the ratio of the received aperture area  $A_r$  to the transmitted beam area  $A_b$  and is given by [13]

$$P_r = I_0 A_r = \frac{2P_t A_r}{\pi \omega^2(z)} = \frac{2A_r}{A_b} P_t \quad (3-12)$$

where  $A_r$  is the receiving aperture area of the lens at the receiver and  $A_b$  is the half-power spot size's area of the transmitted beam at the receiver  $A_b = \pi \omega^2(z)$ . The space loss is obtained as

$$\eta_s = \frac{2A_r}{A_b} \quad (3-13)$$

When the laser beams pass through the atmospheric media, there are many aerosol particles in the paths. These particles absorb and scatter the energy of laser beams and cause the attenuation and dispersion of the optical signal. In the optical link, the signal attenuation due to path loss can be calculated as the difference between the "clear air" signal level and the current air signal level. The first has been evaluated as  $-11\text{dBm}$  [14].

The total path attenuation is then divided by the link's length to obtain the path attenuation  $\alpha_{a\_dB}$  in dB/km. The measured visibility is converted into the path attenuation by applying "Beer's law" [14].

$$\alpha_{a\_dB} = \frac{17.138}{V_s} \left( \frac{\lambda}{550} \right)^{-Dq} \quad (3-14)$$

where  $\alpha_{a\_dB}$  is the path attenuation (dB/km),  $V_s$  is the visibility (km),  $\lambda$  is the wavelength and  $D_q$  is the distribution of particulate with size, which is in the case of low visibility (less than 6 km) as [14]

$$D_q = 0.585(V_s)^{1/3} \quad (3-15)$$

From the above, the path loss can be calculated as

$$\eta_a = 10^{\left(-\frac{\alpha_{a\_dB} \times D_s}{10}\right)} \quad (3-16)$$

According to Eq. (3-16), if the visibility  $V_s = 2 \text{ km}$  and the wavelength  $\lambda = 1550 \text{ nm}$ , the path attenuation is  $\alpha_{a\_dB} = 3.99 \text{ dB/km}$ . If the transmission distance  $D_s = 1 \text{ km}$ , the path loss is  $\eta_a = 10^{\left(-\frac{\alpha_{a\_dB} \times D_s}{10}\right)} = 0.3990$ .

In practice, the optics loss can vary in the range of 2~5dB [3].  $\eta_{t\_dB}$  ( $\eta_t$  in dB) and  $\eta_{r\_dB}$  ( $\eta_r$  in dB) can be about 3dB [3]. The mispointing allowance in dB, expressed as  $\eta_{pt\_dB}$  and  $\eta_{pr\_dB}$ , can be about 3dB [3]. The total loss between the transmitter power and the received power, except the space loss  $\eta_s = \frac{2A_r}{A_b}$ , is

$$\begin{aligned} \alpha &= \eta_t \cdot \eta_{pt} \cdot \eta_a \cdot \eta_r \cdot \eta_{pr} = 10^{\left(-\frac{\alpha_{dB} \times D_s + \eta_{t\_dB} + \eta_{r\_dB} + \eta_{pt\_dB} + \eta_{pr\_dB}}{10}\right)} \\ &= 10^{\left[-\frac{\frac{17.138}{V_s} \left(\frac{\lambda}{550}\right)^{-0.585(V_s)^{\frac{1}{3}}} \times D_s}{10}\right]} 10^{\left(-\frac{\eta_{t\_dB} + \eta_{r\_dB} + \eta_{pt\_dB} + \eta_{pr\_dB}}{10}\right)} \end{aligned} \quad (3-17)$$

If the loss  $\eta_{t\_dB} = 3 \text{ dB}$ ,  $\eta_{r\_dB} = 3 \text{ dB}$ ,  $\eta_{pt\_dB} = 3 \text{ dB}$ ,  $\eta_{pr\_dB} = 3 \text{ dB}$ ,  $\lambda = 1550 \text{ nm}$ ,  $V_s = 2 \text{ km}$ ,  $D_s = 1 \text{ km}$  and  $\eta_s = \frac{2A_r}{A_b}$ , the total loss in one FSO path can be obtained as

$$\alpha \cdot \eta_s = \frac{2A_r}{A_b} 10^{\left(-\frac{\alpha_{dB} \times D_s + \eta_{t\_dB} + \eta_{r\_dB} + \eta_{pt\_dB} + \eta_{pr\_dB}}{10}\right)} = 0.025177 \cdot \frac{2A_r}{A_b} \quad (3-18)$$

The received power of one APD branch from the  $i$ th FSO path for a 1 pulse at the receiver is

$$P_{ril} = \frac{2A_r P_{t il} \alpha}{A_b} \quad 1 \leq i \leq N_t, 1 \leq l \leq N_r \quad (3-19a)$$

The transmitted power of one laser to the  $i$ th FSO path for a 1 pulse at the transmitter is

$$P_{til} = \frac{A_b P_{ril}}{2A_r \alpha} \quad (3-19b)$$

The total energy transmitted by the  $N_t$  lasers array for a 1 pulse at the transmitter is

$$E_s = N_t P_{til} T_b = \frac{A_b P_{ril} T_b N_t}{2A_r \alpha}$$

$$= \frac{A_b h \nu \lambda_{sil} N_t}{2A_r} 10^{\left[ \frac{\frac{17.138 \left( \frac{\lambda}{550} \right)^{-0.585 (V_s)^{\frac{1}{3}}}}{V_s} \times D_s}{10} \right]} 10^{\left( \frac{\eta_{t,dB} + \eta_{r,dB} + \eta_{pt,dB} + \eta_{pr,dB}}{10} \right)} \quad (3-20)$$

where  $P_{ril} T_b = h \nu \lambda_{sil}$ ,  $\lambda_{sil}$  is the average number of the incident signal photons for a 1 pulse from the  $i$ th path and it can be expressed as

$$\lambda_{sil} = \frac{2A_r \alpha E_s}{A_b h \nu N_t} \quad (3-21)$$

The average number  $\lambda_s$  of the incident signal photons in a 1 pulse slot is  $\lambda_s = \sum_{i=1}^{N_t} \lambda_{sil}$ . The received power  $P_r$  in a 1 pulse slot is  $P_r = \sum_{i=1}^{N_t} P_{ril}$ .

During the entire data transmission of the FSO block fading channel, in weak turbulence, the log intensity  $\ell = \ln \left( \frac{I}{\langle I \rangle} \right)$  of laser beams obeys Gaussian distribution with the mean  $m_\ell$  and variance  $\sigma_\ell^2$  [13].  $I$  is the intensity of the laser beam and obeys lognormal distribution [13].  $\langle I \rangle$  is the expected value of the laser beam intensity. The symbol  $\langle \rangle$  denotes an ensemble average. It is proved in the Appendix A that in the  $i$ th path transmission, the laser beam intensity  $I$ , the received power  $P_{r il}$  in a 1 pulse slot

and the average number  $\lambda_{s\ il}$  of the incident signal photons in a 1 pulse slot are related as

$$\ln\left(\frac{I}{\langle I \rangle}\right) = \ln\left(\frac{P_{ril}}{\langle P_{ril} \rangle}\right) = \ln\left(\frac{\lambda_{sil}}{\overline{\lambda_{sil}}}\right) = \ln(\lambda_{sil}) - \ln(\overline{\lambda_{sil}}) \quad (3-22)$$

where  $\langle P_{ril} \rangle$  and  $\overline{\lambda_{sil}}$  are the expected value of the receiver power  $P_{ril}$  and the average number  $\lambda_{sil}$  of the incident signal photons for a 1 pulse, respectively.

The probability density function of the log intensity  $\ell$  is

$$p(\ell) = \frac{1}{\sqrt{2\pi \cdot \sigma_\ell^2}} e^{-\frac{(\ell - m_\ell)^2}{2\sigma_\ell^2}} \quad (3-23)$$

where the mean  $m_\ell = -\frac{\sigma_\ell^2}{2}$  and the variance  $\sigma_\ell^2$ . By noting that  $\langle e^\ell \rangle = \langle \frac{I}{\langle I \rangle} \rangle = 1$ , it can be proved by using Eq. (3-23) and Eq. (3-25a) that the mean of the log intensity  $\ell$  is equal to  $-\frac{\sigma_\ell^2}{2}$ , i.e.  $m_\ell = -\frac{\sigma_\ell^2}{2}$ . The average optical field amplitude is neither attenuated nor amplified if the mean value of log intensity is set to  $-\frac{\sigma_\ell^2}{2}$  [13]. During the transmission of a number of blocks or in the whole transmission duration, the intensity  $I$  of laser beam obeys lognormal distribution [13]. Usually a slot is chosen as the time interval. For the  $i$ th path of the FSO link, the average number  $\lambda_{sil}$  of the incident signal photon for a 1 pulse obeys lognormal distribution with the following PDF as calculated in Appendix B,

$$p_{\lambda_{sil}}(\lambda_{sil}) = p_\ell(\ell) \Big|_{\ell = \ln \lambda_{sil} - \ln \overline{\lambda_{sil}}} \frac{d(\ell)}{d(\lambda_{sil})} = \frac{1}{\sqrt{2\pi \cdot \sigma_\ell^2 \lambda_{sil}}} e^{-\frac{(\ln \lambda_{sil} - \ln \overline{\lambda_{sil}} - m_\ell)^2}{2\sigma_\ell^2}} \quad (3-24)$$

where the mean and variance of the random variable  $\frac{\lambda_{sil}}{\overline{\lambda_{sil}}}$  are calculated in Appendix

B as

$$E\{\lambda_{s\ i l}\} = \overline{\lambda_{s\ i l}} e^{m_\ell + \frac{\sigma_\ell^2}{2}} \quad (3-25a)$$

$$VAR\left\{\frac{\lambda_{s\ i l}}{\overline{\lambda_{s\ i l}}}\right\} = \overline{\lambda_{s\ i l}}^{-2} e^{2m_\ell + \sigma_\ell^2} (e^{\sigma_\ell^2} - 1) \quad (3-25b)$$

where  $m_\ell = -\frac{\sigma_\ell^2}{2}$ . If  $m_\ell = -\frac{\sigma_\ell^2}{2}$ , the average optical field amplitude is neither attenuated nor amplified. The mean value  $E\{\lambda_{s\ i l}\}$  of  $\lambda_{s\ i l}$  is

$$E\{\lambda_{s\ i l}\} = \overline{\lambda_{s\ i l}} = \frac{2A_r \bar{\alpha} E_s}{A_b h \nu N_t} \quad (3-25c)$$

In the reference [13], the variance  $\sigma_\ell^2$  of log intensity is given as

$$\sigma_\ell^2 = 4\sigma_\chi^2 = \begin{cases} 1.23 C_n^2 \kappa^{\frac{7}{6}} R^{\frac{11}{6}} & \text{plane wave} \\ 0.49 C_n^2 \kappa^{\frac{7}{6}} R^{\frac{11}{6}} & \text{spherical wave} \end{cases} \quad (3-26)$$

where  $\kappa = \frac{2\pi}{\lambda}$  and  $\sigma_\chi^2$  is the variance of the log amplitude.  $C_n^2$  is assumed to be uniform over the propagation path and typically ranges from  $10^{-15} m^{-\frac{2}{3}}$  (weak turbulence) to  $10^{-12} m^{-\frac{2}{3}}$  (strong turbulence). The transition from weak to strong turbulence has been found to occur in the range  $1 < \sigma_\ell^2 < 2$ . The ‘‘scintillation index’’ is used to characterize the degree of fading and given as [1]

$$\Psi = e^{4\sigma_\chi^2} - 1 = e^{\sigma_\ell^2} - 1 \quad (3-27)$$

### 3.2.3 Statistical Characteristics of Signals in APD-based Receivers

FSO channels can be modeled as an ergodic, frequency non-selective and block fading channel. The instantaneous channel equation is shown in Eq. (3-7) and Eq. (3-

9), and the matrix channel equations are shown in Eq. (3-1) and Eq. (3-8). The important considerations are:

(a) During the transmission of one block or several blocks, which includes several PPM symbols, the channel gain matrix  $\mathbf{H}$  and the transmitted symbol matrix  $\mathbf{S}$  are deterministic if the transmitted symbols are decided and chosen from the Q-ary PPM symbol set.  $\beta$  is the deterministic parameter in order to make the mean of  $\mathbf{H}$  equal to  $\mathbf{I}$ ,  $E\{\mathbf{H}\} = \mathbf{I}$ .  $E_s$  and  $N_t$  are also deterministic parameters. As there are many noise sources in the systems as discussed in Chapter 2, according to the Central Limit Theorem, the channel noise matrix  $\mathbf{N}$  obeys Gaussian distribution.  $\mathbf{Y}$  is the received signal matrix at the equalizer output current and obeys a Gaussian distribution.

Assuming the time interval in a slot, the instantaneous received signals for a 1 pulse and a 0 pulse in the  $l$ th branch are given as

$$y_l(t_{on}) = \sum_{i=1}^{N_t} \frac{E_s}{N_t} \beta \cdot h_{il}(t_{on}) \cdot s_i(t_{on}) + n_l(t_{on}) \quad (3-28a)$$

$$y_l(t_{off}) = n_l(t_{off}) \quad (3-28b)$$

where  $n_l(t_{on})$  is the total noise in the  $l$ th branch and it obeys the Gaussian distribution with the mean  $\mu_{on} = 0$  and the variance  $\sigma_{on}^2$ ,  $n_l(t_{off})$  is the total noise in the  $l$ th branch and it obeys a zero-mean Gaussian distribution and with variance  $\sigma_{off}^2$ .

For the one-slot interval, the instantaneous incident photon numbers of APD for a 1 pulse and a 0 pulse in the receiver with InGaAs APD, GaAs MESFET transimpedance amplifier, equalizer and decision detector, etc., are

$$k_{rl}(t_{on}) = k_{sl}(t_{on}) + k_{bl}(t_{on}) = \sum_{i=1}^{N_t} k_{sil}(t_{on}) + k_{bj}(t_{on}) \quad (3-29a)$$

$$k_{rl}(t_{off}) = k_{bl}(t_{off}) \quad (3-29b)$$

where  $k_{rl}(t_{on})$ ,  $k_{sl}(t_{on})$  and  $k_{bl}(t_{on})$  are the instantaneous numbers of the total received photon, signal part photon and background noise photon, in a 1 pulse slot for

the  $l$ th branch, respectively.  $k_{rl}(t_{\text{off}})$  and  $k_{bl}(t_{\text{off}})$  are the instantaneous number of the total received photon and background noise photon, in a 0 pulse slot for the  $l$ th branch, respectively.

For the 1 pulse slot, the incident signal photons  $k_{sl}(t_{\text{on}})$  with the average number  $\lambda_{sl}$  contribute to the signal part of the equalizer output current. The incident background noise photons  $k_{bl}(t_{\text{on}})$  with the average number  $\lambda_{bl}$  of a 1 pulse contribute to the background noise part of the total Gaussian-distributed noise in receivers. For the 0 pulse slot, the incident signal photon number is zero,  $k_{sl}(t_{\text{off}}) = 0$ . But the incident background noise photons  $k_{bl}(t_{\text{off}})$  with the average number  $\lambda_{bj}$  still exists and contributes to the background noise part of the total Gaussian-distributed noise in a 0 pulse slot.

In this analysis of the transmission of one block or several blocks, the average number  $\lambda_{sl}$  can be treated as a deterministic value.

(b) During the transmission of a number of consecutive blocks, the channel gain matrix  $\mathbf{H}$  shown in Eq. (3-1) is a random variable and its distribution is calculated in the following section. The noise matrix  $\mathbf{N}$  is the Gaussian-distributed random variable. The transmitted symbol matrix  $\mathbf{S}$  is deterministic if the transmitted symbols are decided and chosen from the Q-ary PPM symbol set.  $\beta$ ,  $E_s$  and  $N_t$  are deterministic.

The instantaneous received signal for a 0 pulse in one branch is the same as Eq. (3-28b). It obeys a zero-mean Gaussian distribution with variance  $\sigma_{\text{off}}^2$ . The instantaneous received signal for a 1 pulse in one branch  $y_l(t_{\text{on}})$  is the same as the one in Eq. (3-28a) and it is impacted by three factors. One factor is the lognormal-distributed intensity of laser beams, which pass through the different FSO paths. The

second factor is the Webb-distributed electron count given out by the ADP. The third is the total noise current added to the equalizer output current and it is a zero-mean Gaussian-distributed with variance  $\sigma_{on}^2$ .

The instantaneous incident photon numbers of the APD in a 1 pulse slot and in a 0 pulse are also be expressed as Eq. (3-29a) and Eq. (3-29b), respectively.

For the APD-based PPM MIMO systems, in each path with the channel gain  $h_{il}$ , the laser beam is exposed to the atmospheric impacts and has attenuation and dispersion. During the transmission of a number of consecutive blocks, in the one-slot interval, the incident signal photon number  $k_{sil}(t_{on})$  of a 1 pulse from the  $i$ th path is a random variable. The average number of the incident signal photons is  $\lambda_{sil}$  and for the  $h_{il}$  path, the probability distribution function (PDF) of  $\lambda_{sil}$  is

$$p_{\lambda_{sil}}(\lambda_{sil}) = \frac{1}{\sqrt{2\pi \cdot \sigma_{\rho}^2 \lambda_{sil}}} e^{-\frac{(\ln \lambda_{sil} - \ln \bar{\lambda}_{sil} - m_{\rho})^2}{2\sigma_{\rho}^2}} \quad (3-30)$$

In receivers, the incident photons are focused to the receiving area of the APD and detected by the APD. Inside the APD, there are two processes shown in Fig 3-4. The first is the primary photon-injecting process and the second is the photon-electron multiplication process.

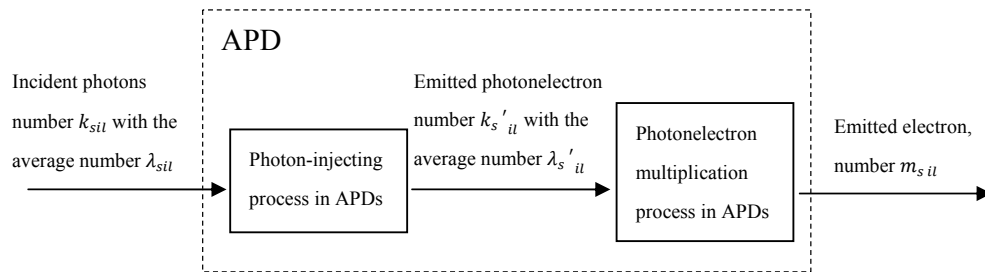


Figure 3.4 Two processes in APDs

For the first process,  $k'_s{}_{il}$  is the total photon-electron number of a 1 pulse emitted by the first photon-injecting process during the one-slot interval. The main

relationship of the incident signal photon number  $k_{s\ il}$  arriving at the APD and the emitted photoelectron number  $k_{s'\ il}$  in the APD can be expressed by the quantum efficiency  $\eta$  as [11]

$$k_{s'\ il} = \eta k_{s\ il} \quad (3-31)$$

According to semiclassical radiation theory, in one slot  $T_b$ , the mean average rate of the emission of the photoelectrons with the received average power  $\bar{P}_r$  and intensity  $\bar{I}$  of the laser beam is [13]

$$\overline{\lambda_{s'\ il}} = \frac{\eta \bar{P}_r}{h\nu} = \frac{\eta \bar{I}_r A_r}{h\nu} \quad (3-32)$$

where  $\bar{I}_r$  is the received laser beam intensity. The emitted photoelectron number  $k_{s'\ il}$  obeys a Poisson distribution and the PDF of  $k_{s'\ il}$  is [13]

$$q(k_{s'\ il}, \lambda_{s'\ il}) = \frac{(\lambda_{s'\ il})^{k_{s'\ il}} \cdot e^{-\lambda_{s'\ il}}}{k_{s'\ il}!} \quad (3-33)$$

We can calculate the PDF of the incident photon number  $k_{s\ il}$  at the receivers as

$$q(k_{s\ il}) = q(k_{s'\ il})|_{k_{s'\ il}=\eta k_{s\ il}} \frac{d(k_{s'\ il})}{d(k_{s\ il})} = \eta \frac{(\lambda_{s'\ il})^{(\eta k_{s\ il})} \cdot e^{-\lambda_{s'\ il}}}{(\eta k_{s\ il})!} \quad (3-34)$$

and the relationship of  $\lambda_{s'\ il}$  and  $\lambda_{s\ il}$  is given as

$$\lambda_{s'\ il} = \eta \lambda_{s\ il} \quad (3-35)$$

The relationship of the average number of  $\lambda_{s'\ il}$  and  $\lambda_{s\ il}$  is

$$\overline{\lambda_{s\ il}} = \frac{\overline{\lambda_{s'\ il}}}{\eta} = \frac{\bar{P}_r T_b}{\eta h\nu} = \frac{\bar{I}_r A_r T_b}{\eta h\nu} = \frac{2A_r P_t T_b \bar{\alpha}}{\eta h\nu A_b} = \frac{2A_r \bar{\alpha} E_s}{A_b h\nu N_t} \quad (3-36)$$

For the second process,  $m_{s\ il}$  is the total electron number in a 1 pulse slot given out by the APD.  $p_{m_{s\ il}}(m_{s\ il} | k_{s'\ il}, \lambda_{s\ il})$  is the probability distribution function of the electron number  $m_{s\ il}$  given out by the APD, on condition of the primary

photoelectron number  $k_s'_{il}$  in the APD and the incident photon number  $k_{s il}$  arriving at the APD. The PDF  $p_{m_{s il}}(m_{s il})$  of the electron count  $m_{s il}$  is given by

$$p_{m_{s il}}(m_{s il}) = \int_{-\infty}^{\infty} \left[ \sum_{k_s'_{il}=1}^{\infty} q_s(m_{s il} | k_s'_{il}, \lambda_{s il}) q(k_s'_{il} | \lambda_{s il}) \right] \cdot p_{\lambda_{s il}}(\lambda_{s il}) \cdot d\lambda_{s il} \quad (3-37)$$

The PDF of the electron number  $m_s$  with the mean primary photoelectron number  $\bar{k}$  in the APD is proposed as the Webb distribution in Chapter 2 [13]

$$p_{sw}(m_s) = \frac{\exp \left\{ - \frac{(m_s - \bar{k}M)^2}{2k_s M^2 F \left[ 1 + \frac{(m_s - \bar{k}M)(F-1)}{\bar{k}MF} \right]} \right\}}{\sqrt{2\pi\bar{k}M^2F} \left[ 1 + \frac{(m_s - \bar{k}M)(F-1)}{\bar{k}MF} \right]^{\frac{3}{2}}} \quad (3-38)$$

This Webb model has the requirement that the emitted electron number should not be smaller than the photon-electron number, i.e.  $m_s \geq \bar{k} \geq 0$ , and the photon-electron pairs generated by the first photon-injecting process obey a Poisson distribution [13].

For 1 pulse slots in the APD-based receiver, the requirements of  $m_{s il} \geq k_s'_{il} \geq 0$  and the Poisson distribution of  $k_s'_{il}$  can be satisfied for APDs that work normally.

Hence, for MIMO FSO systems, the PDF of the electron number  $m_{s il}$  emitted by APD can be expressed as

$$p_{sw}(m_{s il} | \lambda_{s il}) = \sum_{k_s'_{il}=1}^{\infty} q_s(m_{s il} | k_s'_{il}, \lambda_{s il}) q(k_s'_{il} | \lambda_{s il}) \quad (3-39)$$

During the transmission of a number of consecutive blocks, the incident photon average number  $\lambda_{s\ il}$  arriving at the APD is a random variable with the PDF in Eq. (3-30). Since the average values of  $k_{s\ il}'$  and  $k_{s\ il}$  are  $\lambda_{s\ il}'$  and  $\lambda_{s\ il}$ , respectively, and they have the relationships of  $k_{s\ il}' = \eta k_{s\ il}$  and  $\lambda_{s\ il}' = \eta \lambda_{s\ il}$ , the PDF of the electron number  $m_{s\ ij}$  on condition of  $\lambda_{s\ il}$  is

$$\begin{aligned}
 p_{sw}(m_{s\ il} | \lambda_{s\ il}) |_{\lambda_b=0} &= p_{sw}(m_{s\ il}, \lambda_{s\ il}' | \lambda_{s\ il}) |_{\lambda_{s\ il}' = \eta \lambda_{s\ il}, \lambda_b=0} \\
 &= p_{sw}(m_{s\ il}, \eta \lambda_{s\ il} | \lambda_{s\ il}) |_{\lambda_b=0} \\
 &= \frac{\exp \left\{ - \frac{(m_{s\ il} - \eta \lambda_{s\ il} M)^2}{2\eta \lambda_{s\ il} M^2 F \left[ 1 + \frac{(m_{s\ il} - \eta \lambda_{s\ il} M)(F-1)}{\eta \lambda_{s\ il} M F} \right]} \right\}}{\sqrt{2\pi\eta \lambda_{s\ il} M^2 F} \left[ 1 + \frac{(m_{s\ il} - \eta \lambda_{s\ il} M)(F-1)}{\eta \lambda_{s\ il} M F} \right]^{\frac{3}{2}}}
 \end{aligned} \tag{3-40}$$

Then, the probability distribution function of the electron count  $m_{s\ il}$  emitted by the APD can be represented on condition of  $\lambda_{s\ il}$  arriving at the APD

$$p_{m_{s\ il}}(m_{s\ il}) = \int_{-\infty}^{\infty} p_{sw}(m_{s\ il} | \lambda_{s\ il}) \cdot p_{\lambda_{s\ il}}(\lambda_{s\ il}) \cdot d\lambda_{s\ il} \tag{3-41}$$

As  $\lambda_{s\ il} \geq 0$  and the lower limit of the above integral is zero, the PDF of  $m_{s\ il}$  is

$$\begin{aligned}
 p_{m_{s\ il}}(m_{s\ il}) &= \int_0^{\infty} p_{sw}(m_{s\ il} | \lambda_{s\ il}) \cdot p_{\lambda_{s\ il}}(\lambda_{s\ il}) \cdot d\lambda_{s\ il} \\
 &= \int_0^{\infty} \frac{\exp \left\{ - \frac{(m_{s\ il} - \eta \lambda_{s\ il} M)^2}{2\eta \lambda_{s\ il} M^2 F \left[ 1 + \frac{(m_{s\ il} - \eta \lambda_{s\ il} M)(F-1)}{\eta \lambda_{s\ il} M F} \right]} \right\}}{\sqrt{2\pi\eta \lambda_{s\ il} M^2 F} \left[ 1 + \frac{(m_{s\ il} - \eta \lambda_{s\ il} M)(F-1)}{\eta \lambda_{s\ il} M F} \right]^{\frac{3}{2}}} \cdot p_{\lambda_{s\ il}}(\lambda_{s\ il}) \cdot d\lambda_{s\ il} \\
 &= \int_0^{\infty} \frac{1}{\sqrt{2\pi\eta \lambda_{s\ il} M^2 F} \left[ 1 + \frac{(m_{s\ il} - \eta \lambda_{s\ il} M)(F-1)}{\eta \lambda_{s\ il} M F} \right]^{\frac{3}{2}}}
 \end{aligned}$$

$$\begin{aligned}
& \exp \left\{ - \frac{(m_{s\,il} - \eta \lambda_{s\,il} M)^2}{2\eta \lambda_{s\,il} M^2 F \left[ 1 + \frac{(m_{s\,il} - \eta \lambda_{s\,il} M)(F-1)}{\eta \lambda_{s\,il} M F} \right]} \right\} \frac{1}{\sqrt{2\pi \cdot \sigma_\ell^2 \lambda_{s\,il}}} e^{-\frac{(\ln \lambda_{s\,il} - \ln \bar{\lambda}_{s\,il} - m_\ell)^2}{2\sigma_\ell^2}} d\lambda_{s\,il} \\
&= \int_0^\infty \frac{1}{\sqrt{2\pi \eta \lambda_{s\,il} M^2 F}} \frac{1}{\sqrt{2\pi \cdot \sigma_\ell^2 \lambda_{s\,il}}} \left[ 1 + \frac{(m_{s\,il} - \eta \lambda_{s\,il} M)(F-1)}{\eta \lambda_{s\,il} M F} \right]^{-\frac{3}{2}} \\
& \exp \left\{ - \frac{(m_{s\,il} - \eta \lambda_{s\,il} M)^2}{2\eta \lambda_{s\,il} M^2 F \left[ 1 + \frac{(m_{s\,il} - \eta \lambda_{s\,il} M)(F-1)}{\eta \lambda_{s\,il} M F} \right]} - \frac{(\ln \lambda_{s\,il} - \ln \bar{\lambda}_{s\,il} - m_\ell)^2}{2\sigma_\ell^2} \right\} d\lambda_{s\,il}
\end{aligned} \tag{3-42}$$

where  $\bar{\lambda}_{s\,il} = \frac{2A_r \bar{\alpha} E_s}{A_b h \nu N_t}$ . With some parts of the detailed derivation in Appendix C,

$p_{m_{s\,il}}(m_{s\,il})$  can be expressed as

$$\begin{aligned}
p_{m_{s\,il}}(m_{s\,il}) &= \int_0^\infty \frac{\eta F}{2\pi \sigma_\ell M} \left[ \eta \lambda_{s\,il} + \frac{m_{s\,il}(F-1)}{M} \right]^{-\frac{3}{2}} \\
& \exp \left\{ - \frac{(m_{s\,il} - \eta \lambda_{s\,il} M)^2}{2M^2 \eta \lambda_{s\,il} + 2M m_{s\,il}(F-1)} - \frac{(\ln \lambda_{s\,il} - \ln \bar{\lambda}_{s\,il} - m_\ell)^2}{2\sigma_\ell^2} \right\} d\lambda_{s\,il} \\
&= \frac{\eta F}{2\pi \sigma_\ell M} \int_0^\infty \left[ \eta \lambda_{s\,il} + \frac{m_{s\,il}(F-1)}{M} \right]^{-\frac{3}{2}} \\
& \exp \left\{ - \frac{(\eta \lambda_{s\,il} - \frac{m_{s\,il}}{M})^2}{2 \left[ \eta \lambda_{s\,il} + \frac{m_{s\,il}(F-1)}{M} \right]} - \frac{(\ln \lambda_{s\,il} - \ln \bar{\lambda}_{s\,il} - m_\ell)^2}{2\sigma_\ell^2} \right\} d\lambda_{s\,il}
\end{aligned} \tag{3-43}$$

In Eq. (3-43), the following substitution is made

$$x = \frac{\ln \lambda_{s\,il} - \ln \bar{\lambda}_{s\,il} - m_\ell}{\sqrt{2}\sigma_\ell} \tag{3-44a}$$

$$\lambda_{s\,il} = e^{(\sqrt{2}\sigma_\ell x + \ln \bar{\lambda}_{s\,il} + m_\ell)} \tag{3-44b}$$

$$d\lambda_{s\ il} = \frac{d\lambda_{s\ il}}{dx} dx = e^{(\sqrt{2}\sigma_\ell x + \ln\bar{\lambda}_{s\ il} + m_\ell)} \sqrt{2}\sigma_\ell dx \quad (3-44c)$$

Since  $\lambda_{s\ il} \geq 0$ , we can get the range of  $x$  :  $-\infty \leq x \leq \infty$ . The upper limit and lower limit of the integral  $p_{m_{s\ il}}(m_{s\ il})$  are infinity and negative infinity. The PFD can be expressed as

$$\begin{aligned} p_{m_{s\ il}}(m_{s\ il}) &= \frac{\eta F}{2\pi \sigma_\ell M} \int_{-\infty}^{\infty} e^{-x^2} \left[ \eta e^{(\sqrt{2}\sigma_\ell x + \ln\bar{\lambda}_{s\ il} + m_\ell)} + \frac{m_{s\ il}(F-1)}{M} \right]^{-\frac{3}{2}} \\ &\quad \exp \left\{ -\frac{\left[ \eta e^{(\sqrt{2}\sigma_\ell x + \ln\bar{\lambda}_{s\ il} + m_\ell)} - \frac{m_{s\ il}}{M} \right]^2}{2 \left[ \eta e^{(\sqrt{2}\sigma_\ell x + \ln\bar{\lambda}_{s\ il} + m_\ell)} + \frac{m_{s\ il}(F-1)}{M} \right]} \right\} e^{(\sqrt{2}\sigma_\ell x + \ln\bar{\lambda}_{s\ il} + m_\ell)} \sqrt{2}\sigma_\ell dx \\ &= \frac{\eta F}{\sqrt{2\pi} M} \int_{-\infty}^{\infty} e^{-x^2} \left[ \eta e^{(\sqrt{2}\sigma_\ell x + \ln\bar{\lambda}_{s\ il} + m_\ell)} + \frac{m_{s\ il}(F-1)}{M} \right]^{-\frac{3}{2}} \\ &\quad \exp \left\{ -\frac{\left[ \eta e^{(\sqrt{2}\sigma_\ell x + \ln\bar{\lambda}_{s\ il} + m_\ell)} - \frac{m_{s\ il}}{M} \right]^2}{2 \left[ \eta e^{(\sqrt{2}\sigma_\ell x + \ln\bar{\lambda}_{s\ il} + m_\ell)} + \frac{m_{s\ il}(F-1)}{M} \right]} \right\} e^{(\sqrt{2}\sigma_\ell x + \ln\bar{\lambda}_{s\ il} + m_\ell)} dx \end{aligned} \quad (3-45)$$

According to the Gaussian Hermite quadrature rule [16], the integral can be given by the following expression

$$\int_{-\infty}^{\infty} f(x) e^{-x^2} dx \approx \sum_{\substack{u=-N_u \\ u \neq 0}}^{N_u} w_u f(x_u) \quad (3-46a)$$

where  $\{x_u\}$  and  $\{w_u\}$  ( $u = -N_u, N_u + 1, \dots, -1, 1, 2, \dots, N_u - 1, N_u$ ) are the zeros and the weight factors of the Hermite polynomial [4], respectively. This estimation process yields fairly accurate results for values of  $N_u \leq 10$ . Since  $\{x_u\}$  and  $\{w_u\}$  are well-tabulated in reference [4], the tractable means of estimating performance can be obtained. By selecting the suitable  $N_u$ , the calculating error can be very small. Let  $f(x)$  be

$$f(x) = \frac{\eta F}{\sqrt{2\pi} M} \left[ \eta e^{(\sqrt{2}\sigma_\ell x + \ln \bar{\lambda}_{s\ell} + m_\ell)} + \frac{m_{s\ell}(F-1)}{M} \right]^{-\frac{3}{2}}$$

$$\exp \left\{ - \frac{\left[ \eta e^{(\sqrt{2}\sigma_\ell x + \ln \bar{\lambda}_{s\ell} + m_\ell)} - \frac{m_{s\ell}}{M} \right]^2}{2 \left[ \eta e^{(\sqrt{2}\sigma_\ell x + \ln \bar{\lambda}_{s\ell} + m_\ell)} + \frac{m_{s\ell}(F-1)}{M} \right]} \right\} e^{(\sqrt{2}\sigma_\ell x + \ln \bar{\lambda}_{s\ell} + m_\ell)}$$

(3-46b)

Hence, we have

$$p_{m_{s\ell}}(m_{s\ell}) \approx \sum_{\substack{u=-N_u \\ u \neq 0}}^{N_u} w_u \frac{F}{\sqrt{2\pi} M} \left[ \eta e^{(\sqrt{2}\sigma_\ell x_u + \ln \bar{\lambda}_{s\ell} + m_\ell)} + \frac{m_{s\ell}(F-1)}{M} \right]^{-\frac{3}{2}}$$

$$\exp \left\{ - \frac{\left[ \eta e^{(\sqrt{2}\sigma_\ell x_u + \ln \bar{\lambda}_{s\ell} + m_\ell)} - \frac{m_{s\ell}}{M} \right]^2}{2 \left[ \eta e^{(\sqrt{2}\sigma_\ell x_u + \ln \bar{\lambda}_{s\ell} + m_\ell)} + \frac{m_{s\ell}(F-1)}{M} \right]} \right\} \eta e^{(\sqrt{2}\sigma_\ell x_u + \ln \bar{\lambda}_{s\ell} + m_\ell)}$$

(3-47)

$$\text{Let } K_{w_u} = w_u \frac{F}{\sqrt{2\pi} M}$$

(3-48a)

$$K_{x_u} = \eta e^{(\sqrt{2}\sigma_\ell x_u + \ln \bar{\lambda}_{s\ell} + m_\ell)}$$

(3-48b)

$$\text{where } \bar{\lambda}_{s\ell} = \frac{2A_r \alpha E_s}{A_b h\nu N_t}$$

$$p_{m_{s\ell}}(m_{s\ell})$$

$$\approx \sum_{\substack{u=-N_u \\ u \neq 0}}^{N_u} K_{w_u} K_{x_u} \left[ \frac{(F-1)}{M} m_{s\ell} + K_{x_u} \right]^{-\frac{3}{2}} \exp \left\{ - \frac{\left( \frac{m_{s\ell}}{M} - K_{x_u} \right)^2}{2 \left[ \frac{(F-1)}{M} m_{s\ell} + K_{x_u} \right]} \right\}$$

(3-48c)

### 3.2.4 Receiver Noises in MIMO FSO Systems

For MIMO FSO systems, in each transmission path, the optical signal is impacted by the turbulence-induced fading and the additive white Gaussian noise of the free space optical path is added. The AWGN in each FSO path obeys Gaussian distribution  $N(\mu_i, \sigma_i^2)$   $1 \leq i \leq N_t$ . At each receiver shown in Fig. 3.3, the  $N_t$  laser beams from the transmitter array are received by the APDs simultaneously. The total path AWGN at each APD obeys Gaussian distribution  $N(\mu_{path}, \sigma_{path}^2)$  with mean  $\mu_{path} = \sum_{i=1}^{N_t} \mu_i$  and variance  $\sigma_{path}^2 = \sum_{i=1}^{N_t} \sigma_i^2$ . The power spectral density of the path AWGN is  $S_{path} = \sigma_{path}^2$  and the power of the path AWGN is  $P_{path} = \sigma_{path}^2 B$ . But the sum of the noise is much smaller compared to the noise induced in the receiver and it is negligible for the calculation of the error probability.

In MIMO FSO systems, when the post-detection Equal Gain Combining with the envelope detection is implemented, the noise currents in the different branches are assumed as i.i.d Gaussian-distributed random variables and the expression equation is given as

$$y = \sum_{l=1}^{N_r} y_l = \sum_{l=1}^{N_r} \sum_{i=1}^{N_t} \frac{\mathcal{RMAE}_s g}{N_t} h_{il} \cdot s_i + \sum_{l=1}^{N_r} n_l \quad (3-49)$$

According to the discussion of the noise components in Chapter 2, the variances of the noise currents at the decision detector for a 1 pulse and a 0 pulse in MIMO FSO systems are represented as  $\sigma_{on}^2$  and  $\sigma_{off}^2$  with

$$\begin{aligned}
\sigma_{on}^2 &= \frac{1}{B^2} \sum_{l=1}^{N_r} \sigma_{on} l^2 \\
&= \frac{N_r}{B^2} A^2 \left\{ \left[ 2 \frac{\eta q b_{on}}{h\nu T_b} M^2 F + 2\mathcal{R}(P_b + P_c) M^2 F + 2(I_{db} M^2 F + I_{ds}) \right] q I_2 B + \right. \\
&\quad \left. \left( 2q I_{gate} + \frac{4k_B T}{R_b} + \frac{4k_B T \Gamma_e}{g_m \cdot R_b^2} \right) I_2 B + (2\pi C)^2 \frac{4k_B T \Gamma_e}{g_m} I_3 B^3 + \frac{4k_B T}{R_f} I_2 B \right\} \\
&= \frac{N_r}{B^2} A^2 \left\{ \left[ 2 \frac{\eta q b_{on}}{h\nu T_b} M^2 F + 2\mathcal{R}(P_b + P_c) M^2 F + 2(I_{db} M^2 F + I_{ds}) \right] q I_2 B + q^2 B^2 W_{TZ} \right\}
\end{aligned} \tag{3-50a}$$

$$\text{where } W_{TZ} = \frac{1}{q^2 B} \left( 2q I_{gate} + \frac{4k_B T}{R_b} + \frac{4k_B T \Gamma_e}{g_m \cdot R_b^2} \right) I_2 + \left( \frac{2\pi C}{q} \right)^2 \frac{4k_B T \Gamma_e}{g_m} I_3 B + \frac{T_b}{q^2} \frac{4k_B T}{R_f} I_2$$

$$\begin{aligned}
\sigma_{off}^2 &= \frac{1}{B^2} \sum_{l=1}^{N_r} \sigma_{off} l^2 \\
&= \frac{N_r}{B^2} A^2 \left\{ \left[ 2 \frac{\eta q b_{on}}{h\nu T_b} (1 - \gamma_s) M^2 F + 2\mathcal{R}(P_b + P_c) M^2 F + 2(I_{db} M^2 F + I_{ds}) \right] q I_2 B + \right. \\
&\quad \left. \left( 2q I_{gate} + \frac{4k_B T}{R_b} + \frac{4k_B T \Gamma_e}{g_m \cdot R_b^2} \right) I_2 B + (2\pi C)^2 \frac{4k_B T \Gamma_e}{g_m} I_3 B^3 + \frac{4k_B T}{R_f} I_2 B \right\} \\
&= \frac{N_r}{B^2} A^2 \left\{ \left[ 2 \frac{\eta q b_{on}}{h\nu T_b} (1 - \gamma_s) M^2 F + 2\mathcal{R}(P_b + P_c) M^2 F + 2(I_{db} M^2 F + I_{ds}) \right] q I_2 B \right. \\
&\quad \left. + q^2 B^2 W_{TZ} \right\}
\end{aligned} \tag{3-50b}$$

If we assume that the receiver is ideal and linear, and it changes the input optical power to the electrical current with the coefficients ( $\mathcal{R}MAB$ ) linearly, we can calculate the unity gain equivalent variances of the equivalent input power to the receiver in the 1 pulse slot and in the 0 pulse slot as

$$\begin{aligned}
\sigma_{eq\_on}^2 &= \frac{N_r \langle i_N^2 \rangle_{on}}{(\mathcal{R}MAB)^2} \\
&= \frac{N_r}{(\mathcal{R}MAB)^2} (qAB)^2 \left[ \frac{2 \langle i_0 \rangle_1 M^2 F + 2\mathcal{R}(P_b + P_c) M^2 F + 2(I_{db} M^2 F + I_{ds})}{q} T_b I_2 + W_{TZ} \right]
\end{aligned}$$

$$= \left(\frac{h\nu}{\eta}\right)^2 \left[ \frac{2\eta}{h\nu} \left( \frac{b_{on}}{T_b} + P_b + P_c \right) FT_b I_2 + 2T_b I_2 \frac{(I_{db} M^2 F + I_{ds})}{qM^2} + \frac{W_{TZ}}{M^2} \right] \quad (3-51a)$$

$$\begin{aligned} \sigma_{eq\_off}^2 &= \frac{N_r \langle i_N^2 \rangle_{off}}{(\mathcal{R}MAB)^2} \\ &= \frac{N_r}{(\mathcal{R}MAB)^2} (qAB)^2 \left[ \frac{2 \langle i_0 \rangle_0 M^2 F + 2\mathcal{R}(P_b + P_c) M^2 F + 2(I_{db} M^2 F + I_{ds})}{q} T_b I_2 + W_{TZ} \right] \\ &= \left(\frac{h\nu}{\eta}\right)^2 \left[ \frac{2\eta}{h\nu} \left( \frac{b_{on}}{T_b} (1 - \gamma_s) + P_b + P_c \right) FT_b I_2 + 2T_b I_2 \frac{(I_{db} M^2 F + I_{ds})}{qM^2} + \frac{W_{TZ}}{M^2} \right] \end{aligned} \quad (3-51b)$$

### 3.2.5 Signal to Noise Ratio Calculation

For the 1 pulse slots, because the transmitted signal energy is not zero, the signal to noise ratio is not zero, which is very important for the PPM demodulation and the performance analysis. For the 0 pulse slots, the transmitted signal is zero and the signal to noise ratio is zero. As the PPM demodulator detects each slot in one symbol, the values and impacts of SNRs in 1 pulse slots and 0 pulse slots are different. The instantaneous SNR is referred to the one in the 1 pulse slot.

The detailed mean-square signal currents  $\langle i_s^2 \rangle_{on}$  and  $\langle i_s^2 \rangle_{off}$  in the equalizer output current at the APD receiver for a 1 pulse slot and a 0 pulse, respectively, are

$$\langle i_s^2 \rangle_{on} = \left( \frac{\eta q b_{on}}{h\nu T_b} MA \right)^2 = (\mathcal{R}P_s MA)^2 \quad (3-52a)$$

$$\langle i_s^2 \rangle_{off} = \left[ \frac{\eta q b_{on}}{h\nu T_b} MA (1 - \gamma_s) \right]^2 = [\mathcal{R}P_s MA (1 - \gamma_s)]^2 \quad (3-52b)$$

The signal to noise ratio of the equalizer output current is

$$\begin{aligned} SNR_{on} &= \frac{\langle i_s^2 \rangle_{on}}{\sigma_{onl}^2} \\ &= \frac{(\mathcal{R}P_s MA)^2}{A^2 \left\{ \left[ 2 \frac{\eta q b_{on}}{h\nu T_b} M^2 F + 2\mathcal{R}(P_b + P_c) M^2 F + 2(I_{db} M^2 F + I_{ds}) \right] q I_2 B + \left( 2q I_{gate} + \frac{4k_B T}{R_b} + \frac{4k_B T \Gamma_e}{g_m \cdot R_b^2} \right) I_2 B + (2\pi C)^2 \frac{4k_B T \Gamma_e}{g_m} I_3 B^3 + \frac{4k_B T}{R_f} I_2 B \right\}} \end{aligned}$$

$$= \frac{(\mathcal{R}P_s M)^2}{\left\{ 2 \frac{\eta q b_{on}}{h\nu T_b} M^2 F + 2\mathcal{R}(P_b + P_c)M^2 F + 2(I_{db}M^2 F + I_{ds}) \right\} q I_2 B + \left( 2q I_{gate} + \frac{4k_B T}{R_b} + \frac{4k_B T T_e}{g_m \cdot R_b^2} \right) I_2 B + (2\pi C)^2 \frac{4k_B T T_e}{g_m} I_3 B^3 + \frac{4k_B T}{R_f} I_2 B \right\}} \quad (3-53)$$

The signal to noise ratio after the post-detection EGC with the envelop detection at the decision circuit is

$$SNR_{on\_EGC} = \frac{\langle i_s^2 \rangle_{on} N_r^2}{\sigma_{on} l^2 N_r}$$

$$= \frac{N_r (\mathcal{R}P_s M A)^2}{A^2 \left\{ 2 \frac{\eta q b_{on}}{h\nu T_b} M^2 F + 2\mathcal{R}(P_b + P_c)M^2 F + 2(I_{db}M^2 F + I_{ds}) \right\} q I_2 B + \left( 2q I_{gate} + \frac{4k_B T}{R_b} + \frac{4k_B T T_e}{g_m \cdot R_b^2} \right) I_2 B + (2\pi C)^2 \frac{4k_B T T_e}{g_m} I_3 B^3 + \frac{4k_B T}{R_f} I_2 B \right\}}$$

$$= \frac{N_r (\mathcal{R}P_s M)^2}{\left\{ 2 \frac{\eta q b_{on}}{h\nu T_b} M^2 F + 2\mathcal{R}(P_b + P_c)M^2 F + 2(I_{db}M^2 F + I_{ds}) \right\} q I_2 B + \left( 2q I_{gate} + \frac{4k_B T}{R_b} + \frac{4k_B T T_e}{g_m \cdot R_b^2} \right) I_2 B + (2\pi C)^2 \frac{4k_B T T_e}{g_m} I_3 B^3 + \frac{4k_B T}{R_f} I_2 B \right\}} \quad (3-54)$$

The unity gain equivalent signal currents for a 1 pulse slot and a 0 pulse slot are

$$\langle i_{0\_s}^2 \rangle_{on} = \frac{\langle i_s^2 \rangle_{on}}{(\mathcal{R}MAB)^2} = \frac{\left( \frac{\eta q b_{on} M A}{h\nu T_b} \right)^2}{(\mathcal{R}MAB)^2} = b_{on}^2 \quad (3-55a)$$

$$\langle i_{0\_s}^2 \rangle_{off} = \frac{\langle i_s^2 \rangle_{off}}{(\mathcal{R}MAB)^2} = \frac{\left[ \frac{\eta q b_{on} M A (1 - \gamma_s)}{h\nu T_b} \right]^2}{(\mathcal{R}MAB)^2} = [b_{on} (1 - \gamma_s)]^2 \quad (3-55b)$$

The unity gain equivalent SNR for a 1 pulse slot can be expressed as

$$SNR_{eq\_on} = \frac{\langle i_{0\_s}^2 \rangle_{on}}{\sigma_{on}^2} = \frac{b_{on}^2}{\left( \frac{h\nu}{\eta} \right)^2 \left[ \frac{2\eta}{h\nu} \left( \frac{b_{on}}{T_b} + P_b + P_c \right) F T_b I_2 + 2 T_b I_2 \frac{(I_{db} M^2 F + I_{ds})}{q M^2} + \frac{W T Z}{M^2} \right]} \quad (3-56)$$

### 3.3 Probability Density Function Calculation of Channel Gains

For the mathematical model of MIMO FSO systems with block fading given in Section 3.2, the channel gain is a very important parameter for analyzing the system performance. The probabilistic characteristics of the channel gain and received signal are discussed in this section and the equation for the PDF of the channel gain is presented in detail.

At the receiver, the instantaneous signal received from the FSO paths, are expressed in Eq. (3-28a) and (3-28b). We assume that the amplifiers in the receiver work in the linear range and can be treated as a model amplifying the signal  $A$  times and adding the amplifier noise at the same time. In the transmission of MIMO FSO system, the transmitted signals pass through the channels with random channel gains and are added to the Gaussian noise.

The equalizer output current  $y_l$  of the  $l$ th branch of the APD-based receiver can be represented by the function of the transmitted symbol  $s_i$  and the channel gain  $h_{il}$  as

$$y_l = \sum_{i=1}^{N_t} \frac{\mathcal{R}MAE_s g}{N_t T_b} h_{il} \cdot s_i + n_l \quad (3-57)$$

where  $g$  represents the link gain coefficient of the FSO communication channels, which makes the mean channel gain  $h_{il}$  unity,  $E\{h_{il}\} = 1$ . During the processing of the APD-based receiver, the equalizer output current  $y_{ml}$  for one slot can also be represented by the function of the electron count  $m_{sil}$  as

$$y_{ml} = \sum_{i=1}^{N_t} \frac{Aq}{T_b} m_{sil} \cdot s_i + n_l \quad (3-58)$$

The signal parts of Eq. (3-57) and Eq. (3-58) equal to each other:

$$\sum_{i=1}^{N_t} \frac{Aq}{T_b} m_{sil} = \sum_{i=1}^{N_t} \frac{\mathcal{R}MAE_s g}{N_t T_b} h_{il} \cdot s_i \quad (3-59)$$

For each path of the FSO links, we obtain

$$\frac{Aq}{T_b} m_{sil} = \frac{\mathcal{R}MAE_s g}{N_t T_b} h_{il} \cdot s_i \quad (3-60)$$

$$m_{sil} = \frac{\mathcal{R}ME_s g}{q N_t} h_{il} \cdot s_i \quad (3-61)$$

The PDF of the channel gain  $h_{il}$  is obtained from Eq. (3-48c) and is given as

$$\begin{aligned}
p_{h_{il}}(h_{il}) &= p_{m_{sil}}(m_{sil}) \Big|_{m_{sil} = \frac{\mathcal{R}M E_s g}{q N_t} h_{il}} \cdot \frac{dm_{sil}}{dh_{il}} \\
&= \sum_{\substack{u=-N_u \\ u \neq 0}}^{N_u} K_{w_u} K_{x_u} \frac{\mathcal{R}M E_s g}{q N_t} \frac{\exp \left\{ - \frac{\left( \frac{\mathcal{R} E_s g}{q N_t} h_{il} - K_{x_u} \right)^2}{2 \left[ \frac{(F-1) \mathcal{R} E_s g}{q N_t} h_{il} + K_{x_u} \right]} \right\}}{\left[ \frac{(F-1) \mathcal{R} E_s g}{q N_t} h_{il} + K_{x_u} \right]^{\frac{3}{2}}}
\end{aligned} \tag{3-62}$$

where  $K_{w_u}$  and  $K_{x_u}$  are given in Eq. (3-48a) and Eq. (3-48b). The mean expression of the current in Eq. (3-57) and Eq. (3-58) for FSO links are assumed as

$$E\{y_{ml}\} = E\{y_l\} \tag{3-63}$$

$$E\left\{\frac{Aq}{T_b} m_{sil}\right\} + E\{n_l\} = E\left\{\frac{\mathcal{R}M A E_s g}{N_t T_b}\right\} E\{h_{il}\} E\{s_i\} + E\{n_l\} \tag{3-64}$$

Since  $\frac{q}{T_b} m_{sil}$  and  $M \mathcal{R} P_{ril} h_{il}$  (where  $P_{ril} = \frac{E_s}{N_t T_b}$ ) are both the expressions of the APD output current, we can get

$$E\left\{\frac{q}{T_b} m_{sil}\right\} = E\{M \mathcal{R} P_{ril} h_{il}\} \tag{3-65}$$

Substitute Eq. (3-65) for the  $E\left\{\frac{q}{T_b} m_{sil}\right\}$  in Eq. (3-64), we obtain

$$E\left\{\frac{A M \mathcal{R} P_{ril} h_{il}}{T_b}\right\} + E\{n_l\} = E\left\{\frac{\mathcal{R}M A E_s g}{N_t T_b}\right\} E\{h_{il}\} E\{s_i\} + E\{n_l\} \tag{3-66}$$

As  $E\{h_{il}\} = 1$ ,  $E\{s_i\} = 1$  and  $E\{n_l\} = 0$ , Eq. (3-66) can be given as

$$E\left\{\frac{M A \mathcal{R} P_{ril}}{T_b}\right\} = E\left\{\frac{\mathcal{R}M A E_s g}{N_t T_b}\right\} \tag{3-67}$$

$P_{ril}$  and  $E_s$  are random variables. The other parameters, such as  $M$ ,  $A$ ,  $\mathcal{R}$ ,  $T_b$ ,  $N_t$ , are deterministic. The equation can be expressed as

$$M A \overline{\mathcal{R} P_{ril}} = \frac{\mathcal{R}M A \overline{E_s} g}{N_t T_b} \tag{3-68}$$

$$g = \frac{\overline{P_{ril}} N_t T_b}{\overline{E_s}} \tag{3-69}$$

where  $\overline{E_s}$  is the average total transmitting power for a 1 pulse by the laser array,  $\overline{P_{r\ i}}$  is the average incident power received by one APD-based branch from one path. According to Eq. (3-68), it can be obtained that

$$\overline{E_s} = \frac{A_b \overline{P_{r\ i}} N_t T_b}{2A_r \alpha} \quad (3-70)$$

Hence, the link gain coefficient is

$$g = \frac{\overline{P_{r\ i}} N_t T_b}{\frac{A_b \overline{P_{r\ i}} N_t T_b}{2A_r \alpha}} = \frac{2A_r \alpha}{A_b} \quad (3-71)$$

## REFERENCES

- [1]. Neda Cvijetic , Stephen G.Wilson and Maite Brandt-Pearce, “Performance Bounds for Free-Space optical MIMO Systems with APD Receivers in Atmospheric Turbulence,” IEEE Journal on Selected Areas in Communications, VOI.26, No.3, April 2008.
- [2]. Zeinab Hajjarian, Jarir Fadlullah and Mohsen Kavehrad, “MIMO Free Space Optical Communications in Turbid Turbulence Atmosphere”, Journal of Communications Vol. 4, No.8, September 2009.
- [3]. Muthu Jeganathan and Pavel Lonov, “Multi-Gigabits-per-second Optical Wireless Communications”, Optical Crossing Company.
- Website: <http://www.citeseerx.ist.psu.edu/viewdoc/download?doi=10.1.1.110>
- [4]. Marvin K. Simon and Mohamed-Slim Alouini, “Digital Communication over Fading Channels,” 2005, John Wiley & Sons, Inc., second edition.

- [5]. Denis Bushuev and Shlomi Arnon, "Analysis of the performance of a wireless optical multi-input to multi-output communication system," *Optical Society of America, J. Opt. Soc. Am. A*, vol. 23, No.7, July 2006.
- [6]. Hisayoshi Sugiyama and Kiyoshi Nosu, "MPPM: a method for improving the band utilization efficiency in optical PPM," *Journal of lightwave technology*, Vol. 7, No. 3, March 1989.
- [7]. M. K. Simon and V. A. Vlnrotter, "Alamouti-type space-time coding for free-space optical communication with direct detection," *IEEE Trans. Wireless Commun.*, vol. 4, pp. 35–39, January 2005.
- [8]. B. A. Sethuraman, B. Sundar Rajan and V. Shashidhar "Full-Diversity, High-Rate Space-time Block Codes From Division Algebras," *IEEE transaction on information theory*, VOL 49, No. 10 October 2003.
- [9]. Chadi Abou-Rjeily, and Mario Bkassiny, "Alamouti-Type Space-Time Coding for TH-UWB Systems with Unipolar Pulse Position Modulations", 978-1-4244-2644-7/08, 2008.
- [10]. C. Abou-Rjeily and J.-C. Belfiore, "On space-time coding with pulse position and amplitude modulations for time-hopping ultra-wideband systems," *IEEE Trans. Inform. Theory*, vol. 53, no. 7, pp. 2490–2509, July 2007.
- [11]. Gerd Keiser, "Optical Fiber Communications," McGraw Hill, Inc., third edition, 2000.
- [12]. John G. Proakis and Masoud Salehi, "Digital Communications," Mc Graw Hill , fifth edition, 2008.
- [13]. Gregory R. Osche, "Optical Detection Theory for laser Applications," 2002, John Wiley & Sons, Inc.
- [14]. Michele D'Amico, Angelo Leva and Barbara Micheli, "Free-Space Optics

Communication Systems: First Results From a Pilot Field-Trial in the Surrounding Area of Milan, Italy,” IEEE Microwave and wireless Components Letters, vol. 13, No. 8, August 2003.

[15]. The probability definition

[http://en.wikipedia.org/wiki/Probability\\_density\\_function](http://en.wikipedia.org/wiki/Probability_density_function) .

[16]. M. Abramowitz and I. A. Stegun, “ Handbook of Mathematical Functions with Formulas, Graphs and Mathematical Tables”, 9 th ed. New York, NY : Dover Publications,1970.

[17]. S. G. Wilson, M. Brandt-Pearce, Q. Cao, and J.J.H. Leveque, III, “Free-space optical MIMO transmission with Q-ary PPM,” IEEE Trans. Communication. 53, 1402-1412 , 2005.

[18]. George K. Karagiannidis and Athanasios S. Lioumpas “An Improved Approximation for the Gaussian Q-function ”, IEEE communication letters, VOL. 11, NO. 8 , August 2007.

[19]. Frederic M. Davidson and Xiaoli Sun, “Gaussian Approximation Versus Nearly Exact Performance Analysis of Optical Communication System with PPM Signaling and APD Receivers,” IEEE Transaction on Communications, vol. 36, No. 11, November, 1988.

[20]. V. Vilnrotter, A. Biswas, W. Farr, D. Fort, and E. Sigman, “Design and Analysis of a First-Generation Optical Pulse-Position Modulation Receiver,” The Interplanetary Network Progress Report 42-148, October–December 2001, Jet Propulsion Laboratory, Pasadena, California, pp.1–20, February 15, 2002.

## CHAPTER 4

### ERROR PROBABILITY CALCULATION OF MIMO FSO SYSTEMS

#### 4.1 Symbol Error Probability Calculation of MIMO FSO Systems

In practice, the optical signal emitted by a transmitter deviates from the ideal 1 and 0 bit stream. It can be degraded by channel fading during its transmission through free space and by the noise in the optical receiver. Thus the performance of optical receivers is severely limited. MIMO techniques can overcome channel fading and improve the system performance. Based on the analysis of FSO communication systems in Chapter 2 and Chapter 3, we have built up the mathematical model to discuss MIMO FSO communication systems and have derived the closed-form upper bound expressions of the average symbol error probability (SEP), average bit error probability (BEP) and average pairwise error probability (PEP) for MIMO FSO systems with Equal Gain Combining in this chapter. The error analysis for this calculation is given in this chapter.

##### 4.1.1 Symbol Detection of One Q-ary PPM Symbol

The PPM signaling is the orthogonal and power-limit signaling, which is more power efficient but less bandwidth efficient. In the PPM optical receiver, the integrals of the output signal over each time slot are implemented and then the slot of the largest value is chosen as the slot that contains the received light pulse. The Q-ary PPM equal energy orthogonal signaling scheme can be represented as [1]:

$$\begin{aligned}
 s_1 &= (E_s, 0, 0, \dots \dots 0) \\
 s_2 &= (0, E_s, 0, \dots \dots 0) \\
 &\dots \dots \\
 s_L &= (0, 0, 0, \dots \dots E_s)
 \end{aligned} \tag{4-1}$$

The signaling vector representation of the PPM signals can be represented as

$$\begin{aligned}
\mathbf{S}_1 &= (S_1, 0, 0, \dots, 0) \\
\mathbf{S}_2 &= (0, S_2, 0, \dots, 0) \\
&\dots\dots \\
\mathbf{S}_L &= (0, 0, 0, \dots, S_L)
\end{aligned} \tag{4-2}$$

where  $L = 2^Q$  and  $Q$  is  $Q$ -ary PPM signal,  $E_s$  is the total energy of a 1 pulse slot that are transmitted by the laser array,  $\mathbf{S}_1, \mathbf{S}_2 \dots \mathbf{S}_L$  are the symbols in the PPM symbol set and their  $S_1, S_2$  or  $S_L$  slots represent the 1 pulses, respectively, such as  $(0, 0, 0, \dots, 1)$ .  $E_s$  can also be represented by the energy after including the total number  $\lambda_s$  of photons in a 1 pulse slot and  $E_s = h\nu\lambda_s$ .

In optical receivers, the post-detection EGC with envelope detection is used in MIMO FSO communication systems shown in Fig. 3.1 and Fig. 3.3. For one PPM symbol transmission, the received symbols, which are transmitted to the decision detector of the APD-based receiver, have the following vector expression

$$\mathbf{y} = \frac{\mathcal{R}MAE_s g}{N_t} \cdot \mathbf{h} \cdot \mathbf{S}_m + \mathbf{n} \tag{4-3}$$

and the matrix expression is given as

$$\begin{bmatrix} y_{11} & y_{12} & \dots & y_{1L} \\ y_{21} & y_{22} & \dots & y_{2L} \\ \vdots & \vdots & \vdots & \vdots \\ y_{N_r 1} & y_{N_r 2} & \dots & y_{N_r L} \end{bmatrix} = \frac{\mathcal{R}MAE_s g}{N_t} \begin{bmatrix} h_{11} & h_{12} & \dots & h_{1N_t} \\ h_{21} & h_{22} & \dots & h_{2N_t} \\ \vdots & \vdots & \vdots & \vdots \\ h_{N_r 1} & h_{N_r 2} & \dots & h_{N_r N_t} \end{bmatrix} \begin{bmatrix} S_{11} & S_{12} & \dots & S_{1L} \\ S_{21} & S_{22} & \dots & S_{2L} \\ \vdots & \vdots & \vdots & \vdots \\ S_{N_t 1} & S_{N_t 2} & \dots & S_{N_t L} \end{bmatrix} + \begin{bmatrix} n_{11} & n_{12} & \dots & n_{1L} \\ n_{21} & n_{22} & \dots & n_{2L} \\ \vdots & \vdots & \vdots & \vdots \\ n_{N_r 1} & n_{N_r 2} & \dots & n_{N_r L} \end{bmatrix} \tag{4-4}$$

where  $\mathbf{y}$  is the  $N_r \times L$  received signal vector for one PPM symbol, which is sent to the decision detector of the APD receiver,  $\mathbf{h}$  is the  $N_r \times N_t$  channel gain vector with the mean of its element equal to 1,  $E\{h_{il}\} = 1$ ,  $\mathbf{n}$  is the  $N_r \times L$  added white Gaussian noise vector in the APD-based receiver,  $\mathbf{S}_m$  is the  $N_r \times N_t$  transmitted signal vector which is one of the  $L$  possible signals in PPM symbol set and  $1 \leq m \leq L$ . For

example  $\mathbf{S}_2 = (0, S_2, 0, 0 \dots 0)$  and  $S_2 = 1$ .  $\mathbf{y}, \mathbf{h}, \mathbf{S}_m$  and  $\mathbf{n}$  are all the real variable vectors. The signal for the  $l$ th branch before the EGC can be represented by the scalar equation as

$$y_l = \sum_{i=1}^{N_t} \frac{\mathcal{RMAE}_s g}{N_t} h_{il} \cdot s_i + n_l \quad (4-5)$$

The signal after the post-detection EGC with envelope detection is obtained as

$$\begin{aligned} \sum_{l=1}^{N_r} y_l &= \sum_{l=1}^{N_r} \sum_{i=1}^{N_t} \frac{\mathcal{RMAE}_s g}{N_t} h_{il} \cdot s_i + \sum_{l=1}^{N_r} n_l \\ &= \sum_{l=1}^{N_r} \sum_{i=1}^{N_t} \frac{\mathcal{RMAE}_s g}{N_t} h_{il} \cdot s_i + \sum_{l=1}^{N_r} n_l \\ &= \frac{\mathcal{RMAE}_s g}{N_t} h \cdot s_i + \sigma_{\text{on}}^2 \end{aligned} \quad (4-6)$$

where  $h$  is the channel gain  $h = \sum_{l=1}^{N_r} \sum_{i=1}^{N_t} h_{il}$ ,  $\sigma_{\text{on}}^2$  is the variance of the 1 pulse slot and is given in Eq. (3-50a) in Chapter 3.

For equi-probable, equal-energy orthogonal PPM signals, the maximum likelihood detector selects the signal resulting in the largest cross-correlation between the received vector  $\mathbf{y}$  and each of the  $L$  possible transmitted signal vector  $\mathbf{S}_m$  ( $1 \leq m \leq L$ ) as [1]

$$\hat{m} = \arg \max_{1 \leq m \leq L} \mathbf{y} \cdot \mathbf{S}_m \quad (4-7)$$

Due to the symmetry of the constellation and by observing that the distances between any pair of signals in the constellation are equal to  $\sqrt{2}E_s$ , we can conclude that the symbol error probability of one PPM symbol is independent of the transmitted

signal [1]. Therefore, for evaluating the symbol error probability  $P_s(E)$ , we can assume that the signal  $\mathbf{S}_1 = (S_1, 0, 0 \dots 0)$  is transmitted and can calculate the conditional symbol error probability  $P_{s|s1}$ , which is equal to the symbol error probability of this Q-ary PPM. The symbol error probability of the Q-ary PPM can be represented as [1]

$$P_s(E) = \sum_{m=1}^L P_m P_{s|m} = L \frac{1}{L} P_{s|s1} = P_{s|s1} \quad (4-8)$$

where  $P_m$  is the probability that the  $m$ th PPM symbol  $\mathbf{S}_m$  is transmitted. As the PPM symbols are equi-probable,  $P_m$  equal to  $\frac{1}{L}$ ,  $P_{s|s1}$  is the symbol error probability on condition that the  $\mathbf{S}_1$  is transmitted. When  $\mathbf{S}_1 = (S_1, 0, 0 \dots \dots 0)$  is transmitted, the received signal vector is

$$\mathbf{y} = \left( \frac{E_s \mathcal{R} M A g}{N_t} h S_1 + n_1, n_2, n_3, \dots \dots n_L \right) \quad (4-9)$$

$n_1, n_2, n_3 \dots \dots n_L$  are independent identically distributed zero-mean Gaussian random variables,  $n_1$  is the noise in a 1 pulse slot with the variance  $\sigma_{\text{on}}^2$ ,  $n_2, n_3, \dots \dots n_L$  are the noises in the 0 pulse slots with the variance  $\sigma_{\text{off}}^2$ . The PDF of  $n_1$  and  $n_m$  random variables are given as  $p_{n_{\text{on}}}(n_{\text{on}})$  and  $p_{n_{\text{off}}}(n_{\text{off}})$ , respectively, as[1]

$$p_{n_{\text{on}}}(n_{\text{on}}) = \frac{1}{\sqrt{2\pi\sigma_{\text{on}}^2}} \cdot e^{-\frac{n_{\text{on}}^2}{2\sigma_{\text{on}}^2}} \quad (4-10a)$$

$$p_{n_{\text{off}}}(n_{\text{off}}) = \frac{1}{\sqrt{2\pi\sigma_{\text{off}}^2}} \cdot e^{-\frac{n_{\text{off}}^2}{2\sigma_{\text{off}}^2}} \quad (4-10b)$$

Let us define the real decision variable  $R_m$ ,  $1 \leq m \leq L$ , as [1]

$$R_m = \mathbf{y} \cdot \mathbf{S}_m \quad (4-11)$$

With the definition of Eq. (4-11), we can have the following decision variables

$$R_1 = \frac{E_s \mathcal{R} M A g}{N_t} h S_1 S_1 + n_1 S_1 \quad (4-12a)$$

$$R_m = n_m S_m \quad 2 \leq m \leq L \quad (4-12b)$$

where  $h$  is the random variable given as  $h = \sum_{l=1}^{N_r} \sum_{i=1}^{N_t} h_{ij}$  if the post-detection EGC with envelope detection is implemented,  $n_1, n_2, n_3 \dots n_L$  are Gaussian random variables,  $R_1$  and  $R_m$  are also random variables. The random variables  $R_m$  are still Gaussian-distributed with zero mean and variance  $\sigma_{\text{off}}^2$ , i.e.  $R_m \sim N(0, \sigma_{\text{off}}^2)$ . The PDF of  $R_m$  is  $p_{n_{\text{off}}}(n)$  shown in Eq. (4-10b). The random variable  $R_1$  is the sum of the random variable  $\frac{E_s \mathcal{R} M A g}{N_t} h S_1 S_1$  and the Gaussian-distributed variable  $n_1 S_1$  where  $S_1$  and  $S_m$  are deterministic and  $S_1 = 1$ ,  $S_m = 1$ . Then the decision variable can be simplified as

$$R_1 = \frac{E_s \mathcal{R} M A g}{N_t} h + n_1 \quad (4-13a)$$

$$R_m = n_m \quad 2 \leq m \leq L \quad (4-13b)$$

We assume  $k_t = \frac{E_s \mathcal{R} M A g}{N_t}$  and using the variable substitution  $t_s = \frac{E_s \mathcal{R} M A g}{N_t} h = k_t h$ .

Then the decision variable  $R_1$  is  $R_1 = t_s + n_{\text{on}}$  where  $t_s = k_t h$  and  $h$  has the PDF  $p_h(h)$ . The PDF of the random variable  $t_s$  is

$$p_{t_s}(t_s) = p_h(h) \Big|_{h=\frac{t_s}{k_t}} \frac{dh}{dt_s} = \frac{1}{k_t} \cdot p_h\left(\frac{t_s}{k_t}\right) = \frac{1}{k_t} \cdot p_h(h) \quad (4-14)$$

The PDF of the random variable  $R_1$ , which is the sum of  $t_s$  and  $n_{\text{on}}$ , is the convolution of the PDFs of  $t_s$  and  $n_{\text{on}}$  as

$$\begin{aligned} p_{R_1}(r_1) &= p_{t_s}(t_s) * p_{n_{\text{on}}}(n_{\text{on}}) \\ &= \int_{-\infty}^{\infty} p_{t_s}(t_s) \cdot p_{n_{\text{on}}}(r_1 - t_s) \cdot dt_s \\ &= \int_{-\infty}^{\infty} p_{t_s}(r_1 - n_{\text{on}}) \cdot p_{n_{\text{on}}}(n_{\text{on}}) \cdot dn_{\text{on}} \end{aligned}$$

(4-15)

where the upper limit and lower limit of the integration are decided by the range of the random variables  $t_s$  and  $n_{on}$ . We assume that the PPM symbol  $\mathbf{S}_1 = (1,0,0 \dots \dots 0)$  (where  $S_1 = 1, S_2 = 0, S_3 = 0, \dots \dots S_L = 0$ ) is transmitted, and the ML detector makes a correct decision if  $R_1 \geq R_m$  for  $m=2, 3, \dots \dots L$ . Therefore, the probability of a correct decision for one PPM symbol is given by

$$\begin{aligned}
P_c &= P[R_1 \geq R_2, R_1 \geq R_3, \dots \dots R_1 \geq R_L | \mathbf{S}_1 \text{ sent} ] \\
&= P\left[\frac{E_s \mathcal{R}MAG}{N_t} h S_1 S_1 + n_1 S_1 \geq n_2 S_m, \frac{E_s \mathcal{R}MAG}{N_t} h S_1 S_1 + n_1 S_1 \geq n_3 S_m, \right. \\
&\quad \dots \dots \left. \frac{E_s \mathcal{R}MAG}{N_t} h S_1 S_1 + n_1 S_1 \geq n_L S_m | \mathbf{S}_1 \text{ sent} \right] \\
&= P\left[\frac{E_s \mathcal{R}MAG}{N_t} h + n_1 \geq n_2, \frac{E_s \mathcal{R}MAG}{N_t} h + n_1 \geq n_3, \right. \\
&\quad \dots \dots \left. \frac{E_s \mathcal{R}MAG}{N_t} h + n_1 \geq n_L | \mathbf{S}_1 \text{ sent} \right]
\end{aligned} \tag{4-16}$$

Events  $\frac{E_s \mathcal{R}GMAg}{N_t} h + n_1 \geq n_2, \frac{E_s \mathcal{R}MAG}{N_t} h + n_1 \geq n_3, \dots \dots \frac{E_s \mathcal{R}MAG}{N_t} h + n_1 \geq n_L$ , are not independent due to the existence of the random variables  $h$  and  $n_1 = n_{on}$  in all of them. We can assume the condition on  $h$  and  $n_1 = n_{on}$  to make these events independent. Since the  $n_m$ 's are i.i.d random variables for  $m=2,3,\dots \dots M$ , and by using Eq. (4-15) and Eq. (4-16), we can obtain

$$\begin{aligned}
P_{c|h} &= \int_{-\infty}^{\infty} P\left[n_2 \leq \frac{E_s \mathcal{R}GMAg}{N_t} h + n_1, n_3 \leq \frac{E_s \mathcal{R}GMAg}{N_t} h + n_1, \dots \dots n_L \right. \\
&\quad \left. \leq \frac{E_s \mathcal{R}GMAg}{N_t} h + n_1, | \mathbf{S}_1 \text{ sent}, n_1 = n_{on}, h \right] p_{n_{on}}(n_{on}) dn_{on} \\
&= \int_{-\infty}^{\infty} \left\{ P\left[n_2 \leq \frac{E_s \mathcal{R}GMAg}{N_t} h + n_1 | \mathbf{S}_1 \text{ sent}, n_1 = n_{on}, h \right] \right\}^{(L-1)} p_{n_{on}}(n_{on}) dn_{on}
\end{aligned}$$

$$\begin{aligned}
&= \int_{-\infty}^{\infty} \left[ 1 - \left( \int_{\frac{E_s \mathcal{R} \text{MAG}}{N_t} h + n_{on}}^{+\infty} p_{n_{off}}(n_{off}) \cdot dn_{off} \right) \right]^{(L-1)} p_{n_{on}}(n_{on}) dn_{on} \\
&= \int_{-\infty}^{\infty} \int_{-\infty}^{\infty} \left[ 1 - \left( \int_{\frac{E_s \mathcal{R} \text{MAG}}{N_t} h + n_{on}}^{+\infty} p_{n_{off}}(n_{off}) \cdot dn_{off} \right) \right]^{(L-1)} p_{n_{on}}(n_{on}) dn_{on}
\end{aligned} \tag{4-17}$$

The integral of  $\int_{\frac{E_s \mathcal{R} \text{MAG}}{N_t} h + n_{on}}^{+\infty} p_{n_{off}}(n_{off}) \cdot dn_{off}$  is calculated in Appendix D and it is a Q function of the variable  $\frac{E_s \mathcal{R} \text{MAG}}{N_t \sigma_{off}} h + \frac{n_{on}}{\sigma_{off}}$ , i.e.  $Q\left(\frac{E_s \mathcal{R} \text{MAG}}{N_t \sigma_{off}} h + \frac{n_{on}}{\sigma_{off}}\right)$ . Using the definition of the probability density function, it can be obtained

$$\int_{-\infty}^{\infty} \int_{-\infty}^{\infty} 1 \cdot p_{n_{on}}(n_{on}) \cdot dn_{on} \cdot p_{t_s}(t_s) \cdot dt_s = 1 \tag{4-18}$$

Using Eq. (4-15), Eq. (4-17),  $dr_1 = dn_{on}$ , Appendix D and Appendix E, the symbol error probability  $P_s(E)$  is

$$\begin{aligned}
P_s(E) &= P_{s|s_1} = 1 - P_c \\
&= 1 - \int_{-\infty}^{\infty} \int_{-\infty}^{\infty} \left\{ \left[ 1 - Q\left(\frac{E_s \mathcal{R} \text{MAG}}{N_t \sigma_{off}} h + \frac{n_{on}}{\sigma_{off}}\right) \right]^{(L-1)} \right\} \cdot p_{n_{on}}(n_{on}) \cdot dn_{on} \cdot p_{t_s}(t_s) \cdot dt_s
\end{aligned} \tag{4-19}$$

In optical wireless communication, the channel gain  $h$  is nonnegative and  $0 \leq h \leq \infty$ . Using the calculation in Appendix E, the error probability  $P_s(E)$  can also be represented as an integral of the channel gain  $h$

$$P_s(E) = \int_0^{\infty} \left\{ \int_{-\infty}^{\infty} \left\{ 1 - \left[ 1 - Q\left(\frac{E_s \mathcal{R} \text{MAG}}{N_t \sigma_{off}} h + \frac{n_{on}}{\sigma_{off}}\right) \right]^{(L-1)} \right\} p_{n_{on}}(n_{on}) dn_{on} \right\} p_h(h) dh \tag{4-20}$$

where the upper limit and lower limit of the integration are decided by the range of the random variables  $n_{on}$  and  $h$ . According to the reference [2] and Appendix F, the scalar expression of the symbol error probability can also be represented as

$$\begin{aligned} P_s(E) &= \int_0^{\infty} P_s(E|\gamma) \cdot p_\gamma(\gamma) \cdot d\gamma \\ &= \int_0^{\infty} P_s(E|h) \cdot p_h(h) \cdot dh \end{aligned} \quad (4-21)$$

where  $\gamma$  is the signal to noise ratio,  $0 \leq \gamma \leq \infty$ , and  $h$  is the channel gain,  $0 \leq h \leq \infty$ . By comparing Eq. (4-20) and Eq. (4-21), the symbol error probability on condition of  $h$  is obtained as

$$P_s(E|h) = \int_{-\infty}^{\infty} \left\{ 1 - \left[ 1 - Q \left( \frac{E_s \mathcal{R}MAG}{N_t \sigma_{off}} h + \frac{n_{on}}{\sigma_{off}} \right) \right]^{(L-1)} \right\} \cdot p_{n_{on}}(n_{on}) \cdot dn_{on} \quad (4-22)$$

In optical wireless communication, the channel gain  $h$  is nonnegative and  $0 \leq h \leq \infty, 0 \leq t_s \leq \infty$ . The noise in the 1 and 0 pulse slots is Gaussian random variables  $n_{on}$  and  $n_{off}$ , respectively, and they can be positive or negative. For the photodiode current generated in response to an optical signal, its sampled value  $I_s(t)$  fluctuates from bit to bit around an average value  $I_1$  or  $I_0$  [11].  $I_1$  and  $I_0$  correspond to the average values of 1 and 0 bit, respectively. In the decision circuit, the real decision variables  $r_1 = \frac{E_s \mathcal{R}MAG}{N_t} h + n_{on}$  and  $r_m = n_{off}$  are the random variables representing the difference between the sampled value  $I_s(t)$  and the average value  $I_0$ . They can be positive or negative. For the optical receivers under the normal working condition, the signal to noise ratio  $\gamma$  is far above  $\gamma = 0dB$ , i.e.  $\left( \frac{E_s \mathcal{R}MAG}{N_t} E\{h\} \right)^2 \geq \sigma_{on}^2$ . In practice, the noise powers  $\sigma_{on}^2$  and  $\sigma_{off}^2$  are normally smaller than the signal power

$\left(\frac{E_s \mathcal{R}MAG}{N_t} E\{h\}\right)^2$ , i.e.  $\left(\frac{E_s \mathcal{R}MAG}{N_t} E\{h\}\right)^2 \geq \sigma_{on}^2$  and  $\left(\frac{E_s \mathcal{R}MAG}{N_t} E\{h\}\right)^2 \geq \sigma_{off}^2$ ,  $0 \leq h \leq \infty$ . According to the Eq. (3-50a) and Eq. (3-50b) in Chapter 3, it can be proved that  $\sigma_{on}^2 \geq \sigma_{off}^2$ . In this dissertation, the equal gain combining with the envelop detection is used.

Using the Chernov Bound [1] for the AWGN system and Appendix G, the following inequalities are given as

$$\begin{aligned}
& P \left[ n_2 \leq \frac{E_s \mathcal{R}GMAg}{N_t} h + n_1 \mid \mathbf{S}_1 \text{ sent}, n_1 = n_{on}, h \right] \\
&= \int_{-\left| \frac{E_s \mathcal{R}GMAg}{N_t} h + n_{on} \right|}^{\left| \frac{E_s \mathcal{R}GMAg}{N_t} h + n_{on} \right|} \frac{1}{\sqrt{2\pi}} e^{-\frac{n_2^2}{2}} \cdot dn_2 \\
&= 1 - 2Q \left( \left| \frac{E_s \mathcal{R}MAG}{N_t \sigma_{off}} h + \frac{n_{on}}{\sigma_{off}} \right| \right) \\
&\geq 1 - e^{-\frac{\left( \frac{E_s \mathcal{R}MAG}{N_t \sigma_{off}} h + \frac{n_{on}}{\sigma_{off}} \right)^2}{2}}
\end{aligned} \tag{4-23}$$

and

$$0 \leq \left\{ 1 - \left[ 1 - 2Q \left( \frac{E_s \mathcal{R}MAG}{N_t \sigma_{off}} h + \frac{n_{on}}{\sigma_{off}} \right) \right]^{(L-1)} \right\} \leq \left\{ 1 - \left[ 1 - e^{-\frac{\left( \frac{E_s \mathcal{R}MAG}{N_t \sigma_{off}} h + \frac{n_{on}}{\sigma_{off}} \right)^2}{2}} \right]^{(L-1)} \right\} \leq 1 \tag{4-24}$$

Using the calculation in Appendix G, the symbol error probability  $P_s(E)$  of this Q-ary PPM in Eq. (4-20) is given as

$$\begin{aligned}
P_s(E) &= P_{s|s_1} = 1 - P_c \\
&= \int_0^\infty \left\{ \int_{-\infty}^\infty \left\{ 1 - \left[ 1 - 2Q \left( \left| \frac{E_s \mathcal{R}MAG}{N_t \sigma_{off}} h + \frac{n_{on}}{\sigma_{off}} \right| \right) \right]^{(L-1)} \right\} p_{n_{on}}(n_{on}) dn_{on} \right\} p_h(h) dh
\end{aligned}$$

$$\leq \int_0^\infty \left\{ \int_{-\infty}^\infty \left\{ 1 - \left[ 1 - e^{-\frac{(E_s \mathcal{R}MAG_{h+n_{on}})^2}{2N_t \sigma_{off}^2}} \right]^{(L-1)} \right\} p_{n_{on}}(n_{on}) dn_{on} \right\} p_h(h) dh$$
(4-25)

According to Appendix H, the symbol error probability  $P_s(E)$  is

$$P_s(E) \leq \sum_{k=1}^{L-1} \frac{C_{L-1}^k (-1)^{k+1} \sigma_{off}^k}{\sqrt{k\sigma_{on}^2 + \sigma_{off}^2}} \int_0^\infty e^{-\frac{(E_s \mathcal{R}MAG)^2 h^2 k}{2N_t^2 (k\sigma_{on}^2 + \sigma_{off}^2)}} p_h(h) dh$$
(4-26)

The conditional symbol probability is obtained as

$$P_s(E|h) \leq \sum_{k=1}^{L-1} \frac{C_{L-1}^k (-1)^{k+1} \sigma_{off}^k}{\sqrt{k\sigma_{on}^2 + \sigma_{off}^2}} e^{-\frac{k(E_s \mathcal{R}MAG)^2 h^2}{2N_t^2 (k\sigma_{on}^2 + \sigma_{off}^2)}}$$
(4-27)

Letting  $k_l = \frac{k(E_s \mathcal{R}MAG)^2}{2N_t^2 (k\sigma_{on}^2 + \sigma_{off}^2)}$ , Eq. (4-27) can be represented as

$$P_s(E|h) \leq \sum_{k=1}^{L-1} \frac{C_{L-1}^k (-1)^{k+1} \sigma_{off}^k}{\sqrt{k\sigma_{on}^2 + \sigma_{off}^2}} e^{-k_l h^2}$$
(4-28)

#### 4.1.2 Symbol Detection of Transmitted Matrices

When the MIMO PPM symbol matrices are transmitted, the transmission is implemented as the one shown in Fig. 3.3 of Chapter 3. The matrix expressions of the transmission can be represented as

$$\mathbf{Y} = \frac{\mathcal{R}MAE_s g}{N_t} \cdot \mathbf{H} \cdot \mathbf{S} + \mathbf{N}$$
(4-29)

$$\begin{bmatrix} y_{11} & y_{12} & \dots & y_{1N_L} \\ y_{21} & y_{22} & \dots & y_{2N_L} \\ \vdots & \vdots & \ddots & \vdots \\ y_{N_r,1} & y_{N_r,2} & \dots & y_{N_r,N_L} \end{bmatrix} = \frac{\mathcal{RMAE}_{sg}}{N_t} \begin{bmatrix} h_{11} & h_{12} & \dots & h_{1N_t} \\ h_{21} & h_{22} & \dots & h_{2N_t} \\ \vdots & \vdots & \ddots & \vdots \\ h_{N_r,1} & h_{N_r,2} & \dots & h_{N_r,N_t} \end{bmatrix} \begin{bmatrix} s_{11} & s_{12} & \dots & s_{1N_L} \\ s_{21} & s_{22} & \dots & s_{2N_L} \\ \vdots & \vdots & \ddots & \vdots \\ s_{N_t,1} & s_{N_t,2} & \dots & s_{N_t,N_L} \end{bmatrix} + \begin{bmatrix} n_{11} & n_{12} & \dots & n_{1N_L} \\ n_{21} & n_{22} & \dots & n_{2N_L} \\ \vdots & \vdots & \ddots & \vdots \\ n_{N_r,1} & n_{N_r,2} & \dots & n_{N_r,N_L} \end{bmatrix} \quad (4-30)$$

There are  $N$  PPM symbols included in a transmitted matrix and these  $N$  PPM symbols are independent. For the calculations of this chapter, the matrix is coded by simple repetition coding and post-detection EGC with envelope detection is implemented at the receiver. These  $N$  PPM symbols in the receiving matrix at the receiver are decoded together at the same time and then demodulated. The average symbol error probability of one PPM matrix  $P_{e\_matrix}(E)$  can be averaged on the condition of the receiver SNR matrix  $\Gamma$ . In Appendix F, it is proved that  $P_{e\_matrix}(E)$  can also be averaged on the condition of the channel gain matrix  $\mathbf{H}$ .

At the APD-based receiver, the post-detection EGC with envelope detection is used to process the received PPM matrices. For each received PPM symbol in the matrix, the EGC receiver processes the  $N_r$  received replicas from the branches, equally weights them, and then sums them for the decision detection. Hence for the  $L$ -branch receiver, the fading SNR for one branch takes the form [2]

$$\gamma = \left[ \left( \frac{1}{\sqrt{L}} \right) \sum_{l=1}^L \sqrt{\gamma_l} \right]^2 \quad (4-31)$$

In this case, it is more convenient to deal with the square root of the fading SNR for one branch [2]

$$x = \sqrt{\gamma} = \left( \frac{1}{\sqrt{L}} \right) \sum_{l=1}^L \sqrt{\gamma_l} = \left( \frac{1}{\sqrt{L}} \right) \sum_{l=1}^L x_l \quad (4-32)$$

If the channels are assumed independent, this characteristic function (CHF) takes on a product form, namely [2]

$$F_x(j\omega) = \prod_{l=1}^L F_{x_l} \left( \frac{j\omega}{\sqrt{L}} \right) \quad (4-33)$$

Hence for each PPM symbol, the instantaneous received signal  $y$  of a 1 pulse slot after the envelope post-detection EGC is

$$y = \sum_{l=1}^{N_r} y_j = \sum_{l=1}^{N_r} \sum_{i=1}^{N_t} \frac{\mathcal{R}MAE_s g}{N_t} h_{il} \cdot s_i + \sum_{l=1}^{N_r} n_l \quad (4-34)$$

where  $n_l$  ( $1 \leq l \leq N_r$ ) is the i.i.d Gaussian-distributed random variables with the zero mean and the variance  $\sigma_{on}^2$ , i.e.  $n_l \sim N(0, \sigma_{on}^2)$ . The signal to noise ratio for a 1 pulse after the post-detection EGC can be represented as

$$\gamma_{EGC} = \frac{\mathcal{R}^2 M^2 A^2 E_s^2 g^2}{N_t^2 \sigma_{on}^2} \left( \sum_{l=1}^{N_r} \sum_{i=1}^{N_t} h_{il} \right)^2 \quad (4-35)$$

where  $\sigma_{on}^2$  is given in Eq. (3-50a). For the MIMO FSO systems using the post-detection EGC with the envelope detection,  $\mathbf{\Gamma}_{EGC}$  is the SNR matrix for one received matrix,  $\mathbf{\Gamma}_{EGC} = [\boldsymbol{\gamma}_1, \boldsymbol{\gamma}_2 \dots \boldsymbol{\gamma}_m \dots \boldsymbol{\gamma}_N]$  ( $1 \leq m \leq N$ ). If  $\mathcal{S}_1$  PPM symbol is transmitted,  $\boldsymbol{\gamma}_m$  is the SNR vector given as

$$\boldsymbol{\gamma}_m = \left[ \frac{\mathcal{R}^2 M^2 A^2 E_s^2 g^2}{N_t^2 \sigma_{on}^2} h^2, 0, 0 \dots 0 \right] \quad (4-36)$$

where  $\mathbf{h}$  is the channel gain vector and can be represented as

$$\mathbf{h} = [h_{11} \ h_{12} \dots h_{1N_r}; h_{21} \ h_{22} \dots h_{2N_r}; \dots \dots h_{N_t1} \ h_{N_t2} \dots h_{N_tN_r}] \quad (4-37)$$

The instantaneous channel gain  $h$  for one 1 pulse is

$$h = \sum_{l=1}^{N_r} \sum_{i=1}^{N_t} h_{il}$$

(4-38)

where  $h_{il}$  is the channel gain of the  $il$ th path,  $\gamma$  is the SNR for one 1 pulse given as

$$\gamma = \frac{\frac{\mathcal{R}^2 M^2 A^2 E_s^2 g^2}{N_t^2} \left( \sum_{l=1}^{N_r} \sum_{i=1}^{N_t} h_{il} \right)^2}{\sigma_{on}^2} = \frac{\mathcal{R}^2 M^2 A^2 E_s^2 g^2 h^2}{N_t^2 \sigma_{on}^2}$$

(4-39)

where  $\sigma_{on}^2$  is given in Eq. (3-50a). For one received PPM symbol with  $L$  slots, the

decision variable  $r_1$  is

$$\begin{aligned} r_1 &= \sum_{l=1}^{N_r} y_l = \sum_{l=1}^{N_r} \sum_{i=1}^{N_t} \frac{E_s \mathcal{R} M A g s_i}{N_t} h_{il} + \sum_{l=1}^{N_r} n_l \\ &= \frac{E_s \mathcal{R} M A g s_i}{N_t} \sum_{l=1}^{N_r} \sum_{i=1}^{N_t} h_{il} + \sum_{l=1}^{N_r} n_l \\ &= k_t h + \sum_{l=1}^{N_r} n_l \end{aligned}$$

(4-40)

where  $k_t = \frac{E_s \mathcal{R} M A g}{N_t}$  and  $s_i = 1$ .

For the block fading channel assumption of the MIMO FSO systems, the channel gain vector  $\mathbf{h}$  for one PPM symbol is nearly constant. For one receiving matrix, the signals of  $N$  received PPM symbols are i.i.d random variables and their symbol error probabilities are independent. For one  $(N_r \times NL)$  received PPM matrix, the symbol error probability for the matrix  $P_{e\_matrix}(E)$  can be represented on condition of the SNR matrix  $\mathbf{\Gamma} = [\boldsymbol{\gamma}_1, \boldsymbol{\gamma}_2 \dots \dots \boldsymbol{\gamma}_N]$ .

$$\begin{aligned}
P_{e\_matrix}(E) &= P_{rob}[\mathbf{e} < \mathbf{e}_{th}] \\
&= \int_{-\infty}^{\infty} P[\mathbf{e} < \mathbf{e}_{th} | \mathbf{\Gamma}] \cdot p_{\mathbf{\Gamma}}(\mathbf{\Gamma}) \cdot d\mathbf{\Gamma} \\
&= \int_{-\infty}^{\infty} \{P_{e_1}[\mathbf{e}_1 | \boldsymbol{\gamma}_1] P_{e_2}[\mathbf{e}_2 | \boldsymbol{\gamma}_2] \dots P_{e_N}[\mathbf{e}_N | \boldsymbol{\gamma}_N]\} p_{\mathbf{\Gamma}}(\mathbf{\Gamma}) \cdot d\mathbf{\Gamma} \\
&= \int_{-\infty}^{\infty} P_{e_1}[\mathbf{e}_1 | \boldsymbol{\gamma}_1] p_{\boldsymbol{\gamma}_1}(\boldsymbol{\gamma}_1) d\boldsymbol{\gamma}_1 \int_{-\infty}^{\infty} P_{e_2}[\mathbf{e}_2 | \boldsymbol{\gamma}_2] p_{\boldsymbol{\gamma}_2}(\boldsymbol{\gamma}_2) d\boldsymbol{\gamma}_2 \dots \int_{-\infty}^{\infty} P_{e_N}[\mathbf{e}_N | \boldsymbol{\gamma}_N] p_{\boldsymbol{\gamma}_N}(\boldsymbol{\gamma}_N) d\boldsymbol{\gamma}_N \\
&= \prod_{m=1}^N \left[ \int_{-\infty}^{\infty} P_{e_m}[\mathbf{e}_m | \boldsymbol{\gamma}] \cdot p_{\boldsymbol{\gamma}}(\boldsymbol{\gamma}) \cdot d\boldsymbol{\gamma} \right] \\
&= \prod_{m=1}^N \left[ \int_{-\infty}^{\infty} P_{e_m}[\mathbf{e}_m | \mathbf{h}] \cdot p_{\mathbf{h}}(\mathbf{h}) \cdot d\mathbf{h} \right]
\end{aligned} \tag{4-41}$$

where  $\mathbf{e} = (\mathbf{e}_1, \mathbf{e}_2, \dots, \mathbf{e}_m, \dots, \mathbf{e}_N)$  is the error matrix for the transmitted matrix with the  $N$  PPM symbols,  $\mathbf{e}_1, \mathbf{e}_2, \dots, \mathbf{e}_m, \dots, \mathbf{e}_N$  are i.i.d random variable vectors and  $\mathbf{e}_m$  ( $1 \leq m \leq N$ ) is the error vector for one PPM symbol. For the optical wireless communication with PPM, the channel gain  $h$  is nonnegative in the range of  $0 \leq h \leq \infty$ . The signal to noise ratio  $\gamma$  is nonnegative in the range of  $0 \leq \gamma \leq \infty$ .

For one PPM symbol detection, the simplified decision variables are shown in Eq. (4-13a) and Eq. (4-13b). The channel gain  $h$  only impacts the 1 pulse slot and the decision variable  $R_1$  in Eq. (4-13a). In mathematical terms, letting  $R_1|h$  denotes the decision variable on the condition of the channel gain  $h$ . The decision variable  $R_1|h$  can take on positive or negative values whereas the instantaneous channel gain  $h$  is restricted to only nonnegative values. Since  $h = \sum_{l=1}^{N_r} \sum_{i=1}^{N_t} h_{il}$  and  $h_{il} \geq 0$ ,  $h$  is nonnegative  $h \geq 0$ . In addition, the PPM symbols are the positive data bits. In practice, the channel gain should be nonnegative in order to ensure the correct

transmission. The PDF of  $p_{h_{il}}(h_{il})$  is real and nonnegative and is given in Eq. (3-62). The PDF  $p_h(h)$  of  $h$  can be calculated by using  $p_{h_{il}}(h_{il})$ . The conditional probability  $P_{e_m}(\mathbf{e}_m | \mathbf{h})$  for one PPM symbol can be represented on the condition of the instantaneous channel gain  $h$  for one 1 pulse as shown in Eq. (4-41). The integral limit of  $h$  is from zero to infinity. The symbol error probability for one PPM symbol is given in Eq. (4-20) and the conditional symbol error probability for one PPM symbol is given in Eq. (4-22). By using the binomial expansion and Appendix H, Eq. (4-41) can be represented as

$$\begin{aligned}
 P_{e\_matrix}(E) &= \prod_{m=1}^N \left[ \int_0^\infty \int_{-\infty}^\infty \left\{ \sum_{k=1}^{L-1} C_{L-1}^k (-1)^{k+1} \left[ Q \left( \frac{E_s \mathcal{R}MAG}{N_t \sigma_{\text{off}}} h + \frac{n_{\text{on}}}{\sigma_{\text{off}}} \right) \right]^k \right\} p_{n_{\text{on}}}(n_{\text{on}}) dn_{\text{on}} p_h(h) dh \right] \\
 &\quad (4-42)
 \end{aligned}$$

As there is a power function of the Gaussian Q-function in Eq. (4-42), it is difficult to express Eq. (4-42) exactly. By using the Chernov Bound [1] for the AWGN system, and the calculation in Appendix H, Eq. (4-42) can be represented as

$$\begin{aligned}
 P_{e\_matrix}(E) &\leq \prod_{m=1}^N \left[ \sum_{k=1}^{L-1} \frac{C_{L-1}^k (-1)^{k+1} \sigma_{\text{off}}}{\sqrt{k \sigma_{\text{on}}^2 + \sigma_{\text{off}}^2}} \int_0^\infty e^{-\frac{k(E_s \mathcal{R}MAG)^2 h^2}{2N_t^2(k \sigma_{\text{on}}^2 + \sigma_{\text{off}}^2)}} p_h(h) dh \right] \\
 &= \prod_{m=1}^N \left[ \sum_{k=1}^{L-1} \frac{C_{L-1}^k (-1)^{k+1} \sigma_{\text{off}}}{\sqrt{k \sigma_{\text{on}}^2 + \sigma_{\text{off}}^2}} \int_0^\infty e^{-k_l h^2} p_h(h) dh \right] \\
 &\quad (4-43)
 \end{aligned}$$

where  $k_l = \frac{k(E_s \mathcal{R}MAG)^2}{2N_t^2(k \sigma_{\text{on}}^2 + \sigma_{\text{off}}^2)}$  and  $h$  is given in Eq. (4-38). By using the variable

substitution  $t = -h$ , Eq. (4-43) is modified as

$$P_{e\_matrix}(E) \leq \prod_{m=1}^N \left[ \sum_{k=1}^{L-1} \frac{C_{L-1}^k (-1)^{k+1} \sigma_{\text{off}}}{\sqrt{k\sigma_{\text{on}}^2 + \sigma_{\text{off}}^2}} \int_{-\infty}^0 e^{-\frac{k(E_s \mathcal{R}MAg)^2 t^2}{2N_t^2(k\sigma_{\text{on}}^2 + \sigma_{\text{off}}^2)}} p_h(-t) dt \right] \quad (4-44)$$

### 4.1.3 Symbol Error Probability Calculation of Transmitted Matrices

We use the function  $f(t)$  to represent the following part in Eq. (4-44)

$$f(t) = \exp \left[ -\frac{k(E_s \mathcal{R}MAg)^2 t^2}{2N_t^2(k\sigma_{\text{on}}^2 + \sigma_{\text{off}}^2)} \right] \quad (4-45a)$$

The function  $f(t)$  is an even function for . The integral in Eq. (4-44) is an integral of the function  $f(t)p_h(-t)$  given as

$$I = \int_{-\infty}^0 e^{-\frac{k(E_s \mathcal{R}MAg)^2 t^2}{2N_t^2(k\sigma_{\text{on}}^2 + \sigma_{\text{off}}^2)}} \cdot p_h(-t) dt \quad (4-45b)$$

Since the integral limit is from negative infinity to zero, this integral  $I$  can also be considered as a probability of the variable  $t$ , evaluated at  $t_{th} = 0$  as

$$I = P_{rob}[-\infty < t < t_{th}] = \int_{-\infty}^{t_{th}} f(t) p_h(-t) dt = \int_{-\infty}^0 f(t) p_h(-t) dt \quad (4-45c)$$

The PDF of  $t$  is

$$p_t(t) = p_h(h)_{|h=-t} \left| \frac{dh}{dt} \right| = p_h(-t) = p_h(h) \quad (4-46)$$

Substituting Eq. (4-46) into Eq. (4-45b), the integral  $I$  is

$$I = \int_{-\infty}^0 f(t) [p_t(t)] dt \quad (4-47)$$

According to Appendix F, the PDF  $p_h(h)$  is real and nonnegative,  $p_h(h) \geq 0, h \geq 0$ . As shown in Eq. (3-62), the PDF of  $p_{h_{ij}}(h_{ij})$  is real and nonnegative and the characteristic function of the PDF  $p_{h_{ij}}(h_{ij})$  exists. The PDF  $p_h(h)$  of  $h$  can be calculated by using the characteristic function of  $p_{h_{il}}(h_{il})$ .  $F_p(\omega)$  represents the characteristic function of  $p_h(h)$  and  $F_{p_h}(\omega)$  represents the characteristic function of  $p_{h_{il}}(h_{il})$ . The characteristic function of  $p_h(h)$  and the inverse integral can be represented as [3]

$$F_p(\omega) = \int_{-\infty}^{\infty} p_h(h) e^{j\omega h} dh \quad (4-48a)$$

$$p_h(h) = \frac{1}{2\pi} \int_{-\infty}^{\infty} F_p(\omega) e^{-j\omega h} d\omega \quad (4-48b)$$

$$e^{j\omega h} = e^{j\omega(-t)} \quad (0 \leq h \leq \infty, -\infty \leq t \leq 0) \quad (4-48c)$$

$$p_t(t) = p_h(h)|_{h=-t} \left| \frac{dh}{dt} \right| = p_h(-t) = p_h(h) \quad (4-48d)$$

Further the integral in Eq. (4-47) can be represented as

$$\begin{aligned} I &= \int_{-\infty}^0 f(t) [p_t(t)] dt \\ &= \int_{\infty}^0 \{-f(t)[p_t(t)]\} d(-t) \\ &= \int_0^{\infty} f(h) p_h(h) dh \\ &= \int_0^{\infty} f(h) \left[ \frac{1}{2\pi} \int_{-\infty}^{\infty} F_p(\omega) e^{-j\omega h} d\omega \right] dh \end{aligned}$$

$$\begin{aligned}
&= \frac{1}{2\pi} \int_{-\infty}^{\infty} F_p(\omega) \left[ \int_0^{\infty} f(h) e^{-j\omega h} dh \right] d\omega \\
&= \frac{1}{2\pi} \int_{-\infty}^{\infty} \{ \text{Real}[F_p(\omega)F_f(\omega)] + j\text{Imag}[F_p(\omega)F_f(\omega)] \} d\omega
\end{aligned} \tag{4-49}$$

where  $\text{Real}[F_p(\omega)F_f(\omega)]$  is the real part of  $F_p(\omega)F_f(\omega)$  and  $\text{Imag}[F_p(\omega)F_f(\omega)]$  is the imaginary part of  $F_p(\omega)F_f(\omega)$ . For Eq. (4-49), the integral of the real part,  $\text{Real}[F_p(\omega)F_f(\omega)]$ , is the error probability and the integral of the imaginary part,  $\text{Imag}[F_p(\omega)F_f(\omega)]$ , is zero. If  $F_f(\omega) = \int_0^{\infty} f(h) e^{-j\omega h} dh$  is integrated directly as shown in Appendix I, it can be obtained as

$$F_f(\omega) = e^{\frac{-\omega^2}{4k_l}} \sqrt{\frac{\pi}{k_l}} Q\left(\frac{j\omega}{\sqrt{2k_l}}\right) \tag{4-50}$$

where  $k_l = \frac{k(E_s \text{RMAG})^2}{2N_t^2(k\sigma_{\text{on}}^2 + \sigma_{\text{off}}^2)}$ . There is a Gaussian probability function, i.e. Q function, with the complex variable in Eq. (4-50). This causes the difficulty in obtaining further integration of  $\omega$  directly from negative infinity to infinity in the complex domain. The indirect complex integration method for the integral  $I$  is employed here. As the symbol error probability in Eq. (4-43) and Eq. (4-44) is real and nonnegative, the integral  $I$  in Eq. (4-49) is a part of the error probability and can be represented as

$$\begin{aligned}
I &= \text{Real} \left[ \frac{1}{2\pi} \int_{-\infty}^{\infty} F_p(\omega) F_f(\omega) d\omega \right] \\
&= \frac{1}{2\pi} \int_{-\infty}^{\infty} \text{Real}[F_p(\omega)F_f(\omega)] d\omega \\
&= \frac{1}{2\pi} \int_{-\infty}^{\infty} \{ \text{Real}[F_p(\omega)]\text{Real}[F_f(\omega)] - \text{Imag}[F_p(\omega)]\text{Imag}[F_f(\omega)] \} d\omega
\end{aligned}$$

(4-51)

where  $F_f(\omega) = \int_0^\infty f(h)e^{-j\omega h} dh = \int_0^\infty e^{-k_l h^2} e^{-j\omega h} dh$ .

$$\text{Real}[F_f(\omega)] = \int_0^\infty f(h) \cos(\omega h) dh = \int_0^\infty [e^{-k_l h^2} \cos(\omega h)] dh \quad (4-52a)$$

$$\text{Imag}[F_f(\omega)] = \int_0^\infty f(h) \sin(\omega h) dh = \int_0^\infty [-e^{-k_l h^2} \sin(\omega h)] dh \quad (4-52b)$$

$$\text{where } k_l = \frac{k(E_s \mathcal{R}MAG)^2}{2N_t^2(k\sigma_{on}^2 + \sigma_{off}^2)}$$

For MIMO FSO systems, the  $N_t$  lasers transmit the PPM symbol streams through the  $N_t \times N_r$  different paths as shown in Fig. 3.1. From each path, the received laser intensity and the average received photon number  $\lambda_{s\ il}$  are lognormal-distributed random variables. We have obtained the PDF  $p_{h_{il}}(h_{il})$  of the  $il$ th path channel gain  $h_{il}$  in Eq. (3-62). The PPM symbols are the positive data bits. The signal to noise ratio  $\gamma_{il}$  is restricted to only nonnegative values. The channel gain  $h_{il}$  of each path is also a nonnegative value. The decision variable  $r_1$  for a slot can take on positive or negative values, where  $r_1 = \frac{E_s \mathcal{R}MAG}{N_t} h + n_{on}$  and  $h = \sum_{l=1}^{N_r} \sum_{i=1}^{N_t} h_{il}$ . For each  $h_{il}$ , the PDF  $p_{h_{il}}(h_{il})$  is given in Eq. (3-62)

$$p_{h_{il}}(h_{il}) = \sum_{\substack{u=-N_u \\ u \neq 0}}^{N_u} K_{w_u} K_{x_u} \frac{\mathcal{R}M E_s g}{q N_t} \frac{\exp \left\{ - \frac{\left( \frac{\mathcal{R}E_s g}{q N_t} h_{il} - K_{x_u} \right)^2}{2 \left[ \frac{(F-1)\mathcal{R}E_s g}{q N_t} h_{il} + K_{x_u} \right]} \right\}}{\left[ \frac{(F-1)\mathcal{R}E_s g}{q N_t} h_{il} + K_{x_u} \right]^{\frac{3}{2}}} \quad (4-53a)$$

In the above equation, the variable substitution is made

$$K_k = \frac{\Re E_s g}{q N_t} = \frac{\Re E_s 2A_r \alpha}{q N_t A_b} \quad (4-53b)$$

Then the equation is

$$p_{h_{il}}(h_{il}) = \sum_{\substack{u=-N_u \\ u \neq 0}}^{N_u} K_{w_u} K_{x_u} K_k M \frac{\exp\left\{-\frac{(K_k h_{il} - K_{x_u})^2}{2[(F-1)K_k h_{il} + K_{x_u}]}\right\}}{[(F-1)K_k h_{il} + K_{x_u}]^{\frac{3}{2}}} \quad (4-54)$$

The channel gain  $h_{il} \geq 0$  is real and in the range from zero to infinity, the variable  $K_{x_u} = \eta \frac{E_s 2A_r \alpha}{h\nu A_b N_t} e^{m_\ell} e^{\sqrt{2} \sigma_\ell x_u} \geq 0$  and  $\frac{(F-1)\Re E_s g}{q N_t} h_{il} + K_{x_u} \geq 0$ .  $p_{h_{il}}(h_{il})$  is real and nonnegative. The PDF  $p_{h_{il}}(h_{il})$  is real and nonnegative  $p_{h_{il}}(h_{il}) \geq 0$ . The characteristic function  $F_{p_h}(\omega)$  of  $p_{h_{il}}(h_{il})$  exists when  $h_{il} \geq 0$  and the characteristic function  $F_p(\omega)$  of  $p_h(h)$  exists as

$$\begin{aligned} F_{p_h}(\omega) &= \int_{-\infty}^{\infty} p_{h_{il}}(h_{il}) e^{j\omega h_{il}} dh_{il} \\ &= \sum_{\substack{u=-N_u \\ u \neq 0}}^{N_u} K_{w_u} K_{x_u} K_k M \int_0^{\infty} e^{j\omega h_{il}} \frac{\exp\left\{-\frac{(K_k h_{il} - K_{x_u})^2}{2[(F-1)K_k h_{il} + K_{x_u}]}\right\}}{[(F-1)K_k h_{il} + K_{x_u}]^{\frac{3}{2}}} dh_{il} \end{aligned} \quad (4-55)$$

According to the calculation in Appendix J, Eq. (4-55) can be modified to

$$\begin{aligned} F_{p_h}(\omega) &= \sum_{\substack{u=-N_u \\ u \neq 0}}^{N_u} K_{w_u} K_{x_u} K_k M \int_0^{\infty} e^{-h_{il}} [(F-1)K_k h_{il} + K_{x_u}]^{\left(-\frac{3}{2}\right)} \\ &\quad \exp\left\{h_{il} - \frac{K_k (h_{il} - e^{m_\ell} e^{\sqrt{2} \sigma_\ell x_u})^2}{2[(F-1)h_{il} + e^{m_\ell} e^{\sqrt{2} \sigma_\ell x_u}]} + j\omega h_{il}\right\} dh_{il} \end{aligned} \quad (4-56a)$$

where

$$K_{w_u} = w_u \left( \frac{F}{\sqrt{2} \pi M} \right) \quad (4-56b)$$

$$\begin{aligned} K_{x_u} &= \eta \exp \left[ \sqrt{2} \sigma_\ell x_u - \ln \left( \frac{A_b h\nu N_t}{2A_r \alpha E_s} \right) + m_\ell \right] \\ &= \eta \frac{E_s 2A_r \alpha}{h\nu A_b N_t} e^{m_\ell} e^{\sqrt{2} \sigma_\ell x_u} \\ &= K_k e^{m_\ell} e^{\sqrt{2} \sigma_\ell x_u} \end{aligned} \quad (4-56c)$$

$$K_k = \frac{\mathcal{R}E_s g}{qN_t} = \frac{\mathcal{R}E_s 2A_r \alpha}{qN_t A_b} \quad (4-56d)$$

$$\bar{\lambda}_s = \frac{2A_r \alpha E_s}{A_b h\nu N_t} \quad (4-56e)$$

According to the Gaussian Laguerre Integration rule [4], the integral can be given by the following expression

$$\int_0^\infty e^{-x} g(x) dx \approx \sum_{v=1}^{N_v} w_v g(x_v) \quad (4-57)$$

where  $\{x_v\}$  and  $\{w_v\}$  ( $v = 1, 2 \dots N_v - 1, N_v$ ) are the zeros and the weight factors of the Laguerre polynomial [4], respectively. This estimation process yields fairly accurate results for values of  $N_v = 15$ . Since  $\{x_v\}$  and  $\{w_v\}$  are well-tabulated in reference [4], a tractable means of estimating performance can be obtained. By selecting the suitable  $N_v$ , the calculating error can be very small. Eq. (4-55) can be calculated by the Gaussian Laguerre Integration rule and  $g(x)$  represents the following part in Eq. (4-58).

$$\begin{aligned} g(h_{il}) &= [(F - 1)K_k h_{il} + K_{x_u}]^{\left(-\frac{3}{2}\right)} \\ &\quad \exp \left\{ h_{il} - \frac{K_k \left( h_{il} - e^{m_\ell} e^{\sqrt{2} \sigma_\ell x_u} \right)^2}{2[(F - 1)h_{il} + e^{m_\ell} e^{\sqrt{2} \sigma_\ell x_u}]} + j\omega h_{il} \right\} \end{aligned} \quad (4-58)$$

The characteristic function is

$$F_{p_h}(\omega) = \sum_{\substack{u=-N_u \\ u \neq 0}}^{N_u} \sum_{v=1}^{N_v} K_{W_u} K_{x_u} K_k M_{w_v} [(F-1)K_k x_v + K_{x_u}]^{\left(-\frac{3}{2}\right)} \\ \exp \left\{ x_v - \frac{K_k (x_v - e^{m_\ell} e^{\sqrt{2} \sigma_\ell x_u})^2}{2[(F-1)x_v + e^{m_\ell} e^{\sqrt{2} \sigma_\ell x_u}]} + j\omega x_v \right\} \quad (4-59)$$

Because the real nonnegative random variable  $h$  is the sum of the real random variables  $h_{il}$  ( $h_{il} \geq 0$ ), the PDF  $p_h(h)$  is the convolution of the PDFs of each path,  $p_{h_{il}}(h_{il})$  ( $1 \leq i \leq N_t$ ,  $1 \leq l \leq N_r$ ).  $p_h(h)$  is real and nonnegative (Appendix G).

$$p_h(h) = p_{h_{11}}(h_{11}) * p_{h_{12}}(h_{12}) \dots * p_{h_{21}}(h_{21}) * p_{h_{22}}(h_{22}) \dots * p_{h_{N_t N_r}}(h_{N_t N_r}) \quad (4-60)$$

Now the characteristic function  $F_p(\omega)$  of  $p_h(h)$  is the product of the characteristic function  $F_{p_h}(\omega)$  of  $p_{h_{il}}(h_{il})$ . After the detailed calculation in Appendix K,  $F_p(\omega)$  can be represented as

$$F_p(\omega) = \int_{-\infty}^{\infty} p_h(h) e^{j\omega h} dh \\ = \sum_{v_1=1}^{N_v} \sum_{v_2=1}^{N_v} \dots \sum_{v_{N_t N_r}=1}^{N_v} e^{(x_{v_1} + x_{v_2} + \dots + x_{v_{N_t N_r}}) j\omega} \left[ \frac{F e^{m_\ell}}{\pi} \left( \sqrt{\frac{\mathcal{R}E_s A_r \alpha}{q N_t A_b}} \right) \right]^{N_t N_r} \\ \sum_{\substack{u_1=-N_u \\ u_1 \neq 0}}^{N_u} \sum_{\substack{u_2=-N_u \\ u_2 \neq 0}}^{N_u} \dots \sum_{\substack{u_{N_t N_r}=-N_u \\ u_{N_t N_r} \neq 0}}^{N_u} W_{u_1} W_{u_2} \dots W_{u_{N_t N_r}} W_{v_1} W_{v_2} \dots W_{v_{N_t N_r}} \\ \exp \left[ \sqrt{2} \sigma_\ell (x_{u_1} + x_{u_2} \dots + x_{u_{N_t N_r}}) + (x_{v_1} + x_{v_2} \dots + x_{v_{N_t N_r}}) \right] \\ \left[ (F-1)x_{v_1} + e^{m_\ell} e^{\sqrt{2} \sigma_\ell x_{u_1}} \right]^{\left(-\frac{3}{2}\right)} \left[ (F-1)x_{v_2} + e^{m_\ell} e^{\sqrt{2} \sigma_\ell x_{u_2}} \right]^{\left(-\frac{3}{2}\right)} \dots$$

$$\begin{aligned}
& \left[ (F-1)x_{v_{N_t N_r}} + e^{m_\ell} e^{\sqrt{2} \sigma_\ell x_{u_{N_t N_r}}} \right]^{(-\frac{3}{2})} \\
& \exp \left\{ \left( -\frac{K_k}{2} \right) \left[ \frac{(x_{v_1} - e^{m_\ell} e^{\sqrt{2} \sigma_\ell x_{u_1}})^2}{[(F-1)x_{v_1} + e^{m_\ell} e^{\sqrt{2} \sigma_\ell x_{u_1}}]} + \frac{(x_{v_2} - e^{m_\ell} e^{\sqrt{2} \sigma_\ell x_{u_2}})^2}{[(F-1)x_{v_2} + e^{m_\ell} e^{\sqrt{2} \sigma_\ell x_{u_2}}]} \dots \dots \right. \right. \\
& \quad \left. \left. + \frac{(x_{v_{N_t N_r}} - e^{m_\ell} e^{\sqrt{2} \sigma_\ell x_{u_{N_t N_r}}})^2}{[(F-1)x_{v_{N_t N_r}} + e^{m_\ell} e^{\sqrt{2} \sigma_\ell x_{u_{N_t N_r}}]} \right] \right\} \\
& = \sum_{v_1=1}^{N_v} \sum_{v_2=1}^{N_v} \dots \sum_{v_{N_t N_r}=1}^{N_v} K_0 K_f e^{K_d j \omega}
\end{aligned} \tag{4-61}$$

where

$$K_0 = \left( \frac{F e^{m_\ell}}{\pi} \sqrt{\frac{\mathcal{R}E_s A_r \alpha}{q N_t A_b}} \right)^{N_t N_r} \tag{4-62}$$

$$K_f = \sum_{\substack{u_1=-N_u \\ u_1 \neq 0}}^{N_u} \sum_{\substack{u_2=-N_u \\ u_2 \neq 0}}^{N_u} \dots \sum_{\substack{u_{N_t N_r}=-N_u \\ u_{N_t N_r} \neq 0}}^{N_u} W_{u_1} W_{u_2} \dots W_{u_{N_t N_r}} W_{v_1} W_{v_2} \dots W_{v_{N_t N_r}}$$

$$\exp \left[ \sqrt{2} \sigma_\ell (x_{u_1} + x_{u_2} + \dots \dots + x_{u_{N_t N_r}}) + (x_{v_1} + x_{v_2} + \dots + x_{v_{N_t N_r}}) \right]$$

$$\left[ (F-1)x_{v_1} + e^{m_\ell} e^{\sqrt{2} \sigma_\ell x_{u_1}} \right]^{(-\frac{3}{2})} \left[ (F-1)x_{v_2} + e^{m_\ell} e^{\sqrt{2} \sigma_\ell x_{u_2}} \right]^{(-\frac{3}{2})} \dots \dots$$

$$\left[ (F-1)x_{v_{N_t N_r}} + e^{m_\ell} e^{\sqrt{2} \sigma_\ell x_{u_{N_t N_r}}} \right]^{(-\frac{3}{2})}$$

$$\exp \left\{ \left( -\frac{K_k}{2} \right) \left[ \frac{\left( x_{v_1} - e^{m_\ell} e^{\sqrt{2} \sigma_\ell x_{u_1}} \right)^2}{\left[ (F-1)x_{v_1} + e^{m_\ell} e^{\sqrt{2} \sigma_\ell x_{u_1}} \right]} + \frac{\left( x_{v_2} - e^{m_\ell} e^{\sqrt{2} \sigma_\ell x_{u_2}} \right)^2}{\left[ (F-1)x_{v_2} + e^{m_\ell} e^{\sqrt{2} \sigma_\ell x_{u_2}} \right]} \dots \dots \right. \right. \\ \left. \left. + \frac{\left( x_{v_{N_t N_r}} - e^{m_\ell} e^{\sqrt{2} \sigma_\ell x_{u_{N_t N_r}}} \right)^2}{\left[ (F-1)x_{v_{N_t N_r}} + e^{m_\ell} e^{\sqrt{2} \sigma_\ell x_{u_{N_t N_r}}} \right]} \right] \right\} \quad (4-63)$$

$$K_d = x_{v_1} + x_{v_2} + \dots + x_{v_{N_t N_r}} \quad (4-64)$$

$$K_k = \frac{\mathcal{R}E_s g}{qN_t} = \frac{\mathcal{R}E_s 2A_r \alpha}{qN_t A_b} \quad (4-65)$$

In Eq. (4-61), the complex  $F_p(\omega)$  can be represented as

$$\text{Real}[F_p(\omega)] = \sum_{v_1=1}^{N_v} \sum_{v_2=1}^{N_v} \dots \sum_{v_{N_t N_r}=1}^{N_v} K_0 K_f \cos(K_d \omega) \quad (4-66)$$

$$\text{Imag}[F_p(\omega)] = \sum_{v_1=1}^{N_v} \sum_{v_2=1}^{N_v} \dots \sum_{v_{N_t N_r}=1}^{N_v} K_0 K_f \sin(K_d \omega) \quad (4-67)$$

The integral in Eq. (4-51) is

$$I = \frac{1}{2\pi} \int_{-\infty}^{\infty} \{ \text{Real}[F_p(\omega)] \text{Real}[F_f(\omega)] - \text{Imag}[F_p(\omega)] \text{Imag}[F_f(\omega)] \} d\omega$$

$$\begin{aligned}
&= \frac{1}{2\pi} \int_{-\infty}^{\infty} \left\{ \sum_{v_1=1}^{N_v} \sum_{v_2=1}^{N_v} \dots \sum_{v_{N_t N_r}=1}^{N_v} K_0 K_f \cos(K_d \omega) \int_0^{\infty} [e^{-k_l h^2} \cos(\omega h)] dh \right. \\
&\quad \left. + \sum_{v_1=1}^{N_v} \sum_{v_2=1}^{N_v} \dots \sum_{v_{N_t N_r}=1}^{N_v} K_0 K_f \sin(K_d \omega) \int_0^{\infty} [e^{-k_l h^2} \sin(\omega h)] dh \right\} d\omega
\end{aligned} \tag{4-68}$$

Because the integral  $I$  is real, the integrand in the above Eq. (4-68) is even,

$$\begin{aligned}
&Real[F_p(-\omega)]Real[F_f(-\omega)] - Imag[F_p(-\omega)]Imag[F_f(-\omega)] \\
&= \frac{1}{2\pi} \int_{-\infty}^{\infty} \left\{ \sum_{v_1=1}^{N_v} \sum_{v_2=1}^{N_v} \dots \sum_{v_{N_t N_r}=1}^{N_v} K_0 K_f \cos(-K_d \omega) \int_0^{\infty} [e^{-k_l h^2} \cos(-\omega h)] dh \right. \\
&\quad \left. + \sum_{v_1=1}^{N_v} \sum_{v_2=1}^{N_v} \dots \sum_{v_{N_t N_r}=1}^{N_v} K_0 K_f \sin(-K_d \omega) \int_0^{\infty} [e^{-k_l h^2} \sin(-\omega h)] dh \right\} \\
&= \frac{1}{2\pi} \int_{-\infty}^{\infty} \left\{ \sum_{v_1=1}^{N_v} \sum_{v_2=1}^{N_v} \dots \sum_{v_{N_t N_r}=1}^{N_v} K_0 K_f \cos(K_d \omega) \int_0^{\infty} [e^{-k_l h^2} \cos(\omega h)] dh \right. \\
&\quad \left. + \sum_{v_1=1}^{N_v} \sum_{v_2=1}^{N_v} \dots \sum_{v_{N_t N_r}=1}^{N_v} K_0 K_f \sin(K_d \omega) \int_0^{\infty} [e^{-k_l h^2} \sin(\omega h)] dh \right\} \\
&= Real[F_p(\omega)]Real[F_f(\omega)] - Imag[F_p(\omega)]Imag[F_f(\omega)]
\end{aligned} \tag{4-69}$$

where  $k_l = \frac{k(E_s \mathcal{R}MAG)^2}{2N_t^2(k\sigma_{on}^2 + \sigma_{off}^2)}$ . Eq. (4-68) can be represented as

$$\begin{aligned}
I &= \sum_{v_1=1}^{N_v} \dots \sum_{v_{N_t N_r}=1}^{N_v} \frac{K_0 K_f}{\pi} \left\{ \int_0^{\infty} \left[ \cos(K_d \omega) \int_0^{\infty} (e^{-k_l h^2} \cos(\omega h)) dh \right. \right. \\
&\quad \left. \left. + \sin(K_d \omega) \int_0^{\infty} (e^{-k_l h^2} \sin(\omega h)) dh \right] d\omega \right\}
\end{aligned} \tag{4-70}$$

According to the reference [5] (P480 3.896), the following integrals are

$$\int_0^{\infty} [e^{-\beta h^2} \cos(bh)] dh = \frac{1}{2} \sqrt{\frac{\pi}{\beta}} \exp\left(-\frac{b^2}{4\beta}\right) \quad \text{Real } \beta > 0$$

(4-71a)

$$\int_0^{\infty} [e^{-\alpha h^2} \sin(bh)] dh = \frac{b}{2\alpha} \sum_{k=1}^{\infty} \frac{1}{(2k-1)!!} \left(-\frac{b^2}{2\alpha}\right)^{(k-1)} \quad \text{Real } \alpha > 0$$

(4-71b)

Then

$$\int_0^{\infty} [e^{-k_l h^2} \cos(\omega h)] dh = \frac{1}{2} \sqrt{\frac{\pi}{k_l}} \exp\left(-\frac{\omega^2}{4k_l}\right)$$

(4-72)

$$\int_0^{\infty} [e^{-k_l h^2} \sin(\omega h)] dh = \frac{\omega}{2k_l} \sum_{p=1}^{\infty} \frac{1}{(2p-1)!!} \left(-\frac{\omega^2}{2k_l}\right)^{(p-1)}$$

(4-73)

If the variable  $\frac{\omega}{2\sqrt{k_l}}$  is in the range of small values, computing large number of terms in the above series representation can obtain the value of the integral in Eq. (4-73). But if the variable  $\frac{\omega}{2\sqrt{k_l}}$  is in the range of large values, the computing result of Eq. (4-73) becomes oscillated very severely. As the  $\frac{\omega}{2\sqrt{k_l}}$  increases and  $k_l = 82.161$ , the results are shown in Fig. 4.1

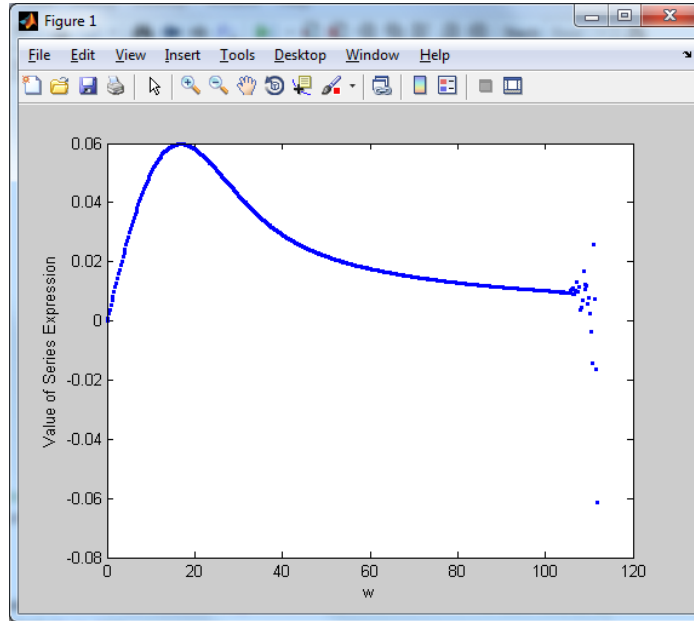


Figure 4.1 Computing result of the series expression in Eq. (4-73)

The following integral in Eq. (4-73) can also be represented by Dawson's integral

$F_D(\omega)$  as

$$\int_0^{\infty} [e^{-k_l h^2} \sin(\omega h)] dh = \frac{1}{\sqrt{k_l}} F_D\left(\frac{\omega}{2\sqrt{k_l}}\right) \quad (4-74)$$

where  $F_D(x)$  denotes Dawson's integral [6],

$$F_D(x) = e^{-x^2} \int_0^x e^{t^2} dt = x\Phi\left(1, \frac{3}{2}, -x^2\right) = x \sum_{p=1}^{\infty} \frac{1}{(2p-1)!!} (-2x^2)^{(p-1)} \quad (4-75)$$

Dawson's integral can be computed more efficiently by using the remarkable approximation due to Rybicki [7]

$$F_D(x) = \lim_{h_d \rightarrow 0} \frac{1}{\sqrt{\pi}} \sum_{z \text{ odd}} \frac{e^{-(x-zh_d)^2}}{z} \quad (4-76)$$

The approximation equation for computing can be represented as [7]

$$F_D(x') \approx \frac{1}{\sqrt{\pi}} \sum_{\substack{z'=-N_D \\ z' \text{ odd}}}^{N_D} \frac{e^{-(x'-z'h_d)^2}}{z' + z_0} \quad (4-77)$$

where  $z_0$  is the even integer nearest to  $\frac{x}{h_d}$ ,  $x_0 = z_0 h_d$ ,  $x' = x - x_0$  and  $z' = z - z_0$ .

The approximate equality is accurate when  $h_d$  is sufficiently small and  $N_D$  is sufficiently large [7]. The computation of this formula in Eq. (4-77) can be greatly speeded up if we note that [7]

$$e^{-(x'-z'h_d)^2} = e^{-x'^2} e^{-(z'h_d)^2} (e^{2x'h_d})^{z'} \quad (4-78)$$

The first factor is computed once, the second is an array of constants to be stored, and the third can be computed recursively. Thus only two exponentials must be evaluated [7]. Advantage is also taken of the symmetry of the coefficients by breaking the summation up into positive and negative values of  $z'$  separately [7]. In order to maintain relative accuracy at values near  $x = 0$  in the calculation of error probability, Dawson's integral is computed by the series in Eq. (4-73) for  $|x| < 0.2$  and by Eq. (4-77) for  $|x| \geq 0.2$ .

$$F_D\left(\frac{\omega}{2\sqrt{k_l}}\right) = \begin{cases} \frac{\omega}{2\sqrt{k_l}} \sum_{p=1}^{N_S} \frac{1}{(2p-1)!!} \left(-\frac{\omega^2}{2k_l}\right)^{(p-1)} & \frac{\omega}{2\sqrt{k_l}} < 0.2 \\ \frac{1}{\sqrt{\pi}} \sum_{\substack{z'=-N_D \\ z' \text{ odd}}}^{N_D} \frac{e^{-\left[\left(\frac{\omega}{2\sqrt{k_l}}\right)-z'h_d\right]^2}}{z' + z_0} & \frac{\omega}{2\sqrt{k_l}} \geq 0.2 \end{cases} \quad (4-79)$$

where  $z_0$  is the even integer nearest to  $\frac{\omega}{h_d 2\sqrt{k_l}}$ ,  $\frac{\omega_0}{h_d 2\sqrt{k_l}} = z_0 h_d$ ,  $\omega' = \omega - \omega_0$ ,  $z' = z - z_0$ ,  $N_S$  and  $N_D$  are the truncating term numbers. As the  $\frac{\omega}{2\sqrt{k_l}}$  increases and  $k_l = 82.161$ , the computing result of Eq. (4-79) by Dawson's integral is shown in Fig.

4.2. The computing result of Eq. (4-79) converges as the  $\omega$  increases.

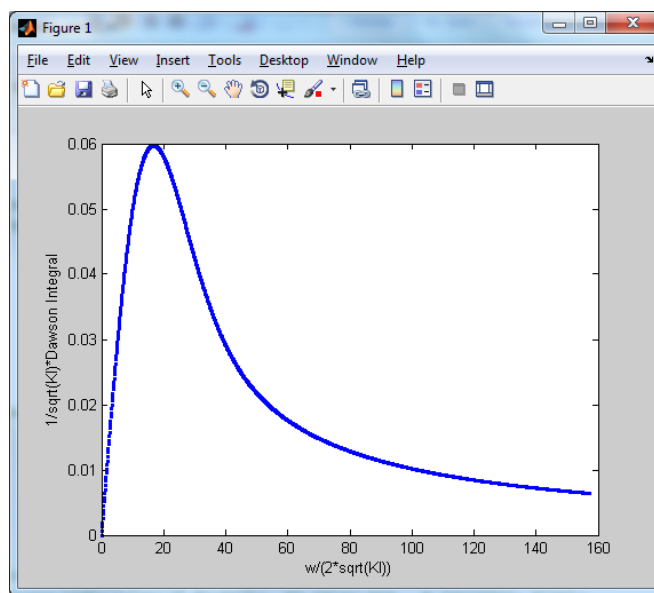


Figure 4.2 Computing result of Eq. (4-73) by Dawson's integral

#### 4.1.4 Fourier Series Method for Calculating the Average SEP

According to reference [3], [6], [8], [9] and Appendix L, the average symbol error probability  $P_s(E)$  for one PPM symbol can be represented by the Fourier series

$$\begin{aligned}
 P_s(E) &= \frac{1}{T_F} \sum_{n=-\infty}^{\infty} \text{Real}\{\Phi_x(n\omega_0)G_x(n\omega_0)\} \\
 &= \frac{\omega_0}{2\pi} \text{Real}\{\Phi_x(0)G_x(0)\} + \frac{2\omega_0}{\pi} \sum_{\substack{n=1 \\ n \text{ odd}}}^{\infty} \text{Real}\{\Phi_x(n\omega_0)G_x(n\omega_0)\}
 \end{aligned}$$

(4-80)

where  $\omega_0 = \frac{2\pi}{T_F}$ ,  $\Phi_x(\omega)$  is the characteristic function of  $P_e(x)$  and  $x \geq 0$ ,  $\Phi_x(\omega) = \int_0^\infty P_e(x)e^{j\omega x}dx$ ,  $G_x(\omega)$  is the Fourier transform of the function  $f(x)$  with the random variable  $x$ ,  $G_x(\omega) = \int_0^\infty f(x)e^{-j\omega x} dx$  [9].  $P_e(x)$  denotes the symbol or bit error probability on an additive white Gaussian noise channel conditioned by the signal-to-noise ration or the combining output envelope [9]. By using Eq. (4-80) in MIMO FSO systems and truncating the infinite summation, a detailed derivation of Eq. (4-80) is given in Appendix L. The average symbol error probability  $P_s(E)$  for one PPM symbol is

$$\begin{aligned}
P_s(E) &\leq \frac{\omega_0}{2\pi} \sum_{v_1=1}^{N_v} \dots \sum_{v_{N_t N_r}=1}^{N_v} K_0 K_f \sum_{k=1}^{L-1} \frac{C_{L-1}^k (-1)^{k+1} \sigma_{\text{off}}}{\sqrt{(k\sigma_{\text{on}}^2 + \sigma_{\text{off}}^2)}} \frac{1}{2} \sqrt{\frac{\pi}{k_l}} \\
&+ \frac{2\omega_0}{\pi} \sum_{\substack{n=1 \\ n \text{ odd}}}^{\infty} \left\{ \int_0^\infty \left[ \sum_{v_1=1}^{N_v} \dots \sum_{v_{N_t N_r}=1}^{N_v} K_0 K_f \cos(K_d \omega) \right] \left[ \int_0^\infty \sum_{k=1}^{L-1} \frac{C_{L-1}^k (-1)^{k+1} \sigma_{\text{off}} e^{-k_l h^2} \cos(\omega h)}{\sqrt{(k\sigma_{\text{on}}^2 + \sigma_{\text{off}}^2)}} dh \right] d\omega \right\} \\
&+ \int_0^\infty \left\{ \sum_{v_1=1}^{N_v} \dots \sum_{v_{N_t N_r}=1}^{N_v} K_0 K_f \sin(K_d \omega) \right\} \left[ \int_0^\infty \sum_{k=1}^{L-1} \frac{C_{L-1}^k (-1)^{k+1} \sigma_{\text{off}}}{\sqrt{(k\sigma_{\text{on}}^2 + \sigma_{\text{off}}^2)}} e^{-k_l h^2} \sin(\omega h) dh \right] d\omega \left. \right\} \\
&= \sum_{k=1}^{L-1} \frac{C_{L-1}^k (-1)^{k+1} \sigma_{\text{off}}}{\sqrt{(k\sigma_{\text{on}}^2 + \sigma_{\text{off}}^2)}} \sum_{v_1=1}^{N_v} \dots \sum_{v_{N_t N_r}=1}^{N_v} K_0 K_f \left\{ \frac{\omega_0}{4\pi} \sqrt{\frac{\pi}{k_l}} \right. \\
&\quad \left. + \frac{2\omega_0}{\pi} \sum_{\substack{n=1 \\ n \text{ odd}}}^{N_F} \left[ \cos(K_d n \omega_0) \frac{1}{2} \sqrt{\frac{\pi}{k_l}} \exp \left[ -\frac{(n\omega_0)^2}{4k_l} \right] \right. \right. \\
&\quad \left. \left. + \sin(K_d n \omega_0) \frac{F_D \left( \frac{n\omega_0}{2\sqrt{k_l}} \right)}{\sqrt{k_l}} \right] \right\} \\
&= \sum_{k=1}^{L-1} \frac{C_{L-1}^k (-1)^{k+1} K_0'}{\sqrt{k}} \sum_{v_1=1}^{N_v} \dots \sum_{v_{N_t N_r}=1}^{N_v} K_f \omega_0
\end{aligned}$$

$$\left\{ \frac{1}{4} + \sum_{\substack{n=1 \\ n \text{ odd}}}^{N_F} \left[ \cos(K_d n \omega_0) \exp \left[ -\frac{(n \omega_0)^2}{4k_l} \right] + \frac{2}{\sqrt{\pi}} \sin(K_d n \omega_0) F_D \left( \frac{n \omega_0}{2\sqrt{k_l}} \right) \right] \right\} \quad (4-81)$$

where

$$K_0' = \frac{\sigma_{\text{off}}}{\sqrt{2\pi}MA} \left( \frac{F e^{m_\ell}}{\pi \sqrt{q}} \right)^{N_t N_r} \left( \frac{\mathcal{R} E_s A_r \alpha}{N_t A_b} \right)^{\left( \frac{N_t N_r}{2} - 1 \right)} \quad (4-82a)$$

$$k_l = \frac{k(E_s \mathcal{R} M A g)^2}{2N_t^2 (k\sigma_{\text{on}}^2 + \sigma_{\text{off}}^2)} \quad (4-82b)$$

$$\omega_0 = \frac{2\pi}{T_F} \quad (4-82c)$$

$$g = \frac{2A_r \alpha}{A_b} \quad (4-82d)$$

$$F_D \left( \frac{n \omega_0}{2\sqrt{k_l}} \right) = \begin{cases} \frac{n \omega_0}{2\sqrt{k_l}} \sum_{p=1}^{N_S} \frac{1}{(2p-1)!!} \left[ -\frac{(n \omega_0)^2}{2k_l} \right]^{(p-1)} & \frac{n \omega_0}{2\sqrt{k_l}} < 0.2 \\ \frac{1}{\sqrt{\pi}} \sum_{\substack{z'=-N_D \\ z' \text{ odd}}}^{N_D} \frac{e^{-\left[ \left( \frac{n \omega_0}{2\sqrt{k_l}} \right) - z' h_d \right]^2}}{z' + z_0} & \frac{n \omega_0}{2\sqrt{k_l}} \geq 0.2 \end{cases} \quad (4-82f)$$

$$K_f = \sum_{\substack{u_1=-N_u \\ u_1 \neq 0}}^{N_u} \sum_{\substack{u_2=-N_u \\ u_2 \neq 0}}^{N_u} \dots \sum_{\substack{u_{N_t N_r}=-N_u \\ u_{N_t N_r} \neq 0}}^{N_u} W_{u_1} W_{u_2} \dots W_{u_{N_t N_r}} W_{v_1} W_{v_2} \dots W_{v_{N_t N_r}}$$

$$\exp \left[ \sqrt{2} \sigma_\ell (x_{u_1} + x_{u_2} + \dots + x_{u_{N_t N_r}}) + (x_{v_1} + x_{v_2} + \dots + x_{v_{N_t N_r}}) \right]$$

$$\left[ (F-1)x_{v_1} + e^{m_\ell} e^{\sqrt{2} \sigma_\ell x_{u_1}} \right]^{\left( -\frac{3}{2} \right)} \left[ (F-1)x_{v_2} + e^{m_\ell} e^{\sqrt{2} \sigma_\ell x_{u_2}} \right]^{\left( -\frac{3}{2} \right)} \dots$$

$$\begin{aligned}
& \left[ (F-1)x_{v_{N_t N_r}} + e^{m_\ell} e^{\sqrt{2}\sigma_\ell x_{u_{N_t N_r}}} \right]^{-\left(\frac{3}{2}\right)} \\
& \exp \left\{ \left( -\frac{K_k}{2} \right) \left[ \frac{(x_{v_1} - e^{m_\ell} e^{\sqrt{2}\sigma_\ell x_{u_1}})^2}{[(F-1)x_{v_1} + e^{m_\ell} e^{\sqrt{2}\sigma_\ell x_{u_1}}]} + \frac{(x_{v_2} - e^{m_\ell} e^{\sqrt{2}\sigma_\ell x_{u_2}})^2}{[(F-1)x_{v_2} + e^{m_\ell} e^{\sqrt{2}\sigma_\ell x_{u_2}}]} \dots \dots \right. \right. \\
& \quad \left. \left. + \frac{(x_{v_{N_t N_r}} - e^{m_\ell} e^{\sqrt{2}\sigma_\ell x_{u_{N_t N_r}}})^2}{[(F-1)x_{v_{N_t N_r}} + e^{m_\ell} e^{\sqrt{2}\sigma_\ell x_{u_{N_t N_r}}]} \right] \right\}
\end{aligned} \tag{4-82g}$$

$$K_d = x_{v_1} + x_{v_2} + \dots + x_{v_{N_t N_r}} \tag{4-82h}$$

$$K_k = \frac{\mathcal{R}E_s g}{qN_t} = \frac{\mathcal{R}E_s 2A_r \alpha}{qN_t A_b} \tag{4-82i}$$

$N_F$  is the truncating term number,  $T_F = \frac{2\pi}{\omega_0}$ ,  $K_0'$ ,  $K_f$ ,  $K_d$  and  $F_D \left( \frac{n\omega_0}{2\sqrt{k_l}} \right)$  are given in Eq.

(4-82a), Eq. (4-82g), Eq. (4-82h) and Eq. (4-82f),  $k_l = \frac{k(E_s \mathcal{R}M A g)^2}{2N_t^2(k\sigma_{on}^2 + \sigma_{off}^2)}$  and  $\omega_0 = \frac{2\pi}{T_F}$

.  $T_F$  is selected such that  $P_e(t \geq T) \leq \varepsilon$ ,  $\varepsilon$  can be set to a very small value and  $T_F$  is also selected as the suitable integer times of  $K_d$ ,  $T_F = n_T K_d$ .  $N_F$  can be selected as the suitable integer times of  $2\pi n_T$ ,  $N_F = n_F 2\pi n_T$ .  $h_d$  is selected sufficiently small, and  $n_T$ ,  $n_F$ ,  $N_D$ ,  $N_S$ ,  $N_v$  and  $N_u$  are sufficiently large such that the calculation error  $\varepsilon$  can be set to a very small value and the accuracy can meet the practical requirement. The computing result of Eq. (4-73) by Dawson's integral is shown in Fig. 4.2 .

The average symbol error probability  $P_{e\_matrix}(E)$  of one transmitted matrix is

$$P_{e\_matrix}(E) = P_S(E)^N$$

$$\begin{aligned}
&\leq \prod_{m=1}^N \sum_{k=1}^{L-1} \frac{C_{L-1}^k (-1)^{k+1} K_0'}{\sqrt{k}} \sum_{v_1=1}^{N_v} \dots \sum_{v_{N_t N_r}=1}^{N_v} K_f \omega_0 \\
&\quad \left\{ \frac{1}{4} + \sum_{\substack{n=1 \\ n \text{ odd}}}^{N_F} \left[ \cos(K_d n \omega_0) \exp \left[ -\frac{(n \omega_0)^2}{4k_l} \right] + \frac{2}{\sqrt{\pi}} \sin(K_d n \omega_0) F_D \left( \frac{n \omega_0}{2\sqrt{k_l}} \right) \right] \right\}
\end{aligned} \tag{4-83}$$

where  $N$  is the number of the PPM symbols that are in one transmitted matrix.

Similarly, the average bit error probability  $P_b(E)$  has the following relationship with the average symbol error probability  $P_s(E)$

$$\begin{aligned}
P_b(E) &= \frac{L}{2(L-1)} P_s(E) = \frac{2^{Q-1}}{2^Q - 1} P_s(E) \\
&\leq \frac{2^{Q-1}}{2^Q - 1} \sum_{k=1}^{L-1} \frac{C_{L-1}^k (-1)^{k+1} K_0'}{\sqrt{k}} \sum_{v_1=1}^{N_v} \dots \sum_{v_{N_t N_r}=1}^{N_v} K_f \omega_0 \\
&\quad \left\{ \frac{1}{4} + \sum_{\substack{n=1 \\ n \text{ odd}}}^{N_F} \left[ \cos(K_d n \omega_0) \exp \left[ -\frac{(n \omega_0)^2}{4k_l} \right] + \frac{2}{\sqrt{\pi}} \sin(K_d n \omega_0) F_D \left( \frac{n \omega_0}{2\sqrt{k_l}} \right) \right] \right\}
\end{aligned} \tag{4-84}$$

The average pairwise error probability  $P_{s \rightarrow s'}(E)$  for one PPM symbol in the MIMO FSO systems can be represented as

$$\begin{aligned}
P_{s \rightarrow s'}(E) &= \frac{1}{(L-1)} P_s(E) \\
&\leq \frac{1}{(L-1)} \sum_{k=1}^{L-1} \frac{C_{L-1}^k (-1)^{k+1} K_0'}{\sqrt{k}} \sum_{v_1=1}^{N_v} \dots \sum_{v_{N_t N_r}=1}^{N_v} K_f \omega_0 \\
&\quad \left\{ \frac{1}{4} + \sum_{\substack{n=1 \\ n \text{ odd}}}^{N_F} \left[ \cos(K_d n \omega_0) \exp \left[ -\frac{(n \omega_0)^2}{4k_l} \right] + \frac{2}{\sqrt{\pi}} \sin(K_d n \omega_0) F_D \left( \frac{n \omega_0}{2\sqrt{k_l}} \right) \right] \right\}
\end{aligned} \tag{4-85}$$

where  $L$  is the number of the slot in one Q-ary PPM symbol,  $L = 2^Q$ .

#### 4.1.5 Modified Gauss-Chebyshev Method for Calculating the Average SEP

The Gauss-Chebyshev quadrature-based numerical technique is used to calculate the average error probability in communication systems [4]. In this dissertation, a modified Gauss-Chebyshev method, the “extended Gauss-Chebyshev quadrature-based technique”, is proposed and employed in the calculation of the average SEP and BEP efficiently.

The following variable substitution is proposed and used for calculating the second integral in Eq. (4-70)

$$\omega = \sqrt{\frac{cx}{1-x}} = \tau_q \quad (4-86)$$

In Appendix M, a detailed derivation of the expressions for  $\omega$  and  $x$  is given. Since the variable  $\omega$  is in the range from zero to infinity, the variable  $x = \frac{1}{1+\frac{c}{\omega^2}}$  is in the range from zero to one. According to Appendix M,  $d\omega$  is given as

$$d\omega = d\left(\sqrt{\frac{cx}{1-x}}\right) = \frac{\sqrt{c}}{2x(1-x)} \sqrt{\frac{x}{1-x}} dx \quad (4-87)$$

According to reference [4] (P889, 25.4.42), we have

$$\int_0^1 f(x) \sqrt{\frac{x}{1-x}} dx = \sum_{q=1}^{N_G} \omega_q f(x_q) + R_n \quad (4-88a)$$

$$x_q = \cos^2 \left[ \left( \frac{2q-1}{2N_G+1} \right) \frac{\pi}{2} \right] \quad (4-88b)$$

$$\omega_q = \frac{2\pi}{(2N_G+1)} x_q$$

(4-88c)

$$\tau_q = \sqrt{\frac{x_q}{1-x_q}} = \cot \left[ \left( \frac{2q-1}{2N_G+1} \right) \frac{\pi}{2} \right]$$

(4-88d)

The integrals in Eq. (4-70) are calculated in Appendix N and represented as

$$\begin{aligned} & \int_0^\infty \sin(K_d \omega) \int_0^\infty [e^{-k_l h^2} \sin(\omega h)] dh d\omega \\ &= \frac{\pi}{(2N_G+1) \sqrt{k_l}} \sum_{q=1}^{N_G} \frac{\sqrt{c} \sin(K_d \tau_q)}{\sin^2 \left[ \left( \frac{2q-1}{2N_G+1} \right) \frac{\pi}{2} \right]} F_D \left( \frac{\tau_q}{2 \sqrt{k_l}} \right) \end{aligned}$$

(4-89a)

$$\int_0^\infty \cos(K_d \omega) \int_0^\infty [e^{-k_l h^2} \cos(\omega h)] dh d\omega = \frac{\pi}{2} \exp(-k_l K_d^2)$$

(4-89b)

where  $\tau_q = \sqrt{\frac{cx_q}{1-x_q}} = \sqrt{c} \cot \left[ \left( \frac{2q-1}{2N_G+1} \right) \frac{\pi}{2} \right]$  and  $F_D \left( \frac{\tau_q}{2 \sqrt{k_l}} \right)$  is given as

$$F_D \left( \frac{\tau_q}{2 \sqrt{k_l}} \right) = \begin{cases} \frac{\tau_q}{2 \sqrt{k_l}} \sum_{p=1}^{N_S} \frac{1}{(2p-1)!!} \left[ -\frac{(\tau_q)^2}{2k_l} \right]^{(p-1)} & \frac{\tau_q}{2 \sqrt{k_l}} < 0.2 \\ \frac{1}{\sqrt{\pi}} \sum_{\substack{z'=-N_D \\ z' \text{ odd}}}^{N_D} \frac{e^{-\left[ \left( \frac{\tau_q}{2 \sqrt{k_l}} \right) - z' h_d \right]^2}}{z' + z_0} & \frac{\tau_q}{2 \sqrt{k_l}} \geq 0.2 \end{cases}$$

(4-90)

The integral in Eq. (4-70) is

$$I = \sum_{v_1=1}^{N_v} \dots \sum_{v_{N_t N_r}=1}^{N_v} K_0 K_f \left\{ \frac{\exp(-k_l K_d^2)}{2} \right. \\ \left. + \frac{1}{(2N_G + 1) \sqrt{k_l}} \sum_{q=1}^{N_G} \frac{\sqrt{c} \sin(K_d \tau_q)}{\sin^2 \left[ \left( \frac{2q-1}{2N_G+1} \right) \frac{\pi}{2} \right]} F_D \left( \frac{\tau_q}{2 \sqrt{k_l}} \right) \right\} \quad (4-91)$$

The average symbol error probability  $P_s(E)$  of one PPM symbol is

$$P_s(E) \leq \sum_{k=1}^{L-1} \frac{C_{L-1}^k (-1)^{k+1} \sigma_{\text{off}} K_0}{\sqrt{(k\sigma_{\text{on}}^2 + \sigma_{\text{off}}^2)}} \sum_{v_1=1}^{N_v} \dots \sum_{v_{N_t N_r}=1}^{N_v} K_f \left\{ \frac{\exp(-k_l K_d^2)}{2} \right. \\ \left. + \frac{1}{(2N_G + 1) \sqrt{k_l}} \sum_{q=1}^{N_G} \frac{\sqrt{c} \sin(K_d \tau_q)}{\sin^2 \left[ \left( \frac{2q-1}{2N_G+1} \right) \frac{\pi}{2} \right]} F_D \left( \frac{\tau_q}{2 \sqrt{k_l}} \right) \right\} \quad (4-92)$$

where  $K_0$ ,  $K_f$ ,  $K_d$  and  $F_D \left( \frac{\tau_q}{2 \sqrt{k_l}} \right)$  are given in Eq. (4-62), Eq. (4-63), Eq. (4-64) and

Eq. (4-90),  $k_l = \frac{k(E_s \mathcal{R}MAG)^2}{2N_t^2(k\sigma_{\text{on}}^2 + \sigma_{\text{off}}^2)}$ ,  $\tau_q = \sqrt{\frac{cx_q}{1-x_q}} = \sqrt{c} \cot \left[ \left( \frac{2q-1}{2N_G+1} \right) \frac{\pi}{2} \right]$ ,  $h_d$  is selected

sufficiently small, and  $n_q$ ,  $N_D$ ,  $N_S$ ,  $N_G$ ,  $N_v$  and  $N_u$  are sufficiently large such that the

calculation error  $\varepsilon$  can be set to a very small value and the accuracy can meet the

practical requirement. The parameter  $\sqrt{c}$  is selected as the suitable integer times of

$K_d$ ,  $\sqrt{c} = 1/(n_q K_d)$ , and  $\sqrt{c}$  is also selected by making the integral of the imaginary

part in Eq. (4-49) equal to zero,  $\frac{1}{2\pi} \int_{-\infty}^{\infty} \text{Imag}[F_p(\omega)F_f(\omega)] d\omega = 0$ .

The average symbol error probability  $P_{e\_matrix}(E)$  of one matrix is

$$P_{e\_matrix}(E) = P_s(E)^N$$

$$\begin{aligned}
&\leq \prod_{m=1}^N \sum_{k=1}^{L-1} \frac{C_{L-1}^k (-1)^{k+1} \sigma_{\text{off}} K_0}{\sqrt{(k\sigma_{\text{on}}^2 + \sigma_{\text{off}}^2)}} \sum_{v_1=1}^{N_v} \dots \sum_{v_{N_t N_r}=1}^{N_v} K_f \left\{ \frac{\exp(-k_l K_d^2)}{2} \right. \\
&\quad \left. + \frac{1}{(2N_G + 1) \sqrt{k_l}} \sum_{q=1}^{N_G} \frac{\sqrt{c} \sin(K_d \tau_q)}{\sin^2 \left[ \left( \frac{2q-1}{2N_G + 1} \right) \frac{\pi}{2} \right]} F_D \left( \frac{\tau_q}{2 \sqrt{k_l}} \right) \right\}
\end{aligned} \tag{4-93}$$

The average bit error probability  $P_b(E)$  has the following relationship with the average symbol error probability  $P_s(E)$

$$\begin{aligned}
P_b(E) &= \frac{L}{2(L-1)} P_s(E) = \frac{2^{Q-1}}{2^Q - 1} P_s(E) \\
&\leq \frac{2^{Q-1}}{2^Q - 1} \sum_{k=1}^{L-1} \frac{C_{L-1}^k (-1)^{k+1} \sigma_{\text{off}} K_0}{\sqrt{(k\sigma_{\text{on}}^2 + \sigma_{\text{off}}^2)}} \sum_{v_1=1}^{N_v} \dots \sum_{v_{N_t N_r}=1}^{N_v} K_f \left\{ \frac{\exp(-k_l K_d^2)}{2} \right. \\
&\quad \left. + \frac{1}{(2N_G + 1) \sqrt{k_l}} \sum_{q=1}^{N_G} \frac{\sqrt{c} \sin(K_d \tau_q)}{\sin^2 \left[ \left( \frac{2q-1}{2N_G + 1} \right) \frac{\pi}{2} \right]} F_D \left( \frac{\tau_q}{2 \sqrt{k_l}} \right) \right\}
\end{aligned} \tag{4-94}$$

The average pairwise error probability  $P_{s \rightarrow s'}(E)$  for one PPM symbol in the MIMO FSO systems can be represented as

$$\begin{aligned}
P_{s \rightarrow s'}(E) &= \frac{1}{(L-1)} P_s(E) \\
&\leq \frac{1}{2^Q - 1} \sum_{k=1}^{L-1} \frac{C_{L-1}^k (-1)^{k+1} \sigma_{\text{off}} K_0}{\sqrt{(k\sigma_{\text{on}}^2 + \sigma_{\text{off}}^2)}} \sum_{v_1=1}^{N_v} \dots \sum_{v_{N_t N_r}=1}^{N_v} K_f \left\{ \frac{\exp(-k_l K_d^2)}{2} \right. \\
&\quad \left. + \frac{1}{(2N_G + 1) \sqrt{k_l}} \sum_{q=1}^{N_G} \frac{\sqrt{c} \sin(K_d \tau_q)}{\sin^2 \left[ \left( \frac{2q-1}{2N_G + 1} \right) \frac{\pi}{2} \right]} F_D \left( \frac{\tau_q}{2 \sqrt{k_l}} \right) \right\}
\end{aligned}$$

(4-95)

where  $L$  is the number of the slot in one Q-ary PPM symbol,  $L = 2^Q$ .

## 4.2 Symbol Error Probability Calculation of SISO FSO Systems

The average error probabilities of MIMO systems with lognormal fading channels are analyzed in Section 4.1. By using these equations given for MIMO system, the average error probabilities for SISO have been obtained.

### 4.2.1 SEP Calculation of SISO FSO Systems By Fourier Series Method

For the SISO FSO system with lognormal fading channel, the average symbol error probability of one PPM symbol is

$$P_s(E) \leq \sum_{k=1}^{L-1} \frac{C_{L-1}^k (-1)^{k+1} K_{s0}'}{\sqrt{k}} \sum_{v_1=1}^{N_v} K_{sf} \omega_0 \left\{ \frac{1}{4} + \sum_{\substack{n=1 \\ n \text{ odd}}}^{N_F} \left[ \cos(K_d n \omega_0) \exp \left[ -\frac{(n \omega_0)^2}{4k_l} \right] + \frac{2}{\sqrt{\pi}} \sin(K_d n \omega_0) F_D \left( \frac{n \omega_0}{2\sqrt{k_l}} \right) \right] \right\} \quad (4-96)$$

where

$$F_D \left( \frac{n \omega_0}{2\sqrt{k_l}} \right) = \begin{cases} \frac{n \omega_0}{2\sqrt{k_l}} \sum_{p=1}^{N_S} \frac{1}{(2p-1)!!} \left[ -\frac{(n \omega_0)^2}{2k_l} \right]^{(p-1)} & \frac{n \omega_0}{2\sqrt{k_l}} < 0.2 \\ \frac{1}{\sqrt{\pi}} \sum_{\substack{z'=-N_D \\ z' \text{ odd}}}^{N_D} \frac{e^{-\left[ \left( \frac{n \omega_0}{2\sqrt{k_l}} \right) - z' h_d \right]^2}}{z' + z_0} & \frac{n \omega_0}{2\sqrt{k_l}} \geq 0.2 \end{cases}$$

(4-97a)

$$K_{s0}' = \frac{\sigma_{\text{off}}}{\sqrt{2\pi}MA} \left( \frac{F e^{m_\ell}}{\pi \sqrt{q}} \right) \left( \frac{\mathcal{R}E_s A_r \alpha}{A_b} \right)^{\left(-\frac{1}{2}\right)} \quad (4-97b)$$

$$K_{sf} = \sum_{\substack{u_1=-N_u \\ u_1 \neq 0}}^{N_u} w_{u_1} w_{v_1} \exp\left(\sqrt{2} \sigma_\ell x_{u_1} + x_{v_1}\right) \left[ (F-1)x_{v_1} + e^{m_\ell} e^{\sqrt{2} \sigma_\ell x_{u_1}} \right]^{\left(-\frac{3}{2}\right)} \\ \exp\left\{ \left(-\frac{K_k}{2}\right) \left[ \frac{\left(x_{v_1} - e^{m_\ell} e^{\sqrt{2} \sigma_\ell x_{u_1}}\right)^2}{\left[(F-1)x_{v_1} + e^{m_\ell} e^{\sqrt{2} \sigma_\ell x_{u_1}}\right]} \right] \right\} \quad (4-97c)$$

$$K_d = x_{v_1} \quad (4-97d)$$

$$K_k = \frac{\mathcal{R}E_s g}{qN_t} = \frac{\mathcal{R}E_s 2A_r \alpha}{qN_t A_b} \quad (4-97e)$$

$N_F$  is the truncating term number,  $T_F = \frac{2\pi}{\omega_0}$ ,  $K_{s0}'$ ,  $K_{sf}$ ,  $K_d$  and  $F_D \left(\frac{n\omega_0}{2\sqrt{k_l}}\right)$  are given in

Eq. (4-97b), Eq. (4-97c), Eq. (4-97d) and Eq. (4-97a),  $k_l = \frac{k(E_s \mathcal{R}M A g)^2}{2N_t^2(k\sigma_{\text{on}}^2 + \sigma_{\text{off}}^2)}$  and

$\omega_0 = \frac{2\pi}{T_F}$ .  $T_F$  is selected such that  $P_e(t \geq T) \leq \varepsilon$ ,  $\varepsilon$  can be set to a very small value.

$T_F$  is also selected as the suitable integer times of  $K_d$ ,  $T_F = n_T K_d$ .  $N_F$  can be selected as the suitable integer times of  $2\pi n_T$ ,  $N_F = n_F 2\pi n_T$ .  $h_d$  is selected sufficiently small, and  $n_T$ ,  $n_F$ ,  $N_D$ ,  $N_S$ ,  $N_v$  and  $N_u$  are sufficiently large such that the calculation error  $\varepsilon$  can be set to a very small value and the accuracy can meet the practical requirement.

The average symbol error probability  $P_{e\_matrix}(E)$  of one transmitted matrix for SISO FSO systems is

$$P_{e\_matrix}(E) = P_s(E)^N$$

$$\begin{aligned}
&\leq \prod_{m=1}^N \sum_{k=1}^{L-1} \frac{C_{L-1}^k (-1)^{k+1} K_{s0}'}{\sqrt{k}} \sum_{v_1=1}^{N_v} K_{sf} \omega_0 \\
&\quad \left\{ \frac{1}{4} + \sum_{\substack{n=1 \\ n \text{ odd}}}^{N_F} \left[ \cos(K_d n \omega_0) \exp \left[ -\frac{(n \omega_0)^2}{4k_l} \right] + \frac{2}{\sqrt{\pi}} \sin(K_d n \omega_0) F_D \left( \frac{n \omega_0}{2\sqrt{k_l}} \right) \right] \right\}
\end{aligned} \tag{4-98}$$

where  $N$  is the number of the PPM symbols in one transmitted matrix.

The average bit error probability  $P_b(E)$  for SISO FSO systems has the following relationship with the average symbol error probability  $P_s(E)$

$$\begin{aligned}
P_b(E) &= \frac{L}{2(L-1)} P_s(E) = \frac{2^{Q-1}}{2^Q - 1} P_s(E) \\
&\leq \frac{2^{Q-1}}{2^Q - 1} \sum_{k=1}^{L-1} \frac{C_{L-1}^k (-1)^{k+1} K_{s0}'}{\sqrt{k}} \sum_{v_1=1}^{N_v} K_{sf} \omega_0 \\
&\quad \left\{ \frac{1}{4} + \sum_{\substack{n=1 \\ n \text{ odd}}}^{N_F} \left[ \cos(K_d n \omega_0) \exp \left[ -\frac{(n \omega_0)^2}{4k_l} \right] + \frac{2}{\sqrt{\pi}} \sin(K_d n \omega_0) F_D \left( \frac{n \omega_0}{2\sqrt{k_l}} \right) \right] \right\}
\end{aligned} \tag{4-99}$$

The average pairwise error probability  $P_{s \rightarrow s'}(E)$  for one PPM symbol in the SISO FSO systems can be represented as

$$\begin{aligned}
P_{s \rightarrow s'}(E) &= \frac{1}{(L-1)} P_s(E) \\
&\leq \frac{1}{(L-1)} \sum_{k=1}^{L-1} \frac{C_{L-1}^k (-1)^{k+1} K_{s0}'}{\sqrt{k}} \sum_{v_1=1}^{N_v} K_{sf} \omega_0 \\
&\quad \left\{ \frac{1}{4} + \sum_{\substack{n=1 \\ n \text{ odd}}}^{N_F} \left[ \cos(K_d n \omega_0) \exp \left[ -\frac{(n \omega_0)^2}{4k_l} \right] + \frac{2}{\sqrt{\pi}} \sin(K_d n \omega_0) F_D \left( \frac{n \omega_0}{2\sqrt{k_l}} \right) \right] \right\}
\end{aligned} \tag{4-100}$$

where  $L$  is the number of the slot in one Q-ary PPM symbol,  $L = 2^Q$ .

#### 4.2.2 SEP Calculation of SISO FSO Systems By Modified Gauss-Chebyshev

##### Method

The computing equations in Section 4.1.5 by the modified Gauss-Chebyshev method can be used to calculate the average SEP of SISO system as  $N_t = 1$ ,  $N_r = 1$ .

The average symbol error probability  $P_s(E)$  of one PPM symbol for SISO systems is

$$P_s(E) \leq \sum_{k=1}^{L-1} \frac{C_{L-1}^k (-1)^{k+1} \sigma_{\text{off}} K_{c0}}{\sqrt{(k\sigma_{\text{on}}^2 + \sigma_{\text{off}}^2)}} \sum_{v_1=1}^{N_b} K_f \left\{ \frac{\exp(-k_l K_d^2)}{2} \right. \\ \left. + \frac{1}{(2N_G + 1) \sqrt{k_l}} \sum_{q=1}^{N_G} \frac{\sqrt{c} \sin(K_d \tau_q)}{\sin^2 \left[ \left( \frac{2q-1}{2N_G+1} \right) \frac{\pi}{2} \right]} F_D \left( \frac{\tau_q}{2 \sqrt{k_l}} \right) \right\} \quad (4-101)$$

where

$$K_{c0} = \left( \frac{F e^{m_\ell}}{\pi} \sqrt{\frac{\mathcal{R} E_s A_r \alpha}{q N_t A_b}} \right) \quad (4-102a)$$

$$K_{sf} = \sum_{\substack{u_1 = -N_u \\ u_1 \neq 0}}^{N_u} w_{u_1} w_{v_1} \exp(\sqrt{2} \sigma_\ell x_{u_1} + x_{v_1}) \left[ (F-1)x_{v_1} + e^{m_\ell} e^{\sqrt{2} \sigma_\ell x_{u_1}} \right]^{(-\frac{3}{2})} \\ \exp \left\{ \left( -\frac{K_k}{2} \right) \left[ \frac{(x_{v_1} - e^{m_\ell} e^{\sqrt{2} \sigma_\ell x_{u_1}})^2}{[(F-1)x_{v_1} + e^{m_\ell} e^{\sqrt{2} \sigma_\ell x_{u_1}}]} \right] \right\} \quad (4-102b)$$

$$K_d = x_{v_1} \quad (4-102c)$$

$$K_k = \frac{\mathcal{R}E_s g}{qN_t} = \frac{\mathcal{R}E_s 2A_r \alpha}{qN_t A_b} \quad (4-102d)$$

where  $K_{c0}$ ,  $K_{sf}$ ,  $K_d$  and  $F_D \left( \frac{\tau_q}{2\sqrt{k_l}} \right)$  are given in Eq. (4-102a), Eq. (4-102b), Eq. (4-102c) and Eq. (4-90),  $k_l = \frac{k(E_s \mathcal{R}M A g)^2}{2N_t^2(k\sigma_{on}^2 + \sigma_{off}^2)}$ ,  $\tau_q = \sqrt{\frac{cx_q}{1-x_q}} = \sqrt{c} \cot \left[ \left( \frac{2q-1}{2N_G+1} \right) \frac{\pi}{2} \right]$ ,  $h_d$  is selected sufficiently small,  $T_F$  is the suitable integer times of  $K_d$ , and  $n_q$ ,  $N_D$ ,  $N_S$ ,  $N_G$ ,  $N_v$  and  $N_u$  are sufficiently large such that the calculation error  $\varepsilon$  can be set to a very small value and the accuracy can meet the practical requirement. The parameter  $\sqrt{c}$  is selected as a suitable integer times of  $K_d$ ,  $\sqrt{c} = 1/(n_q K_d)$  and  $\sqrt{c}$  is also selected by making the integral of the imaginary part in Eq. (4-49) equal to zero,  $\frac{1}{2\pi} \int_{-\infty}^{\infty} \text{Imag}[F_p(\omega)F_f(\omega)] d\omega = 0$ .

The average symbol error probability  $P_{e\_matrix}(E)$  of one matrix is

$$P_{e\_matrix}(E) = P_s(E)^N$$

$$\leq \prod_{m=1}^N \sum_{k=1}^{L-1} \frac{C_{L-1}^k (-1)^{k+1} \sigma_{off} K_{c0}}{\sqrt{(k\sigma_{on}^2 + \sigma_{off}^2)}} \sum_{v_1=1}^{N_v} K_f \left\{ \frac{\exp(-k_l K_d^2)}{2} \right.$$

$$\left. + \frac{1}{(2N_G + 1) \sqrt{k_l}} \sum_{q=1}^{N_G} \frac{\sqrt{c} \sin(K_d \tau_q)}{\sin^2 \left[ \left( \frac{2q-1}{2N_G+1} \right) \frac{\pi}{2} \right]} F_D \left( \frac{\tau_q}{2\sqrt{k_l}} \right) \right\} \quad (4-103)$$

The average bit error probability  $P_b(E)$  has the following relationship with the average symbol error probability  $P_s(E)$  as

$$\begin{aligned}
P_b(E) &= \frac{L}{2(L-1)} P_s(E) = \frac{2^{Q-1}}{2^Q - 1} P_s(E) \\
&\leq \frac{2^{Q-1}}{2^Q - 1} \sum_{k=1}^{L-1} \frac{C_{L-1}^k (-1)^{k+1} \sigma_{\text{off}} K_{c0}}{\sqrt{(k\sigma_{\text{on}}^2 + \sigma_{\text{off}}^2)}} \sum_{v_1=1}^{N_v} K_f \left\{ \frac{\exp(-k_l K_d^2)}{2} \right. \\
&\quad \left. + \frac{1}{(2N_G + 1) \sqrt{k_l}} \sum_{q=1}^{N_G} \frac{\sqrt{c} \sin(K_d \tau_q)}{\sin^2 \left[ \left( \frac{2q-1}{2N_G + 1} \right) \frac{\pi}{2} \right]} F_D \left( \frac{\tau_q}{2 \sqrt{k_l}} \right) \right\}
\end{aligned} \tag{4-104}$$

The average pairwise error probability  $P_{s \rightarrow s'}(E)$  for one PPM symbol in the SISO FSO systems can be represented as

$$\begin{aligned}
P_{s \rightarrow s'}(E) &= \frac{1}{(L-1)} P_s(E) \\
&\leq \frac{1}{2^Q - 1} \sum_{k=1}^{L-1} \frac{C_{L-1}^k (-1)^{k+1} \sigma_{\text{off}} K_{c0}}{\sqrt{(k\sigma_{\text{on}}^2 + \sigma_{\text{off}}^2)}} \sum_{v_1=1}^{N_v} K_f \left\{ \frac{\exp(-k_l K_d^2)}{2} \right. \\
&\quad \left. + \frac{1}{(2N_G + 1) \sqrt{k_l}} \sum_{q=1}^{N_G} \frac{\sqrt{c} \sin(K_d \tau_q)}{\sin^2 \left[ \left( \frac{2q-1}{2N_G + 1} \right) \frac{\pi}{2} \right]} F_D \left( \frac{\tau_q}{2 \sqrt{k_l}} \right) \right\}
\end{aligned} \tag{4-105}$$

where  $L$  is the number of the slots in one Q-ary PPM symbol,  $L = 2^Q$ .

### 4.3 Error Analysis for SEP and BEP Calculations

The average error probabilities of MIMO and SISO systems with lognormal fading channels are calculated in Section 4.1 and Section 4.2. The errors introduced by numerical calculations and truncations are analyzed in this section in detail.

#### 4.3.1 Error Analysis for the Average SEP and BEP Calculation

As the complexity of MIMO transmissions, the calculation employs the Chernov Bound, Gaussian Hermite numerical integration, Gaussian Laguerre numerical integration, Gauss Chebyshev numerical integration, Fourier series and Dawson integral approximation. These calculations employ the summation of infinite series and numerical calculation. In order to make the calculation tractable, the infinite summations are truncated. Thus, the discretization error and truncation error are introduced. If the discretization step is sufficiently small and the number of terms in the truncated summation is sufficiently large, the discretization error and truncation error are negligible. If the calculation of the error probabilities employs the Fourier series method, the total error  $E(e)$  can be represented as

$$E(e) = E_{CB}(\delta) + E_{GH}(N_u) + E_{GL}(N_v) + E_{FS}(N_F) + E_{TFS}(N_F) + E_D(N_D) + E_{TD}(N_D) \quad (4-106)$$

If the calculation employs the Gaussian Chebyshev method, the total error  $E(e)$  can be represented as

$$E(e) = E_{CB}(\delta) + E_{GH}(N_u) + E_{GL}(N_v) + E_{GC}(N_G) + E_D(N_D) + E_{TD}(N_D) \quad (4-107)$$

Where  $E_{CB}(\delta)$ ,  $E_{GH}(N_u)$ ,  $E_{GL}(N_v)$ ,  $E_{FS}(N_F)$ ,  $E_{GC}(N_G)$ ,  $E_D(N_D)$  are the calculation errors of the Chernov bound, Gaussian Hermite numerical integration, Gaussian Laguerre numerical integration, Fourier series technique, Gauss Chebyshev

numerical integration and Dawson integral approximation, respectively.  $E_{TFS}(N_F)$  and  $E_{TD}(N_D)$  are the truncation error of the Fourier series method and Dawson's Integral approximation.

For Dawson's integral approximation in Eq. (4-76), Eq. (4-77), (4-78) and Eq. (4-79), if the choices of the step  $h_d = 0.4$  and the term number  $N_D = 11$  are made, the accuracy of the result is about  $2 \times 10^{-7}$ [7]. This is small enough for the error probability calculation of MIMO FSO systems.

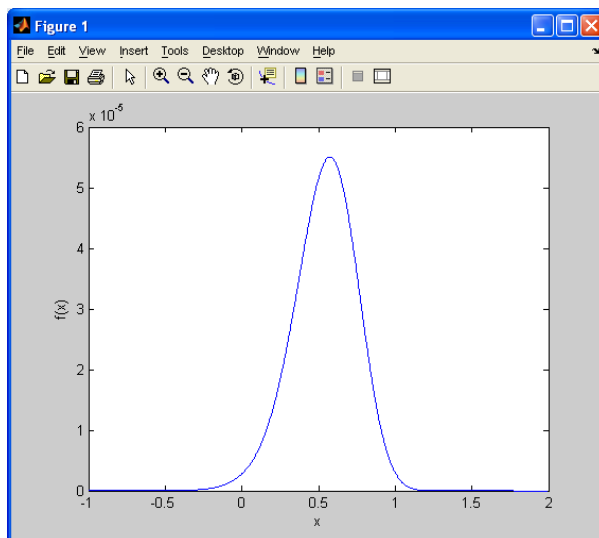
For Gaussian Hermite numerical integration, Gaussian Laguerre numerical integration and Gaussian Chebyshev numerical integration, the computation error is given in the reference [4]. From Eq. (3-45), the error of the Gaussian Hermite numerical integration is [4]

$$E_{GH}(N_u) = \frac{N_u! \sqrt{\pi}}{2^{N_u} (2N_u)!} f^{(2N_u)}(x) \quad -\infty < x < \infty \quad (4-108)$$

The function  $f(x)$  in Eq. (3-45) is

$$f(x) = \frac{\eta^F}{\sqrt{2\pi} M} \left[ \eta e^{(\sqrt{2}\sigma_\ell x + \ln \bar{\lambda}_{s_{ij}} + m_\ell)} + \frac{m_{s_{ij}}(F-1)}{M} \right]^{-\frac{3}{2}} \exp \left\{ - \frac{\left( \eta e^{(\sqrt{2}\sigma_\ell x + \ln \bar{\lambda}_{s_{ij}} + m_\ell)} - \frac{m_{s_{ij}}}{M} \right)^2}{2 \left[ \eta e^{(\sqrt{2}\sigma_\ell x + \ln \bar{\lambda}_{s_{ij}} + m_\ell)} + \frac{m_{s_{ij}}(F-1)}{M} \right]} + \sqrt{2}\sigma_\ell x + \ln \bar{\lambda}_{s_{ij}} + m_\ell \right\} \quad (4-109)$$

Figure 4.3 shows the plot of  $f(x)$  with  $\bar{\lambda}_{s_{ij}} = 800$ ,  $m_{s_{ij}} = 32000$ ,  $\sigma_\ell = 0.4458$ ,  $m_\ell = -\frac{\sigma_\ell^2}{2}$ ,  $\eta = 78\%$ ,  $M = 40$ ,  $F = M^{0.7}$  for InGaAs APD. If the parameters change, the plot of  $f(x)$  changes from that in Fig 4.3, but it still converges in the similar manner.

Figure 4.3 Plot of  $f(x)$  in Eq. (4-109)

The first order derivative of the function  $f(x)$  is calculated in Appendix O and can be represented as

$$\begin{aligned} \frac{d[f(x)]}{dx} = & \frac{\eta F}{\sqrt{2\pi} M} \left[ \eta e^{(\sqrt{2}\sigma_\ell x + \ln\bar{\lambda}_{sij} + m_\ell)} + \frac{m_{sij}(F-1)}{M} \right]^{-\frac{3}{2}} \\ & \exp \left\{ - \frac{\left[ \eta e^{(\sqrt{2}\sigma_\ell x + \ln\bar{\lambda}_{sij} + m_\ell)} - \frac{m_{sij}}{M} \right]^2}{2 \left[ \eta e^{(\sqrt{2}\sigma_\ell x + \ln\bar{\lambda}_{sij} + m_\ell)} + \frac{m_{sij}(F-1)}{M} \right]} + \sqrt{2}\sigma_\ell x + \ln\bar{\lambda}_{sij} + m_\ell \right\} \\ & \left\{ - \frac{\eta e^{(\sqrt{2}\sigma_\ell x + \ln\bar{\lambda}_{sij} + m_\ell)} \sqrt{2}\sigma_\ell \left\{ 3 + 2 \left[ \eta e^{(\sqrt{2}\sigma_\ell x + \ln\bar{\lambda}_{sij} + m_\ell)} - \frac{m_{sij}}{M} \right] \right\}}{2 \left[ \eta e^{(\sqrt{2}\sigma_\ell x + \ln\bar{\lambda}_{sij} + m_\ell)} + \frac{m_{sij}(F-1)}{M} \right]} \right. \\ & \left. + \frac{\left[ \eta e^{(\sqrt{2}\sigma_\ell x + \ln\bar{\lambda}_{sij} + m_\ell)} - \frac{m_{sij}}{M} \right]^2 \eta e^{(\sqrt{2}\sigma_\ell x + \ln\bar{\lambda}_{sij} + m_\ell)} \sqrt{2}\sigma_\ell}{2 \left[ \eta e^{(\sqrt{2}\sigma_\ell x + \ln\bar{\lambda}_{sij} + m_\ell)} + \frac{m_{sij}(F-1)}{M} \right]^2} + \sqrt{2}\sigma_\ell \right\} \end{aligned} \quad (4-110)$$

Figure 4.4 shows the plot of  $\frac{d[f(x)]}{dx}$  with  $\bar{\lambda}_{sij} = 800$ ,  $m_{sij} = 32000$ ,  $\sigma_\ell = 0.4458$ ,

$m_\ell = -\frac{\sigma_\ell^2}{2}$ ,  $\eta = 78\%$ ,  $M = 40$ ,  $F = M^{0.7}$  for InGaAs APD.

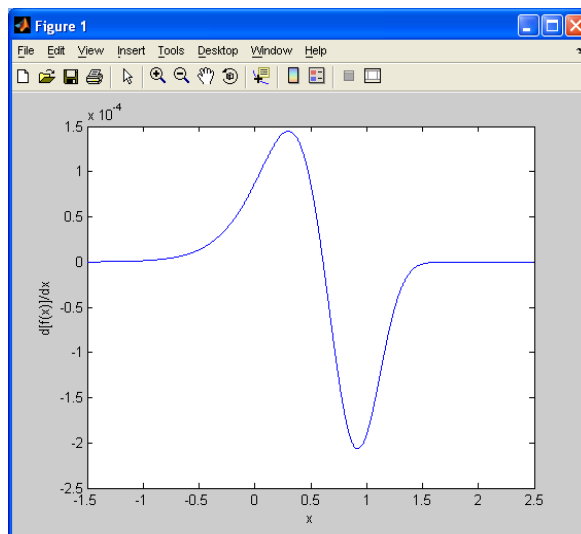


Figure 4.4 Plot of  $\frac{d[f(x)]}{dx}$  in Eq. (4-110)

The first order derivative  $\frac{d[f(x)]}{dx}$  of  $f(x)$  is the slope of the curve of  $f(x)$  in Fig. 4.3. According to the calculation in Appendix O and the plots of  $f(x)$  and  $\frac{d[f(x)]}{dx}$  in Fig. 4.3 and Fig. 4.4, the curves of  $f(x)$  and  $\frac{d[f(x)]}{dx}$  have upper bounds. The high order derivatives of  $f(x)$  also have the upper bounds. It can be assumed that the  $N_u$ -order derivative of  $f(x)$  has the upper bound  $f(x) \leq C_{GH}$ , for  $-\infty \leq x < \infty$ . If  $N_u = 20$ , the value of  $\frac{N_u! \sqrt{\pi}}{2^{N_u} (2N_u)!}$  part in Eq. (4-108) is  $5.0403 \times 10^{-36}$ . The value of the error in Eq. (4-108) has the upper bound  $5.0403 \times 10^{-36} C_{GH}$ . The error value can be sufficiently small if  $N_u$  is sufficiently large.

In the calculation of Eq. (4-57), the error equation of the Gaussian Laguerre integral is [4]

$$E_{GL}(N_v) = \frac{(N_v!)^2}{(2N_v)!} f^{(2N_v)}(x) \quad 0 < x < \infty \quad (4-111)$$

The function  $f(x)$  in Eq. (4-57) is

$$\begin{aligned}
g(h_{il}) &= [(F-1)K_k h_{il} + K_{x_u}]^{(-\frac{3}{2})} \exp \left\{ h_{il} - \frac{K_k (h_{il} - e^{m_\ell e^{\sqrt{2} \sigma_\ell x_u})^2}}{2[(F-1)h_{il} + e^{m_\ell e^{\sqrt{2} \sigma_\ell x_u}]} + j\omega h_{il} \right\} \\
&= [(F-1)K_k h_{il} + K_{x_u}]^{(-\frac{3}{2})} \exp \left\{ h_{il} - \frac{K_k (h_{il} - e^{m_\ell e^{\sqrt{2} \sigma_\ell x_u})^2}}{2[(F-1)h_{il} + e^{m_\ell e^{\sqrt{2} \sigma_\ell x_u}]} \right\} \cos(\omega h_{il}) \\
&\quad + j [(F-1)K_k h_{il} + K_{x_u}]^{(-\frac{3}{2})} \exp \left\{ h_{il} - \frac{K_k (h_{il} - e^{m_\ell e^{\sqrt{2} \sigma_\ell x_u})^2}}{2[(F-1)h_{il} + e^{m_\ell e^{\sqrt{2} \sigma_\ell x_u}]} \right\} \sin(\omega h_{il}) \\
&= g_1(h_{il}) + jg_2(h_{il}) \tag{4-112}
\end{aligned}$$

where  $0 \leq h_{il} < \infty$ . According to the values of the parameters in Eq. (4-112), the plots of  $g_1(h_{il})$  and  $g_2(h_{il})$  vary as  $h_{il} \geq 0$  and  $h_{il}$  increases but the forms of these plots are similar. For example, plots of  $g_1(h_{il})$  and  $g_2(h_{il})$  are shown in Fig. 4.5 and Fig. 4.6.

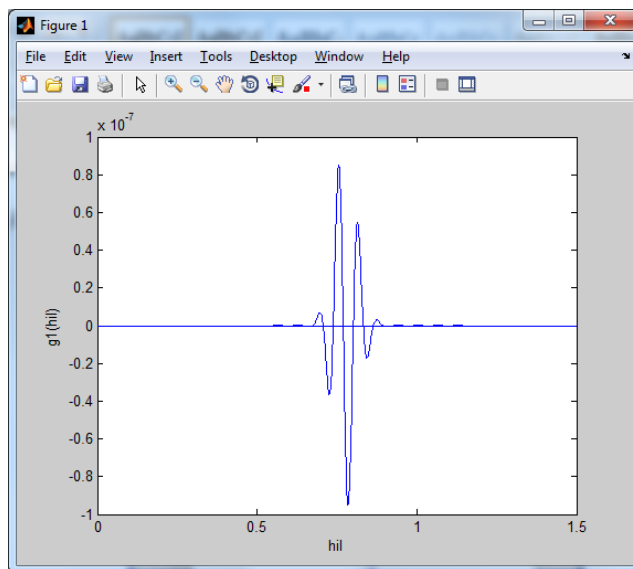


Figure 4.5 Plot of  $g_1(h_{il})$  in Eq. (4-112)

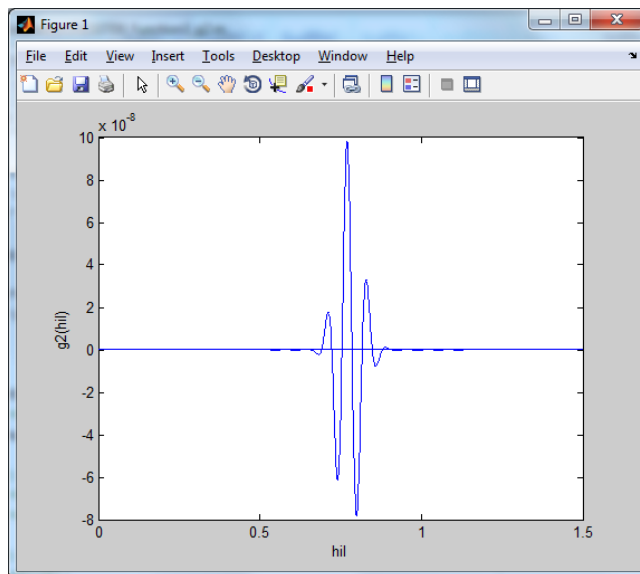


Figure 4.6 Plot of  $g_2(h_{il})$  in Eq. (4-112)

According to the example plots in Fig. 4.5 and Fig. 4.6, the functions  $g_1(h_{il})$  and  $g_2(h_{il})$  have the upper bounds. The calculations of the first order derivative of  $g_1(h_{il})$  and  $g_2(h_{il})$  are similar to the calculations for  $f(x)$  in Appendix O and they are bounded above. It can be assumed that the high order derivatives of  $g_1(h_{il})$  and  $g_2(h_{il})$  have also the upper bound  $C_{GL}$ . If  $N_v = 15$ , the value of  $\frac{(N_v!)^2}{(2N_v)!}$  part in Eq. (4-111) is  $6.4467 \times 10^{-9}$ . According to the calculation of the derivatives, the computation errors in  $g_1(h_{il})$  and  $g_2(h_{il})$  in Eq. (4-112) have the upper bound  $6.4467 \times 10^{-9} \times C_{GL}$ . The error value can be sufficiently small if  $N_v$  is large enough.

For the Fourier series of Eq. (4-80) and Eq. (4-81), the calculation result turns out to be a trapezoidal rule approximation. The error usually associated with the trapezoidal rule is simply determined by the step size  $T_F = \frac{2\pi}{\omega_0}$ . The discretization error can be made sufficiently small by choosing the step size  $T_F$  sufficiently small. To obtain a specified numerical accuracy, we must contend with the error due to the truncation of the Fourier series. In all practical problems, the series is usually

truncated after  $N_F$  terms. It is the well-known that the partial sum of the Fourier series truncated after  $(N_F + 1)$  term is given by [12]

$$f_N(t) = \frac{1}{\pi} \int_{-\pi}^{\pi} f(x) C_N(x-t) dx \quad (4-113)$$

where the kernel is defined as [12]

$$C_N(x) = \sin \left[ \left( N + \frac{1}{2} \right) x \right] \left[ \sin \left( N + \frac{x}{2} \right) \right]^{-1} \quad (4-114)$$

A more practical determination is found by using the fact that for an oscillating series, the error in truncating the series is approximately the value of the term at which the truncation is made [12]. The computational time of the Fourier series can be reduced significantly by using the Fast Fourier Transforms [12].

In the analysis of MIMO FSO systems, the average error probability for the conditions of either the fading channel gain  $h$  or the received signal to noise ratio  $\gamma$  is employed [2,3]. The conditional error probability for L-ary PPM signaling employing the noncoherent detection scheme includes the Gaussian probability integral  $Q(\cdot)$  function. Thus, there is a tradeoff between the accuracy and the simplicity of the error probability calculation. The Chernov bound is a very tight and useful bound frequently employed in communication systems. In this dissertation, the Chernov bound for the AWGN channel is used to calculate the error probability.

For optical receivers under normal working condition, the signal to noise ratio  $\gamma$  is much bigger than  $\gamma = 0dB$ ,  $\left( \frac{E_s \mathcal{R}MAg}{N_t} E\{h\} \right)^2 \geq \sigma_{on}^2$ ,  $\left( \frac{E_s \mathcal{R}MAg}{N_t} E\{h\} \right)^2 \geq \sigma_{off}^2$  and  $\sigma_{on}^2 \geq \sigma_{off}^2$ . Assuming  $E\{h\} = 1$ , the mean value  $M_{\gamma_1}$  of the variable  $\frac{E_s \mathcal{R}MAg}{N_t \sigma_{off}} h + \frac{n_{on}}{\sigma_{off}}$  is

$$\begin{aligned}
M_{\gamma_1} &= E \left\{ \frac{E_s \mathcal{R}MAG}{N_t \sigma_{\text{off}}} h + \frac{n_{on}}{\sigma_{\text{off}}} \right\} \\
&= \frac{E_s \mathcal{R}MAG}{N_t \sigma_{\text{off}}} E\{h\} + \frac{E\{n_{on}\}}{\sigma_{\text{off}}} \\
&= \frac{E_s \mathcal{R}MAG}{N_t \sigma_{\text{off}}} \\
&\geq 1
\end{aligned}$$

(4-115)

The calculations in Appendix G employ the inequality of Eq. (4-23) to obtain the computation error.

$$\begin{aligned}
&P \left[ n_2 \leq \frac{E_s \mathcal{R}GMAg}{N_t} h + n_1 \mid \mathbf{S}_1 \text{ sent}, n_1 = n_{on}, h \right] \\
&= 1 - 2Q \left( \left| M_{\gamma_1} h + \frac{n_{on}}{\sigma_{\text{off}}} \right| \right) \\
&\geq 1 - e^{-\frac{\left( M_{\gamma_1} h + \frac{n_{on}}{\sigma_{\text{off}}} \right)^2}{2}}
\end{aligned}$$

(4-116)

When the signal to noise ratio  $\gamma$  is zero,  $\gamma = 0dB$ , the value of  $M_{\gamma_1}$  is around 1, i.e.  $M_{\gamma_1} \approx 1$ . Under most working conditions, the signal to noise ratio is far above 0dB, as  $\gamma = 10dB$  and  $M_{\gamma_1} \gg 1$ . Letting  $x = \frac{n_{on}}{\sigma_{\text{off}}}$  and  $\gamma_1 = M_{\gamma_1} h$ , the functions are

$$2Q \left( \left| M_{\gamma_1} h + \frac{n_{on}}{\sigma_{\text{off}}} \right| \right) = 2Q(|M\gamma_1 + x|)$$

(4-117)

$$\left[ e^{-\frac{\left( M_{\gamma_1} h + \frac{n_{on}}{\sigma_{\text{off}}} \right)^2}{2}} \right] = \left[ e^{-\frac{(M\gamma_1 + x)^2}{2}} \right]$$

(4-118)

The diagrams of the functions  $2Q\left(\left|M_{\gamma_1} h + \frac{n_{on}}{\sigma_{off}}\right|\right)$  and  $\left[e^{-\frac{\left(M_{\gamma_1} h + \frac{n_{on}}{\sigma_{off}}\right)^2}{2}}\right]$  with

$M_{\gamma_1} = 1$  ( $\gamma = 0dB$ ) and  $M_{\gamma_1} = 6$  ( $\gamma = 7.7815dB$ ) are shown in Fig. 4.7 and Fig. 4.8, respectively.

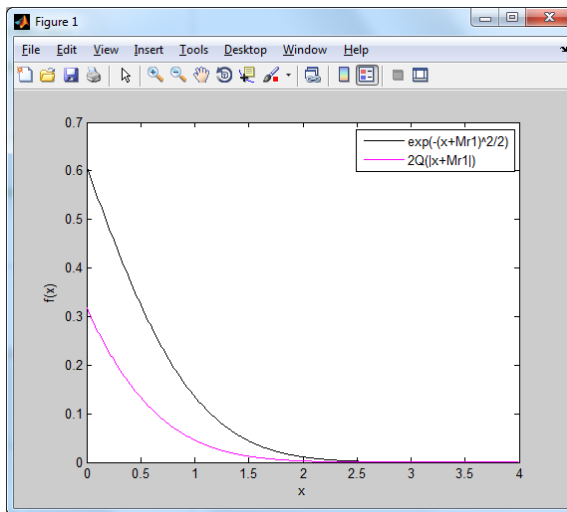


Figure 4.7 Plot of the functions in Eq. (4-117) and Eq. (4-118) with  $M_{\gamma_1} = 1$

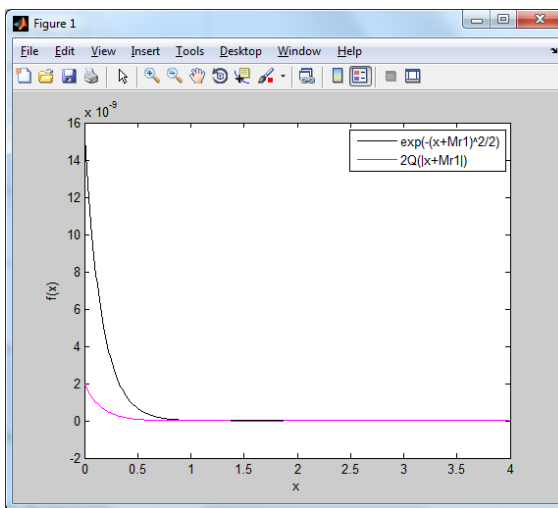


Figure 4.8 Plot of the functions in Eq. (4-117) and Eq. (4-118) with  $M_{\gamma_1} = 6$

where  $x = \frac{n_{on}}{\sigma_{off}}$  and  $f(x) = 2Q\left(\left|M_{\gamma_1} h + x\right|\right)$  or  $\left[e^{-\frac{\left(M_{\gamma_1} h + x\right)^2}{2}}\right]$ . At  $M_{\gamma_1} = 1$  and the signal to noise ratio around 0dB, the calculation error using the inequality in Eq. (4-

117) is about 0.3. As the variant  $M\gamma_1$  changes, the calculation error changes as shown in Fig. 4.7 and Fig. 4.8. The Chernov bound provides an upper bound on the error probability and makes the calculation simpler.

The error of Gauss Chebyshev numerical integration is [4]

$$E_{GC}(N_G) = \frac{\pi}{(2N_G)!2^{4N_G+1}} f^{(2N_G)}(x) \quad 0 < x < 1 \quad (4-119)$$

The function  $f(x)$  for the Eq. (4-89a) is

$$g(x) = \sin\left(K_d \sqrt{\frac{cx}{1-x}}\right) \frac{1}{\sqrt{k_l}} F_D\left(\frac{1}{2\sqrt{k_l}} \sqrt{\frac{cx}{1-x}}\right) \frac{\sqrt{c}}{2x(1-x)} \quad 0 \leq x \leq 1 \quad (4-120)$$

The diagram of  $g(x)$  in Eq. (4-120) as  $0 \leq x \leq 1$  and  $x$  increases is shown in Fig. 4.9

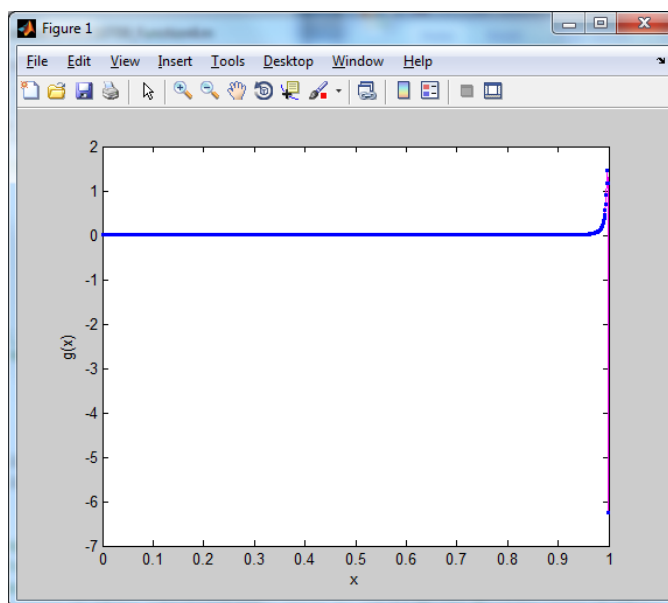


Figure 4.9 Plot of  $g(x)$  in Eq. (4-120)

In Fig. 4.9, as  $x$  reaches near to 1, the diagram of Eq. (4-120) becomes highly oscillatory and does not converge. The derivative of  $g(x)$  is the slope of the curve. If  $N_G = 20$ , the value of  $\frac{\pi}{(2N_G)!2^{(4N_G+1)}}$  part in Eq. (4-119) is  $1.5925 \times 10^{-72}$ . It is difficult to obtain the value of Eq. (4-120). Thus it is difficult to calculate the value or

the upper bound of the error value in Eq. (4-119), but the error value can be small if  $N_G$  is larger.

### REFERENCES

- [1]. John G. Proakis and Masoud Salehi, "Digital Communicaitons," McGraw Hill, Inc., fifth edition, 2008.
- [2]. Marvin K. Simon and Mohamed-Slim Alouini, "Digital Communication over Fading Channels," 2005, John Wiley & Sons, Inc., second edition.
- [3]. A. Annamalai and C. Tellambura and Vijay K. Bhargava, " A general method for calculating Error Probabilities over fading Channels" , IEEE Transactions on Communications, Vol. 53, No.5, May 2005.
- [4]. M. Abramowitz and I. A. Stegun, " Handbook of Mathematical Functions with Formulas, Graphs and Mathematical Tables", 9th ed. New York, NY : Dover Publications,1970.
- [5]. I.S. Gradshteyn and I.M. Ryzhik "Table of integrals, series and products ",1980.
- [6]. A. Annamalai and C. Tellambura and Vijay K. Bhargava, "Unified Analysis of Equal-Gain Diversity on Rician and Nakagami Fading Channels", IEEE Wireless Communications and Networking Conference, 1999, pp10 - 14, vol.1, 0-7803-5668-3
- [7]. "Dawson's Integral. Numerical Recipes in Fortran 77: the art of scientific computing" (ISBN 0-521-43064-X) Copyright (C) 1986-1992, Cambridge University

Press, [http://www.mpi-hd.mpg.de/astrophysik/HEA/internal/Numerical\\_Recipes/f6-10.pdf](http://www.mpi-hd.mpg.de/astrophysik/HEA/internal/Numerical_Recipes/f6-10.pdf).

[8]. H. Dubner and J. Abate “Numerical inversion of Laplace Transforms by Relating them to the finite Fourier Cosine Transform” Journal of the Association for Computing Machinery , Vol. 15, No. 1, January 1968, pp 115-123.

[9]. A. Annamalai and C. Tellambura and Vijay K. Bhargava, “A General Method for Calculation Error Probabilities Over Fading Channels”, IEEE Transactions on Communication, Vol. 53, No.5, May 2005.

[10]. Gerd Keiser, “Optical Fiber Communicaitons,” third edition, McGraw-Hill, Inc. 2000.

[11]. Govind P. Agrawal, “Fiber-optic Communication Systems”, second edition, 1997, pp170-171.

[12]. H. Dubner and J. Abate “Numerical inversion of Laplace Transforms by Relating them to the finite Fourier Cosine Transform” Journal of the Association for Computing Machinery , Vol. 15, No. 1, January 1968, pp 115-123.

## CHAPTER 5

### SYSTEM MODEL AND ANALYTICAL RESULTS

#### 5.1 MIMO FSO System Model and Results

According to average error probability calculations in Chapter 4, the system performance has been obtained from the given SEP and BEP equations. In this chapter, the model used for the analysis is designed and the parameters are set as shown in Table 5-1.

##### 5.1.1 Model Used for Analysis

The structure of a MIMO FSO system is shown in Fig. 3.1 and Fig. 3.3 and a detailed description and analysis were presented in Chapter 3 and Chapter 4. At the receivers,  $N_r$  receiving branches are included and each branch includes the InGaAs APD, GaAs MESFET amplifier, matched filter and equalizer, sampling circuit and decision detector, etc. All these components are suitable for practical multi-gigabit-per-second (multi-Gb/s) short range (up to 2~3 km) links in MIMO FSO systems. Typical values of the parameters generally used in optical devices are given in Table 5-1. Analytical results of the average error probabilities for MIMO FSO systems are presented in this section, emphasizing the role of parameters such as  $N_t$ ,  $N_r$ ,  $M$ ,  $A$ ,  $L$  and  $\sigma_\ell$ , etc.

Lognormal fading channels describe FSO communication under weak turbulence, which are the most common working conditions for FSO. By noting that  $\langle e^\ell \rangle = \langle \frac{I}{I} \rangle = 1$  and Eq. (3-25a), the mean of the log intensity  $\ell$  is equal to  $-\frac{\sigma_\ell^2}{2}$ , i.e.  $m_\ell = -\frac{\sigma_\ell^2}{2}$ , and the average optical field amplitude is neither attenuated nor amplified. The research and analysis in this dissertation focus on the lognormal fading

channel. At the receivers, InGaAs APD working at 1550nm wavelength is employed and GaAs MESFETs are used as the preamplifier and main amplifier working in the linear region of their characteristics. During the transmission in free space, laser beams are scattered and bent along the paths and the PPM pulses suffer attenuation and dispersion. The parameter  $\gamma_s$  represents the percentage of the energy that is kept in the 1 pulse slot. In practice, the sampling time of the optical receiver fluctuates from bit to bit due to the nature of the noise in the input to the clock-recovery circuit. Such fluctuations are called timing jitter and this can also cause the pulse energy to fall out of the 1 pulse slot. The matched filter and equalizer are used in the receivers. EGC with envelope detection and maximum likelihood detection are implemented in the decision parts. It is assumed that the lasers operate on a peak-power constraint and the total transmitting power for one 1 pulse by the laser array is constrained as  $E_s$ . Thus the performance of SISO and MIMO systems can be easily compared. The Fourier series for the SEP and BEP calculation is mainly used in the calculation and analysis.

### **5.1.2 Parameters of MIMO FSO Systems**

The parameters used in the analysis of this chapter are set according to Table 5-1, unless otherwise specified. The parameters for the InGaAs APD are set as the values of the generic operating parameters given in Ref [1, pp267, Table 6-1]. The parameters of GaAs MESFETs are set as the typical values given in Ref [1, pp308, Table 7-2], Ref [1, pp301, Fig. 7-13] and Ref [1, pp302, Fig. 7-14]. The parameters of the free space optical channel are given in Ref [2]. The parameters for the link budget are given by Ref [3].

Table 5-1  
Parameters of MIMO FSO systems

Parameter	Value	Unit
$N_r$	2	
$N_t$	2	
$L$	4	
$\lambda$	1550	nm
$T$	293	K
$C_n^2$	$1 \times 10^{-14}$	$m^{(-\frac{2}{3})}$
$\eta$	75%	
$M$	40	
$A$	40	
$x$	0.7	For InGaAs
$R_b$	1000	$\Omega$
$R_f$	$10^6$	$\Omega$
$g_m$	$30 \times 10^{-3}$	$mS$
$C$	10	$pF$
$B$	$1 \times 10^9$	$bit/s$
$P_c$	$1 \times 10^{-20}$	A
$P_b$	$3 \times 10^{-20}$	A
$I_{db}$	$50 \times 10^{-9}$	A
$I_{ds}$	$2 \times 10^{-9}$	A
$\Gamma_e$	1.1	
$I_{gate}$	$50 \times 10^{-9}$	nA
$\gamma_s$	0.95	

$I_2$	0.45	
$I_3$	0.0855	
$d_r$	0.075	m
$d_b$	1	m
$A_r$	$4.4156 \times 10^{-3}$	$m^2, A_r = \pi \left(\frac{d_r}{2}\right)^2$
$A_b$	0.785	$m^2, A_b = \pi \left(\frac{d_b}{2}\right)^2$
$V_s$	2	km
$D_s$	1	km
$\alpha_{a\_dB}$	3.99	dB/km
$\eta_{t\_dB}$	3	dB
$\eta_{r\_dB}$	3	dB
$\eta_{pt\_dB}$	3	dB
$\eta_{pr\_dB}$	3	dB
$h_d$	0.4	
$N_D$	11	

## 5.2 Results and Analysis of the Average Error Probability

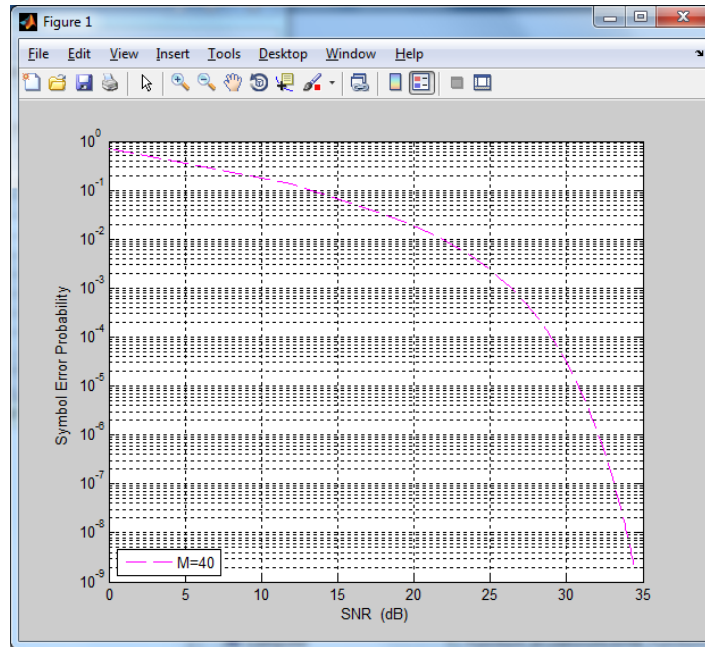
The system models for the analysis of MIMO FSO system are designed and discussed in Chapters 2, 3, 4 and Section 5.1. The components with the corresponding probabilistic characteristics in these models are analyzed. Different parameters of these components are set in Section 5.2. The analytical results are represented through various plots and the results have been discussed in this section in detail.

### 5.2.1 SISO and MIMO Comparison

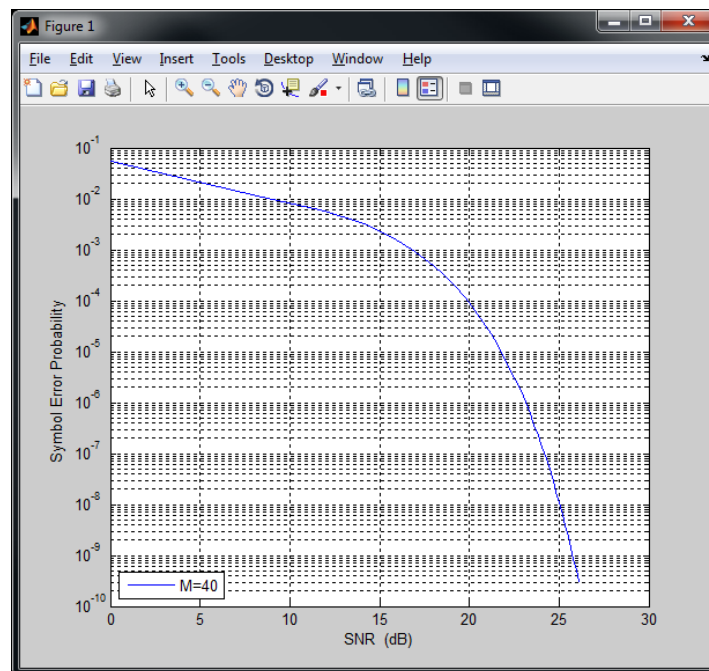
In SISO wireless optical communication systems, link performance can be seriously impaired by adverse atmospheric conditions. In particular, one important atmospheric effect is the attenuation due to scattering and absorption. Another important effect is scintillation due to turbulence and the free space channel is modeled as the lognormal fading channel. One method to reduce these impacts is to use the MIMO technique to transmit the redundant symbols to overcome channel fading.

A detailed calculation of the error probabilities for SISO and MIMO systems has been discussed in Chapter 4. The parameter setting is given in Subsection 5.1.2. The equation of average SEP and BEP are obtained in Eq. (4-81), Eq. (4-84), Eq. (4-92) and Eq. (4-94). Under atmospheric turbulence with  $\sigma_\ell^2 = 0.19877$ ,  $C_n^2 = 10^{-14} m^{(-\frac{2}{3})}$  and the pulse dispersion as  $\gamma_s = 0.95$ , the plots of the average SEP corresponding to average SNR for SISO and MIMO systems are shown in Fig. 5.1(a) and Fig. 5.1(b). The numbers of the transmitting laser and the receiving APDs in the MIMO systems are  $N_t = 2$  and  $N_r = 2$  and the length of the transmitted PPM symbol is  $L = 2$ . In the SISO systems, the average SEP of  $L = 2$  PPM symbols is about 0.71 at  $SNR = 0dB$ . MIMO systems result in lower average SEP and BEP than SISO systems under similar conditions and the same average SNR. Thus MIMO systems have a better performance than SISO systems. For different services, like voice, data and video, the required BEP of communication links are different. For  $SEP = 10^{-6}$  which is in the range of common working conditions for normal services, the required

SNR of MIMO systems is about 23.13dB , which is about 9dB lower than the required 32d.01B SNR of SISO systems.



(a)



(b)

Figure 5.1 (a) Average SEP of SISO FSO systems with  $L = 2$  PPM symbols(b) Average SEP of MIMO FSO systems with  $L = 2$  PPM symbols

The relationship between the average BEP and the received optical energy is analyzed for FSO communication systems. The received optical energy for free space PPM transmission is given by

$$\bar{J}_r(dBJ) = 10\log\left(J_{s1}\frac{B}{L}\right) \quad (5-1a)$$

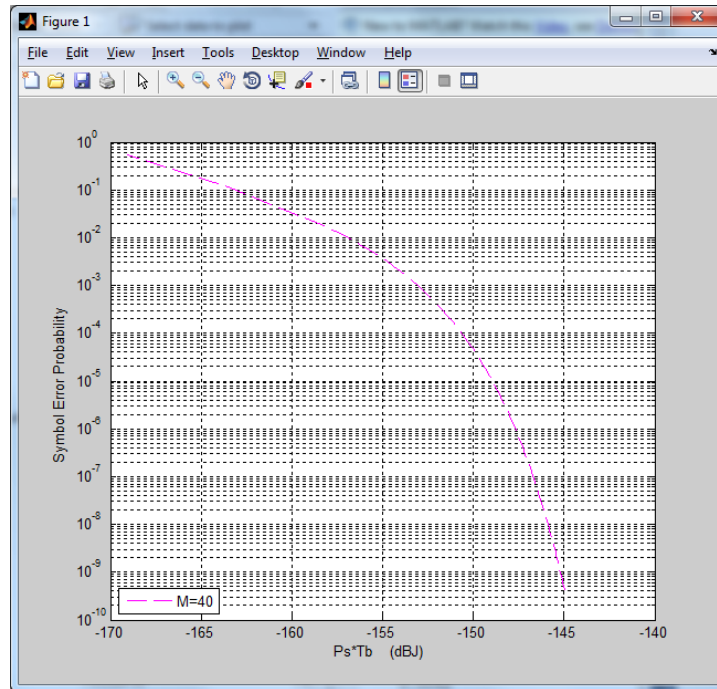
where  $\bar{J}_r(dBJ)$  is the received optical energy in dBJ,  $J_{s1}$  is the energy for one 1 pulse in  $J$ ,  $B$  is the data rate and  $L$  is the number of the slots in one Q-ary PPM symbol,  $L = 2^Q$ .

The average BEP corresponding to the received optical power for free space PPM transmission is given by

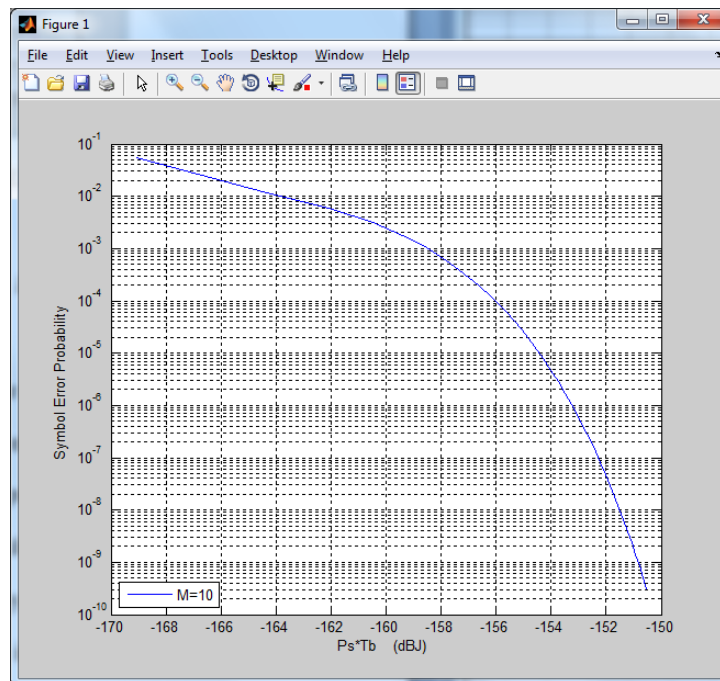
$$\bar{P}_r(dBm) = 10\log\left(P_{s1}\frac{B}{L}\right) \quad (5-1b)$$

where  $\bar{P}_r(dBm)$  is the received optical power in dBm,  $P_{s1}$  is the power for one 1 pulse in Watt,  $B$  is the data rate and  $L$  is the number of the slots in one Q-ary PPM symbol,  $L = 2^Q$ .

For the parameter values of Table 5-1 and with the bandwidth of  $B = 1Gb/s$ , the SEPs of SISO and MIMO systems corresponding to the received optical energy are shown in Fig. 5.2(a) and Fig. 5.2(b). At average  $SEP = 10^{-6}$ , the received optical energy required for MIMO systems is about -153.24dBJ, which is about 6.5dB lower than the -147.75dBJ of SISO systems. The average SEPs of SISO and MIMO systems corresponding to the received optical power are shown in Fig. 5.2(c) and Fig. 5.2(d). At average  $SEP = 10^{-6}$ , the received optical power required for MIMO systems is about -33.3dBm, which is lower than -27.75dBm of SISO systems. These results show that MIMO can improve the system performance, especially in the normal working range of the average  $SEP = 10^{-3} \sim 10^{-7}$ .

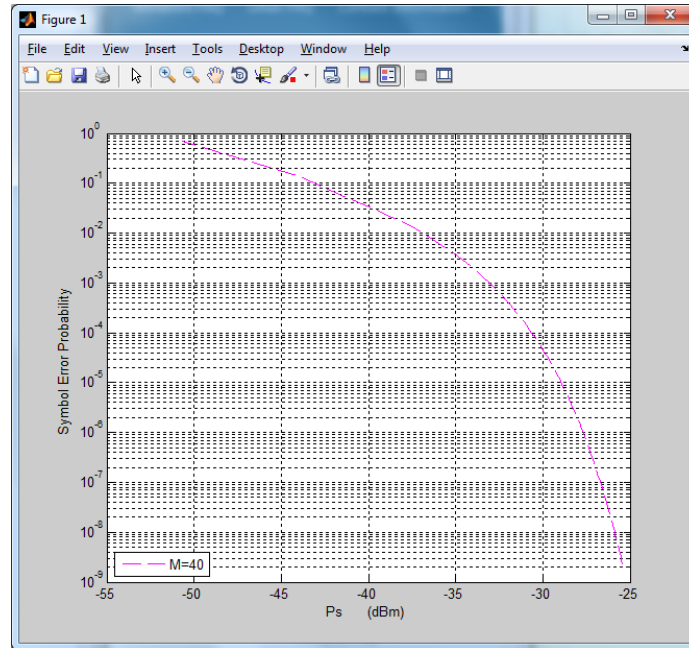


(a)

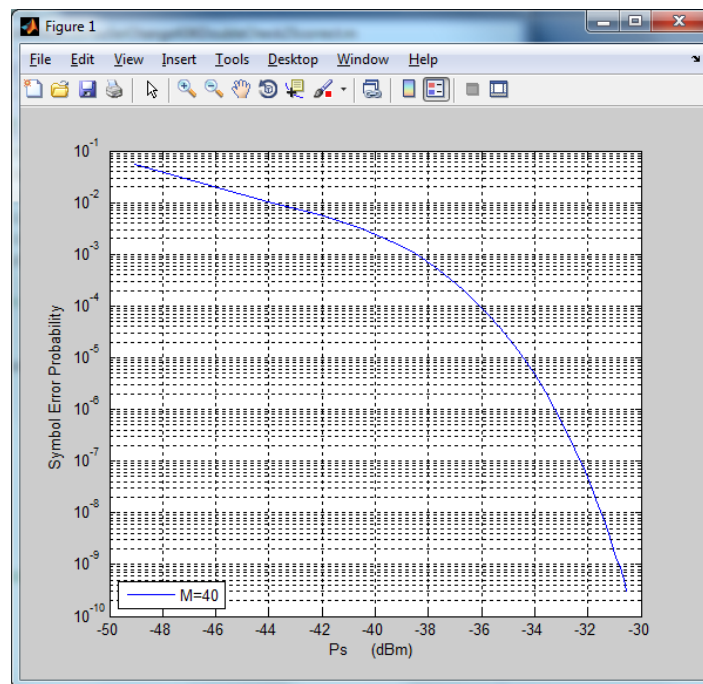


(b)

Figure 5.2 (a) Average SEP of SISO FSO systems with  $L = 2$  PPM symbol(b) Average SEP of MIMO FSO systems with  $L = 2$  PPM symbol



(c)



(d)

Figure 5.2 (c) Average SEP of SISO FSO systems with  $L = 2$  PPM symbol(d) Average SEP of MIMO FSO systems with  $L = 2$  PPM symbol

## 5.2.2 Optical Device Impact

### (a) Performance Comparison of APDs

In Chapter 2, the wavelength choice is discussed and 1550nm is considered as the suitable wavelength in FSO. There are different types of commercial lasers available at 1550 nm wavelength. For photodetectors, there are three widely used materials, silicon (Si), germanium (Ge) and indium gallium arsenide (InGaAs). For short distance applications, Si devices operating around 850nm provide relatively inexpensive solutions for most links and longer links usually require operation in the 1300nm and 1550nm [10]. Ge APDs and InGaAs APDs both work at 1550nm and can be considered for a multi-gigabit-per-second (multi-Gb/s) bandwidth. The generic operating parameters of commercial Si, Ge and InGaAs avalanche photodiodes are given in Ref [1, pp267, Table 6-1]. For Ge APDs, the product of APD gain and bandwidth, i.e.  $M \times B$ , is fixed in the range of 20~40 GHz. As the avalanche gain  $M$  of Ge APDs is in the range of 50~200, there is a tradeoff between the APD gain and the bandwidth of Ge APDs. PD-LD, Inc. provides one Ge APD “PDGAJ1001FCA-0-0-01” working at 1550nm with 1.5GHz bandwidth [5]. But the APD gain is not provided in the data sheet. Hamamatsu, Inc. provides one InGaAs APD “G8931-04” working at 1550nm with 2.5GHz bandwidth and the cutoff bandwidth of 3GHz at  $M = 10$  [6]. For the multi-gigabit-per-second (multi-Gb/s) bandwidth FSO systems, the InGaAs APD is the preferred choice in the receivers. The generic operating parameters of Ge and InGaAs APDs are given in the reference [1] and are shown in Table 5-2. According to the parameters provided by the reference [1] and the data sheets of the APD products online, the values of the parameter used in the analysis are shown in Table 5-2.

Table 5-2

Generic operating parameters of Ge and InGaAs APDs

Parameter	Symbol	Unit	Ge		InGaAs	
			range	value	range	value
Wavelength range	$\lambda$	nm	800~1650	1550	1100~1700	1550
Responsivity	$\mathcal{R}$	A/W	0.4~0.5	0.5	0.75~0.95	0.95
Avalanche gain	$M$	—	50~200	70	10~40	40
Dark current	$I_D$	nA	50~500	500	10~50	50
Rise time	$\tau_r$	ns	0.5~0.8	0.5	0.1~0.5	0.5
Gain*Bandwidth	$M \cdot B$	GHz	2~10	10	20~250	40
Bandwidth	$B$	GHz		0.143		1
Bias voltage	$V_B$	V	20~40	40	20~30	30
Parameter $x$ in the excess noise factor $F = M^x$			1.0	1.0	0.7	0.7

Ge APD has lower responsivity  $\mathcal{R}$ , bigger dark current  $I_D$  and lower bandwidth  $B$  compared to the InGaAs APD. But the APD gain  $M$  of Ge APDs can be much higher than InGaAs APDs. The average BEP curves corresponding to the received optical energy for the Ge APD and the InGaAs APD are shown in Fig. 5.3(a). The parameter values are set according to Table 5-2. In Fig. 5.3(a), it is evident that the Ge APD required more received optical energy than that of the InGaAs APD for the specified average BEP. This can limit the distance that Ge

APD system can transmit. Thus the InGaAs APD is the normal choice for the multi-gigabit-per-second (multi-Gb/s) bandwidth FSO systems.

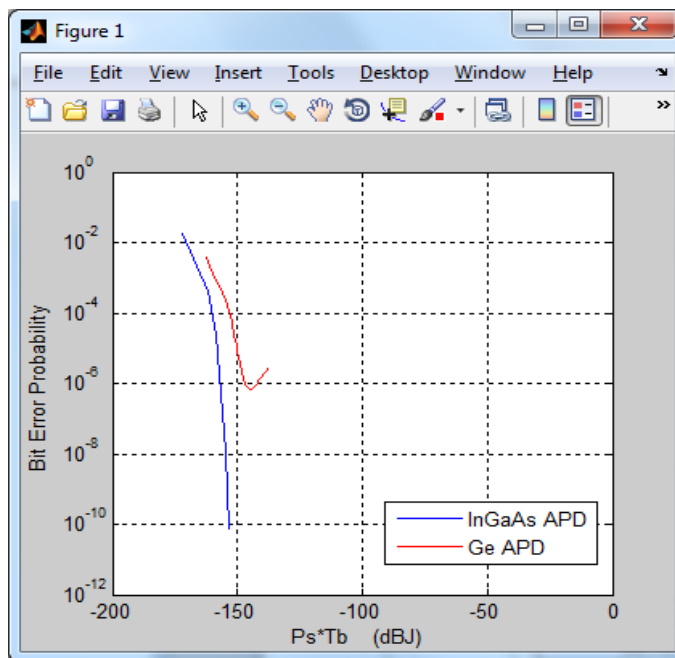


Figure 5.3(a) Average BEP of Ge APDs and the InGaAs APDs

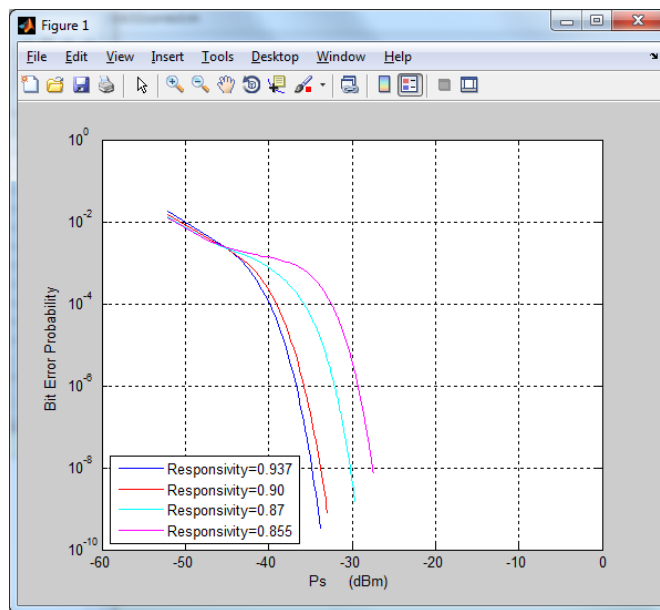


Figure 5.3(b) Average BEP of InGaAs APDs with the different responsivity

The average BEP curves of the InGaAs APD with different responsivity corresponding to the received optical power are shown in Fig. 5.3(b). It is clear that at the specified BEP, as the responsivity increases, the required received optical power becomes lower.

### (b) APD Gain Impact

The APD gain  $M$  plays an important role in the calculation of the average SEP and BEP in Eq. (4-81) and Eq. (4-84). First,  $M$  has an impact on the excess noise factor of APDs as  $F = M^x$  [1].  $F$  is in the  $K_0'$  function in Eq. (4-82a) and  $K_0'$  can be represented as

$$\begin{aligned} K_0' &= M^{xN_tN_r-1} \frac{\sigma_{\text{off}}}{\sqrt{2\pi A}} \left( \frac{e^{m_\ell}}{\pi \sqrt{q}} \right)^{N_tN_r} \left( \frac{\mathcal{R}E_s A_r \alpha}{N_t A_b} \right)^{\left(\frac{N_tN_r}{2}-1\right)} \\ &= M^{1.8} \frac{\sigma_{\text{off}}}{\sqrt{2\pi A}} \left( \frac{e^{m_\ell}}{\pi \sqrt{q}} \right)^{N_tN_r} \left( \frac{\mathcal{R}E_s A_r \alpha}{N_t A_b} \right)^{\left(\frac{N_tN_r}{2}-1\right)} \end{aligned} \quad (5-2)$$

where  $x = 0.7$  for InGaAs APDs,  $N_t = 2$ ,  $N_r = 2$  for MIMO ,

$$\sigma_{\text{off}}^2 = \frac{N_r}{B^2} A^2 \left\{ \left[ 2 \frac{\eta q b_{\text{on}}}{h\nu T_b} (1 - \gamma_s) M^2 F + 2\mathcal{R}(P_b + P_c) M^2 F + 2(I_{\text{db}} M^2 F + I_{\text{ds}}) \right] q I_2 B + q^2 B^2 W_{\text{TZ}} \right\} \quad (5-3)$$

As  $M$  increases and  $M \geq 1$ ,  $\sigma_{\text{off}}$  becomes larger and thus  $K_0'$  also increases.  $F$  also appears in the function  $K_f$  in Eq. (4-82g). As the excess noise factor  $F$  increases, the exponential part of  $K_f$  increases and the fractional part of  $K_f$  decreases. Thus, the trend of  $K_f$  is uncertain.  $M$  also impacts  $\sigma_{\text{on}}^2$  and  $\sigma_{\text{off}}^2$  in Eq. (3-50a) and Eq. (3-50b) . As the APD gain  $M$  increases, the noise variances  $\sigma_{\text{on}}^2$  and  $\sigma_{\text{off}}^2$  increase.  $k_l$  in Eq. (4-82b) can be represented as

$$k_l = \frac{k(E_s \mathcal{R} A g)^2}{2N_t^2 \left( \frac{k\sigma_{on}^2 + \sigma_{off}^2}{M^2} \right)} \quad (5-4a)$$

where

$$\begin{aligned} & \frac{k\sigma_{on}^2 + \sigma_{off}^2}{M^2} \\ &= \frac{kN_r}{B^2} A^2 \left\{ \left[ 2 \frac{\eta q b_{on}}{h\nu T_b} M^x + 2\mathcal{R}(P_b + P_c)M^x + 2(I_{ab}M^x) \right] qI_2B + \frac{2I_{ds}qI_2B + q^2B^2W_{TZ}}{M^2} \right\} \\ & \quad + \frac{N_r}{B^2} A^2 \left\{ \left[ 2 \frac{\eta q b_{on}}{h\nu T_b} (1 - \gamma_s)M^x + 2\mathcal{R}(P_b + P_c)M^x + 2(I_{ab}M^x) \right] qI_2B + \frac{2I_{ds}qI_2B + q^2B^2W_{TZ}}{M^2} \right\} \end{aligned} \quad (5-4b)$$

As  $M$  increases and  $M \geq 1$ , the trend of  $k_l$  is uncertain and thus  $F_D \left( \frac{n\omega_0}{2\sqrt{k_l}} \right)$  in Eq. (4-82f) is uncertain. As the gain  $M$  of the InGaAs APD increases from 10 to 40 and the FSO channel is under weak turbulence with  $\sigma_\ell^2 = 0.19877$ , the average BEP curves corresponding to the average SNR are shown in Fig. 5.4. The different gains  $M$  have varied impacts on the average BEP curves during normal working condition with  $BEP = 10^{-3} \sim 10^{-7}$ . Thermal noise characteristic is represented as

$$W_{TZ} = \frac{1}{q^2 B} \left( 2qI_{gate} + \frac{4k_B T}{R_b} + \frac{4k_B T \Gamma_e}{g_m \cdot R_b^2} \right) I_2 + \left( \frac{2\pi C}{q} \right)^2 \frac{4k_B T \Gamma_e}{g_m} I_3 B + \frac{T_b}{q^2} \frac{4k_B T}{R_f} I_2 \quad (5-5)$$

Thermal noise has no relationship with the APD gain and it is part of the total noise at the decision circuit. As the APD gain decreases, more optical power at the APDs is needed in order to overcome the noise and to achieve the desired signal level or SNR in the decision circuit. This

higher received optical power  $P_{s1}$  induces more noise and makes the total noise in Eq. (3-50a) and Eq. (3-50b) larger.

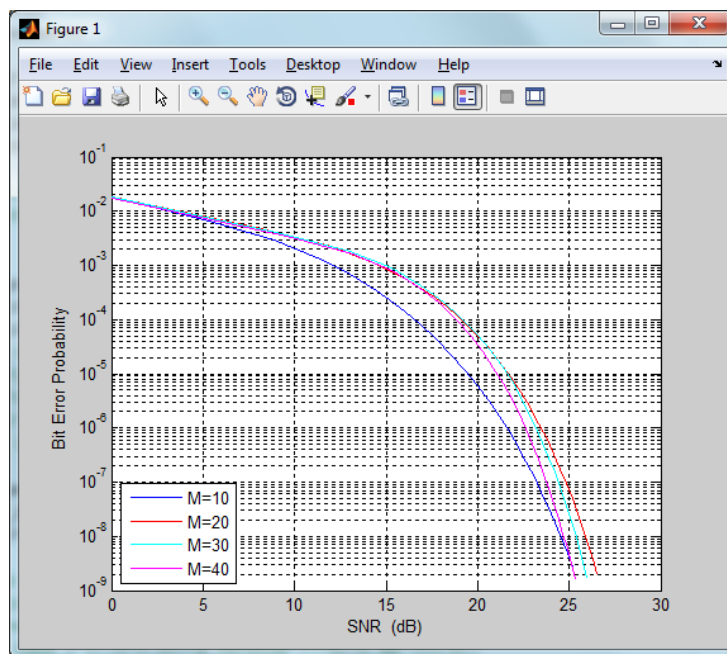
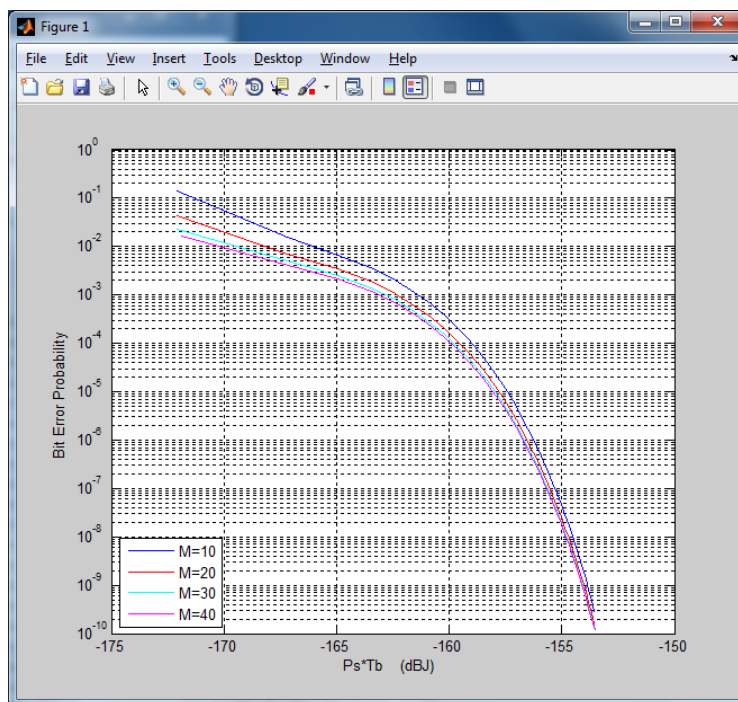
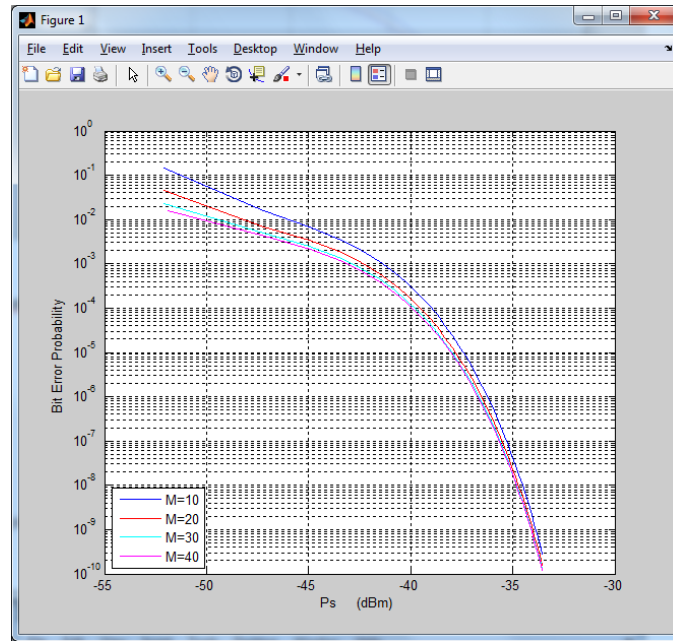


Figure 5.4 Average BEP with different APD gains  $M$



(a)



(b)

Figure 5.5 (a) Average BEP with different  $M$  corresponding to  $P_s T_b$  (dBJ)(b) Average BEP with different  $M$  corresponding to  $P_s$  (dBm)

The average BEP curves corresponding to the received optical energy (dBJ) or the received optical power (dBm) with different APD gains are shown in Fig. 5.5(a) and Fig. 5.5(b). At  $BEP = 10^{-6}$ , the received optical energy under the small APD gain  $M = 10$  is about -156.15dBJ, which is 0.7dBJ higher than the -156.85dBJ receiver energy at  $M = 40$ . At  $BEP = 10^{-6}$ , the received optical power for small APD gain  $M = 10$  is about -36.18dBm, which is more than the -36.91dBm receiver power for  $M = 40$ .

To determine the impact of gain under different turbulence, a plot of average BEP corresponding to the APD gain is shown in Fig. 5.6. The degree of the turbulence is represented by variance  $\sigma_\ell^2$  of the log intensity. As the turbulence increases, the BEP becomes larger but the change of BEP is not exactly proportional to that of  $\sigma_\ell^2$ . At around the fixed receiver optical energy -157.74dBJ,  $BEP = 10^{-5}$  and with turbulence and dispersion, the average BEP of the

APD gains  $M$  at around 40 is smaller than those of the other gains.

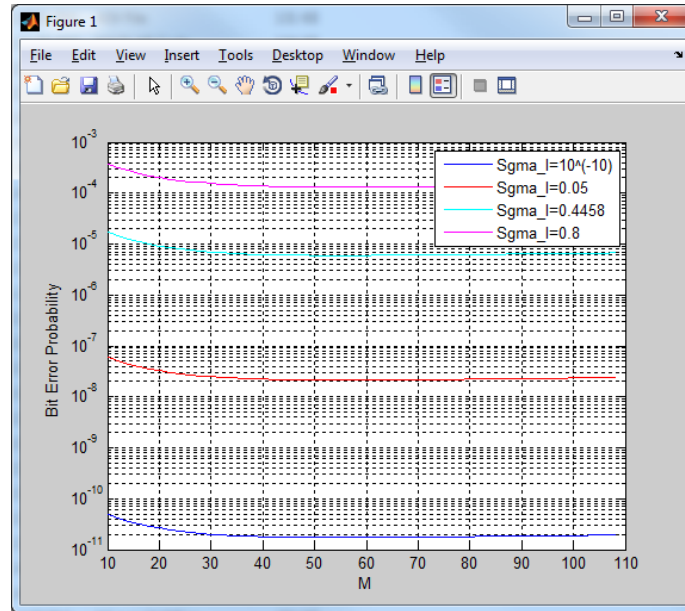


Figure 5.6 Average BEP with different APD gains  $M$  and different turbulence

## 5.2.3 Electrical Device Impact

### (a) Amplifier Impact

It is assumed that the amplifiers in the optical receiver work in the linear range and provide a gain  $A$ . The input signal is amplified by  $A$  times and it also adds the noise to the signal. The noise added by the amplifier is included in the total noise equations of Eq. (3-50a) and Eq. (3-50b). The amplifier gain  $A$  has impacts on the  $K_0'$  in Eq. (4-82a),  $k_l$  in Eq. (4-82b) and  $F_D \left( \frac{n\omega_0}{2\sqrt{k_l}} \right)$  in Eq. (4-82f). The signal to noise ratio after the post-detection EGC with the envelop detection at the decision circuit is given in Eq. (3-54) as

$$\text{SNR} = \frac{N_r (\mathcal{R}P_s M)^2}{\left\{ \left[ 2 \frac{\eta q b_{\text{on}}}{h\nu T_b} M^2 F + 2\mathcal{R}(P_b + P_c) M^2 F + 2(I_{\text{db}} M^2 F + I_{\text{ds}}) \right] q I_2 B + \left( 2q I_{\text{gate}} + \frac{4k_B T}{R_b} + \frac{4k_B T T_e}{g_m \cdot R_b^2} \right) I_2 B + (2\pi C)^2 \frac{4k_B T T_e}{g_m} I_3 B^3 + \frac{4k_B T}{R_f} I_2 B \right\}} \quad (5-6)$$

The SNR of the input signal in the amplifier is similar to the SNR of the output signal. The amplifier gain  $A$  does not impact the SNR shown in Eq. (5-6). The plots of the average SEP with different amplifier gains are shown in Fig. 5-7. As the amplifier gain increases, the curves with the different amplifier gains overlap. Since the amplifiers amplify the noise as well as the signals, the increase of the amplifier gain does not improve the system performance. At the same time, the noise added by the amplifiers is small and the variation in the noise due to the increase in the amplifier gain is small. The change of the amplifier gain  $A$  in the electrical part does not impact the average BEP performance.

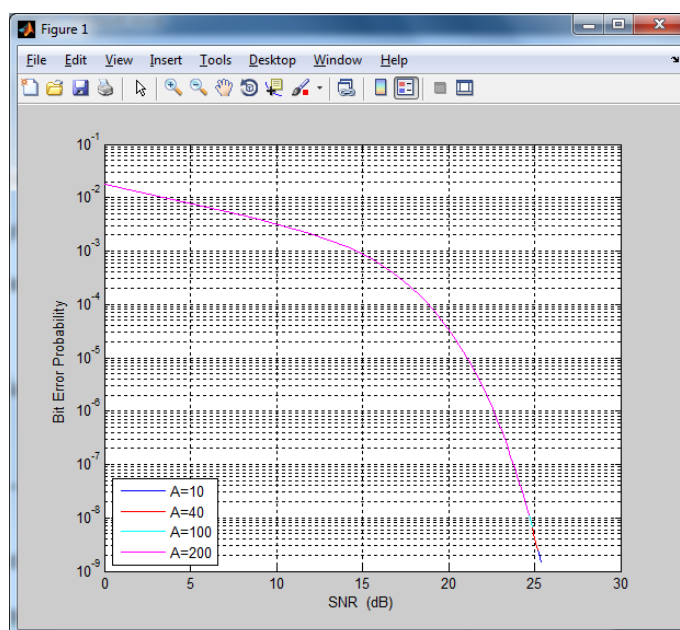


Figure 5.7 Average BEP with the different amplifier gains

### (b) Temperature Impact

In optical wireless communication, the receiver should be able to operate over a wide temperature range, for example  $-40\sim 85^{\circ}\text{C}$ . In the noise variances of Eq. (3-50a) and Eq. (3-50b), the temperature  $T$  is included in the numerator of the thermal noise part. Thus  $T$  influences the noise of the receivers and the system performance. In the average bit error probability of Eq.

(4-81), the temperature  $T$  impacts the noise variances  $\sigma_{\text{on}}^2$  and  $\sigma_{\text{off}}^2$  in the factor  $K_0'$  in Eq. (4-82a) and the  $k_l$  of the Dawson's integral in Eq. (4-82b) and Eq. (4-82f). As the temperature  $T$  increases, the noise variances  $\sigma_{\text{on}}^2$  and  $\sigma_{\text{off}}^2$  increase. On the other hand, the gain mechanism of an APD is very temperature-sensitive at higher bias voltage, where small changes in temperature can cause large variation in gain [1]. A compensation circuit is usually incorporated in the receiver and it adjusts the applied bias voltage on the photodetector when temperature changes [1]. Thus the impact of the temperature can be reduced and becomes negligible. In this section, it is assumed that the temperature impact on APD gain using the compensation circuit is negligible and the temperature impact on the thermal noise is mainly considered in this dissertation. Under different temperatures  $243K \sim 333K$  and as the  $BEP$  is around  $10^{-5}$ , the curves corresponding to the different APD gains are shown in Fig. 5.8. As the temperature increases, the  $BEP$  increases. This is because the noise variances in Eq. (3-50a) and Eq. (3-50b) increase as the temperature increases and the increased noise power makes the  $BEP$  larger.

The curves under different temperatures  $70K \sim 400K$  corresponding to different APD gains are shown in Fig. 5.9. The received optical power in Fig. 5.9 is about  $-157.74$  dBJ at  $BEP = 10^{-5}$ . From Fig. 5.8 and Fig. 5.9, as the temperature  $T$  increases, the average  $BEP$  increases and the system performance deteriorates.

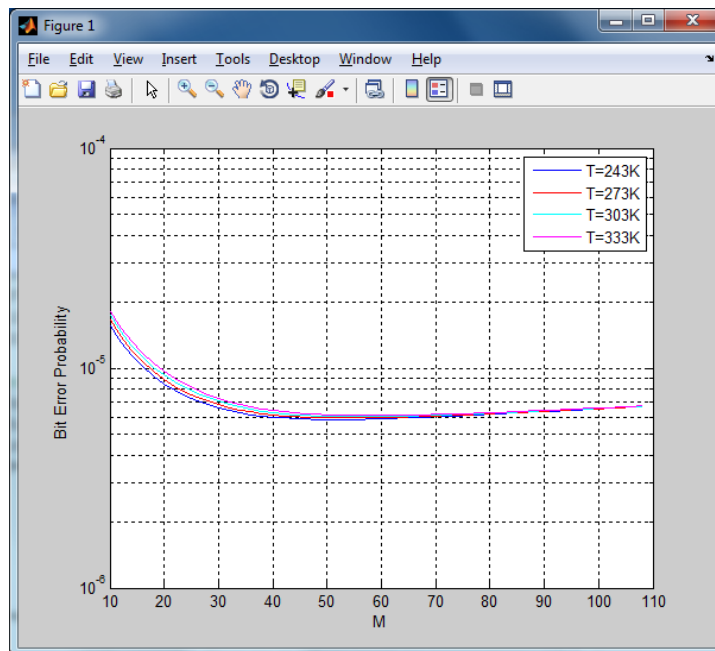


Figure 5.8 Average BEP under the different temperatures at  $P_s T_b = -157.74 \text{ dB}$

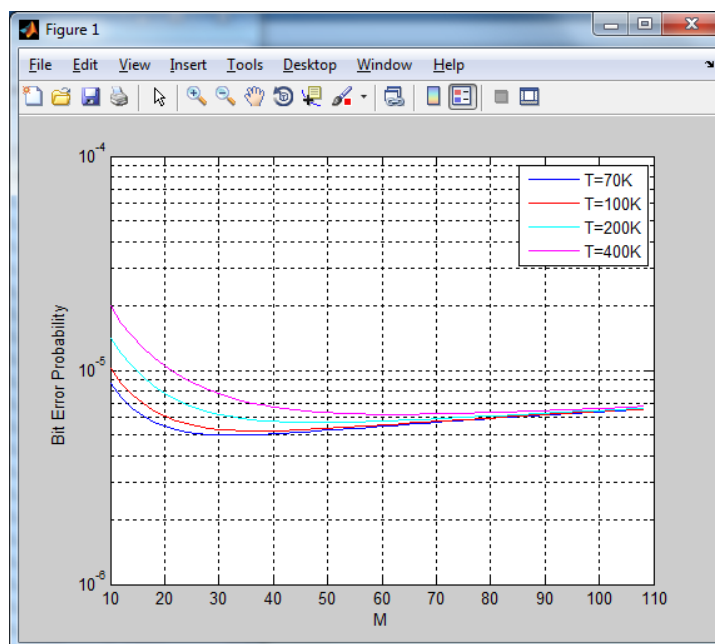


Figure 5.9 Average BEP under the different temperatures at  $P_s T_b = -157.74 \text{ dB}$

**(c) Average BER Comparison of Systems with the different  $\gamma_s$ ,  $I_2$  and  $I_3$**

In order to consider the clear sky condition and bad weather condition completely, the added noise and pulse dispersion of the PPM symbols are considered and analyzed in Section 3.2.3. The parameters, associated with the pulse dispersion and the added noise, are included in the noise variances of Eq. (3-50a) and Eq. (3-50b). The parameters,  $\gamma_s$ ,  $I_2$  and  $I_3$ , which are related to the bias circuit, the amplifier and equalizer and impact the sensitivity of the receivers, are discussed in Ref [1] in detail. The values of the parameters are given in Ref [1, pp308, Table 7-2], Ref [1, pp301, Fig. 7-13] and Ref [1, pp302, Fig. 7-14]. The average BEP curves for different dispersions are shown in Fig. 5.10 and the related parameters are set in Table 5-3. As the energy fraction  $\gamma_s$  in one 1 pulse slot decreases, more received optical power is required.

Table 5-3

Values of the parameters  $\gamma_s$ ,  $I_2$  and  $I_3$  for MIMO FSO systems

Parameter	Value	Value	Value	Value
$\gamma_s$	1	0.95	0.9	0.85
$I_2$	0.375	0.45	0.57	0.65
$I_3$	0.03001	0.0855	0.0905	0.13
$\alpha$	0	0.25	0.3	0.35

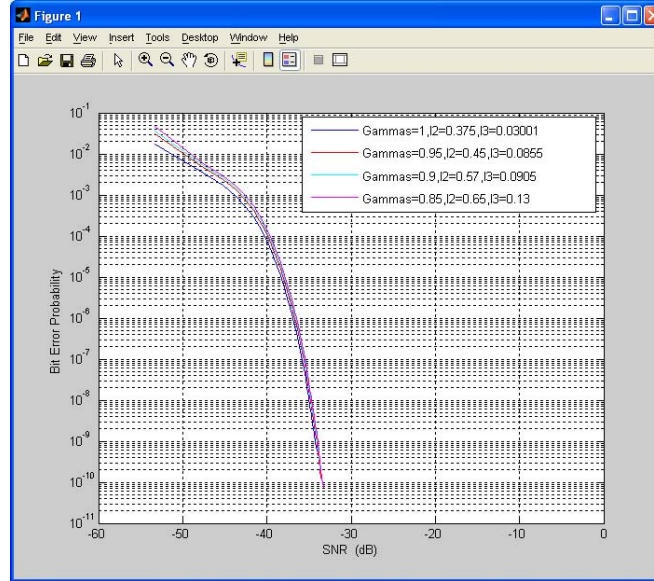


Figure 5.10 Average BEP of MIMO FSO systems with the different  $\gamma_s$ ,  $I_2$  and  $I_3$

#### (d) Bias Resistance Impact

The noise in the optical receiver is discussed in Section 3.2.3 of Chapter 3 and the noise variances are given in Eq. (3-50a) and Eq. (3-50b). In practice, typical FET amplifiers have very large input resistance  $R_a$ , usually greater than  $10^6\Omega$  [1]. For the transimpedance amplifier, the feedback resistance  $R_f$  is much greater than the amplifier input resistance  $R_a$  [1]. In the equivalent circuit of a typical optical receiver in Ref [1, pp279, Fig. 7-4], the parallel combination of  $R_a$  and  $R_b$  reduces to the value of the detector bias resistor  $R_b$  [1]. The detector bias resistor  $R_b$  impacts the thermal characteristics, and thus impacts the thermal noise in the optical receiver. As the detector bias resistor  $R_b$  increases, the thermal characteristic decreases and the noise variances  $\sigma_{on}^2$  and  $\sigma_{off}^2$  decrease. The thermal noise characteristic is represented as

$$W_{TZ} = \frac{1}{q^2 B} \left( 2qI_{gate} + \frac{4k_B T}{R_b} + \frac{4k_B T \Gamma_e}{g_m \cdot R_b^2} \right) I_2 + \left( \frac{2\pi C}{q} \right)^2 \frac{4k_B T \Gamma_e}{g_m} I_3 B + \frac{T_b}{q^2} \frac{4k_B T}{R_f} I_2 \quad (5-7)$$

The average BEP curves with different detector bias resistances  $R_b$  are shown in Fig. 5.11. The change in the noise variances due to changes in  $R_b$  is very small, and thus changes in BEP due to changes in  $R_b$  are very small.  $R_b$  impacts the average BEP but the change is very limited.

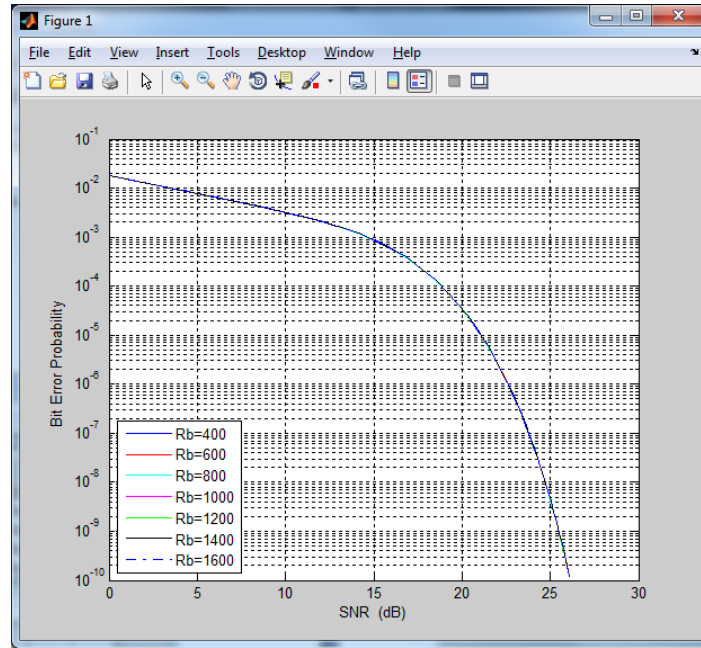
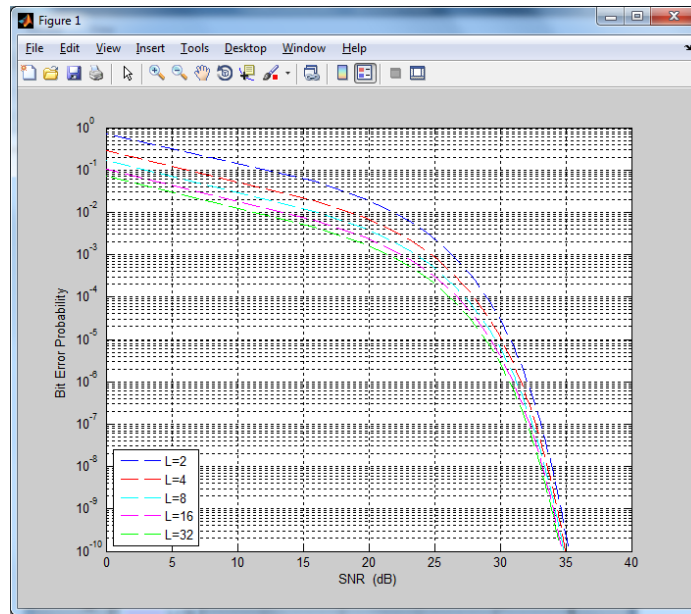


Figure 5.11 Average BEP with the different bias resistances  $R_b$

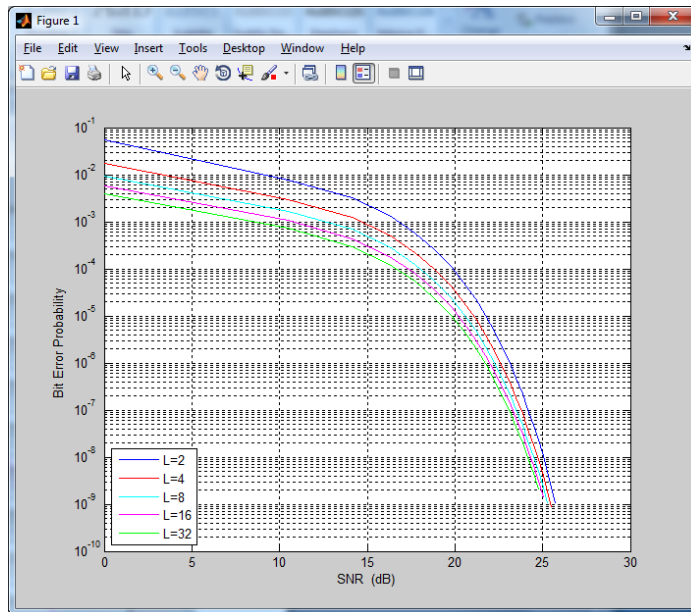
#### 5.2.4 PPM Symbol Length and MIMO Diversity Impact

For orthogonal PPM signaling with repetition coding, the order of diversity is equal to the number of times that a symbol is repeated in the block orthogonal coding. The length of PPM symbols  $L$  impacts the summation terms in Eq. (4-81). The numbers of the transmitting lasers and the receiving APDs,  $N_t$  and  $N_r$ , have impact on the summation terms,  $K_0'$  in Eq. (4-82a),  $K_f$  in Eq. (4-82g) and  $K_d$  in Eq. (4-82h). The BEP curves of different PPM lengths are plotted as a function of SNR per bit in Fig. 5-12(a) and Fig. 5-12(b). It is apparent from these figures that the BEP becomes lower and the receiver performance improves as  $N_t$ ,  $N_r$  and  $L = 2^Q$  increases for a

specified SNR. The average BEP decreases and performance increases much more drastically by increasing  $N_t$  and  $N_r$  compared to a corresponding increase in  $L$ .



(a)



(b)

Figure 5.12 (a) Average BEP with the different  $L$  and different  $N_t$  and  $N_r$  for SISO

(b) Average BEP with the different  $L$  and different  $N_t$  and  $N_r$  for MIMO

### 5.2.5 Turbulence Impact

Atmospheric turbulence has a large impact on the system performance, especially on the average BEP. The atmospheric impact of the FSO channel is analyzed in Section 2.3 and Section 3.2.2. Channel fading is modeled as the lognormal distribution of Eq. (3-23) and Eq. (3-24). The average error probabilities are calculated in Section 4.1. The equations for the average SEP and BEP are given in Eq. (4-81) and Eq. (4-84). The parameters  $m_\ell$  and  $\sigma_\ell^2$  are the mean and the variance of the log intensity  $\ell$ , respectively. The mean  $m_\ell$  can be set as  $-\frac{\sigma_\ell^2}{2}$  for the normal working condition. The variance  $\sigma_\ell^2$ , which is associated with the scintillation index  $\Psi$  in Eq. (3-27), represents the degree of fading of FSO channels. The  $\sigma_\ell^2$  has impacts on  $K_0'$  in Eq. (4-82a) and  $K_f$  in Eq. (4-81) is given as

$$\begin{aligned}
 K_f = & \sum_{\substack{u_1=-N_u \\ u_1 \neq 0}}^{N_u} \sum_{\substack{u_2=-N_u \\ u_2 \neq 0}}^{N_u} \dots \sum_{\substack{u_{N_t N_r}=-N_u \\ u_{N_t N_r} \neq 0}}^{N_u} W_{u_1} W_{u_2} \dots W_{u_{N_t N_r}} W_{v_1} W_{v_2} \dots W_{v_{N_t N_r}} \\
 & \exp \left[ \sqrt{2} \sigma_\ell \left( x_{u_1} + x_{u_2} + \dots + x_{u_{N_t N_r}} \right) + \left( x_{v_1} + x_{v_2} + \dots + x_{v_{N_t N_r}} \right) \right] \\
 & \left[ (F-1)x_{v_1} + e^{m_\ell} e^{\sqrt{2} \sigma_\ell x_{u_1}} \right]^{(-\frac{3}{2})} \left[ (F-1)x_{v_2} + e^{m_\ell} e^{\sqrt{2} \sigma_\ell x_{u_2}} \right]^{(-\frac{3}{2})} \dots \dots \\
 & \left[ (F-1)x_{v_{N_t N_r}} + e^{m_\ell} e^{\sqrt{2} \sigma_\ell x_{u_{N_t N_r}}} \right]^{(-\frac{3}{2})} \\
 & \exp \left\{ \left( -\frac{K_k}{2} \right) \left[ \frac{\left( x_{v_1} - e^{m_\ell} e^{\sqrt{2} \sigma_\ell x_{u_1}} \right)^2}{\left[ (F-1)x_{v_1} + e^{m_\ell} e^{\sqrt{2} \sigma_\ell x_{u_1}} \right]} + \frac{\left( x_{v_2} - e^{m_\ell} e^{\sqrt{2} \sigma_\ell x_{u_2}} \right)^2}{\left[ (F-1)x_{v_2} + e^{m_\ell} e^{\sqrt{2} \sigma_\ell x_{u_2}} \right]} \dots \dots \right. \right. \\
 & \left. \left. + \frac{\left( x_{v_{N_t N_r}} - e^{m_\ell} e^{\sqrt{2} \sigma_\ell x_{u_{N_t N_r}}} \right)^2}{\left[ (F-1)x_{v_{N_t N_r}} + e^{m_\ell} e^{\sqrt{2} \sigma_\ell x_{u_{N_t N_r}}} \right]} \right] \right\}
 \end{aligned}
 \tag{5-8}$$

The average BEP curves under weak turbulence with  $\sigma_\ell = 10^{-10}$ ,  $\sigma_\ell = 0.05$ ,  $\sigma_\ell = 0.4458$  and  $\sigma_\ell = 0.8$  are shown in Fig. 5.13(a) and Fig. 5.13(b). The curve with  $\sigma_\ell = 10^{-10}$ , shows the performance under very small turbulence. For the specified SNR, as  $\sigma_\ell$  increases, the average BER becomes larger and the system performance deteriorates. The changes in BEP are not exactly proportional to changes in the variance  $\sigma_\ell^2$ .

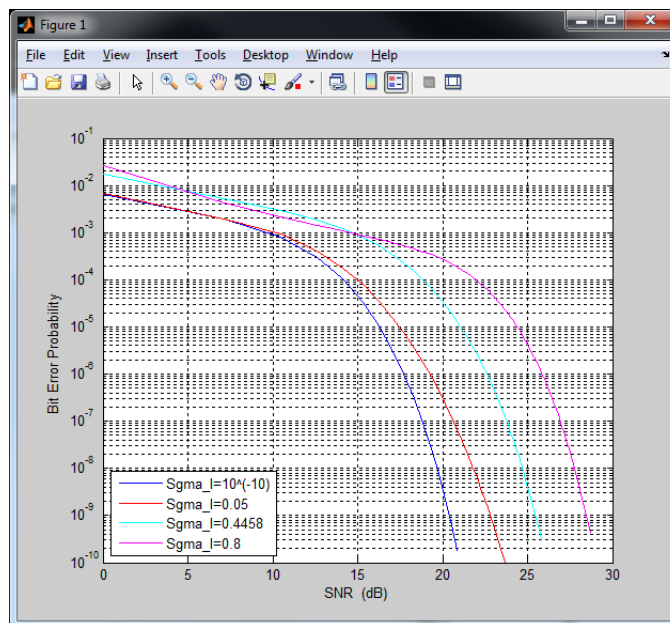


Figure 5.13 Average BEP with the different variance of the log intensity

## REFERENCES

- [1]. Gerd Keiser, "Optical Fiber Communications," McGraw-Hill, Inc., third edition, 2000, pp267.
- [2]. Gregory R. Osche, "Optical Detection Theory for laser Applications," 2002, John Wiley & Sons, Inc.
- [3]. Muthu Jeganathan and Pavel Lonov, "Multi-Gigabits-per-second Optical Wireless Communications", Optical Crossing Company, Website: <http://www.citeseerx.ist.psu.edu/viewdoc/downloaddoi=10.1.1.110>
- [4]. Govind P. Agrawal, "Fiber-optic Communication Systems", John Wiley & Sons, Inc. , second edition, 1997, pp170-171.
- [5]. Data Sheet of Ge APDs "PDGAJ1001FCA-0-0-01", PD-LD Inc. <http://www.pd-ld.com/> .
- [6]. Data Sheet of InGaAs APDs "G8931-04", Hamamatsu Inc.  
<http://sales.hamamatsu.com/en/products/solid-state-division/ingaas-pin-photodiodes/apd/part-g8931-04.php> .

## CHAPTER 6

### CONCLUSION AND FUTURE RESEARCH DIRECTIONS

A comprehensive study of Free Space Optical communication using MIMO techniques has been presented. The modulation and wavelength suitable for MIMO FSO systems are discussed. The characteristics of FSO channels and the impact of FSO channels on the optical signal are analyzed by modeling the optical beams as Gaussian beams. The APD-based receiver for MIMO FSO systems under normal working conditions has been designed. At the same time the characteristics of its components, such as InGaAs APDs, GaAs MESFET transimpedance amplifiers, a matched filter and an equalizer, etc., have been discussed. A probabilistic analysis of FSO channel, APDs and noise in the FSO systems has been carried out. The FSO channel fading obeys the lognormal distribution while electrons emitted by APDs obey the Webb distribution. The noise in the optical receivers obeys a Gaussian distribution. The distributions of the received signals and channel gains are analyzed.

The main contributions in this dissertation are: obtaining the detailed closed-form expressions for the upper bounds of the error probabilities, analyzing the impacts of different parameters in MIMO FSO systems, and thorough analysis of a more complex model of the MIMO FSO system involving Webb distribution for APD-based optical receiver, the probabilistic analysis of the detection for PPM signaling and transmitted symbol matrix for MIMO FSO equal gain combining systems.

Detailed expressions of the closed-form upper bounds for the average symbol error probability, average bit error probability and average pairwise probability have been obtained. The equations for the error probabilities have been obtained by using Fourier series analysis

method in Chapter 4. The modified Gauss-Chebyshev method for calculating average SEP, average BEP and average PEP are proposed and corresponding equations have been derived. The results for average SEP and average BEP under different parameters are obtained in Chapter 5. The impact of the parameters in the MIMO FSO systems is also discussed and plotted. The error analysis of the calculations of error probabilities is given in Chapter 5.

According to the analyses in Chapter 4 and Chapter 5, it is observed that the MIMO technique can improve the performance of optical wireless communication systems remarkably. For numerical method used in the error probability expressions of the closed-form upper bound, if suitable computing parameters are selected, the computation error and the truncation errors can be sufficiently small.

MIMO FSO systems are very complicated systems and still there are several aspects that must be investigated further.

The following areas can be addressed in future research works:

1. Closed-form expressions or closed-form upper bound expressions of the error probabilities for MIMO FSO systems with negative exponential distributed channel fading and Gamma-Gamma distributed channel fading. These analyses would provide the results for strong and weak/strong turbulences in the air medium, respectively.
2. Exploring the closed-form expressions or the closed-form upper bound expressions of the error probabilities for MIMO FSO systems with the square-law equal gain combining. This would improve the performance results of the system,
3. Design of the STBC schemes suitable for MIMO FSO systems using PPM, which would reduce the error probability and improve the system performance. At the same

time comparison among various proposed STBC schemes would help in the selection of the most suitable one.

4. Lognormal channel estimation using Kalman filtering for improved channel gain estimation and accurate demodulation.

## APPENDIX A

This is the derivation for Eq. (3-22).

The log intensity  $\ell = \ln \left( \frac{I}{\langle I \rangle} \right)$  of laser beams obeys Gaussian distribution with the mean  $m_\ell$  and variance  $\sigma_\ell^2$  [13]. According to Eq. (4-8), Eq. (4-9), Eq. (4-18) and  $P_{ril}T_b = h\nu \lambda_{sil}$ , the intensity of a Gaussian beam in the  $il$ th path is

$$I = I_0 e^{\frac{-2r^2}{\omega^2(z)}} = \frac{2P_{til}}{\pi\omega^2(z)} e^{\frac{-2r^2}{\omega^2(z)}} = \frac{A_b P_{ril}}{\pi\omega^2(z)A_r\alpha} e^{\frac{-2r^2}{\omega^2(z)}} = \frac{A_b h\nu \lambda_{sil}}{\pi\omega^2(z)A_r\alpha T_b} e^{\frac{-2r^2}{\omega^2(z)}}$$

The mean values of  $I$ ,  $P_{ril}$ ,  $\lambda_{sil}$  are

$$\langle I \rangle = \frac{2\langle P_{til} \rangle}{\pi\omega^2(z)} e^{\frac{-2r^2}{\omega^2(z)}} = \frac{A_b \langle P_{ril} \rangle}{\pi\omega^2(z)A_r\alpha} e^{\frac{-2r^2}{\omega^2(z)}} = \frac{A_b h\nu \langle \lambda_{sil} \rangle}{\pi\omega^2(z)A_r\alpha T_b} e^{\frac{-2r^2}{\omega^2(z)}}$$

Then the following ratios exist

$$\frac{I}{\langle I \rangle} = \frac{P_{ril}}{\langle P_{ril} \rangle} = \frac{\lambda_{sil}}{\langle \lambda_{sil} \rangle}$$

Where  $\langle \lambda_{sil} \rangle = \overline{\lambda_{sil}}$

The log intensity  $\ell$  is

$$\ln \left( \frac{I}{\langle I \rangle} \right) = \ln \left( \frac{P_{ril}}{\langle P_{ril} \rangle} \right) = \ln \left( \frac{\lambda_{sil}}{\langle \lambda_{sil} \rangle} \right) = \ln(\lambda_{sil}) - \ln(\overline{\lambda_{sil}})$$

## APPENDIX B

This is the derivation for Eq. (3-24).

The log intensity  $\ell = \ln \left( \frac{\lambda_{sil}}{\langle \lambda_{sil} \rangle} \right)$  of laser beams obeys Gaussian distribution with the mean  $m_\ell$  and variance  $\sigma_\ell^2$  [13].

$$p_\ell(\ell) = \frac{1}{\sqrt{2\pi\sigma_\ell^2}} e^{-\frac{(\ell-m_\ell)^2}{2\sigma_\ell^2}}$$

The probability density function of  $\lambda_{sil}$  is

$$\begin{aligned}
 p_{\lambda_{sil}}(\lambda_{sil}) &= p_{\ell}(\ell) \Big|_{\ell=\ln\left(\frac{\lambda_{sil}}{\bar{\lambda}_{sil}}\right)} \frac{d\ell}{d\lambda_{sil}} \\
 &= \frac{1}{\sqrt{2\pi \cdot \sigma_{\ell}^2}} \exp \left\{ -\frac{\left[ \ln\left(\frac{\lambda_{sil}}{\bar{\lambda}_{sil}}\right) - m_{\ell} \right]^2}{2\sigma_{\ell}^2} \right\} \frac{1}{\frac{\lambda_{sil}}{\bar{\lambda}_{sil}}} \frac{1}{\bar{\lambda}_{sil}} \\
 &= \frac{1}{\sqrt{2\pi \cdot \sigma_{\ell}^2} \lambda_{sil}} \exp \left\{ -\frac{[\ln(\lambda_{sil}) - \ln(\bar{\lambda}_{sil}) - m_{\ell}]^2}{2\sigma_{\ell}^2} \right\}
 \end{aligned}$$

The mean of  $\lambda_{sil}$  is

$$\begin{aligned}
 E\{\lambda_{sil}\} &= \int_{-\infty}^{\infty} \lambda_{sil} \cdot p_{\lambda_{sil}}(\lambda_{sil}) \cdot d\lambda_{sil} \\
 &= \int_{-\infty}^{\infty} \lambda_{sil} \cdot \frac{1}{\sqrt{2\pi \cdot \sigma_{\ell}^2} \lambda_{sil}} \exp \left\{ -\frac{[\ln(\lambda_{sil}) - \ln(\bar{\lambda}_{sil}) - m_{\ell}]^2}{2\sigma_{\ell}^2} \right\} \cdot d\lambda_{sil} \\
 &= \int_{-\infty}^{\infty} \frac{1}{\sqrt{2\pi \cdot \sigma_{\ell}^2}} \exp \left\{ -\frac{[\ln(\lambda_{sil}/\bar{\lambda}_{sil}) - m_{\ell}]^2}{2\sigma_{\ell}^2} \right\} \cdot d\lambda_{sil}
 \end{aligned}$$

Using  $t = \ln\left(\frac{\lambda_{sil}}{\bar{\lambda}_{sil}}\right)$ ,  $\lambda_{sil} = \bar{\lambda}_{sil} e^t$

$$\begin{aligned}
 E\{\lambda_{sil}\} &= \int_{-\infty}^{\infty} \frac{1}{\sqrt{2\pi \cdot \sigma_{\ell}^2}} \exp \left\{ -\frac{[t - m_{\ell}]^2}{2\sigma_{\ell}^2} \right\} \bar{\lambda}_{sil} e^t dt \\
 &= \bar{\lambda}_{sil} \int_{-\infty}^{\infty} \frac{1}{\sqrt{2\pi \cdot \sigma_{\ell}^2}} \exp \left\{ -\frac{[t - m_{\ell}]^2}{2\sigma_{\ell}^2} \right\} e^t dt \\
 &= \bar{\lambda}_{sil} \int_{-\infty}^{\infty} \frac{1}{\sqrt{2\pi \cdot \sigma_{\ell}^2}} \exp \left\{ -\frac{[t - m_{\ell} - \sigma_{\ell}^2]^2 - 2\sigma_{\ell}^2 \left(m_{\ell} + \frac{\sigma_{\ell}^2}{2}\right)}{2\sigma_{\ell}^2} \right\} dt \\
 &= \bar{\lambda}_{sil} e^{m_{\ell} + \frac{\sigma_{\ell}^2}{2}} \int_{-\infty}^{\infty} \frac{1}{\sqrt{2\pi \cdot \sigma_{\ell}^2}} \exp \left\{ -\frac{[t - m_{\ell} - \sigma_{\ell}^2]^2}{2\sigma_{\ell}^2} \right\} dt
 \end{aligned}$$

$$= \bar{\lambda}_{sil} e^{m_\ell + \frac{\sigma_\ell^2}{2}}$$

The second moment of  $\lambda_{sil}$  is

$$E\{\lambda_{sil}^2\} = \int_{-\infty}^{\infty} \lambda_{sil}^2 \cdot p_{\lambda_{sil}}(\lambda_{sil}) \cdot d\lambda_{sil}$$

$$\int_{-\infty}^{\infty} \lambda_{sil}^2 \cdot \frac{1}{\sqrt{2\pi \cdot \sigma_\ell^2} \lambda_{sil}} \exp\left\{-\frac{[\ln(\lambda_{sil}) - \ln(\bar{\lambda}_{sil}) - m_\ell]^2}{2\sigma_\ell^2}\right\} \cdot d\lambda_{sil}$$

Using  $t = \ln\left(\frac{\lambda_{sil}}{\bar{\lambda}_{sil}}\right)$ ,  $\lambda_{sil} = \bar{\lambda}_{sil} e^t$

$$E\{\lambda_{sil}^2\} = \int_{-\infty}^{\infty} \frac{1}{\sqrt{2\pi \cdot \sigma_\ell^2}} \exp\left\{-\frac{[t - m_\ell]^2}{2\sigma_\ell^2}\right\} \bar{\lambda}_{sil}^{-2} e^{2t} dt$$

$$= \bar{\lambda}_{sil}^{-2} \int_{-\infty}^{\infty} \frac{1}{\sqrt{2\pi \cdot \sigma_\ell^2}} \exp\left\{-\frac{[t - m_\ell - \sigma_\ell^2]^2 - 2\sigma_\ell^2(2m_\ell + 2\sigma_\ell^2)}{2\sigma_\ell^2}\right\} dt$$

$$= \bar{\lambda}_{sil}^{-2} e^{2m_\ell + 2\sigma_\ell^2} \int_{-\infty}^{\infty} \frac{1}{\sqrt{2\pi \cdot \sigma_\ell^2}} \exp\left\{-\frac{[t - m_\ell - \sigma_\ell^2]^2}{2\sigma_\ell^2}\right\} dt$$

$$= \bar{\lambda}_{sil}^{-2} e^{2m_\ell + 2\sigma_\ell^2}$$

The variance of  $\lambda_{sil}$  is

$$VAR\{\lambda_{sil}\} = E\{\lambda_{sil}^2\} - [E\{\lambda_{sil}\}]^2$$

$$= \bar{\lambda}_{sil}^{-2} e^{2m_\ell + 2\sigma_\ell^2} - \left(\bar{\lambda}_{sil} e^{m_\ell + \frac{\sigma_\ell^2}{2}}\right)^2$$

$$= \bar{\lambda}_{sil}^{-2} e^{2m_\ell + \sigma_\ell^2} (e^{\sigma_\ell^2} - 1)$$

## APPENDIX C

This is the derivation for Eq. (3-43).

$$\begin{aligned}
& \frac{1}{\sqrt{2\pi \eta \lambda_{s il} M^2 F}} \frac{1}{\sqrt{2\pi \cdot \sigma_\ell^2 \lambda_{s il}}} \left[ 1 + \frac{(m_{s il} - \eta \lambda_{s il} M)(F - 1)}{\eta \lambda_{s il} M F} \right]^{-\frac{3}{2}} \\
&= \frac{\eta}{2\pi (\eta \lambda_{s il})^{\frac{3}{2}} \sigma_\ell M \sqrt{F}} \left[ 1 + \frac{(m_{s il} - \eta \lambda_{s il} M)(F - 1)}{\eta \lambda_{s il} M F} \right]^{-\frac{3}{2}} \\
&= \frac{\eta}{2\pi \sigma_\ell M \sqrt{F}} \left[ \eta \lambda_{s il} + \frac{m_{s il}(F - 1) - \eta \lambda_{s il} M F + \eta \lambda_{s il} M}{M F} \right]^{-\frac{3}{2}} \\
&= \frac{\eta}{2\pi \sigma_\ell M \sqrt{F}} \left[ \frac{\eta \lambda_{s il} M F - \eta \lambda_{s il} M F + m_{s il}(F - 1) + \eta \lambda_{s il} M}{M F} \right]^{-\frac{3}{2}} \\
&= \frac{\eta F}{2\pi \sigma_\ell M (F)^{\frac{3}{2}}} \left[ \frac{m_{s il}(F - 1) + \eta \lambda_{s il} M}{M F} \right]^{-\frac{3}{2}} \\
&= \frac{\eta F}{2\pi \sigma_\ell M} \left[ \frac{m_{s il}(F - 1) + \eta \lambda_{s il} M}{M} \right]^{-\frac{3}{2}} \\
&= \frac{\eta F}{2\pi \sigma_\ell M} \left[ \eta \lambda_{s il} + \frac{m_{s il}(F - 1)}{M} \right]^{-\frac{3}{2}} \\
& 2\eta \lambda_{s il} M^2 F \left\{ 1 + \frac{(m_{s il} - \eta \lambda_{s il} M)(F - 1)}{\eta \lambda_{s il} M F} \right\} \\
&= 2M^2 F \left\{ \eta \lambda_{s il} + \frac{(m_{s il} - \eta \lambda_{s il} M)(F - 1)}{M F} \right\} \\
&= 2M^2 F \left\{ \frac{\eta \lambda_{s il} M F + m_{s il}(F - 1) - \eta \lambda_{s il} M F + \eta \lambda_{s il} M}{M F} \right\}
\end{aligned}$$

$$\begin{aligned}
&= 2M^2 F \left\{ \frac{m_{s\,il}(F-1) + \eta \lambda_{s\,il} M}{MF} \right\} \\
&= 2M^2 \eta \lambda_{s\,il} + 2M m_{s\,il} (F-1)
\end{aligned}$$

## APPENDIX D

This is the derivation of Eq. (4-19).

The integral of  $\int_{\frac{E_s \mathcal{R}MAG}{N_t} h + n_{on}}^{+\infty} p_{n_{off}}(n_{off}) \cdot dn_{off}$  is a function of  $n_{on}$  and its value can be represented as

$$\begin{aligned}
g(n_{on}) &= \int_{\frac{E_s \mathcal{R}MAG}{N_t} h + n_{on}}^{+\infty} p_{n_{off}}(n_{off}) \cdot dn_{off} \\
&= \int_{\frac{E_s \mathcal{R}MAG}{N_t} h + n_{on}}^{+\infty} \frac{1}{\sqrt{2\pi\sigma_{off}^2}} \cdot e^{-\frac{n_{off}^2}{2\sigma_{off}^2}} \cdot dn_{off} \\
&= \int_{\frac{E_s \mathcal{R}MAG}{N_t \sigma_{off}} h + \frac{n_{on}}{\sigma_{off}}}^{+\infty} \frac{1}{\sqrt{2\pi}} \cdot e^{-\frac{\left(\frac{n_{off}}{\sigma_{off}}\right)^2}{2}} \cdot d\left(\frac{n_{off}}{\sigma_{off}}\right)
\end{aligned}$$

In the above equation, the variable substitution  $t = \frac{n_{off}}{\sigma_{off}}$  is made resulting in

$$\begin{aligned}
g(r_1) &= \frac{1}{\sqrt{2\pi}} \int_{\frac{E_s \mathcal{R}MAG}{N_t \sigma_{off}} h + \frac{n_{on}}{\sigma_{off}}}^{+\infty} e^{-\frac{(t)^2}{2}} \cdot d(t) \\
&= Q\left(\frac{E_s \mathcal{R}MAG}{N_t \sigma_{off}} h + \frac{n_{on}}{\sigma_{off}}\right) \quad \text{where } r_1 = \frac{E_s \mathcal{R}MAG}{N_t} h + n_{on} \\
&= Q\left(\frac{r_1}{\sigma_{off}}\right)
\end{aligned}$$

## APPENDIX E

This is the derivation for Eq. (4-19).

Letting  $r_1 = \frac{E_s \mathcal{R}MAG}{N_t} h + n_{on}$  in Eq. (4-19), the integral  $\int_{-\infty}^{\infty} \left\{ 1 - \left[ 1 - Q \left( \frac{r_1}{\sigma_{off}} \right) \right]^{(L-1)} \right\} \cdot p_{n_{on}}(r_1 - t_s) \cdot dr_1$  is a function of  $t_s$  and we assume that the function  $f(t_s)$  is the following part in Eq. (4-19)

$$f(t_s) = \int_{-\infty}^{\infty} \left\{ 1 - \left[ 1 - Q \left( \frac{r_1}{\sigma_{off}} \right) \right]^{(L-1)} \right\} \cdot p_{n_{on}}(r_1 - t_s) \cdot dr_1$$

Hence

$$P_s(E) = \int_{-\infty}^{\infty} f(t_s) \cdot p_{t_s}(t_s) \cdot dt_s$$

By using the variable substitution  $t_s = k_t h$  ( $0 \leq t_s \leq \infty, 0 \leq h \leq \infty$ ),  $k_t = \frac{E_s \mathcal{R}MAG}{N_t}$ ,  $h = \frac{t_s}{k_t}$  and

$p_{t_s}(t_s) = \frac{1}{k_t} \cdot p_h(h)$ , it can be obtained

$$\begin{aligned} f(t_s) \cdot p_{t_s}(t_s) \cdot dt_s &= \left[ f(t_s) \cdot p_{t_s}(t_s) \cdot dt_s \right]_{|t_s=k_t h} \\ &= f(k_t h) \cdot p_{t_s}(k_t h) \cdot d(k_t h) \\ &= f(k_t h) \cdot \frac{1}{k_t} \cdot p_h \left( \frac{k_t h}{k_t} \right) \cdot k_t \cdot dh \\ &= f(k_t h) \cdot p_h(h) \cdot dh \end{aligned}$$

For the optical wireless communication, the channel gain  $h$  is nonnegative and  $0 \leq t_s \leq \infty, 0 \leq h \leq \infty$ . In the Eq. (4-19), using the above equation and the variable substitution  $t_s = k_t h$ , the symbol error probability  $P_s(E)$  for one PPM symbol can be obtained as

$$P_s(E) = \int_0^{\infty} \left\{ \int_{-\infty}^{\infty} \left\{ 1 - \left[ 1 - Q \left( \frac{r_1}{\sigma_{off}} \right) \right]^{(L-1)} \right\} p_{n_{on}}(r_1 - k_t h) \cdot dr_1 \right\} \cdot p_h(h) dh$$

or

$$P_s(E) = \int_0^\infty \left\{ \int_{-\infty}^\infty \left\{ 1 - \left[ 1 - Q \left( \frac{E_s \mathcal{R}MAG}{N_t \sigma_{\text{off}}} h + \frac{n_{\text{on}}}{\sigma_{\text{off}}} \right) \right]^{(L-1)} \right\} p_{n_{\text{on}}}(n_{\text{on}}) dn_{\text{on}} \right\} p_h(h) dh$$

where the upper limit and lower limit of the integration are decided by the range of the random variables  $r_1 = \frac{E_s \mathcal{R}MAG}{N_t \sigma_{\text{off}}} h + \frac{n_{\text{on}}}{\sigma_{\text{off}}}$  and  $h$ .

## APPENDIX F

This is the derivation for Eq. (4-21).

The error probability  $P_e(E)$  of the FSO MIMO systems can be expressed as the error probability integral on condition of the signal to noise ratio  $\gamma$  for a 1 pulse as

$$\begin{aligned} P_e(E) &= \int_0^\infty P[E | \gamma] \cdot p_\gamma(\gamma) \cdot d\gamma \\ &= \int_0^\infty P[n < n_{th} | \gamma] \cdot p_\gamma(\gamma) \cdot d\gamma \\ &= \int_0^\infty \int_{n_{th}}^\infty p_{n|\gamma}(n, \gamma) dn \cdot p_\gamma(\gamma) \cdot d\gamma \end{aligned}$$

By using the variable substitution of

$$\gamma = f(h)$$

$$p_\gamma(\gamma) = p_\gamma(h)|_{h=f(\gamma)} \cdot \frac{dh}{d\gamma}$$

Hence

$$\begin{aligned} P_e(E) &= \int_0^\infty \int_{n_{th}}^\infty [p_{n|\gamma}(n, \gamma) \cdot p_\gamma(\gamma)]|_{\gamma=f(h)} \cdot dn \cdot \frac{dh}{d\gamma} \cdot d\gamma \\ &= \int_0^\infty \int_{n_{th}}^\infty [p_{n|f(h)}(n, f(h)) \cdot p_\gamma(f(h))] \cdot dn \cdot dh \\ &= \int_0^\infty \int_{n_{th}}^\infty p_{n|h}(n, h) \cdot dn \cdot p_\gamma[f(h)] \cdot dh \end{aligned}$$

Using the variable substitution  $p_h(h) = p_\gamma[f(h)]$

$$\begin{aligned} P_e(E) &= \int_0^\infty P[n < n_{th} | h] \cdot p_h(h) \cdot dh \\ &= \int_0^\infty P(E | h) \cdot p_h(h) \cdot dh \end{aligned}$$

Where  $p_h(h) = p_\gamma[f(h)]$  is a PDF function of the channel gain random variable  $h$  for a 1 pulse.

$P(E | h)$  is the error probability on the condition of the random variable vector  $h$ .

### APPENDIX G

This is the derivation for Eq. (4-23).

By using the Chernov Bound [12], for the AWGN system ( $0 \leq x \leq \infty$ ), we can get

$$0 \leq \int_x^\infty \frac{1}{\sqrt{2\pi}} e^{-\frac{t^2}{2}} \cdot dt \leq \frac{1}{2} e^{-\frac{x^2}{2}} \leq 1$$

In practice, for the optical receiver under the normally working condition, the unified noise

powers  $\sigma_{on}^2$  and  $\sigma_{off}^2$  are smaller than the unified signal power  $\left(\frac{E_s \mathcal{R}MAG}{N_t} h\right)^2$  and  $\frac{E_s \mathcal{R}MAG}{N_t} h \geq$

$\sigma_{on}$ ,  $\frac{E_s \mathcal{R}MAG}{N_t} h \geq \sigma_{off}$ ,  $0 \leq h \leq \infty$ . The signal to noise ratio is far above 0dB, which means

$$\left(\frac{E_s \mathcal{R}MAG}{N_t} h\right)^2 \geq \sigma_{on}^2.$$

Letting  $r_1 = \frac{E_s \mathcal{R}MAG}{N_t} h + n_{on}$  and the following inequality exists

$$P\left[n_2 \leq \frac{E_s \mathcal{R}MAG}{N_t} h + n_1 \mid \mathbf{S}_1 \text{ sent}, n_1 = n_{on}\right]$$

$$\geq \int_{-\left(\frac{E_s \mathcal{R}MAG}{N_t} h + n_{on}\right)}^{\left|\frac{E_s \mathcal{R}MAG}{N_t} h + n_{on}\right|} \frac{1}{\sqrt{2\pi}} e^{-\frac{n_2^2}{2}} \cdot dn_2$$

$$\begin{aligned}
&= \int_{-\left(\frac{E_s \mathcal{RGMAG}_{h+n_{on}}}{N_t}\right)}^0 \frac{1}{\sqrt{2\pi}} e^{-\frac{n_2^2}{2}} \cdot dn_2 + \int_0^{\left|\frac{E_s \mathcal{RGMAG}_{h+n_{on}}}{N_t}\right|} \frac{1}{\sqrt{2\pi}} e^{-\frac{n_2^2}{2}} \cdot dn_2 \\
&= 2 \int_0^{\left|\frac{E_s \mathcal{RGMAG}_{h+n_{on}}}{N_t}\right|} \frac{1}{\sqrt{2\pi}} e^{-\frac{n_2^2}{2}} \cdot dn_2 \\
&= 2 \left[ \frac{1}{2} - Q \left( \left| \frac{E_s \mathcal{RGMAG}_{h+n_{on}}}{N_t} \right| \right) \right] \\
&\geq 2 \left[ \frac{1}{2} - \frac{1}{2} e^{-\frac{\left(\frac{E_s \mathcal{RGMAG}_{h+n_{on}}}{N_t}\right)^2}{2}} \right] \\
&= 1 - e^{-\frac{\left(\frac{E_s \mathcal{RGMAG}_{h+n_{on}}}{N_t}\right)^2}{2\sigma_{\text{off}}^2}} \\
&= 1 - e^{-\frac{1}{2} \left( \frac{E_s \mathcal{RGMAG}_{h+n_{on}}}{\sigma_{\text{off}} N_t} + \frac{n_{on}}{\sigma_{\text{off}}} \right)^2}
\end{aligned}$$

In Eq. (4-20), the following Q function inequality equation exists

$$\begin{aligned}
1 &\geq 1 - Q \left( \frac{E_s \mathcal{RGMAG}_{h+n_{on}}}{\sigma_{\text{off}} N_t} + \frac{n_{on}}{\sigma_{\text{off}}} \right) \geq 1 - e^{-\frac{1}{2} \left( \frac{E_s \mathcal{RGMAG}_{h+n_{on}}}{\sigma_{\text{off}} N_t} + \frac{n_{on}}{\sigma_{\text{off}}} \right)^2} \geq 0 \\
1 &\geq \left[ 1 - Q \left( \frac{E_s \mathcal{RGMAG}_{h+n_{on}}}{\sigma_{\text{off}} N_t} + \frac{n_{on}}{\sigma_{\text{off}}} \right) \right]^{(L-1)} \geq \left[ 1 - e^{-\frac{1}{2} \left( \frac{E_s \mathcal{RGMAG}_{h+n_{on}}}{\sigma_{\text{off}} N_t} + \frac{n_{on}}{\sigma_{\text{off}}} \right)^2} \right]^{(L-1)} \geq 0 \\
0 &\leq 1 - \left[ 1 - Q \left( \frac{E_s \mathcal{RGMAG}_{h+n_{on}}}{\sigma_{\text{off}} N_t} + \frac{n_{on}}{\sigma_{\text{off}}} \right) \right]^{(L-1)} \leq 1 - \left[ 1 - e^{-\frac{1}{2} \left( \frac{E_s \mathcal{RGMAG}_{h+n_{on}}}{\sigma_{\text{off}} N_t} + \frac{n_{on}}{\sigma_{\text{off}}} \right)^2} \right]^{(L-1)} \leq 1
\end{aligned}$$

The PDF of  $p_{n_{on}}(n_{on})$  is nonnegative  $p_{n_{on}}(n_{on}) \geq 0$  and the following inequality equation exists

$$\begin{aligned}
0 &\leq \left\{ 1 - \left[ 1 - Q \left( \frac{E_s \mathcal{RGM}Ag h}{\sigma_{\text{off}} N_t} + \frac{n_{\text{on}}}{\sigma_{\text{off}}} \right) \right]^{(L-1)} \right\} p_{n_{\text{on}}}(n_{\text{on}}) \\
&\leq \left\{ 1 - \left[ 1 - e^{-\frac{1}{2} \left( \frac{E_s \mathcal{RGM}Ag h + n_{\text{on}}}{\sigma_{\text{off}}} \right)^2} \right]^{(L-1)} \right\} p_{n_{\text{on}}}(n_{\text{on}})
\end{aligned}$$

If this inequality is integrated on both sides from negative infinity to infinity, this inequality is also satisfied as

$$\begin{aligned}
0 &\leq \int_{-\infty}^{\infty} \left\{ 1 - \left[ 1 - Q \left( \frac{E_s \mathcal{RGM}Ag h}{\sigma_{\text{off}} N_t} + \frac{n_{\text{on}}}{\sigma_{\text{off}}} \right) \right]^{(L-1)} \right\} p_{n_{\text{on}}}(n_{\text{on}}) \cdot dn_{\text{on}} \\
&\leq \int_{-\infty}^{\infty} \left\{ 1 - \left[ 1 - e^{-\frac{1}{2} \left( \frac{E_s \mathcal{RGM}Ag h + n_{\text{on}}}{\sigma_{\text{off}}} \right)^2} \right]^{(L-1)} \right\} p_{n_{\text{on}}}(n_{\text{on}}) \cdot dn_{\text{on}}
\end{aligned}$$

where  $k_t = \frac{E_s \mathcal{RMA}g}{N_t}$ . As the integrand of the above integral is real,  $r_1$  is real and the integral in

Eq. (4-20) is a probability, the integration result is real.

In Eq. (3-62), the channel gain  $h_{il} \geq 0$  is real, the variable

$$K_{x_u} = \eta \frac{E_s 2A_r \alpha}{h\nu A_b N_t} e^{m_\ell} e^{\sqrt{2} \sigma_\ell x_u} \geq 0 \quad \text{and} \quad \frac{(F-1)\mathcal{R}E_s g}{qN_t} h_{il} + K_{x_u} \geq 0. \quad p_{h_{il}}(h_{il}) \text{ is real and}$$

nonnegative and has a singularity of  $h_{il} = 0$ . Since  $h = \sum_{l=1}^{N_r} \sum_{i=1}^{N_t} h_{il}$ ,  $p_h(h)$  is the convolution

of  $p_{h_{il}}(h_{il})$  ( $0 \leq i \leq N_t, 0 \leq l \leq N_r$ ). According to the properties of the convolution of the

real and nonnegative functions, the PDF  $p_h(h)$  is real and nonnegative. The inequality is

satisfied when the two sides of the above inequality are multiplied by  $p_h(h)$  ( $p_h(h) \geq 0$ ) and

integrated on both sides as

$$0 \leq \left[ \int_{-\infty}^{\infty} \left\{ 1 - \left[ 1 - Q \left( \frac{E_s \mathcal{RGM}Ag h}{\sigma_{\text{off}} N_t} + \frac{n_{\text{on}}}{\sigma_{\text{off}}} \right) \right]^{(L-1)} \right\} p_{n_{\text{on}}}(n_{\text{on}}) \cdot dn_{\text{on}} \right] p_h(h)$$

$$\leq \left[ \int_{-\infty}^{\infty} \left\{ 1 - \left[ 1 - e^{-\frac{1}{2} \left( \frac{E_s \mathcal{R}GMAG}{\sigma_{\text{off}} N_t} h + \frac{n_{\text{on}}}{\sigma_{\text{off}}} \right)^2} \right]^{(L-1)} \right\} p_{n_{\text{on}}}(n_{\text{on}}) \cdot dn_{\text{on}} \right] p_h(h)$$

Then

$$\begin{aligned} & \int_0^{\infty} \left[ \int_{-\infty}^{\infty} \left\{ 1 - \left[ 1 - Q \left( \frac{E_s \mathcal{R}GMAG h}{\sigma_{\text{off}} N_t} + \frac{n_{\text{on}}}{\sigma_{\text{off}}} \right) \right]^{(L-1)} \right\} p_{n_{\text{on}}}(n_{\text{on}}) \cdot dn_{\text{on}} \right] \cdot p_h(h) dh \\ & \leq \int_0^{\infty} \left[ \int_{-\infty}^{\infty} \left\{ 1 - \left[ 1 - e^{-\frac{1}{2} \left( \frac{E_s \mathcal{R}GMAG}{\sigma_{\text{off}} N_t} h + \frac{n_{\text{on}}}{\sigma_{\text{off}}} \right)^2} \right]^{(L-1)} \right\} p_{n_{\text{on}}}(n_{\text{on}}) \cdot dn_{\text{on}} \right] \cdot p_h(h) dh \end{aligned}$$

The symbol error probability  $P_s(E)$  of this Q-ary PPM in Eq. (4-20) is

$$\begin{aligned} P_s(E) &= P_{s|s_1} = 1 - P_c \\ &= \int_0^{\infty} \left[ \int_{-\infty}^{\infty} \left\{ 1 - \left[ 1 - Q \left( \frac{E_s \mathcal{R}GMAG h}{\sigma_{\text{off}} N_t} + \frac{n_{\text{on}}}{\sigma_{\text{off}}} \right) \right]^{(L-1)} \right\} p_{n_{\text{on}}}(n_{\text{on}}) \cdot dn_{\text{on}} \right] \cdot p_h(h) dh \\ &\leq \int_0^{\infty} \left[ \int_{-\infty}^{\infty} \left\{ 1 - \left[ 1 - e^{-\frac{1}{2} \left( \frac{E_s \mathcal{R}GMAG}{\sigma_{\text{off}} N_t} h + \frac{n_{\text{on}}}{\sigma_{\text{off}}} \right)^2} \right]^{(L-1)} \right\} p_{n_{\text{on}}}(n_{\text{on}}) \cdot dn_{\text{on}} \right] \cdot p_h(h) dh \end{aligned}$$

## APPENDIX H

This is the derivation for Eq. (4-26).

Letting  $k_t = \frac{E_s \mathcal{R}MAG}{N_t}$ , the symbol error probability in Eq. (4-19) is

$$\begin{aligned} P_s(E) &= P_{s|s_1} = 1 - P_c \\ &= \int_0^{\infty} \left\{ \int_{-\infty}^{\infty} \left\{ 1 - \left[ 1 - Q \left( \frac{k_t h + n_{\text{on}}}{\sigma_{\text{off}}} \right) \right]^{(L-1)} \right\} p_{n_{\text{on}}}(n_{\text{on}}) dn_{\text{on}} \right\} p_h(h) dh \\ &= \int_0^{\infty} \left\{ \int_{-\infty}^{\infty} \left\{ 1 - \left[ 1 - \int_{\frac{k_t h + n_{\text{on}}}{\sigma_{\text{off}}}}^{\infty} \frac{1}{\sqrt{2\pi}} e^{-\frac{t^2}{2}} \cdot dt \right]^{(L-1)} \right\} p_{n_{\text{on}}}(n_{\text{on}}) dn_{\text{on}} \right\} p_h(h) dh \end{aligned}$$

$$\begin{aligned}
&\leq \int_0^\infty \left\{ \int_{-\infty}^\infty \left\{ 1 - \left[ 1 - e^{-\frac{(k_t h + n_{\text{on}})^2}{2\sigma_{\text{off}}^2}} \right]^{(L-1)} \right\} p_{n_{\text{on}}}(n_{\text{on}}) dn_{\text{on}} \right\} p_h(h) dh \\
&= \int_0^\infty \left\{ \int_{-\infty}^\infty \left\{ 1 - \left[ 1 - e^{-\frac{(k_t h + n_{\text{on}})^2}{2\sigma_{\text{off}}^2}} \right]^{(L-1)} \right\} \frac{e^{-\frac{n_{\text{on}}^2}{2\sigma_{\text{on}}^2}}}{\sqrt{2\pi\sigma_{\text{on}}^2}} dn_{\text{on}} \right\} p_h(h) dh \\
&= \int_0^\infty \left\{ \int_{-\infty}^\infty \left\{ 1 - \sum_{k=0}^{L-1} C_{L-1}^k (-1)^k e^{-\frac{k(k_t h + n_{\text{on}})^2}{2\sigma_{\text{off}}^2}} \right\} \frac{e^{-\frac{n_{\text{on}}^2}{2\sigma_{\text{on}}^2}}}{\sqrt{2\pi\sigma_{\text{on}}^2}} dn_{\text{on}} \right\} p_h(h) dh \\
&= \int_0^\infty \left\{ \int_{-\infty}^\infty \left\{ 1 - C_{L-1}^0 (-1)^0 e^{-\frac{0(k_t h + n_{\text{on}})^2}{2\sigma_{\text{off}}^2}} \right. \right. \\
&\quad \left. \left. - \sum_{k=1}^{L-1} C_{L-1}^k (-1)^k e^{-\frac{k(k_t h + n_{\text{on}})^2}{2\sigma_{\text{off}}^2}} \right\} \frac{e^{-\frac{n_{\text{on}}^2}{2\sigma_{\text{on}}^2}}}{\sqrt{2\pi\sigma_{\text{on}}^2}} dn_{\text{on}} \right\} p_h(h) dh \\
&= \int_0^\infty \left\{ \int_{-\infty}^\infty \left\{ \sum_{k=1}^{L-1} C_{L-1}^k (-1)^{k+1} e^{-\frac{k(k_t h + n_{\text{on}})^2}{2\sigma_{\text{off}}^2}} \right\} \frac{e^{-\frac{n_{\text{on}}^2}{2\sigma_{\text{on}}^2}}}{\sqrt{2\pi\sigma_{\text{on}}^2}} dn_{\text{on}} \right\} p_h(h) dh \\
&= \int_0^\infty \left\{ \sum_{k=1}^{L-1} \frac{C_{L-1}^k (-1)^{k+1}}{\sqrt{2\pi\sigma_{\text{on}}^2}} \int_{-\infty}^\infty e^{-\frac{k(k_t h + n_{\text{on}})^2}{2\sigma_{\text{off}}^2}} e^{-\frac{n_{\text{on}}^2}{2\sigma_{\text{on}}^2}} dn_{\text{on}} \right\} p_h(h) dh \\
&= \int_0^\infty \sum_{k=1}^{L-1} \frac{C_{L-1}^k (-1)^{k+1}}{\sqrt{2\pi\sigma_{\text{on}}^2}} \int_{-\infty}^\infty e^{-\frac{k\sigma_{\text{on}}^2(k_t h)^2 + k\sigma_{\text{on}}^2 2k_t h n_{\text{on}} + k\sigma_{\text{on}}^2 n_{\text{on}}^2 + \sigma_{\text{off}}^2 n_{\text{on}}^2}{2\sigma_{\text{off}}^2 \sigma_{\text{on}}^2}} dn_{\text{on}} \\
&\quad \cdot p_h(h) dh \\
&= \int_0^\infty \sum_{k=1}^{L-1} \frac{C_{L-1}^k (-1)^{k+1}}{\sqrt{2\pi\sigma_{\text{on}}^2}} \int_{-\infty}^\infty e^{-\frac{(k\sigma_{\text{on}}^2 + \sigma_{\text{off}}^2)n_{\text{on}}^2 + k\sigma_{\text{on}}^2 2k_t h n_{\text{on}} + k\sigma_{\text{on}}^2 (k_t h)^2}{2\sigma_{\text{off}}^2 \sigma_{\text{on}}^2}} dn_{\text{on}} p_h(h) dh
\end{aligned}$$

$$\begin{aligned}
&= \int_0^\infty \sum_{k=1}^{L-1} \frac{C_{L-1}^k (-1)^{k+1}}{\sqrt{2\pi\sigma_{\text{on}}^2}} \int_{-\infty}^\infty e^{-\frac{\left[ \sqrt{(k\sigma_{\text{on}}^2 + \sigma_{\text{off}}^2)} n_{\text{on}} + \frac{k\sigma_{\text{on}}^2 k_t h}{\sqrt{(k\sigma_{\text{on}}^2 + \sigma_{\text{off}}^2)}} \right]^2}{2\sigma_{\text{off}}^2 \sigma_{\text{on}}^2} - \frac{(k\sigma_{\text{on}}^2 k_t h)^2}{(k\sigma_{\text{on}}^2 + \sigma_{\text{off}}^2)} + k\sigma_{\text{on}}^2 (k_t h)^2} dh \\
&\quad \frac{\sigma_{\text{on}} \sigma_{\text{off}}}{\sqrt{(k\sigma_{\text{on}}^2 + \sigma_{\text{off}}^2)}} d \left( \frac{\sqrt{(k\sigma_{\text{on}}^2 + \sigma_{\text{off}}^2)}}{\sigma_{\text{on}} \sigma_{\text{off}}} n_{\text{on}} \right) p_h(h) dh \\
&= \int_0^\infty \sum_{k=1}^{L-1} \frac{C_{L-1}^k (-1)^{k+1}}{\sqrt{2\pi\sigma_{\text{on}}^2}} \frac{\sigma_{\text{on}} \sigma_{\text{off}}}{\sqrt{(k\sigma_{\text{on}}^2 + \sigma_{\text{off}}^2)}} e^{\frac{(k\sigma_{\text{on}}^2 k_t h)^2}{(k\sigma_{\text{on}}^2 + \sigma_{\text{off}}^2)} - k\sigma_{\text{on}}^2 (k_t h)^2} \\
&\quad \int_{-\infty}^\infty e^{-\frac{\left[ \sqrt{(k\sigma_{\text{on}}^2 + \sigma_{\text{off}}^2)} n_{\text{on}} + \frac{k\sigma_{\text{on}}^2 k_t h}{\sqrt{(k\sigma_{\text{on}}^2 + \sigma_{\text{off}}^2)}} \right]^2}{2\sigma_{\text{off}}^2 \sigma_{\text{on}}^2}} d \left( \frac{\sqrt{(k\sigma_{\text{on}}^2 + \sigma_{\text{off}}^2)}}{\sigma_{\text{on}} \sigma_{\text{off}}} n_{\text{on}} \right) p_h(h) dh
\end{aligned}$$

where  $k_t = \frac{E_s \mathcal{R} \text{MAG}}{N_t}$ . Using the variable substitution  $t = \frac{\sqrt{(k\sigma_{\text{on}}^2 + \sigma_{\text{off}}^2)} n_{\text{on}} + \frac{k\sigma_{\text{on}}^2 k_t h}{\sqrt{(k\sigma_{\text{on}}^2 + \sigma_{\text{off}}^2)}}}{\sigma_{\text{on}} \sigma_{\text{off}}}$ , the

following integral is

$$\int_{-\infty}^\infty e^{-\frac{\left[ \sqrt{(k\sigma_{\text{on}}^2 + \sigma_{\text{off}}^2)} n_{\text{on}} + \frac{k\sigma_{\text{on}}^2 k_t h}{\sqrt{(k\sigma_{\text{on}}^2 + \sigma_{\text{off}}^2)}} \right]^2}{2\sigma_{\text{off}}^2 \sigma_{\text{on}}^2}} d \left( \frac{\sqrt{(k\sigma_{\text{on}}^2 + \sigma_{\text{off}}^2)}}{\sigma_{\text{on}} \sigma_{\text{off}}} n_{\text{on}} \right) = \int_{-\infty}^\infty e^{-\frac{t^2}{2}} dt$$

Since the function  $\frac{1}{\sqrt{2\pi}} e^{-\frac{t^2}{2}}$  is the PDF of the Gaussian distribution, its integral from negative

infinity to infinity equal to 1, i.e.  $\int_{-\infty}^\infty \frac{1}{\sqrt{2\pi}} e^{-\frac{t^2}{2}} dt = 1$ . The symbol error probability is obtained

as

$$\begin{aligned}
P_s(E) &\leq \int_0^\infty \sum_{k=1}^{L-1} \frac{C_{L-1}^k (-1)^{k+1}}{\sqrt{2\pi\sigma_{\text{on}}^2}} \frac{\sigma_{\text{on}}\sigma_{\text{off}}}{\sqrt{(k\sigma_{\text{on}}^2 + \sigma_{\text{off}}^2)}} e^{-\frac{(k\sigma_{\text{on}}^2 k_t h)^2}{(k\sigma_{\text{on}}^2 + \sigma_{\text{off}}^2)} - k\sigma_{\text{on}}^2 (k_t h)^2} \sqrt{2\pi} p_h(h) dh \\
&= \int_0^\infty \sum_{k=1}^{L-1} \frac{C_{L-1}^k (-1)^{k+1} \sigma_{\text{off}}}{\sqrt{(k\sigma_{\text{on}}^2 + \sigma_{\text{off}}^2)}} e^{-\frac{(k\sigma_{\text{on}}^2 k_t h)^2 - k\sigma_{\text{on}}^2 (k_t h)^2 (k\sigma_{\text{on}}^2 + \sigma_{\text{off}}^2)}{2\sigma_{\text{off}}^2 \sigma_{\text{on}}^2 (k\sigma_{\text{on}}^2 + \sigma_{\text{off}}^2)}} p_h(h) dh \\
&= \int_0^\infty \sum_{k=1}^{L-1} \frac{C_{L-1}^k (-1)^{k+1} \sigma_{\text{off}}}{\sqrt{(k\sigma_{\text{on}}^2 + \sigma_{\text{off}}^2)}} e^{-\frac{(k\sigma_{\text{on}}^2 k_t h)^2 - k^2 \sigma_{\text{on}}^4 (k_t h)^2 - k\sigma_{\text{on}}^2 (k_t h)^2 \sigma_{\text{off}}^2}{2\sigma_{\text{off}}^2 \sigma_{\text{on}}^2 (k\sigma_{\text{on}}^2 + \sigma_{\text{off}}^2)}} p_h(h) dh \\
&= \int_0^\infty \sum_{k=1}^{L-1} \frac{C_{L-1}^k (-1)^{k+1} \sigma_{\text{off}}}{\sqrt{(k\sigma_{\text{on}}^2 + \sigma_{\text{off}}^2)}} e^{-\frac{k(k_t h)^2}{2(k\sigma_{\text{on}}^2 + \sigma_{\text{off}}^2)}} p_h(h) dh \\
&= \int_0^\infty \sum_{k=1}^{L-1} \frac{C_{L-1}^k (-1)^{k+1} \sigma_{\text{off}}}{\sqrt{(k\sigma_{\text{on}}^2 + \sigma_{\text{off}}^2)}} e^{-\frac{k(E_s \mathcal{R}MAG)^2 h^2}{2N_t^2 (k\sigma_{\text{on}}^2 + \sigma_{\text{off}}^2)}} p_h(h) dh
\end{aligned}$$

## APPENDIX I

This is the derivation for Eq. (4-50).

The function  $F_f(\omega)$  is calculated as

$$\begin{aligned}
F_f(\omega) &= \int_0^\infty f(h) e^{-j\omega h} dh \\
&= \int_0^\infty e^{-k_l h^2} e^{-j\omega h} dh \\
&= \int_0^\infty e^{-k_l \left[ h^2 + \frac{j\omega h}{k_l} + \left( \frac{j\omega}{2k_l} \right)^2 \right] + \frac{(j\omega)^2}{4k_l}} dh \\
&= e^{\frac{(j\omega)^2}{4k_l}} \int_0^\infty e^{-k_l \left( h + \frac{j\omega}{2k_l} \right)^2} dh
\end{aligned}$$

$$= \frac{1}{\sqrt{2k_l}} e^{\frac{-\omega^2}{4k_l}} \int_0^\infty e^{-\frac{\left(\sqrt{2k_l}h + \frac{j\omega}{\sqrt{2k_l}}\right)^2}{2}} d(\sqrt{2k_l} h)$$

$$\text{Letting } x = \sqrt{2k_l}h + \frac{j\omega}{\sqrt{2k_l}}$$

$$= \frac{1}{\sqrt{2k_l}} e^{\frac{-\omega^2}{4k_l}} \left[ \int_{\frac{j\omega}{\sqrt{2k_l}}}^\infty e^{-\frac{(x)^2}{2}} dx \right]$$

$$= \frac{1}{\sqrt{2k_l}} e^{\frac{-\omega^2}{4k_l}} \sqrt{2\pi} \left[ Q\left(\frac{j\omega}{\sqrt{2k_l}}\right) \right]$$

$$= e^{\frac{-\omega^2}{4k_l}} \sqrt{\frac{\pi}{k_l}} Q\left(\frac{j\omega}{\sqrt{2k_l}}\right)$$

$$\text{where } k_l = \frac{k(E_s R M A g)^2}{2N_t^2(k\sigma_{on}^2 + \sigma_{off}^2)}$$

## APPENDIX J

This is the derivation for Eq. (4-56a).

In Eq. (4-55), the numerator part of the variable in the exponential function can be calculated as

$$\begin{aligned} (K_k h_{il} - K_{x_u})^2 &= K_k^2 h_{il}^2 - 2K_k h_{il} K_{x_u} + K_{x_u}^2 \\ &= \{-2[(F-1)K_k h_{ij} + K_{x_u}]h_{il}\} + (K_k h_{il} - K_{x_u})^2 + 2[(F-1)K_k h_{il}^2 + K_{x_u} h_{il}] \\ &= \{-2[(F-1)K_k h_{il} + K_{x_u}]h_{il}\} + K_k^2 \left(h_{il} - \frac{K_{x_u}}{K_k}\right)^2 + 2[(F-1)K_k h_{il}^2 + K_{x_u} h_{il}] \\ &= \{-2[(F-1)K_k h_{il} + K_{x_u}]h_{il}\} + K_k^2 \left(h_{il} - qe^{m_\ell} e^{\sqrt{2}\sigma_\ell x_u}\right)^2 + 2[(F-1)K_k h_{il}^2 + K_{x_u} h_{il}] \end{aligned}$$

In Eq. (4-55), the denominator part of the variable in the exponential function can be calculated

as

$$\begin{aligned}
2[(F-1)K_k h_{il} + K_{x_u}] &= 2K_k \left[ (F-1)h_{il} + \frac{K_{x_u}}{K_k} \right] \\
&= 2K_k \left[ (F-1)h_{il} + qe^{m_\ell} e^{\sqrt{2}\sigma_\ell x_u} \right]
\end{aligned}$$

Then the part in Eq. (4-55) is

$$\begin{aligned}
&\exp \left\{ -\frac{(K_k h_{il} - K_{x_u})^2}{2[(F-1)K_k h_{il} + K_{x_u}]} \right\} \\
&= e^{-h_{il}} \cdot \exp \left\{ h_{il} - \frac{K_k (h_{il} - qe^{m_\ell} e^{\sqrt{2}\sigma_\ell x_u})^2}{2[(F-1)h_{il} + qe^{m_\ell} e^{\sqrt{2}\sigma_\ell x_u}]} \right\}
\end{aligned}$$

Eq. (4-55) can be represented as

$$\begin{aligned}
F_{p_h}(\omega) &= \sum_{\substack{u=-N_u \\ u \neq 0}}^{N_u} K_{w_u} K_{x_u} K_k M \int_0^\infty e^{-h_{il}} [(F-1)K_k h_{il} + K_{x_u}]^{(-\frac{3}{2})} \\
&\quad \exp \left\{ h_{il} - \frac{K_k (h_{il} - e^{m_\ell} e^{\sqrt{2}\sigma_\ell x_u})^2}{2[(F-1)h_{il} + e^{m_\ell} e^{\sqrt{2}\sigma_\ell x_u}]} + j\omega h_{il} \right\} dh_{il}
\end{aligned}$$

## APPENDIX K

This is the derivation for Eq. (4-61).

Then the characteristic function  $F_p(\omega)$  of  $p_h(h)$  can be represented as

$$\begin{aligned}
F_p(\omega) &= \int_{-\infty}^{\infty} p_h(h) e^{j\omega h_{il}} dh \\
&= \int_{-\infty}^{\infty} p_{h_{11}}(h_{11}) e^{j\omega h_{11}} dh_{11} \int_{-\infty}^{\infty} p_{h_{12}}(h_{12}) e^{j\omega h_{12}} dh_{12} \dots \dots
\end{aligned}$$

$$\int_{-\infty}^{\infty} p_h(h_{N_t N_r}) e^{j\omega h_{N_t N_r}} dh_{N_t N_r}$$

$$\begin{aligned}
&= F_{p_{h_{11}}}(\omega) F_{p_{h_{12}}}(\omega) \dots \dots F_{p_{h_{1N_r}}}(\omega) F_{p_{h_{21}}}(\omega) \dots \dots F_{p_{h_{N_t N_r}}}(\omega) \\
&= \prod_{l=1}^{N_r} \prod_{i=1}^{N_t} F_{p_h}(\omega) \\
&= \prod_{l=1}^{N_r} \prod_{i=1}^{N_t} \sum_{\substack{u=-N_u \\ u \neq 0}}^{N_u} \sum_{v=1}^{N_v} K_{w_u} K_{x_u} K_k M_{w_v} [(F-1)K_k x_v + K_{x_u}]^{(-\frac{3}{2})} \\
&\quad \exp \left\{ x_v - \frac{K_k (x_v - e^{m_\ell} e^{\sqrt{2} \sigma_\ell x_u})^2}{2[(F-1)x_v + e^{m_\ell} e^{\sqrt{2} \sigma_\ell x_u}]} + j\omega x_v \right\} \\
&= \prod_{l=1}^{N_r} \prod_{i=1}^{N_t} \sum_{\substack{u=-N_u \\ u \neq 0}}^{N_u} \sum_{v=1}^{N_v} K_{w_u} K_{x_u} K_k M_{w_v} [(F-1)K_k x_v + K_{x_u}]^{(-\frac{3}{2})} \\
&\quad \exp \left\{ x_v - \frac{K_k (x_v - e^{m_\ell} e^{\sqrt{2} \sigma_\ell x_u})^2}{2[(F-1)x_v + e^{m_\ell} e^{\sqrt{2} \sigma_\ell x_u}]} \right\} \exp\{j\omega x_v\} \\
&= \sum_{\substack{u_1=-N_u \\ u_1 \neq 0}}^{N_u} \sum_{\substack{u_2=-N_u \\ u_2 \neq 0}}^{N_u} \dots \sum_{\substack{u_{N_t N_r}=-N_u \\ u_{N_t N_r} \neq 0}}^{N_u} \sum_{v_1=1}^{N_v} \sum_{v_2=1}^{N_v} \dots \sum_{v_{N_t N_r}=1}^{N_v} \left[ \frac{F e^{m_\ell}}{\pi} \left( \sqrt{\frac{R E_s A_r \alpha}{q N_t A_b}} \right) \right]^{N_t N_r} \\
&W_{u_1} W_{u_2} \dots W_{u_{N_t N_r}} W_{v_1} W_{v_2} \dots W_{v_{N_t N_r}} \\
&\exp \left[ \sqrt{2} \sigma_\ell (x_{u_1} + x_{u_2} + \dots \dots + x_{u_{N_t N_r}}) + (x_{v_1} + x_{v_2} + \dots + x_{v_{N_t N_r}}) \right] \\
&\left[ (F-1)x_{v_1} + e^{m_\ell} e^{\sqrt{2} \sigma_\ell x_{u_1}} \right]^{(-\frac{3}{2})} \left[ (F-1)x_{v_2} + e^{m_\ell} e^{\sqrt{2} \sigma_\ell x_{u_2}} \right]^{(-\frac{3}{2})} \dots \dots \\
&\left[ (F-1)x_{v_{N_t N_r}} + e^{m_\ell} e^{\sqrt{2} \sigma_\ell x_{u_{N_t N_r}}} \right]^{(-\frac{3}{2})}
\end{aligned}$$

$$\begin{aligned}
& \exp \left\{ \left( -\frac{K_k}{2} \right) \left[ \frac{(x_{v_1} - e^{m_\ell} e^{\sqrt{2} \sigma_\ell} x_{u_1})^2}{[(F-1)x_{v_1} + e^{m_\ell} e^{\sqrt{2} \sigma_\ell} x_{u_1}]} + \frac{(x_{v_2} - e^{m_\ell} e^{\sqrt{2} \sigma_\ell} x_{u_2})^2}{[(F-1)x_{v_2} + e^{m_\ell} e^{\sqrt{2} \sigma_\ell} x_{u_2}]} \dots \dots \right. \right. \\
& \quad \left. \left. + \frac{(x_{v_{N_t N_r}} - e^{m_\ell} e^{\sqrt{2} \sigma_\ell} x_{u_{N_t N_r}})^2}{[(F-1)x_{v_{N_t N_r}} + e^{m_\ell} e^{\sqrt{2} \sigma_\ell} x_{u_{N_t N_r}}]} \right] \right\} e^{(x_{v_1} + x_{v_2} + \dots + x_{v_{N_t N_r}}) j \omega} \\
& = \sum_{v_1=1}^{N_v} \sum_{v_2=1}^{N_v} \dots \sum_{v_{N_t N_r}=1}^{N_v} e^{(x_{v_1} + x_{v_2} + \dots + x_{v_{N_t N_r}}) j \omega} \left[ \frac{F e^{m_\ell}}{\pi} \left( \sqrt{\frac{\mathcal{R} E_s A_r \alpha}{q N_t A_b}} \right) \right]^{N_t N_r} \\
& \quad \sum_{\substack{u_1=-N_u \\ u_1 \neq 0}}^{N_u} \sum_{\substack{u_2=-N_u \\ u_2 \neq 0}}^{N_u} \dots \sum_{\substack{u_{N_t N_r}=-N_u \\ u_{N_t N_r} \neq 0}}^{N_u} W_{u_1} W_{u_2} \dots W_{u_{N_t N_r}} W_{v_1} W_{v_2} \dots W_{v_{N_t N_r}} \\
& \exp \left[ \sqrt{2} \sigma_\ell (x_{u_1} + x_{u_2} \dots + x_{u_{N_t N_r}}) + (x_{v_1} + x_{v_2} \dots + x_{v_{N_t N_r}}) \right] \\
& \quad [(F-1)x_{v_1} + e^{m_\ell} e^{\sqrt{2} \sigma_\ell} x_{u_1}]^{(-\frac{3}{2})} [(F-1)x_{v_2} + e^{m_\ell} e^{\sqrt{2} \sigma_\ell} x_{u_2}]^{(-\frac{3}{2})} \dots \dots \\
& \quad [(F-1)x_{v_{N_t N_r}} + e^{m_\ell} e^{\sqrt{2} \sigma_\ell} x_{u_{N_t N_r}}]^{(-\frac{3}{2})} \\
& \exp \left\{ \left( -\frac{K_k}{2} \right) \left[ \frac{(x_{v_1} - e^{m_\ell} e^{\sqrt{2} \sigma_\ell} x_{u_1})^2}{[(F-1)x_{v_1} + e^{m_\ell} e^{\sqrt{2} \sigma_\ell} x_{u_1}]} + \frac{(x_{v_2} - e^{m_\ell} e^{\sqrt{2} \sigma_\ell} x_{u_2})^2}{[(F-1)x_{v_2} + e^{m_\ell} e^{\sqrt{2} \sigma_\ell} x_{u_2}]} \dots \dots \right. \right. \\
& \quad \left. \left. + \frac{(x_{v_{N_t N_r}} - e^{m_\ell} e^{\sqrt{2} \sigma_\ell} x_{u_{N_t N_r}})^2}{[(F-1)x_{v_{N_t N_r}} + e^{m_\ell} e^{\sqrt{2} \sigma_\ell} x_{u_{N_t N_r}}]} \right] \right\} \\
& = \sum_{v_1=1}^{N_v} \sum_{v_2=1}^{N_v} \dots \sum_{v_{N_t N_r}=1}^{N_v} K_0 K_f e^{K_d j \omega}
\end{aligned}$$

## APPENDIX L

This is the derivation for Eq. (4-80).

By using the Fourier series expression in the reference [6] in Chapter 4, the average symbol error probability for one PPM symbol in Eq. (4-80) can be represented as [6]

$$\begin{aligned}
 P_s(E) &= \frac{1}{T} \sum_{n=-\infty}^{\infty} \text{Real}\{G(n\omega_0)\Phi_x(n\omega_0)\} \\
 &= \frac{\omega_0}{2\pi} \sum_{n=-\infty}^{\infty} \text{Real}\{G(n\omega_0)\Phi_x(n\omega_0)\} \\
 &= \frac{\omega_0}{2\pi} \text{Real}\{G(0)\Phi_x(0)\} + \frac{\omega_0}{\pi} \sum_{n=1}^{\infty} \text{Real}\{G(n\omega_0)\Phi_x(n\omega_0)\} \\
 &= \frac{\omega_0}{2\pi} \text{Real}\{G(0)\Phi_x(0)\} + \frac{2\omega_0}{\pi} \sum_{\substack{n=1 \\ n \text{ odd}}}^{\infty} \text{Real}\{G(n\omega_0)\Phi_x(n\omega_0)\}
 \end{aligned}$$

where  $\omega_0 = \frac{2\pi}{T}$ ,  $\Phi_x(\omega)$  is the characteristic function of  $P_e(x)$  and  $x \geq 0$ ,  $\Phi_x(\omega) = \int_0^{\infty} P_e(x)e^{j\omega x} dx$ ,  $G_x(\omega)$  is the Fourier transform of the function  $f(x)$  with the random variable  $x$ ,  $G_x(\omega) = \int_0^{\infty} f(x)e^{-j\omega x} dx$  [9].  $P_e(x)$  denotes the symbol or bit error probability on an additive white Gaussian noise channel conditioned by the signal-to-noise ration or the combiner output envelope [9]. By using Eq. (4-80) in For the MIMO FSO system, the  $\text{Real}\{G(n\omega_0)\Phi_x(n\omega_0)\}$  part is

$$\begin{aligned}
 &\text{Real}\{G(n\omega_0)\Phi_x(n\omega_0)\} \\
 &= \int_0^{\infty} \left[ \sum_{v_1=1}^{N_v} \dots \sum_{v_{N_t N_r}=1}^{N_v} K_0 K_f \cos(K_d \omega) \right] \left[ \int_0^{\infty} \sum_{k=1}^{L-1} \frac{C_{L-1}^k (-1)^{k+1} \sigma_{\text{off}}}{\sqrt{(k\sigma_{\text{on}}^2 + \sigma_{\text{off}}^2)}} e^{-k_1 h^2} \cos(\omega h) dh \right] d\omega
 \end{aligned}$$

$$\begin{aligned}
& + \int_0^\infty \left[ \sum_{v_1=1}^{N_v} \dots \sum_{v_{N_t N_r}=1}^{N_v} K_0 K_f \sin(K_d \omega) \right] \left[ \int_0^\infty \sum_{k=1}^{L-1} \frac{C_{L-1}^k (-1)^{k+1} \sigma_{\text{off}}}{\sqrt{(k\sigma_{\text{on}}^2 + \sigma_{\text{off}}^2)}} e^{-k_l h^2} \sin(\omega h) dh \right] d\omega \\
& = \sum_{k=1}^{L-1} \frac{C_{L-1}^k (-1)^{k+1} \sigma_{\text{off}}}{\sqrt{(k\sigma_{\text{on}}^2 + \sigma_{\text{off}}^2)}} \sum_{v_1=1}^{N_v} \dots \sum_{v_{N_t N_r}=1}^{N_v} K_0 K_f \left\{ \int_0^\infty \cos(K_d \omega) \left[ \int_0^\infty e^{-k_l h^2} \cos(\omega h) dh \right] d\omega \right. \\
& \quad \left. + \int_0^\infty \sin(K_d \omega) \left[ \int_0^\infty e^{-k_l h^2} \sin(\omega h) dh \right] d\omega \right\} \\
& = \sum_{k=1}^{L-1} \frac{C_{L-1}^k (-1)^{k+1} \sigma_{\text{off}}}{\sqrt{(k\sigma_{\text{on}}^2 + \sigma_{\text{off}}^2)}} \sum_{v_1=1}^{N_v} \dots \sum_{v_{N_t N_r}=1}^{N_v} K_0 K_f \left\{ \int_0^\infty \cos(K_d \omega) \frac{1}{2} \sqrt{\frac{\pi}{k_l}} \exp\left(-\frac{\omega^2}{4k_l}\right) d\omega \right. \\
& \quad \left. + \int_0^\infty \sin(K_d \omega) \frac{1}{\sqrt{k_l}} F_D\left(\frac{\omega}{2\sqrt{k_l}}\right) d\omega \right\} \\
\text{Real}\{G(0)\Phi_x(0)\} & = \cos(K_d 0) \frac{1}{2} \sqrt{\frac{\pi}{k_l}} \exp\left(-\frac{0^2}{4k_l}\right) + \sin(K_d 0) \frac{1}{\sqrt{k_l}} F_D\left(\frac{0}{2\sqrt{k_l}}\right) \\
& = \frac{1}{2} \sqrt{\frac{\pi}{k_l}}
\end{aligned}$$

The average symbol error probability for one PPM symbol is

$$\begin{aligned}
P_s(E) & = \sum_{k=1}^{L-1} \frac{C_{L-1}^k (-1)^{k+1} \sigma_{\text{off}}}{\sqrt{(k\sigma_{\text{on}}^2 + \sigma_{\text{off}}^2)}} \sum_{v_1=1}^{N_v} \dots \sum_{v_{N_t N_r}=1}^{N_v} K_0 K_f \\
& \quad \left\{ \frac{\omega_0}{2\pi} \frac{1}{2} \sqrt{\frac{\pi}{k_l}} + \frac{2\omega_0}{\pi} \sum_{\substack{n=1 \\ n \text{ odd}}}^{\infty} \left[ \cos(K_d n \omega_0) \frac{1}{2} \sqrt{\frac{\pi}{k_l}} \exp\left[-\frac{(n\omega_0)^2}{4k_l}\right] + \sin(K_d n \omega_0) \frac{1}{\sqrt{k_l}} F_D\left(\frac{n\omega_0}{2\sqrt{k_l}}\right) \right] \right\} \\
& = \sum_{k=1}^{L-1} \frac{C_{L-1}^k (-1)^{k+1} \sigma_{\text{off}}}{\sqrt{(k\sigma_{\text{on}}^2 + \sigma_{\text{off}}^2)}} \sum_{v_1=1}^{N_v} \dots \sum_{v_{N_t N_r}=1}^{N_v} K_0 K_f
\end{aligned}$$

$$\left\{ \frac{\omega_0}{4\pi} \sqrt{\frac{\pi}{k_l}} + \frac{2\omega_0}{\pi} \sum_{\substack{n=1 \\ n \text{ odd}}}^{\infty} \left[ \cos(K_d n \omega_0) \frac{1}{2} \sqrt{\frac{\pi}{k_l}} \exp\left[-\frac{(n\omega_0)^2}{4k_l}\right] + \sin(K_d n \omega_0) \frac{1}{\sqrt{k_l}} F_D\left(\frac{n\omega_0}{2\sqrt{k_l}}\right) \right] \right\}$$

where

$$K_0 = \left( \frac{F e^{m_\ell}}{\pi} \sqrt{\frac{\mathcal{R}E_s A_r \alpha}{q N_t A_b}} \right)^{N_t N_r}$$

$$k_l = \frac{k(E_s \mathcal{R}M A g)^2}{2N_t^2(k\sigma_{\text{on}}^2 + \sigma_{\text{off}}^2)}$$

$$\omega_0 = \frac{2\pi}{T_F}$$

$$g = \frac{2A_r \alpha}{A_b}$$

The equation of the error probability can be simplified further as

$$\begin{aligned} P_s(E) &\leq \sum_{k=1}^{L-1} \frac{C_{L-1}^k (-1)^{k+1} \sigma_{\text{off}}}{\sqrt{(k\sigma_{\text{on}}^2 + \sigma_{\text{off}}^2)}} \sum_{v_1=1}^{N_v} \dots \sum_{v_{N_t N_r}=1}^{N_v} \frac{K_0 K_f \omega_0}{\sqrt{\pi k_l}} \\ &\quad \left\{ \frac{1}{4} + \sum_{\substack{n=1 \\ n \text{ odd}}}^{N_F} \left[ \cos(K_d n \omega_0) \exp\left[-\frac{(n\omega_0)^2}{4k_l}\right] + \frac{2}{\sqrt{\pi}} \sin(K_d n \omega_0) F_D\left(\frac{n\omega_0}{2\sqrt{k_l}}\right) \right] \right\} \\ &= \sum_{k=1}^{L-1} \frac{C_{L-1}^k (-1)^{k+1} \sigma_{\text{off}}}{\sqrt{(k\sigma_{\text{on}}^2 + \sigma_{\text{off}}^2)}} \sum_{v_1=1}^{N_v} \dots \sum_{v_{N_t N_r}=1}^{N_v} \frac{K_0 K_f \omega_0}{\frac{E_s \mathcal{R}M A g}{N_t} \sqrt{\frac{\pi k}{2(k\sigma_{\text{on}}^2 + \sigma_{\text{off}}^2)}}} \\ &\quad \left\{ \frac{1}{4} + \sum_{\substack{n=1 \\ n \text{ odd}}}^{N_F} \left[ \cos(K_d n \omega_0) \exp\left[-\frac{(n\omega_0)^2}{4k_l}\right] + \frac{2}{\sqrt{\pi}} \sin(K_d n \omega_0) F_D\left(\frac{n\omega_0}{2\sqrt{k_l}}\right) \right] \right\} \end{aligned}$$

$$\begin{aligned}
&= \sum_{k=1}^{L-1} \frac{C_{L-1}^k (-1)^{k+1} \sigma_{\text{off}} K_0}{\frac{E_s \mathcal{R} M A g}{N_t} \sqrt{\frac{\pi k}{2}}} \sum_{v_1=1}^{N_v} \dots \sum_{v_{N_t N_r}=1}^{N_v} K_f \omega_0 \\
&\quad \left\{ \frac{1}{4} + \sum_{\substack{n=1 \\ n \text{ odd}}}^{N_F} \left[ \cos(K_d n \omega_0) \exp \left[ -\frac{(n \omega_0)^2}{4k_l} \right] + \frac{2}{\sqrt{\pi}} \sin(K_d n \omega_0) F_D \left( \frac{n \omega_0}{2\sqrt{k_l}} \right) \right] \right\} \\
&= \sum_{k=1}^{L-1} \frac{C_{L-1}^k (-1)^{k+1} \sigma_{\text{off}}}{2MA \frac{\mathcal{R} E_s A_r \alpha}{N_t A_b} \sqrt{\frac{\pi k}{2}}} \left( \frac{F e^{m_\ell}}{\pi} \sqrt{\frac{\mathcal{R} E_s A_r \alpha}{q N_t A_b}} \right)^{N_t N_r} \sum_{v_1=1}^{N_v} \dots \sum_{v_{N_t N_r}=1}^{N_v} K_f \omega_0 \\
&\quad \left\{ \frac{1}{4} + \sum_{\substack{n=1 \\ n \text{ odd}}}^{N_F} \left[ \cos(K_d n \omega_0) \exp \left[ -\frac{(n \omega_0)^2}{4k_l} \right] + \frac{2}{\sqrt{\pi}} \sin(K_d n \omega_0) F_D \left( \frac{n \omega_0}{2\sqrt{k_l}} \right) \right] \right\} \\
&= \sum_{k=1}^{L-1} \frac{C_{L-1}^k (-1)^{k+1} \sigma_{\text{off}}}{\frac{\mathcal{R} E_s A_r \alpha}{N_t A_b} MA \sqrt{2\pi k}} \left( \frac{F e^{m_\ell}}{\pi \sqrt{q}} \sqrt{\frac{\mathcal{R} E_s A_r \alpha}{N_t A_b}} \right)^{N_t N_r} \sum_{v_1=1}^{N_v} \dots \sum_{v_{N_t N_r}=1}^{N_v} K_f \omega_0 \\
&\quad \left\{ \frac{1}{4} + \sum_{\substack{n=1 \\ n \text{ odd}}}^{N_F} \left[ \cos(K_d n \omega_0) \exp \left[ -\frac{(n \omega_0)^2}{4k_l} \right] + \frac{2}{\sqrt{\pi}} \sin(K_d n \omega_0) F_D \left( \frac{n \omega_0}{2\sqrt{k_l}} \right) \right] \right\} \\
&= \sum_{k=1}^{L-1} \frac{C_{L-1}^k (-1)^{k+1} \sigma_{\text{off}}}{MA \sqrt{2\pi k}} \left( \frac{F e^{m_\ell}}{\pi \sqrt{q}} \right)^{N_t N_r} \left( \frac{\mathcal{R} E_s A_r \alpha}{N_t A_b} \right)^{\left( \frac{N_t N_r}{2} - 1 \right)} \sum_{v_1=1}^{N_v} \dots \sum_{v_{N_t N_r}=1}^{N_v} K_f \omega_0 \\
&\quad \left\{ \frac{1}{4} + \sum_{\substack{n=1 \\ n \text{ odd}}}^{N_F} \left[ \cos(K_d n \omega_0) \exp \left[ -\frac{(n \omega_0)^2}{4k_l} \right] + \frac{2}{\sqrt{\pi}} \sin(K_d n \omega_0) F_D \left( \frac{n \omega_0}{2\sqrt{k_l}} \right) \right] \right\} \\
&= \sum_{k=1}^{L-1} \frac{C_{L-1}^k (-1)^{k+1} K_0'}{\sqrt{k}} \sum_{v_1=1}^{N_v} \dots \sum_{v_{N_t N_r}=1}^{N_v} K_f \omega_0
\end{aligned}$$

$$\left\{ \frac{1}{4} + \sum_{\substack{n=1 \\ n \text{ odd}}}^{N_F} \left[ \cos(K_d n \omega_0) \exp \left[ -\frac{(n \omega_0)^2}{4k_l} \right] + \frac{2}{\sqrt{\pi}} \sin(K_d n \omega_0) F_D \left( \frac{n \omega_0}{2\sqrt{k_l}} \right) \right] \right\}$$

where

$$K_0' = \frac{\sigma_{\text{off}}}{\sqrt{2\pi}MA} \left( \frac{F e^{m_\ell}}{\pi \sqrt{q}} \right)^{N_t N_r} \left( \frac{\mathcal{R} E_s A_r \alpha}{N_t A_b} \right)^{\left( \frac{N_t N_r}{2} - 1 \right)}$$

$$k_l = \frac{k(E_s \mathcal{R} M A g)^2}{2N_t^2 (k\sigma_{\text{on}}^2 + \sigma_{\text{off}}^2)}$$

$$\omega_0 = \frac{2\pi}{T_F}$$

$$g = \frac{2A_r \alpha}{A_b}$$

## APPENDIX M

This is the derivation for Eq. (4-87).

$$\omega = \sqrt{\frac{cx}{1-x}}$$

$$\omega^2 - \omega^2 x = cx$$

$$\omega^2 = (c + \omega^2)x$$

$$x = \frac{\omega^2}{(c + \omega^2)}$$

$$x = \frac{1}{\left( \frac{c}{\omega^2} + 1 \right)}$$

If  $\omega$  tends to infinity, the value of  $x$  is unity. If  $\omega$  is zero, the value of  $x$  is also zero.

$$\begin{aligned}
d\omega &= d\left(\sqrt{\frac{cx}{1-x}}\right) \\
&= \frac{1}{2}\left(\frac{cx}{1-x}\right)^{-\frac{1}{2}}\left[\frac{c}{1-x} + \frac{-cx(-1)}{(1-x)^2}\right] dx \\
&= \frac{\sqrt{c}}{2}\left(\frac{1-x}{x}\right)^{\frac{1}{2}}\left[\frac{1-x+x}{(1-x)^2}\right] dx \\
&= \frac{\sqrt{c}}{2}\left(\frac{1-x}{x}\right)^{\frac{1}{2}}\left[\frac{1-x+x}{(1-x)^2}\right] dx \\
&= \frac{\sqrt{c}}{2x(1-x)}\sqrt{\frac{x}{1-x}} dx
\end{aligned}$$

## APPENDIX N

This is the derivation for Eq. (4-89a).

$$\begin{aligned}
&\int_0^\infty \sin(K_d\omega) \int_0^\infty [e^{-k_l h^2} \sin(\omega h)] dh d\omega \\
&= \int_0^\infty \sin(K_d\omega) \frac{1}{\sqrt{k_l}} F_D\left(\frac{\omega}{2\sqrt{k_l}}\right) d\omega \\
&= \int_0^1 \sin\left(K_d\sqrt{\frac{cx}{1-x}}\right) \frac{1}{\sqrt{k_l}} F_D\left(\frac{1}{2\sqrt{k_l}}\sqrt{\frac{cx}{1-x}}\right) \frac{\sqrt{1-x}}{2x(1-x)} dx \\
&= \sum_{q=1}^{N_G} \frac{2\pi x_q}{(2N_G+1)} \sin(K_d\tau_q) \frac{1}{\sqrt{k_l}} F_D\left(\frac{\tau_q}{2\sqrt{k_l}}\right) \frac{\sqrt{c}}{2x_q(1-x_q)} \\
&= \frac{\pi}{(2N_G+1)\sqrt{k_l}} \sum_{q=1}^{N_G} \frac{\sqrt{c} \sin(K_d\tau_q)}{\sin^2\left[\left(\frac{2q-1}{2N_G+1}\right)\frac{\pi}{2}\right]} F_D\left(\frac{\tau_q}{2\sqrt{k_l}}\right)
\end{aligned}$$

$$\begin{aligned}
& \int_0^\infty \cos(K_d \omega) \int_0^\infty [e^{-k_l h^2} \cos(\omega h)] dh d\omega \\
&= \frac{1}{2} \sqrt{\frac{\pi}{k_l}} \int_0^\infty \left\{ \exp\left(-\frac{\omega^2}{4k_l}\right) \cos(K_d \omega) \right\} d\omega \\
&= \frac{1}{2} \sqrt{\frac{\pi}{k_l}} \frac{1}{2} \sqrt{4k_l \pi} \exp\left(-\frac{K_d^2}{4 \frac{1}{4k_l}}\right) \\
&= \frac{\pi}{2} \exp(-k_l K_d^2)
\end{aligned}$$

## APPENDIX O

This is the derivation for Eq. (4-110).

$$\begin{aligned}
\frac{d[f(x)]}{dx} &= \frac{\eta F}{\sqrt{2\pi} M} \left[ \eta e^{(\sqrt{2}\sigma_\ell x + \ln \bar{\lambda}_{s\ell} + m_\ell)} + \frac{m_{s\ell}(F-1)}{M} \right]^{-\frac{5}{2}} \left( -\frac{3}{2} \right) \eta e^{(\sqrt{2}\sigma_\ell x + \ln \bar{\lambda}_{s\ell} + m_\ell)} \sqrt{2}\sigma_\ell \\
&\quad \exp \left\{ -\frac{\left[ \eta e^{(\sqrt{2}\sigma_\ell x + \ln \bar{\lambda}_{s\ell} + m_\ell)} - \frac{m_{s\ell}}{M} \right]^2}{2 \left[ \eta e^{(\sqrt{2}\sigma_\ell x + \ln \bar{\lambda}_{s\ell} + m_\ell)} + \frac{m_{s\ell}(F-1)}{M} \right]} + \sqrt{2}\sigma_\ell x + \ln \bar{\lambda}_{s\ell} + m_\ell \right\} \\
&+ \frac{\eta F}{\sqrt{2\pi} M} \left[ \eta e^{(\sqrt{2}\sigma_\ell x + \ln \bar{\lambda}_{s\ell} + m_\ell)} + \frac{m_{s\ell}(F-1)}{M} \right]^{-\frac{3}{2}} \\
&\quad \exp \left\{ -\frac{\left[ \eta e^{(\sqrt{2}\sigma_\ell x + \ln \bar{\lambda}_{s\ell} + m_\ell)} - \frac{m_{s\ell}}{M} \right]^2}{2 \left[ \eta e^{(\sqrt{2}\sigma_\ell x + \ln \bar{\lambda}_{s\ell} + m_\ell)} + \frac{m_{s\ell}(F-1)}{M} \right]} + \sqrt{2}\sigma_\ell x + \ln \bar{\lambda}_{s\ell} + m_\ell \right\} \\
&\quad \left\{ -\frac{2 \left[ \eta e^{(\sqrt{2}\sigma_\ell x + \ln \bar{\lambda}_{s\ell} + m_\ell)} - \frac{m_{s\ell}}{M} \right] \eta e^{(\sqrt{2}\sigma_\ell x + \ln \bar{\lambda}_{s\ell} + m_\ell)} \sqrt{2}\sigma_\ell}{2 \left[ \eta e^{(\sqrt{2}\sigma_\ell x + \ln \bar{\lambda}_{s\ell} + m_\ell)} + \frac{m_{s\ell}(F-1)}{M} \right]} \right. \\
&\quad \left. + \frac{\left[ \eta e^{(\sqrt{2}\sigma_\ell x + \ln \bar{\lambda}_{s\ell} + m_\ell)} - \frac{m_{s\ell}}{M} \right]^2 \eta e^{(\sqrt{2}\sigma_\ell x + \ln \bar{\lambda}_{s\ell} + m_\ell)} \sqrt{2}\sigma_\ell}{2 \left[ \eta e^{(\sqrt{2}\sigma_\ell x + \ln \bar{\lambda}_{s\ell} + m_\ell)} + \frac{m_{s\ell}(F-1)}{M} \right]^2} + \sqrt{2}\sigma_\ell \right\} \\
&= \frac{\eta F}{\sqrt{2\pi} M} \left[ \eta e^{(\sqrt{2}\sigma_\ell x + \ln \bar{\lambda}_{s\ell} + m_\ell)} + \frac{m_{s\ell}(F-1)}{M} \right]^{-\frac{3}{2}}
\end{aligned}$$

$$\begin{aligned}
& \exp \left\{ - \frac{\left[ \eta e^{(\sqrt{2}\sigma_\ell x + \ln \bar{\lambda}_{s\ell} + m_\ell)} - \frac{m_{s\ell}}{M} \right]^2}{2 \left[ \eta e^{(\sqrt{2}\sigma_\ell x + \ln \bar{\lambda}_{s\ell} + m_\ell)} + \frac{m_{s\ell}(F-1)}{M} \right]} + \sqrt{2}\sigma_\ell x + \ln \bar{\lambda}_{s\ell} + m_\ell \right\} \\
& \left\{ - \frac{3\eta e^{(\sqrt{2}\sigma_\ell x + \ln \bar{\lambda}_{s\ell} + m_\ell)} \sqrt{2}\sigma_\ell}{2 \left[ \eta e^{(\sqrt{2}\sigma_\ell x + \ln \bar{\lambda}_{s\ell} + m_\ell)} + \frac{m_{s\ell}(F-1)}{M} \right]} - \frac{2 \left[ \eta e^{(\sqrt{2}\sigma_\ell x + \ln \bar{\lambda}_{s\ell} + m_\ell)} - \frac{m_{s\ell}}{M} \right] \eta e^{(\sqrt{2}\sigma_\ell x + \ln \bar{\lambda}_{s\ell} + m_\ell)} \sqrt{2}\sigma_\ell}{2 \left[ \eta e^{(\sqrt{2}\sigma_\ell x + \ln \bar{\lambda}_{s\ell} + m_\ell)} + \frac{m_{s\ell}(F-1)}{M} \right]} \right. \\
& \quad \left. + \frac{\left[ \eta e^{(\sqrt{2}\sigma_\ell x + \ln \bar{\lambda}_{s\ell} + m_\ell)} - \frac{m_{s\ell}}{M} \right]^2 \eta e^{(\sqrt{2}\sigma_\ell x + \ln \bar{\lambda}_{s\ell} + m_\ell)} \sqrt{2}\sigma_\ell}{2 \left[ \eta e^{(\sqrt{2}\sigma_\ell x + \ln \bar{\lambda}_{s\ell} + m_\ell)} + \frac{m_{s\ell}(F-1)}{M} \right]^2} + \sqrt{2}\sigma_\ell \right\} \\
& = \frac{\eta^F}{\sqrt{2}\pi M} \left[ \eta e^{(\sqrt{2}\sigma_\ell x + \ln \bar{\lambda}_{s\ell} + m_\ell)} + \frac{m_{s\ell}(F-1)}{M} \right]^{-\frac{3}{2}} \\
& \exp \left\{ - \frac{\left[ \eta e^{(\sqrt{2}\sigma_\ell x + \ln \bar{\lambda}_{s\ell} + m_\ell)} - \frac{m_{s\ell}}{M} \right]^2}{2 \left[ \eta e^{(\sqrt{2}\sigma_\ell x + \ln \bar{\lambda}_{s\ell} + m_\ell)} + \frac{m_{s\ell}(F-1)}{M} \right]} + \sqrt{2}\sigma_\ell x + \ln \bar{\lambda}_{s\ell} + m_\ell \right\} \\
& \left\{ - \frac{\eta e^{(\sqrt{2}\sigma_\ell x + \ln \bar{\lambda}_{s\ell} + m_\ell)} \sqrt{2}\sigma_\ell \left\{ 3 + 2 \left[ \eta e^{(\sqrt{2}\sigma_\ell x + \ln \bar{\lambda}_{s\ell} + m_\ell)} - \frac{m_{s\ell}}{M} \right] \right\}}{2 \left[ \eta e^{(\sqrt{2}\sigma_\ell x + \ln \bar{\lambda}_{s\ell} + m_\ell)} + \frac{m_{s\ell}(F-1)}{M} \right]} \right. \\
& \quad \left. + \frac{\left[ \eta e^{(\sqrt{2}\sigma_\ell x + \ln \bar{\lambda}_{s\ell} + m_\ell)} - \frac{m_{s\ell}}{M} \right]^2 \eta e^{(\sqrt{2}\sigma_\ell x + \ln \bar{\lambda}_{s\ell} + m_\ell)} \sqrt{2}\sigma_\ell}{2 \left[ \eta e^{(\sqrt{2}\sigma_\ell x + \ln \bar{\lambda}_{s\ell} + m_\ell)} + \frac{m_{s\ell}(F-1)}{M} \right]^2} + \sqrt{2}\sigma_\ell \right\}
\end{aligned}$$